University of Leoben

Dissertation

Fracture toughness and microstructural stability of heavily deformed tungsten materials

M.Sc. Vladica Nikolić

Leoben, September 2018

Erich Schmid Institute of Materials Science
Austrian Academy of Sciences
Jahnstraße 12
A-8700 Leoben

Affidavit

I declare in lieu of oath, that I wrote this thesis and performed the associated research myself, using only literature cited in this volume.

M.Sc. Vladica Nikolić

Leoben, September 2018

Acknowledgments

It is my pleasure to acknowledge the contribution of many people who helped with completion of my dissertation and supported me in different ways over the past years.

First and foremost, I would like to express my biggest gratitude to Professor Dr. Reinhard Pippan, who gave me the opportunity to pursue my PhD and supported me throughout the way. His immense knowledge and expertise, unwavering optimism, patience and tranquillity in various situations, made all of this a truly remarkable and valuable experience. So, thank you for welcoming me to the always exciting world of fracture mechanics!

All of the employees at the Erich Schmid Institute contributed a lot to the success of this work. I would particularly like to highlight the continuously helpful and highly skilled workshop team: Franz Hubner and Robin Neubauer. A big thanks go to Silke Modritsch, for untiring preparation of the samples and Peter Kutleša, for useful advices regarding experimental setup. Our lovely secretaries Sabine Wilfling and Daniela Brunner are recognized for all the administrative and organizational support, which is always provided so impeccably.

For the financial support of the project, I would like to thank the EUROfusion consortium and in particular people in charge of the HHFM group – Dr. Jens Reiser and Dr. Gerald Pintsuk. Your inspiring enthusiasm and insightful discussions enriched our project meetings and made them very pleasant. A big thank you also to Dr. Johann Riesch for a very interesting and fruitful collaboration.

I also owe a great deal of appreciation to a very important group of people – my co-doctoral colleagues, post-docs, diploma students, student assistants and all the friends at ESI, who supported me in both professional as well as private matters and were a big help during the last years. Firstly, I would like to thank the preceding "tungsten dude" Stefan Wurster, who was a great help from the very beginning – from initial administrative tasks and showing me all the equipment, to the many insightful discussions, constructive criticism, proof reading and catching all those skipped articles. Thank you! I am grateful to Daniel Firneis for the help with experiments and also for sharing the load of all those tough times when tungsten was trying to break us. Special thanks go to Babsi and Benji for their friendship and fun times outside the institute. Thank you Mr. Schuh for interesting conference trips, as well as travelling together to all those amazing destinations. To our "laser guy" and a fellow commuter Manuel for supporting me in my last experiments and for all the cheerful conversations that made those train rides quite nice. Toni is appreciated for his willingness to help whenever needed, Megan for organizing girls' evenings and Andi for nice and calm office times. Furthermore, I would like to thank everyone, including those whom I have not named, for extremely pleasant working atmosphere and all those non-scientific discussions over a cup of coffee or during our entertaining workshop gatherings. It was truly an honour to be a part of the ESI family.

It is also my pleasure to thank all the friends, both here and abroad, for wonderful times that we shared together, your support and encouragement throughout this journey. I am grateful to have you in my life. Special thanks go to my FOM family: Branka, Ana, Maša and Miloš, for your optimism, time and motivating ideas in our common aspiration of bringing fusion research to students back home.

In the end, I would like to express my deepest and sincerest gratitude to my family, for their unconditional love and unwavering support. Svojim roditeljima, Mileni i Rajku, sam beskrajno zahvalna na nezamenjivoj podršci i bezuslovnoj ljubavi, što su mi omogućili da ostvarim svoje ciljeve, čak i ako je to podrazumevalo da se odselim daleko i što su uvek verovali u mene, čak i kada ja sama nisam. Volim vas puno! My sister Vanja was also there every step of the way, to keep me grounded when needed and to have my back no matter what. A person could not ask for a better sister, friend and companion in life! Last, but not the least, I want to thank you my love, for your devotion, unconditional support and unlimited patience. You kept my spirit up during challenging moments and made the end of this journey significantly calmer and that more enjoyable. From the bottom of my heart, thank you all so, so much!

Abstract

Different tungsten and tungsten-based materials are recognised as leading candidates for the divertor and plasma facing components of a nuclear fusion device. A unique suitability of these metals for the very challenging fusion reactor application is due to their excellent high temperature properties. However, a significant drawback for the structural application of tungsten is its poor fracture toughness and low ductility at room temperature (RT), coupled with a high ductile-to-brittle transition temperature (DBTT). These properties cause serious restrictions in both its performance in demanding applications, as well as its workability. Therefore, progress and success of using tungsten for structural components are strongly dependant on the development of toughening mechanisms, making tungsten in such a way a more fracture resistant material. Hence, a comprehensive understanding of the fundamentals of fracture properties of tungsten is essential, as well as determining the influence of different parameters on the underlying micromechanisms controlling the fracture process.

The main focus of this thesis was devoted to the investigation of the fracture behaviour of heavily deformed tungsten materials - *foils and wires*, with an additional emphasis on their microstructural stability upon annealing. Crack resistance of pure and potassium doped, ultrafine grained 100µm tungsten foils was investigated as a function of testing direction and temperature in the range from -196°C to 800°C. To study the influence of the anisotropic microstructure on the fracture process, the single-edge-notched specimens were extracted in three different crack orientations relative to the rolling direction. This thorough investigation shows the positive impact of deformation induced grain refinement through extraordinary high values of fracture toughness and a reduction of the DBTT to about room temperature. Furthermore, it was demonstrated that the grain shape anisotropy and a strong rotated cubic texture are decisive factors for anisotropic fracture properties. Fracture surface investigations reveal distinctive behaviour with an increase in temperature. The pronounced transition in failure mode was observed going from brittle, transcrystalline fracture at -196°C towards pronounced delamination at intermediate temperatures and to ductile failure at highest temperatures.

The purpose of the work regarding drawn tungsten wires was to perform a systematic study on the effect of heat treatments and investigate how microstructural and fracture properties develop upon annealing, with a special focus on the relationship between the investigated features. A comprehensive microstructural characterization of the 150µm pure and potassium doped tungsten wires was performed through detailed analyses of the evolution of different aspects of the microstructure (nature of grain boundaries, grain shape and size, texture). Annealing in the temperature range from 900-1600°C enables the investigation of the microstructural stability of the two materials and arising annealing phenomena - recovery, recrystallization and grain growth. The results demonstrate that pure tungsten wires recrystallize fully in the temperature range 1300-1500°C accompanied with tremendous coarsening and a complete loss of the initial fibrous, elongated grain structure. In contrast to this, potassium doped wire shows superior high temperature properties, where the performed heat treatments cause milder microstructural changes, consequently suppressing recrystallization and grain growth to temperatures well above the highest investigated one. Room temperature fracture toughness

measurements of the wires were conducted with the emphasis on the evolution of the fracture micromechanisms in respect to annealing treatments. Single-edge-notched specimens were used, with the crack growth direction perpendicular to the drawing axis of the wire. The occurrence of either a brittle or a ductile response in the as-received state of both materials is a strong indication that the ductile-to-brittle transition temperature is around room temperature. Pure, annealed tungsten wires experience a tremendous deterioration of the fracture toughness with a very prominent transition of the failure mode. The observed embrittlement by annealing can be related to the loss of the fibrous, elongated microstructure. In contrast to this, the results of the annealed, doped wires demonstrate that the microstructural stability and preservation of the initial, beneficial grain structure is directly reflected in the crack resistance of the material. Predominately ductile behaviour, with characteristic knife-edge necking, is seen even after annealing at 1600°C.

In addition, a preliminary study on binary tungsten thin film alloys was conducted, exploring in such a way a prospect of performing a high-throughput study in a wide range of compositions and determining the exact influence of a particular alloying element on the resulting properties. Combinatorial magnetron co-sputtering was applied to produce thin film composition spread materials libraries with well-defined, continuous composition gradients. Chemical, morphological and microstructural analyses were performed, revealing a strong influence of the concentration of the alloying elements. The prospects of studying potential enhancements of mechanical properties by solid solutions are outlined, emphasising the necessary microstructural requirements for valuable micromechanical tests.

Content

1

Motivation and aim of the work

The sustainable development and modernisation of our civilization is strongly dependent on the energy supply. A rapid urbanization and the growth of the world's population greatly increase the overall energy demands, while the limitation of available resources and the environmental requirements of reduced pollution are driving forces for the development of alternative energy solutions. Nuclear fusion is considered to be an attractive option for the future global energy mix and by the middle of this century should acquire the key role in tackling global energy needs. The exceptional potential of fusion power is seen through its key benefits over conventional approaches, these being that it is a potential source of inherently safe, non-carbon emitting and virtually limitless energy.

In the past decades, the technical feasibility of human engineered fusion has already been demonstrated on a small scale in dozens of experimental fusion facilities. However, the success of fusion as an energy provider will greatly depend on whether existing challenges of upscaling the process to commercial proportions will be met in an efficient, economical and environmentally benign way. The next step towards this goal is the International Thermonuclear Experimental Reactor (ITER), currently under construction in the southern France. ITER has been designed as the essential experimental link between today's fusion research machines and tomorrow's fusion power plants, thus answering the question of how viable it is to harness the fusion power. And while the main task of ITER will be to demonstrate the technological and scientific feasibility of fusion energy, the consecutive machine, before building a real commercial reactor, called DEMO (Demonstration Power Plant), will be the prototype of the fusion reactor towards its industrial and commercial exploitation. Although the final design and concept of DEMO will to a large extent depend on results collected from ITER and other fusion experiments, it is already evident that the operating environment will be even more challenging than in the case of ITER. As a result, the development of advanced structural and plasma facing materials, able to withstand extreme working conditions for acceptable minimum operating time, is essential. Thus, the future of nuclear fusion will strongly be influenced by the capability of materials science to deliver material options fulfilling fusion-specific harsh requirements.

When thinking of highly exposed high-heat flux reactor parts, such as the divertor and the first wall, tungsten (W) based materials appear to be the best choice at the moment. However, the mechanical properties of available W materials are not yet suitable for structural purposes due to their intrinsic brittleness at low temperatures and rather high ductile-to-brittle transition temperature. Therefore, the progress of structural application of tungsten is strongly related to the development of toughening

mechanisms, making tungsten in such a way a more fracture resistant material. Among several proposed strategies aimed at improving its fracture toughness and mitigating the brittleness issue, the development of W-based composites seems to be a very promising method. Focusing here only on the fibre reinforced and laminated/3D composites, it is indicated that their key structural components are heavily deformed ultrafine grained (UFG) tungsten materials, in a form of wires and foils, respectively. In order to produce such a fine grained material, a very high degree of deformation is imposed, leading to the development of unique microstructures, which are known to be amongst the main influences on the fracture behaviour of the material.

The aim of the work presented in this thesis is to investigate fracture behaviour of commercially available thin tungsten foils and drawn tungsten wires, looking into different parameters influencing the fracture process. Special focus is given to the investigation of the microstructural stability upon annealing and determining whether additions of potassium lead to the preservation of advantageous properties. The obtained results have a great significance for the next steps in the composite development and are essential part in comprehensive understanding of the fracture characteristics of the composites themselves.

Furthermore, a part of the work will review capabilities and limitations of different tungsten alloys, giving an overview of decades of scientific research regarding the ductility enhancement by solid solutions. Related to this topic is a preliminary study on binary tungsten alloys, in the form of thin films produced by magnetron co-sputtering technique. The prospect of performing a high-throughput study in a wide range of compositional gradients will be explored, with the idea of determining the exact influence of a particular alloying element on the resulting properties and potentially finding an element with a beneficial effect on tungsten.

2

Introduction

"We say that we want to put the sun into the box. The idea is pretty. The problem is, we don't know how to make the box"

Pierre-Gilles de Gennes

2.1. Nuclear fusion

Nuclear fusion denotes a nuclear reaction in which two light atomic nuclei are fused, forming a heavier and a more stable nucleus whilst releasing energy which is converted from the mass defect of the reaction. This is the main mechanism that powers the sun and stars, where most of the energy comes from the fusion of hydrogen atoms into helium (pp chain reaction). In order to achieve controlled thermonuclear fusion in terrestrial conditions, the efforts are concentrated on a reaction between isotopes of hydrogen, deuterium and tritium, as it has the most efficient reaction rate among other possible candidates for efficient fusion reaction [1]. The following D-T reaction

$$_1^2D + \ _1^3T \ \rightarrow \ \alpha(3.5 \ MeV) + \ _0^1n(14.1MeV) \tag{1}$$
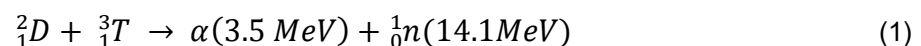
is the leading candidate for the fusion program due to the highest cross section at energies achievable at the present level of technology [2]. The products of this reaction are an alpha particle (an ionized helium atom) with an energy of 3.5MeV and a neutron carrying 14.1MeV of kinetic energy. Both deuterium and tritium are isotopes of hydrogen, however their natural abundance differs strongly. While the deuterium is easily obtained from the water, tritium is a radioactive hydrogen isotope with a half-life of 12.32 years, hence naturally occurring tritium is extremely rare. As a major requirement for fusion to be a fuel self-sufficient energy source [3] tritium needs to be bred in the reactor, which could be achieved by irradiating lithium targets with neutrons already produced in the D-T fusion reaction. The great advantage of using lithium is that it is a very abundant element in the Earth's crust, making the whole fusion fuel cycle practically unlimited in resources.

For fusion to take place, the particles of the fuel, which are in the state of ionized plasma, need to overcome the Coulomb repulsive forces between like-charged nuclei. Thus, certain conditions must be met so that the particles are brought to fuse. This requirement of igniting a D-T plasma and keeping it burning is described by the Lawson criterion [4],which is given as the triple product of the plasma

density, the energy confinement time and the ion temperature. Essentially, the ignition condition means that the plasma temperature needs to be high enough to overcome the repulsive forces and a sufficiently large number of particles (high density) needs to be confined for long enough time to allow numerous fusion reactions to happen. In the case of stellar bodies, these conditions are met naturally as a result of enormous heat and extremely high gravitational pressure. The implementation of the same approach in the laboratory setting is impossible, making the task of "taming the sun" in terrestrial conditions a very tough challenge. The most common way to satisfy the aforementioned criterion is presented by the magnetic confinement fusion concept [5], where the plasma confinement is achieved by applying a suitable magnetic field. At the time being, this is the most advanced concept for energy generating fusion reactors. An alternative approach of inertial confinement [6], [7] is the concept of laser driven fusion, where the small values of confinement time are coupled with enormously high densities of the fuel.

Already back in the 50's and simultaneously in several different countries, the research of harnessing the energy of sun on Earth was taken in the direction of controlled magnetic fusion [8]. Among several different conceptual schemes of achieving magnetic confinement, the leading design in the fusion research is a tokamak device [2]. It is a machine where plasma is stored in a doughnut-shaped metallic vessel and confined with magnetic fields originating from toroidal and poloidal coils. The reactor core is arranged in different layers with the most inner part being the vacuum chamber, which encloses the space where plasma is confined and fusion reactions take place. This area is surrounded by the blanket and the divertor, both parts constituting the so-called first wall. This is the first element which encounters the hot plasma. Neutrons provided by the fusion reaction are uncharged particles, thus magnetic fields do not confine them, allowing in such a way a transfer of their energy to the first wall via inelastic collision. Generally speaking, all the plasma facing components (PFCs) are under enormous heat flux, hence an active cooling system is a necessity for large-scaled fusion devices. The aforementioned divertor is situated at the bottom of the vacuum vessel and is a particularly important reactor part. Its primary function is to pump helium ash and impurities, making the divertor a region with highest heat fluxes and erosion rate. Furthermore, the coils of the magnetic field are located outside the vacuum vessel and since the magnets are superconductors and operate at very low temperatures, the entire reactor core is situated inside a cryostat.

The outlined concept of a tokamak design is the one chosen for the world's mostly known reactor - ITER (Figure 1) [9], [10]. **I**nternational **T**hermonuclear **E**xperimental **R**eactor (lat. for "the way") is presently the most important long-term scientific fusion experiment. Its construction is currently ongoing in southern France with the first plasma experiment less than a decade away. The ITER project represents one of the most ambitious energy projects in the world nowadays and since it results from a collaboration of 35 nations, it is also seen as the most prominent international, multinational scientific community. The ITER members - European Union, China, India, Japan, Korea, Russia and the United States, have combined their available resources to conquer one of the greatest frontiers in science and are working together to prove the feasibility of fusion as a large-scale energy resource. Thus, the main goals set for this reactor are quite challenging. Designed to produce a ten-fold return of energy (Q=10), ITER will be the first fusion reactor to produce long pulses of energy release on a significant scale. Put

in numbers, this means that 50MW of auxiliary heating power injected in plasma will give 500MW of fusion power as an output [9], [11]. In previous experimental efforts, more energy was used to drive the fusion process than energy that could be obtained, with the world record for fusion power held by the currently biggest JET tokamak (Q=0.67). Among ITER's prime scientific and engineering goals is to combine different fusion technologies and components for a future fusion reactor, with a very important mission at the later stage of operation - to demonstrate the feasibility of producing tritium within the blanket. It will be the first fusion device to test the integrated technologies, materials and physics regimes necessary for commercial production of fusion based electricity. Thus, the main achievement of the ITER's experimental campaign towards advancing fusion science and preparing the way for the fusion power plants of tomorrow, will be to provide the necessary knowledge for the design of a succeeding demonstration fusion reactor - DEMO [12], [13]. DEMO will be a larger scale prototype designed to produce electricity and required to satisfy all the basic functions of a power plant. As an intermediate step between ITER and a commercial reactor, it will give the ultimate answer about fusion power viability.
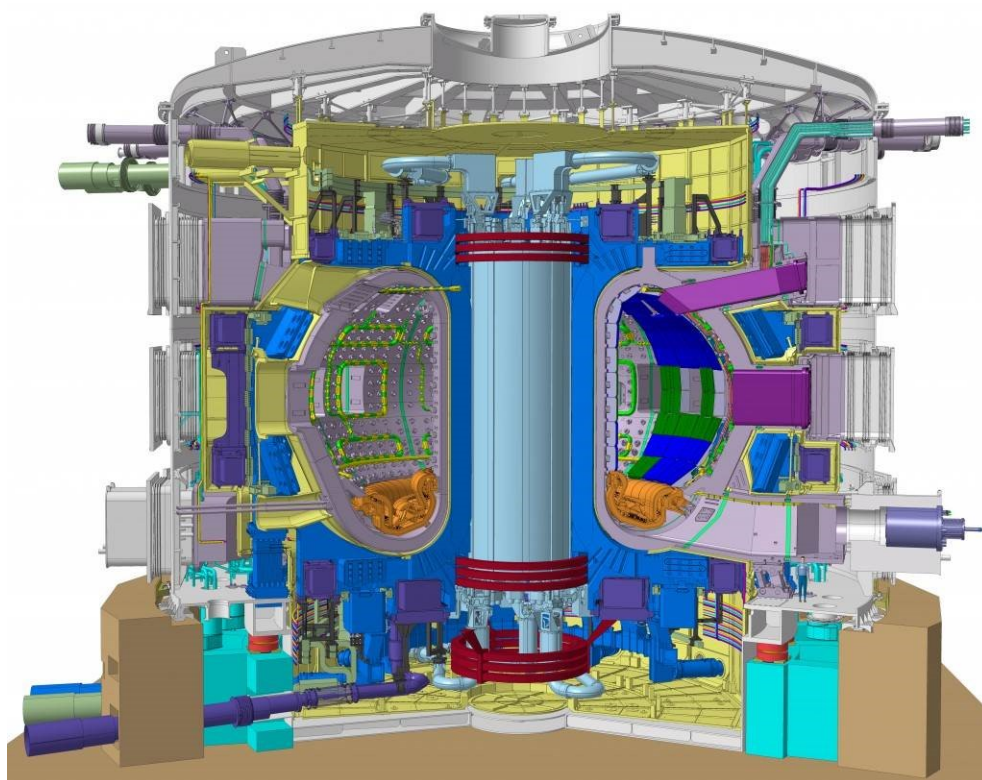
Figure 1. *International **T**hermonuclear **E**xperimental **R**eactor fusion reactor - a cutaway view. Taken from* [10].

2.2. Materials requirements and the role of tungsten

A perspective of nuclear fusion as a clean, abundant source of energy for the "near future" in reality represents one of the greatest scientific, technical and industrial challenges. Materials science takes a central role in the fusion development, with a difficult task of selecting and delivering material options

capable to endure a harsh and extreme environment of a commercial fusion reactor. Compatibility between the fusion plasma and the surrounding materials needs to be established for the construction of future devices and for satisfying performance requirements. Thus, the development of suitable plasma facing components is one of the key issues [14]–[16] as they are, regardless of the tokamak size, reactor parts exposed to high heat and particle fluxes coming from the plasma. The main aim for these most unprotected areas in a reactor is to develop materials which are heat-resistant, thermally conductive, resistant to physical and chemical erosion and show low fuel retention [14]. Furthermore, all of these properties need to be maintained over long-term operational time, so the ideal materials need to be able to meet the design life of 20 years under severe operating conditions.

One of the most critical requirements for plasma facing and structural materials is to be, as much as possible, resistant against radiation damage. Irradiated materials might undergo dramatic modification of mechanical properties, in addition to becoming radioactive through transmutation. Radiation generates lattice defects and produces He bubble, which leads to swelling and embrittlement of the materials. The fast, highly energetic 14MeV neutrons produced in the fusion reaction are not restricted by the magnetic field and can easily penetrate the walls and will cause severe damage on atomic level to different reactor parts. Through collision cascades displacement of atoms from their lattice sites occur, which is also used as a measure for radiation damage. One dpa (displacement per atom) means that on average each atom was displaced one time from its lattice site. Consequently, it is of utmost importance to gain a comprehensive understanding of the impact of the high flux of 14MeV neutrons and their interaction with matter. As such a fusion - relevant neutron spectrum currently does not exist, a very important milestone in the fusion program on a roadmap to DEMO is the development of the International Fusion Materials Irradiation Facility (IFMIF) [17]–[19]. It will be a large-scale irradiation and testing laboratory where candidate materials will be tested in conditions similar to those found in a fusion reactor. The necessary fast neutrons will be generated by hitting a lithium liquid target with accelerated deuterium beams.

The selection of materials to be used for the first wall has to be made very carefully, so that neutron activated radioactivity is kept at minimum and no long-living radioisotopes are produced. Hence, the starting criteria for all the materials in a reactor core is the requirement of low activation, meaning that all the materials should be suitable for recycling and disposal in non-active landfills one hundred years after removal from the reactor [20]. Figure 2 shows the radioactivity of different elements after exposure to neutron irradiation as a function of the time [21]. The horizontal line is the so called "hands-on-level" which should be reached after a minimum of time to keep the storing time as low as possible. As clearly seen, the use of certain elements such as molybdenum, aluminium, niobium, nickel and cobalt should be prevented even as alloying elements in low concentrations. Thus, engineering materials proposed to be used for fusion applications are limited to C, Si, Fe, Mn, V, Cr, W, Be and Ta. Low activation criteria coupled with the requirement of a relatively high toughness, high creep strength and chemical compatibility leads to the choice of the following reduced activation structural materials [22]–[24]:

- Reduced activation ferritic/martensitic steels
- Oxide dispersion strengthened steels

Introduction

- Tungsten-based materials
- Vanadium alloys
- SiC/SiC ceramic composites
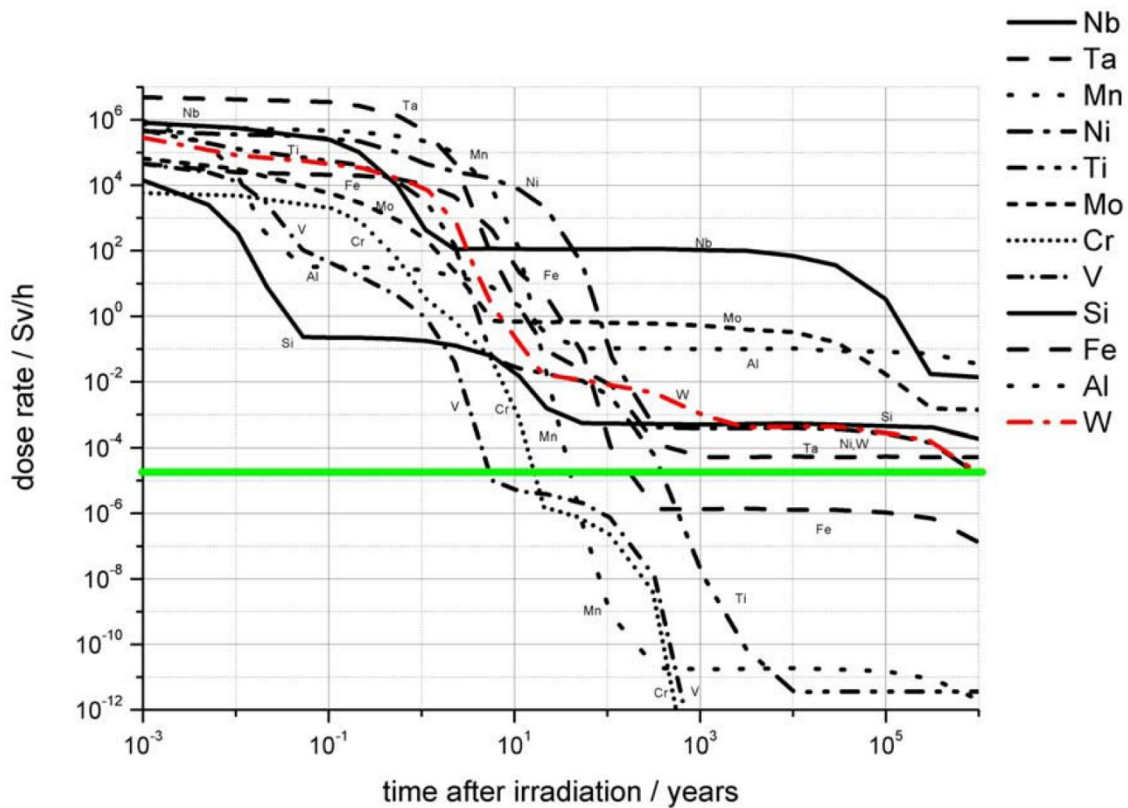
Figure 2. *Induced radioactivity of selected elements as a function time after exposure to a neutron fluence of 12.5MWy/m². W is highlighted in red, while the green line depicts hands-on level. Data taken from* [21].

Furthermore, in order to be able to deal with high heat and neutron fluxes, apart from low activation, an ideal material should also be light enough (low Z) to minimize pollution of the plasma core, non-reactive with plasma species, an excellent thermal conductor, resistant to thermal shocks and resistant to erosion processes. Reality is that such a material does not exist. The majority of currently available machines operate with PFCs made of beryllium or carbon, however, these are not acceptable for reactor class devices. In the case of ITER, a combination of three different materials was introduced into design [25]–[27]. The largest part of the first wall will be covered with the low-Z element beryllium due to its good plasma compatibility [9], while tungsten and carbon will be used for the divertor [28], [29]. The selection of these three materials should allow obtaining optimal parameters for ITER operation. However, thinking of the next step, the requirements of electricity generation and tritium self-sufficiency in DEMO lead to a significant challenge in the selection of materials. Scaling up in the size of new reactors inevitably increases operation temperature, fusion power, irradiation dose and helium levels, which implies that the irradiation induced changes in the material will become the central problem [30]. What is known with certainty is that the materials will have to cope with a tougher ambient for a longer

time. However, the capability to reliably predict the behaviour of divertor in the future devices, is lacking due to a very unique environment, where a knowledge of true materials performance is still uncertain. Overcoming these difficulties will be the key to a successful power plant and it remains to be seen whether new, advanced materials with enhanced properties can be delivered in time for a next generation fusion reactor.

Tungsten and tungsten-based materials have been recognized as leading candidates for the divertor and plasma facing components with extensive R&D activities currently ongoing which are investigating a wide range of tungsten fusion relevant issues and topics [31], [32]. A unique suitability of this metal for the harsh fusion application is due to its excellent high-temperature properties. Apart from having the highest melting point of all metals (3422°C [33]) the following beneficial properties defined its valuable status in nuclear engineering: a good thermal conductivity, low coefficient of thermal expansion, high creep resistance, high-temperature strength, good thermal shock resistance, low vapour pressure, a high threshold energy for physical sputtering, hence the low sputtering yield, low tritium/deuterium retention and a low hydrogen solubility [34], [35]. Furthermore, tungsten was listed together with titanium, vanadium and chromium as low induced activation material [36], which is as previously mentioned, a key point in materials selection. For all of the outlined reasons, tungsten has taken a fundamental role as the baseline material for the state-of-the-art plasma-facing component technology [37].

However, several issues and risks are associated with the use of tungsten. As it is a metal with a body-centred cubic (bcc) crystal structure, it is inherently brittle material at low temperatures coupled with a relatively high DBTT, even in an unirradiated state. Furthermore, it is characterized by low ductility, poor fracture toughness, low machinability and fabricability [34]. The existence of DBTT well above room temperature (RT) can cause serious operational problems - any thermal damage induced during high heat loading on the material might lead to immediate failure of the component in the cooling down phase. Recrystallization is one of the most important processes that has to be kept in mind, as it is the process accompanied by substantial microstructural changes and therefore could increase brittleness. Thus, the use of W at very high temperatures (above recrystallization temperature) is strictly prohibited due to the safety issues related to deterioration of mechanical properties [38], [39]. Further drawbacks of tungsten are related to high embrittlement due to irradiation at low temperatures and increase of DBTT with an increase of radiation level. However, further investigations are necessary so that a complete understanding of interconnections between ductility, fracture and irradiation can be obtained.

As a final remark, it is outlined that the useful operational temperature limit of tungsten and tungsten-based materials is determined by two restricting limits - the lower one is defined by the DBTT (coupled with the radiation embrittlement) and the higher bound is given by the recrystallization temperature [24], [40]. Outlined drawbacks of tungsten are being addressed through various areas of research with the intention of making W more reliable for future fusion devices and explore the possibilities of expanding the operating temperature window by enhancement of its properties.

2.3. Fracture behaviour of tungsten

Despite having a central role in an extensive research on different divertor concepts and being the prime material candidate for the first wall of a reactor, there still remains a significant challenge in the structural application of different tungsten-based materials. The aforementioned poor fracture toughness and low ductility at room temperature, coupled with a high DBTT cause serious restrictions in both its performance in demanding applications and its workability. Thus, it is essential to address these issues and investigate different toughening strategies, which could lead to the necessary improvement of these properties. A complete description of the fracture behaviour of tungsten is a natural first step in tacking the brittleness problem. However, giving a simple overview of its crack resistance is not an easy task and despite decades of scientific research, a full understanding of all the underlying processes has not been completely realized.

Comprehensive descriptions of fracture processes in tungsten single crystals were obtained through an extensive study performed in the nineties [41], [42], revealing that the {100} planes are primary occurring cleavage planes with <110> being the preferred crack propagation direction. {110} planes are designated as secondary cleavage planes, with the same <110> dominant direction. Apart from investigating the effect of the crystallographic orientation on the critical stress intensity factor, determining the influence of other parameters, such as temperature and loading rate, was of great interest [43], [44]. The obtained results of fracture toughness, K_{IC}, for the tests performed at liquid nitrogen, were 2.4MPa(m)$^{1/2}$ and 2.8MPa(m)$^{1/2}$ for the {100}<110> and {110}<110> crack systems, respectively. The temperature dependence is seen through a pronounced increase of K_{IC} already at room temperature, with the toughness values of 6.4MPa(m)$^{1/2}$ ({100}<110> system) and 12.9MPa(m)$^{1/2}$ ({110}<110> system), which is related to increased crack tip plasticity in the semi-brittle regime. Furthermore, the strong dependence of the DBTT and fracture toughness on the loading rate [45] is an indication that the dislocation availability and/or mobility at the crack tip is controlling the transition process. The Arrhenius relationship of the strain rate and the activation energy for the double-kink formation on screw dislocations, suggests that their motion controls the DBTT [45], [46].

In contrast to the good description of fracture processes in single crystals, the complete understanding of fracture properties of tungsten materials with more complex microstructures i.e. industrially produced polycrystalline W is still not fully obtained. The difficulty associated with discussing the material properties of W is the fact that the resulting fracture toughness and occurring failure mode is tremendously influenced and controlled by many different parameters. Temperature is one of the main factors with the influence seen through the occurrence of aforementioned DBTT - there is a transition region from a brittle fracture at low temperatures to a ductile and tough behaviour at high temperatures. A similar transition temperature is commonly observed in most bcc metals. The problem with tungsten is that the transition temperature is relatively high (well above ambient temperatures for typical bulk materials), additionally complicating the machining at low temperatures. Besides, the DBTT is not a simple material constant i.e. a general value cannot be given, as it strongly depends on the microstructure, testing direction, strain rate and the type of mechanical test [45], [47], [48]. Thus, relating different experimental results is not that straightforward and moreover, as the DBTT can be defined in

many different ways, care needs to be taken when making comparisons even for the same material. Apart from the influence of the testing temperature, the underlying microstructure of tungsten materials has a tremendous influence on its crack resistance. The characteristic structure of the grains is established through several deformation steps, during the production of the different grades of materials, like rods, sheets and wires. It has been shown that there is a strong correlation between manufacturing history (sintering, rolling, swaging, hot/cold work...) and the resulting material's microstructure and mechanical properties [49]. The most important microstructural features that affect the fracture toughness and play a decisive role in the resulting failure mode are grain size, grain shape and texture, which quite often also lead to the anisotropic fracture behaviour of the deformed tungsten materials [50], [51].

Identifying tungsten as the main plasma facing material in fusion reactors, increased in recent years the amount of research activities which address the low temperature brittleness issue and the work on enhancing the mechanical properties of different tungsten materials. Determining a way of decreasing the DBTT and increasing ductility and fracture toughness is the crucial milestone in fusion research, as the improved properties will significantly impact the manufacturing and variety of applications of tungsten. So, what are the ways of obtaining a tougher tungsten and improving its ductility? Since fracture properties of tungsten are strongly dependent on a wide range of parameters, different ductilization strategies have been proposed in the attempt of enhancing its fracture performance [31], [32], [52]. The current research is primarily focused on the main three approaches being i) alloying to promote solid solutions, ii) microstructural design by nanostructuring and iii) synthesis of various composite materials. The following paragraphs will give a brief overview of the outlined methods.

Alloying is by far the most explored and well-known approach for improving the ductility of tungsten, with initial studies going back to the mid-50s and the work of Geach and Jaffe [53], [54]. At first, the research was mainly focused on the investigation of the influence of Re additions to W materials [55], [56], the only element known that undoubtedly improves the fracture properties of W. Since then, an extensive research has been carried out [50], [57]–[59] investigating different alloying elements [60]–[63], as well as performing various calculations and simulations [64]–[66]. A comprehensive overview of capabilities of alloying and associated limitations is given in Publication F, particularly focusing on the discussion of tungsten alloys which fulfil the low activation requirement, hence the feasibility of application in future fusion reactors is addressed. Summarizing the relevant findings, it can be concluded that the ductility and toughness of tungsten can be significantly enhanced by formation of solid solution when adding Re, since many experimental results show e.g. improved toughness and lower DBTT. Based on computational results, the explanation of the so-called „rhenium effect" is attributed to the modification of the core symmetry of screw dislocation, the reduction of the Peierls stress and the increase of the number of slip planes [66]. However, despite the big technological and industrial relevance of the rhenium ductilizing effect, its use is limited by the fact that rhenium is a rare element and therefore, very expensive. When thinking of a fusion application, tungsten alloying with rhenium has been ruled out due to neutron activation issues, cost, reduced thermal conductivity and radiation induced intermetallic phases leading to changes in materials properties [64], [67]. Research effort has also been directed towards investigation of other possible alloying candidates, which might

have a similar effect as rhenium in tungsten toughening. However, up until now, there was very little experimental evidence that has demonstrated positive influence of other elements, although more detailed studies should be conducted before definite conclusions can be made. In addition, it should be emphasized that the majority of the reported studies over past decades were performed on different materials processed by different production techniques. Hence, microstructures and purity levels differ and it is very challenging to make a comparison between available datasets and to judge the exact influence of a single alloying element on a particular materials property. In Publication E, an alternative approach of studying the effect of different alloying elements and their concentrations on the properties of W thin films is explored. The possibility of a high-throughput investigation of binary tungsten alloys systems is achieved by magnetron sputter co-deposition techniques.

The second strategy relies on the microstructural design approach enabling alternation of the microstructure to the ultrafine grain size through various methods of severe plastic deformation such as equal channel angular pressing (ECAP) [68], high pressure torsion (HPT) [63] or heavy rolling [69]. In such a way, a deformation induced grain refinement can lead to the development of a beneficial UFG microstructure of tungsten having enhanced both strength and ductility. A strong sensitivity of mechanical properties to the deformed microstructure is seen through a general correlation between an increase in the amount of thermomechanical deformation and a decrease of grain size, resulting in a reduction of the DBTT and improved fracture toughness. Rolling of tungsten plates below the recrystallization temperature results in a pancake-shaped layered microstructure elongated in the rolling direction, which is favourable for good toughness in two out of three principal loading directions and with the decrease in thickness, the DBTT is shifted to lower temperatures [70]. Taking a step forward and going to even more refined material - tungsten foil, it can be seen that the ultrafine grained elongated microstructure leads to some extraordinary mechanical properties. Such a material behaves ductile in a tensile experiment at RT [71], reaching a maximum of 4 to 7% elongation strain [69]. However, a systematic study and thorough fracture mechanical investigation of ultrafine grained tungsten foils are still lacking. It is clear that the underlying microstructure established during the production has a tremendous influence on the resulting properties, but it is also very important to determine the exact influence of different microstructural features. Publications A and B are tackling the mentioned issues with a focus on providing answers to the following questions: How do fracture properties change if tungsten plate material is submitted to even higher degrees of rolling (deformation) resulting in commercially available 100μm thin tungsten foil? Are the values of fracture toughness higher in comparison to other tungsten materials? What happens to the DBTT in case of such highly deformed foils?

Development of various tungsten composite materials has been proposed and investigated as another approach to ductilize tungsten. Among several different composite types, very promising results are seen in the research regarding laminated and fibre reinforced composites, where the principal structural reinforcement components are in the form of polycrystalline tungsten foils and wires, respectively. Tungsten laminates synthesized by assembling multilayers of ultrafine grained tungsten foils [72] are an approach towards expanding advantageous mechanical properties of the foils to a ductile bulk tungsten materials. Charpy impact test results of the laminated plates show a significant

increase in impact energy and a reduction of the DBTT by 300°C [73]. In some He-cooled divertor concepts being currently investigated, the use of structural, pressurized W cooling pipes will be used, which will be exposed to 600°C and 100bar [74]. Typical manufacturing processes like extrusion or drilling of holes in rods are challenging and additionally, in this way, the alignment of elongated grains i.e. the preferred crack propagation path would be coinciding with the expected fracture direction of the pressurized pipe, which has to be avoided. Therefore, the option of synthesizing the structural tungsten pipe by rolling up and joining of tungsten foils seems to be very promising, since the best case scenario of microstructural design, where the direction of low fracture toughness follows the contour of the pipe, can be obtained.

Tungsten fibre-reinforced composites (W$_f$/W) are extensively investigated as a second very promising composite option for ductilization of tungsten [75]. This composite structure is obtained by embedding commercially available drawn tungsten wires in a tungsten matrix which is produced either by powder metallurgy [76] or by a chemical deposition process [77]. The advantage of W$_f$/W is in its pseudo ductile behaviour and thereby increased toughness as a consequence of extrinsic toughening mechanism such as crack bridging by intact fibres, fibre pull-out, crack deflection and ductile deformation of fibres [78]. In such a way, the brittleness of W can be mitigated, making W$_f$/W composite a feasible PFC alternative. The drawn tungsten wires used as reinforcements are the key components which determine the structural integrity of W$_f$/W composite. This sets the requirement of exceptional properties and brings an interest in studying them. Crack resistance properties of the wires at moderate temperatures and a complete understanding of the underlying micromechanisms controlling the fracture process is of fundamental importance for the composite development. The study presented in Publications C and D evaluated the fracture toughness of the wires with a special focus on recrystallization phenomena, embrittlement by annealing and interconnection between different microstructural features and resulting mechanical properties. As a last comment regarding the toughness enhancement of tungsten by composite development, it should be noted that despite very optimistic results, a common drawback of these materials is that the scaling up of the production processes to industrial size is not a trivial task and is still very distant from current state of the research.

Finally, a common goal of all the different ductilization strategies is the preservation of the advantageous properties at elevated temperatures i.e. recrystallization temperature needs to be precisely determined, as well as the resulting degree of property degradation. Part of the work within this thesis is also related to the investigation of the recrystallization phenomena, with a focus on the stabilization of the beneficial, ultrafine grained microstructure - the most important controlling factor in overall fracture behaviour of tungsten.

3

Summary of the results

In this summary chapter the most important results of the thesis are outlined, alongside with the discussion of the significance of the findings for the application of tungsten materials in fusion research. According to the type of the investigated materials, the section is divided into three parts: UFG tungsten foils, drawn tungsten wires and thin film tungsten alloys. In each part, the main conclusions of published results (Publications A - F) are summarized, together with unpublished work, which is relevant for giving a comprehensive overview of the problems/answers addressed within the thesis.

3.1. UFG tungsten foils

The first part of the work is devoted to the fracture mechanical assessment of ultrafine grained tungsten foils. The materials of interest are commercially available 99.97wt.% pure tungsten and potassium (0.005 wt.%) doped tungsten (WVM) foils with a thickness of 100μm. To obtain such a small dimension of the foil, a tungsten plate is submitted to a very high degree of deformation during the rolling process, which has a crucial impact on the resulting beneficial microstructure. Thus, the selection of this foil thickness enables investigating a correlation between deformation induced grain refinement to the ultrafine grained region and resulting superior fracture properties of the foils.

An overview of the foil microstructure is given in Figure 3a, where orientation maps acquired in three principal directions of a rolled plate (RD - along longitudinal, rolling direction, TD - perpendicular to and in plane with the rolling direction and SD - short transverse direction) are projected on a cuboid. As it can be perceived the long, very thin grains are elongated in the direction of rolling, forming a characteristic pancake-like microstructure. Furthermore, the investigated foil has a pronounced rotated-cube crystallographic texture, which is commonly observed in bcc metals [79], with a most dominant {001} <110> orientation, giving in addition to the anisotropic microstructure, orientation dependent mechanical properties.

Due to the size and thickness restrictions of the foil, specimen dimensions required by the ASTM standard [80] could not be achieved. Thus, at the initial stage of the investigation, designing a suitable experimental set-up and optimizing sample preparation procedure was required. Specifications and all the details regarding the specimen fabrication, crack initiation and brazing process are outlined in Publication A. In all the experiments, single-edge notched tension (SENT) specimens were fabricated,

with a specimen size of 20x5x0.1mm^3. Notches introduced by a diamond wire saw were further sharpened by a razor blade polishing, while the final sharp pre-crack was introduced by a FIB.

The main focus of the presented study was to investigate the fracture behaviour of the foils and variation of the properties in respect to two key parameters: testing temperature and testing direction. Thus, in order to elucidate the influence of the first parameter all of the tests were performed in the temperature range from -196°C to 800°C. For the analysis of the influence of the orientation of the microstructure on the anisotropy of fracture properties, samples were taken with three different orientations of the pre-crack in respect to the rolling direction: parallel to the RD (T-L system), perpendicular to the RD (L-T system) and with 45° angle (45° system) as depicted in Figure 3b. The two letter crack plane orientation nomenclature is according to the ASTM standard, with the first letter designating the direction normal to the crack plane and the second letter the expected direction of the crack propagation.
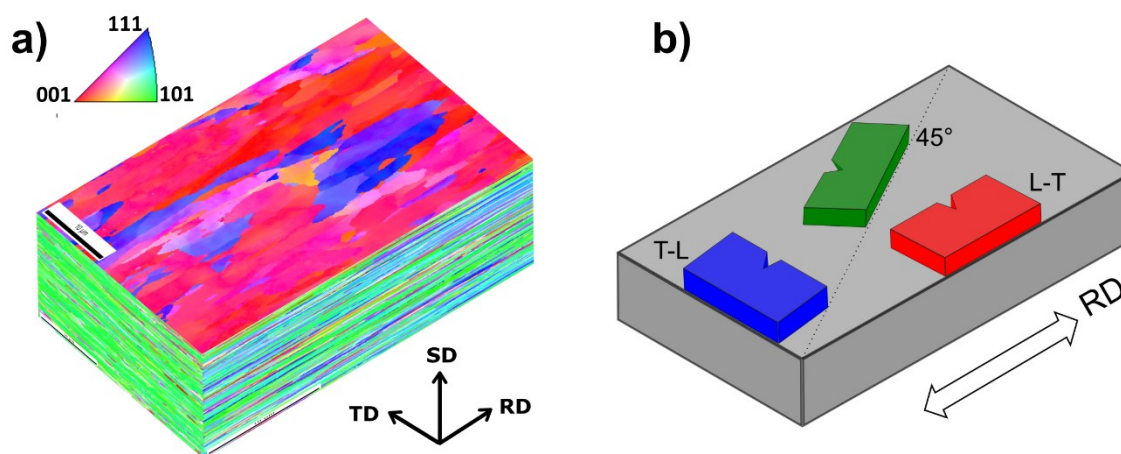
Figure 3. a) Inverse Pole Figures (IPF) of pure 0.1mm tungsten foil in as-received condition in three principal directions of a rolled plate: RD, TD and SD. EBSD maps are projected on a cuboid to better visualize the pancake-like microstructure, with thin, elongated grains along the rolling direction. Colour coded unit triangle representing <100>, <110> and <111> crystallographic directions perpendicular to the sample surface. b) An illustration of the orientation of different SENT specimen types.

3.1.1. Influence of the testing temperature

The results obtained in fracture experiments are displayed in Figure 4, where the conditional fracture toughness, Kq, is plotted as a function of testing temperature, T, for different testing directions. A comparison is made between pure and doped foil with the associated values also shown in Table 1. For both material types, a similar trend is seen, where the lowest K_q are obtained for experiments performed in liquid nitrogen. With the increase in testing temperature, as expected, values of fracture toughness increase up until room temperature or 200°C, after which an apparent decrease is observed. In all the cases, the standard method given by the ASTM procedure [80] was used for evaluation of the conditional fracture toughness, where the application of linear elastic fracture mechanics (LEFM)

assumes that certain geometry and sample size criteria are met. However, due to the sample size restrictions of the foil, the majority of the results do not meet all the validity requirements, especially regarding thickness, so that the plane strain conditions are not fulfilled. For a comprehensive discussion and details regarding limits of validity and necessary criteria, the reader is referred to Publication B. Furthermore, regardless of the size requirements, in the regime of increased ductility occurring at higher temperatures LEFM loses validity. Thus, the obtained values of conditional fracture toughness are underestimations, which is indicated by small arrows next to the data points and above RT an increase in fracture toughness is to be assumed.
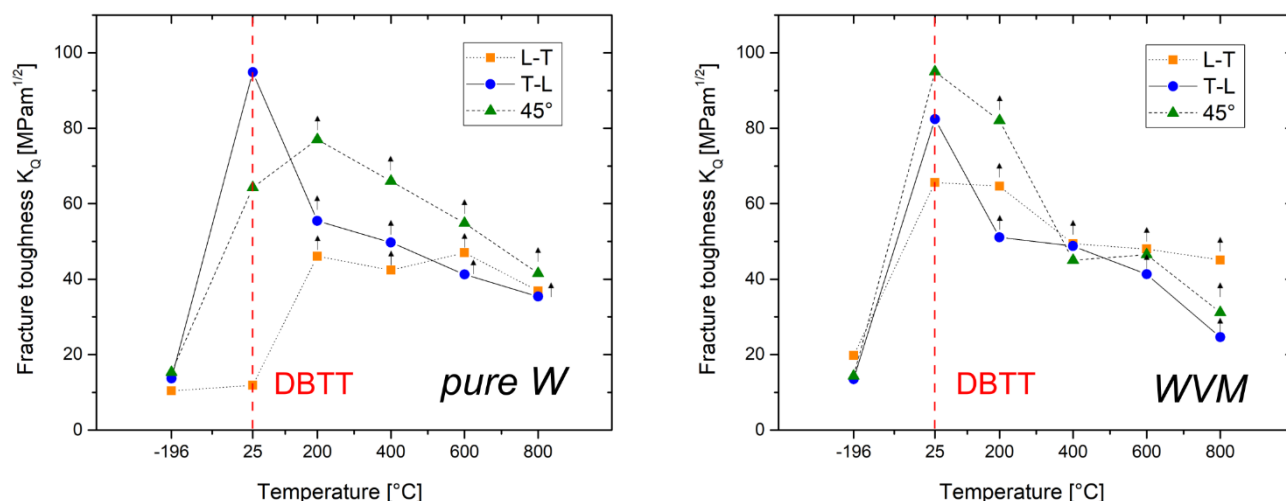
Figure 4. *Fracture toughness K_q of the 100µm thin pure and potassium doped tungsten foils as a function of testing temperature for three different specimen orientations. Test were done in air at -196°C, room temperature and 200°C, while a vacuum chamber was used for the experiments at elevated temperatures. All the specimens were tested in crosshead displacement control at 0.4mm/min.*

Table 1. *K_q values of 100µm thin pure and potassium doped tungsten foils tested in the temperature range from -196°C to 800°C; the values for different loading geometries are compared.*

Temperature[°C]	Fracture toughness [MPa(m)$^{1/2}$]					
	L-T system		T-L system		45° system	
	W	WVM	W	WVM	W	WVM
-196	10.4	19.8	13.7	13.5	15.4	14.3
RT	11.9	65.7	94.8	82.4	64.3	95.0
200	46.1	64.7	55.5	51.1	77.0	82.1
400	42.4	49.4	49.8	48.8	66.7	45.0
600	47.0	48.0	41.2	41.3	54.8	46.5
800	36.9	45.1	37.9	24.6	41.6	31.2

Summary of the results

The performed fracture investigations indicate a superior behaviour of thin tungsten foils and extraordinarily high values of fracture toughness. For the sake of comparison, it is noted that the 200°C fracture toughness of a pure sintered tungsten material was measured as $6.1\text{MPa(m)}^{1/2}$ [50], which is even smaller than the lowest obtained K_q at cryogen temperatures. Particularly high values of fracture toughness indicate a positive impact of deformation induced grain refinement, which is an efficient strengthening mechanisms, but usually leads to a loss in ductility, brittle behaviour and poor toughness [81]. However, the tested 100µm tungsten foil is an example where an extraordinary combination of increased strength and high fracture resistance can be achieved. The key reason for these exceptional mechanical properties lies within the development of a beneficial microstructure of thin elongated grains.

Most interesting is the result of the foil tested at room temperature where a large scatter of data has been observed. In Publication A, the example of the L-T system is outlined, where a variation of K_q goes from about $12\text{MPa(m)}^{1/2}$ to incredible $106\text{MPa(m)}^{1/2}$. Such a spread of data is in good accordance with the fracture surface observations, demonstrating that this is the temperature region where brittle to ductile transition takes place, for this crack front orientation. The fact that for ultrafine grained tungsten foil this distinctive transition occurs at ambient temperatures represent an incredible result for tungsten materials. A clearly defined DBTT cannot be given for W, as it strongly depends on various parameters (microstructure, testing method, strain rate etc.); however, it is very pronounced for both single and polycrystalline materials and can vary for several hundred °C. To give an example, Charpy impact test results of 3mm tungsten plates, for the T-L orientation of the samples, indicate that DBTT occurs at 500°C [82].

The final remark is related to the level of underestimation of the calculated fracture toughness in the region of elevated temperatures. The expected increase of fracture toughness with temperature, associated with an increase in crack tip plasticity, is not reflected by the LEFM estimated fracture toughness values. Since high temperature results are associated with increased ductility of the tungsten foil, LEFM becomes invalid. However, the extent of blunting of the crack tip before the crack starts to propagate can be measured through the critical crack tip opening displacement (CTOD) parameter which enables the determination of more accurate values of fracture toughness, K_{CTOD}, in the region of increased ductility. In order to measure the CTOD parameter, the depth information from the SEM fractographs is reconstructed by stereophotogrammetric methods [83], [84]. The obtained anaglyph pictures are further processed with an automatic image system which allows the generation of digital elevation models (DEM) of the investigated surfaces. The obtained 3D information is used to retrieve the microscopic topography of the fracture surfaces, from which the degree of local plastic deformation can be calculated. An example of the procedure is presented for the 45° system sample tested at 800°C (Figure 5), where the lower band value of K_q yields $41.6\text{MPa(m)}^{1/2}$. Using an automatic fracture surface analysis system, the 3D models of fracture surfaces were calculated from which an average value of the CTOD of 54.6 ± 3.5µm was determined, with relating average fracture toughness of $115.9\pm3.7\text{MPa(m)}^{1/2}$. A difference of K_{CTOD} and K_q by nearly a factor of three emphasizes the importance of determining a more accurate value of fracture toughness in the elastic-plastic regime.
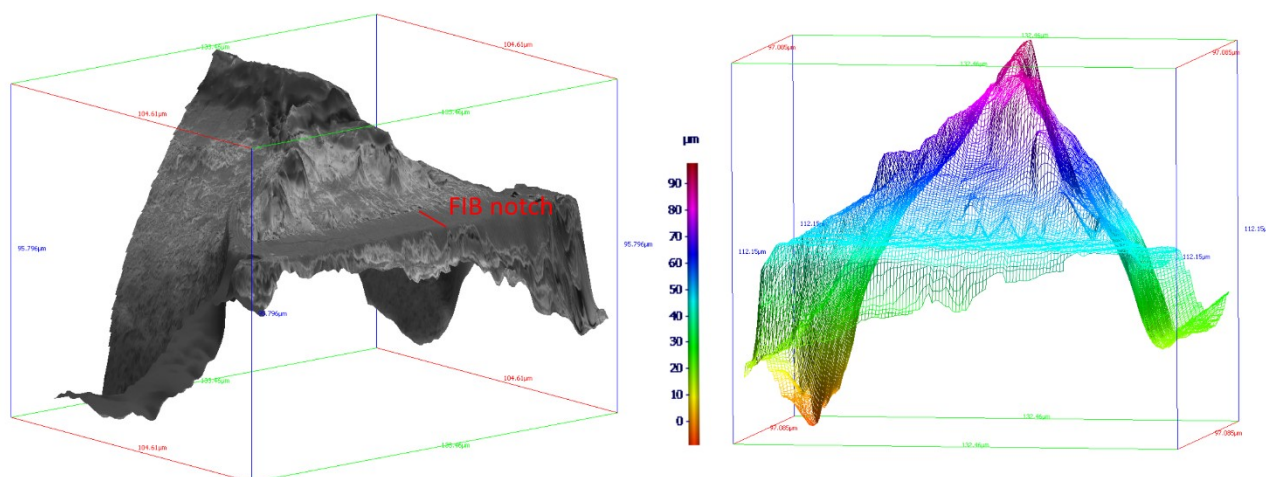
Figure 5. *An example of the CTOD determination procedure of a 45°system sample tested at 800°C. Digital elevation models (DEM) representing a 3D topography reconstruction of the two fractured halves, represented in optical image and pseudocolour view. The viewing direction is along the crack propagation direction with the blue "mountain" showing the plastically deformed ligament. Colour code indicates height in µm.*

3.1.2. Influence of the microstructure

A microstructural influence on the resulting anisotropic fracture toughness is demonstrated by a comparison of the obtained values of K_q of all three tested systems. For both pure and doped tungsten foil, samples orientated at 45° show highest fracture toughness for nearly all testing temperatures. The observed variation of the fracture toughness values within different systems can be attributed to two aspects of the elongated microstructure: a) strong <110> rotated cubic texture and b) the grain shape anisotropy along the rolling direction. The crack orientation dependence is related to the spatial distribution of weak sites for fracture initiated propagation such as cleavage planes and boundaries of elongated grains. The tendency of the samples with a crack at 45° in respect to RD towards higher values of fracture toughness might be attributed to the texture of the foil, which allows the main slip direction of bcc metals, the <111> direction, to be congruent to the maximum shear stress. Fracture properties of samples with crack propagating perpendicular and parallel to the RD are in similar range. A small variance in fracture toughness of L-T and T-L systems is related to the difference in the amount of grain boundaries appearing in the crack propagation direction. The grain shape and orientation effect might not be as influential when the failure is in the ductile regime or when it fails completely brittle, as the fracture toughness anisotropy is less pronounced at these temperatures. The difference in material response could also be attributed to the geometrical arrangement of areas with low and high fracture toughness with respect to the crack system. Anisotropic distribution can be a result of different contributions from the grain boundary toughness, K^{gb} and toughness of the grains, K^{grains}.

Alongside with studying the origin of the high fracture toughness and its dependence on the loading direction and testing temperature, it is very important to determine deformation characteristics and micromechanisms controlling the fracture process by analysing the obtained fractographs. Thus, SEM

investigations of the fracture surfaces were conducted, revealing distinctive behaviour for different testing temperature regimes with a very pronounce evolution of fracture modes in respect to an increase in testing temperature. Both pure and doped foils behave in a very similar manner and the observed anisotropy of the fracture toughness for three tested systems is not reflected in fractographic transition. Thus, not all fractographs for different temperatures and testing directions will be shown here and displayed examples correspond to the WVM foil tested in the T-L system. The results for low/intermediate and high testing temperatures are shown in Figures 6 and 7, respectively. For further SEM fracture images of a pure tungsten foil, the reader is referred to Publications A and B.

Figure 6. Fracture surface micrographs of the potassium doped tungsten foils tested in the low and intermediate temperature range, for the T-L crack orientation direction. A sample tested at -196°C shows a typical brittle, transcrystalline fracture, whereas for samples tested at RT and 200°C pronounced delaminations can be perceived. In some of the micrographs the FIB induced pre-crack is clearly visible on the left side.

Summary of the results

At liquid nitrogen temperature (-196°C), all the samples fracture in classical brittle, transcrystalline manner associated with the lowest values of fracture toughness. In the obtained fracture surfaces, aligned grains can be perceived as horizontal lines. At these temperatures, no significant plastic deformation within the pancake like grains takes place and the micromechanisms controlling the fracture toughness is a de-cohesion process by cleavage of the individual grains predominately along (100) crystallographic planes. Thus, the crack easily propagates in the designated crack growth direction yielding low K_Q values.

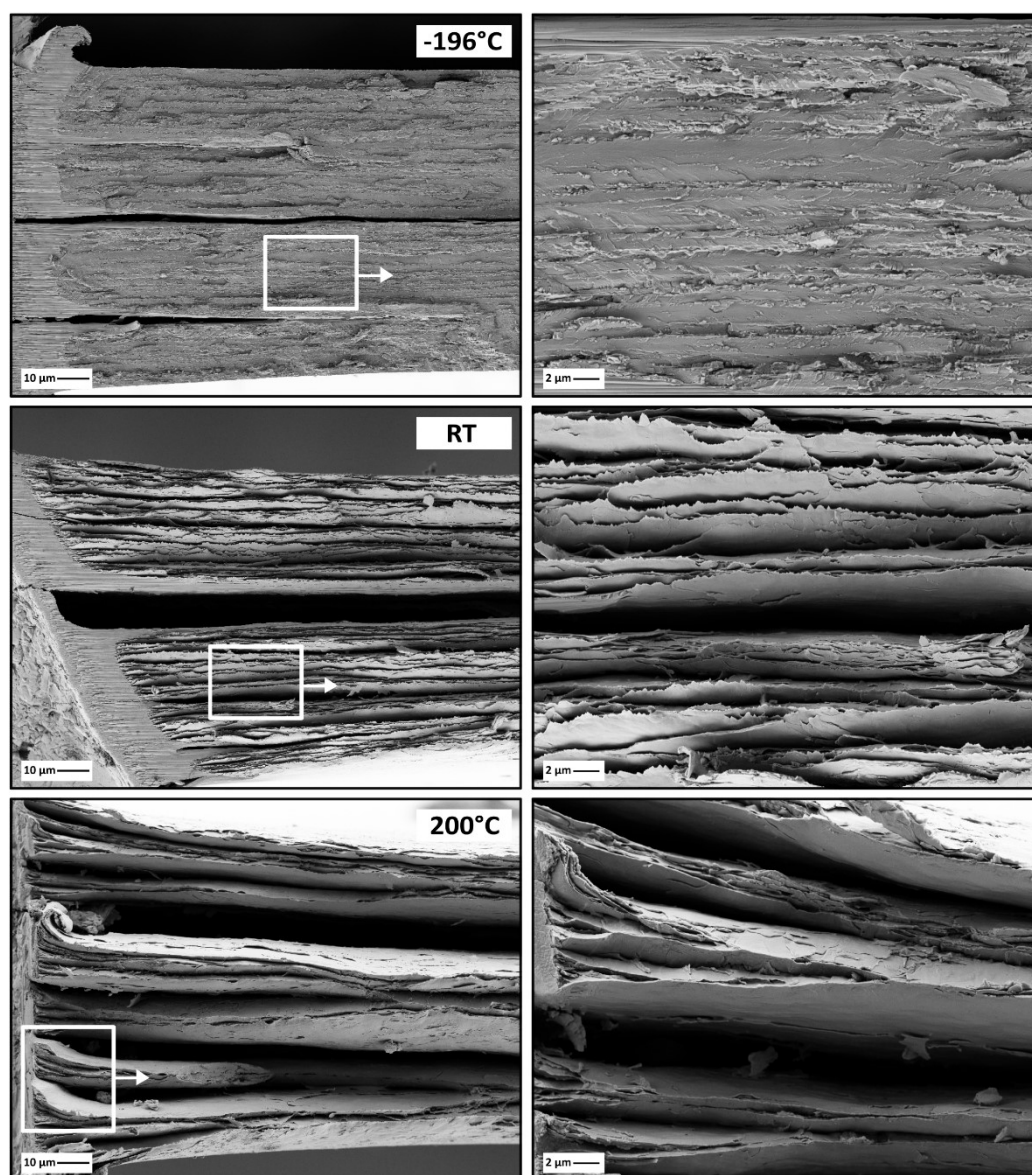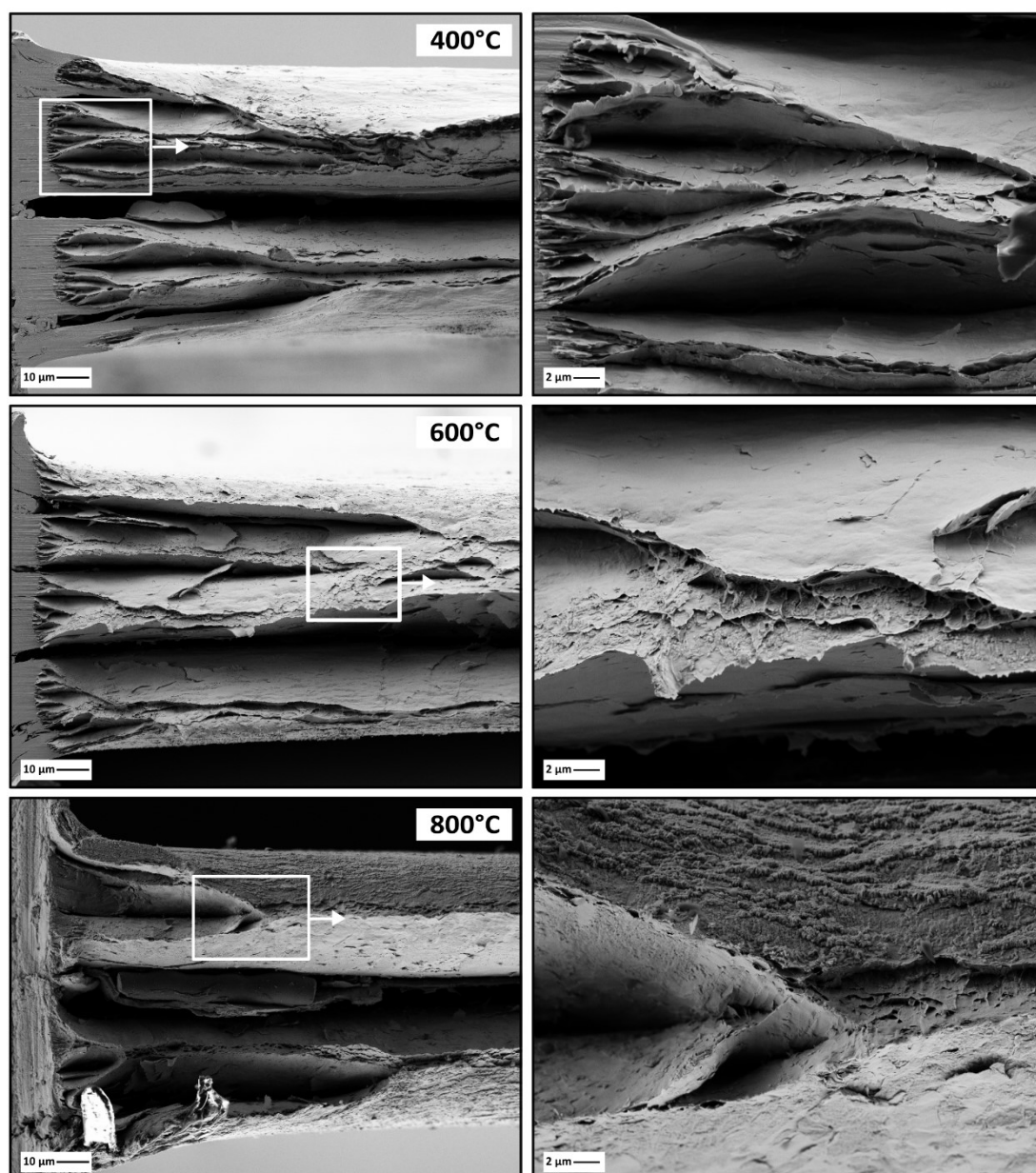**Figure 7.** *Fracture surface micrographs of the potassium doped tungsten foils tested in the high temperature range, for the T-L crack orientation direction. Increasing the temperature from 400°C to 800°C, surfaces evolve from a coarse delamination to a more ductile fracture.*

Summary of the results

In the intermediate temperature range (RT and 200°C) the situation differs significantly with fracture surfaces showing pronounced delamination along the foil plane, with a significant amount of small crack openings within the foil plane. Such a fan-out topography is a direct consequence of the characteristic microstructure and the weak adherence of the elongated grains. The anisotropy of the grain shape and the ability of the individual grains to deform plastically allow the delamination process to take place. Under the applied load, the delaminated grains are elongated and small openings are formed near the notch root. With further deformation small cracks propagate along the large sides of pancake-like grains, while the conjunct ligaments are further elongated and thinned out until the fracture takes place. With an increase in temperature to 200°C the delamination takes place somewhat less frequently followed by a larger crack opening. With a further increase of testing temperature, a transition of fracture surfaces continues towards a more ductile behaviour. The highest number of single lamellas is at room temperature and with increasing temperature this number decreases. Already at 400°C strong delamination is less pronounced with a significantly smaller amount of individual lamellae. From a microstructural point of view, conjunct grains in a form of thicker ligaments show increased plasticity and certain amount of necking, before they fail ductile.

Pronounced alignment and elongation of the microstructure in the principal deformation direction is the essential microstructural feature which controls the fracture process of the investigated foil. The observed enhanced fracture toughness and reduction of the DBTT for ultrafine grained tungsten foil can mostly be attributed to the mechanism of delamination toughening. This mechanism leads to the characteristic appearance because of the secondary microscopic crack systems propagating perpendicular to the primary crack growing plane. As a consequence of the formation of the microscopic delamination cracks, a sample is locally divided into many thin sheet ligaments which deform plastically in a nearly plane stress state. Following delamination, thin ligaments as the remaining areas between the delaminations will further stretch and eventually fail in a ductile manner. The origin of the micro-delamination is connected to weak crack planes of low fracture toughness parallel to the foil plane, so that the splitting between grain boundaries can easily occur. The introduction of delaminations leads to a drastic change in the stress state from plane strain to a plane stress dominated one (see schematic Figure B.9 in Publication B). Delaminations of the interfaces, which are perpendicular to the crack plane, relax the stress component in thickness direction, which further results in the reduction of tensile stress triaxiality. So, when delamination occurs, the effective thickness of the sample is reduced and at each ligament the σ_{zz} stress goes to nearly zero, reaching plane stress condition which will result in higher toughness. Consequently, the sample behaves like a stack of even thinner foils instead of one thick sample. So, the extend of fracture toughness is determined by the stress state at the crack tip and it increases with decreasing tensile stress triaxiality.

3.1.3. Influence of thermal treatments

As already outlined, the extraordinary ductile fracture behaviour of the analysed tungsten foil can directly be related to the beneficial ultrafine grained and nearly lamellar microstructure developed during the rolling process. Since fine grained materials are very sensitive to annealing and recrystallization phenomena, it is very important to look into the effect of heat treatments on the microstructural stability and determine whether this leads to deterioration of the obtained superior fracture properties.

To begin with, the influence of thermal treatments was investigated through detailed microstructural characterization consisting of the identification of changes of the grain shape and size, analyses of the grain boundaries and evolution of the developed texture. An overview of the microstructural changes is seen in Figure 8, where a comparison is made between EBSD orientation maps of pure tungsten foil in the as-received and different annealing states. Heat treatments were performed in vacuum at 1200°C, 1400°C and 1600°C, with a holding time of 1h. The shown IPF maps, as stated before, reveal that the material in the as-received condition has long, thin grains elongated in the rolling direction (with the shortest grain lengths parallel to SD) forming a characteristic pancake-like microstructure, with grains having a large aspect ratio. Heat treatments considerably affect the thin foil microstructure through a complete loss of elongated grain shape and onset of significant grain coarsening. The large, quasi-symmetric, globular μm sized grains are formed at about 1400°C for pure tungsten and in accordance to the shape alterations, aspect ratio is tremendously changed. Furthermore, simultaneously with grain growth during the heat treatments, the grain boundary area is tremendously reduced, consisting almost exclusively of high angle grain boundaries. In-depth discussion regarding different aspects of microstructural modifications, such as determination of grain size, the nature of grain boundaries and preferential orientation of the grains is given in Publication B.
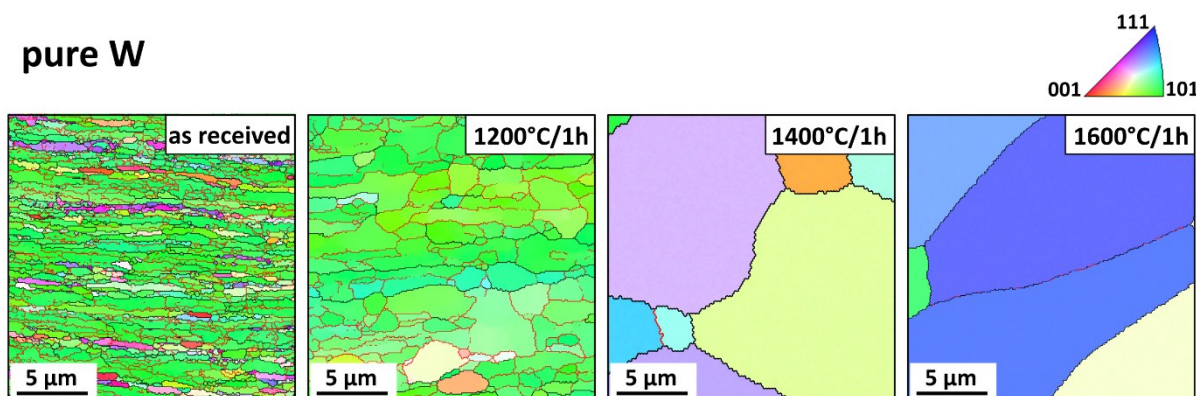
Figure 8. *Inverse Pole Figures (IPF) maps acquired along longitudinal, rolling direction of pure 0.1mm tungsten foil in the as-received and annealed conditions: 1200°C, 1400°C and 1600°C for 1h.*

The observed alternations of the grain structure of the UFG foil can be related to the processes of recovery and subsequent recrystallization of the material, which have an enormous effect on the resulting mechanical properties. Due to the high amount of stored energy in the material, which is present in the form of grain boundaries and dislocations, the microstructure will change upon thermal treatments. Recovery refers to changes in material's microstructure prior to recrystallization and it easily

occurs in worked materials having high concentration of defects. During this process, the stored energy of the material is lowered by e.g. the movement and arrangement of dislocations. In contrast to that, recrystallization involves the formation of new grains, which might be unevenly distributed over the specimen separating the microstructure into recrystallized and not recrystallized parts. New grains formed during recrystallization may have individual lattice orientation, which can be independent of the one resulting from the cold work during the manufacturing process. Thus, once a beneficial microstructure is obtained, it is crucial to stabilize it at elevated temperatures. In the case of pure tungsten, the heat treatment of 1400°C leads to full recrystallization and therefore this was the material condition which was chosen for looking into the effect of annealing on the fracture toughness.

The first impression of the impact of annealing on the resulting fracture behaviour can be seen in Figure 9, where fractographs of the foils in as-received and annealed condition are compared. Tests were done at 200°C and in the case of heat treated foil a decrease in fracture toughness from 46.5MPa(m)$^{1/2}$ to 38.6MPa(m)$^{1/2}$ is detected. The grain coarsening during annealing induces a significant reduction in yield stress, which permits the development of a plane stress dominated plastic zone, which then induces the relatively high fracture toughness despite the brittle appearance of the fracture. Comparing SEM fractographs of the two samples, a substantial transition in failure modes can be seen. Delamination only occurs for the foil in as-received state, while the annealed foil fails in a brittle, mixed fracture mode (trans and intercrystalline mode). A closer look on its fracture surface reveals that the specimen fails predominately by transgranular cleavage on significantly enlarged grains and only a small amount of intergranular fracture surfaces can be seen near the edges. This is an indication that for the annealed foil, the ductile-to-brittle transition temperature is shifted to significantly higher temperatures even for such thin foils (at least above 200°C). The beneficial elongated, fine grained microstructure leading to the improved fracture properties of the as-received tungsten foil should be preserved at higher temperatures and processes like grain growth and recrystallization should be avoided at all circumstances. For tungsten materials in fusion application it is very important to precisely know at what temperature recrystallization happens, as the material properties deteriorate and this sets the higher temperature operating limit [40].
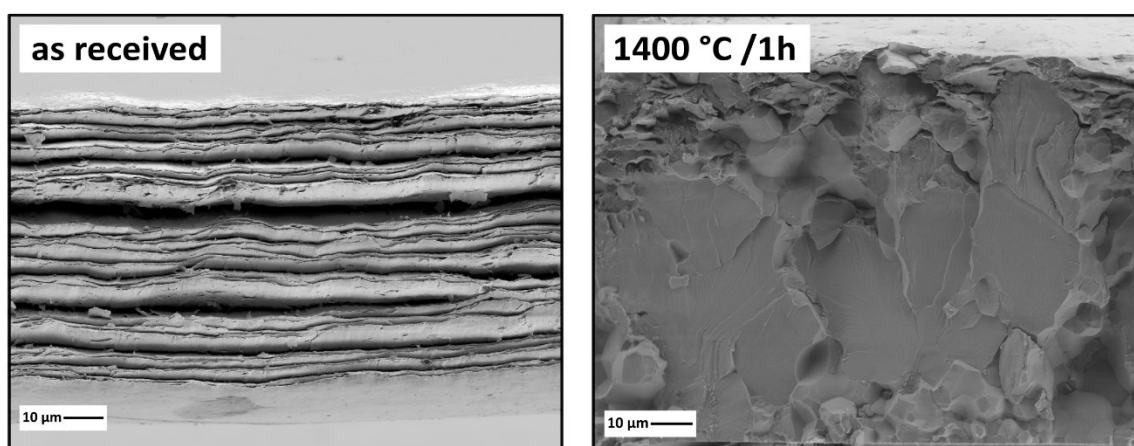

Figure 9. Comparison of fractured surfaces of the sample tested at 200°C for as-received foil showing strong delamination (left) and annealed foil failed by a mixed transgranular/intergranular failure mode (right).

Based on presented results regarding ultrafine grained tungsten foil, it can be concluded that a deformation induced grain refinement and a formation of beneficial microstructure of thin, elongated grains is a successful recipe for obtaining a tungsten material with exceptional fracture properties. Fracture toughness in ultrafine grained materials can be enhanced by the mechanism of delamination toughening which is mainly controlled by features of anisotropic microstructure: small grain size in SD direction, the elongated grain shape and the <110> rotated cube deformation texture. The effect of branching of the main crack along the weak boundary sites parallel to the longitudinal direction, is associated with a relaxation of the triaxial stress state towards a state of biaxial tension. As a final remark, it can be stated that the tungsten-related problems of poor fracture resistance at low temperatures and high DBTT can be overcome by a proper microstructural design, thus potentially extending the use of W as a structural component, making tungsten materials a very interesting option for nuclear fusion applications.

3.2. Drawn tungsten wires

The second major part of the work conducted within the thesis is devoted to the microstructural and mechanical characterization of tungsten wires which are used as reinforcement material in the advanced tungsten fibre-reinforced composited (W_f/W) [75]. The purpose of this work was to perform a systematic study on the effect of heat treatments in a broad range of annealing temperatures and investigate how microstructural and fracture properties develop upon annealing, with the special focus on the relationship between the investigated features. The investigated materials were once again commercially available pure and potassium doped (K-W, 60 ppm) tungsten, with a wire diameter of 150µm. The final, desired diameter of such a material is obtained by drawing processes, which have a significant influence on the resulting microstructure. Imposed high degree of deformation leads to the development of a unique wire structure consisting of extremely elongated grains along the drawing direction, while perpendicular to the drawing axis, uniformly distributed and curled grains have significantly smaller dimensions. The first impression of the deformed, as-received microstructure is seen in Figure 10, where the backscatter electron (BSE) images are taken in the longitudinal section (Figure 10a) and cross section (Figure 10b) of the wire. The given example is of the doped tungsten wire, however, both materials have a very similar initial appearance.

The investigation of the microstructural stability of the two materials and arising annealing phenomena - recovery, recrystallization and grain growth was conducted on series of heat treated samples. Annealing was performed in vacuum in the temperature range from 900-1600°C with a holding time of 1h. For each material and annealing condition, EBSD scans with an area of 25 x 25µm^2, were obtained in two principal viewing directions: longitudinal section (plane parallel to the drawing axis) and cross section (plane perpendicular to the drawing axis), as shown in the schematic drawing in Figure 10. The use of advanced microscopy tools allowed comprehensive analyses of the evolution of different aspects of the microstructure, thus enabling the assessment of the different stages of occurring phenomena. The systematic study consisted of identifying the grain shape and size changes, analyzing the grain boundaries and assessing the evolution of the developed texture. Furthermore, in order to

give the first impression of a correlation between the microstructure and mechanical properties, Vickers hardness measurements were performed for both wires in the as-received and all annealed states.
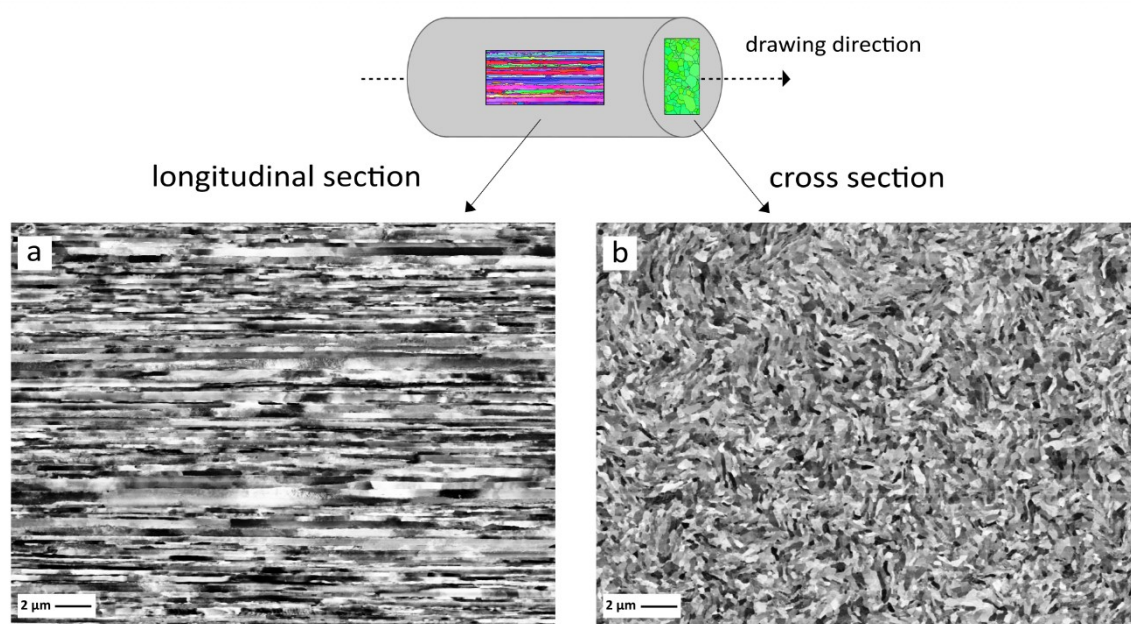
Figure 10. *Scanning electron micrographs of the as-received potassium doped tungsten wire in the BSE mode taken in the central area across a) longitudinal section and b) cross-section. The schematic drawing on the top shows the principle direction of deformation, as well as the position of the typical scanning areas in respect to the drawing direction.*

The performance of tungsten wires and in particular their crack resistance properties at moderate temperatures are of fundamental importance when being used as reinforcement elements in the composite materials. Thus, the second part of this study was directed towards the room temperature fracture toughness assessment, particularly focusing on the evolution of the fracture mechanisms in respect to different heat treatments. Based on the microstructural characterization, two annealing temperatures were chosen: 1300°C and 1600°C, enabling in such a way determination of the relation between the microstructural evolution and the embrittlement by annealing and/or ductility conservation. The fracture experiments were conducted in one principal testing direction with the crack growth direction perpendicular to the drawing axis of the wires. Thus, the damage tolerance of tungsten wires was investigated on single-edge notched tension specimens. The typical sample length of the wire was about 20mm with the notch depth, introduced by the femtosecond (fs) laser, being about one third of the wire diameter. Furthermore, in order to investigate the influence of a nearly atomically-sharp flaw in the material, some of the as-received samples also contained a pre-crack like notch introduced by a FIB. An example of a top view of a laser notch (perpendicular to the drawing axis) as well as the position of the FIB cut can be seen in Figure 11. During the experiments, the load-displacement curves were recorded and the maximum obtained load was used in evaluating the critical stress intensity factor K.

The minimal length of the crack is taken for all the calculations, which is determined from fracture surfaces by a straight line parallel to the end of a notch, as shown in Figure 11b.
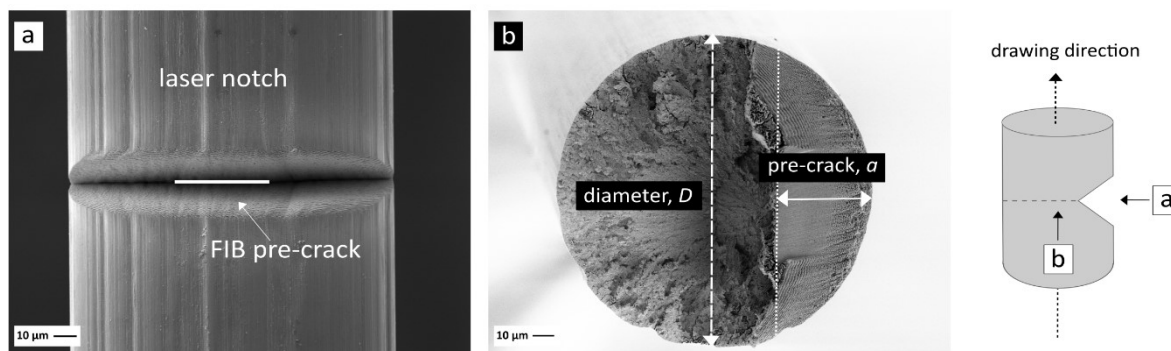
Figure 11. Scanning electron micrographs of a) a top view of a laser notch with designated position of a FIB cut and b) an exemplary fracture surface showing how a minimal length of a pre-crack was measured. The schematic drawing on the right illustrates a characteristic SENT specimen with indicated viewing directions.

3.2.1. Microstructural stability

The main characteristics of the wire microstructure in the as-received state (shown in Figure 10) are fibrous grains elongated along the axial direction and the development of a very pronounced <110> fibre texture. Such an appearance is typically seen in heavily deformed bcc wires [85] and as expected, the results of as-received pure and K doped tungsten are very similar. Another peculiar feature observed in the cross section of the wire is a distinctive pattern known as grain curling or the so called Van Gogh sky structures [86]. The origin of the formation of such ribbon-shaped grains lies within the tendency of textured grains to deform by plane strain elongation [87]. In the course of severe plastic deformation during the drawing process, the microstructure of the wire is severely altered from the initially equiaxed grains (of the sintered ingot) to the elongated grains parallel to the axial direction and the shape change of each grain must be compatible with that of the neighbouring grains. However, with plane strain flow, this can only be accomplished by twisting of grains around each other. In such a way, grains become shaped like ribbons, curled around the wire axis establishing a very pronounced, sharp <110> fibre texture. The analyses of the pole figures obtained from EBSD data confirm this strong, preferential orientation of the grains with the <110> direction parallel to the wire axis. The evolution of the developed texture does not seem to be influenced by isothermal annealing treatments. Even at the highest annealing temperature of 1600°C very little effect can be seen on the lattice orientation, as the texture remains the same with a very dominant <110> direction.

The effect of different heat treatments on the microstructural stability was studied through series of EBSD orientation maps by making a comparison between data acquired in the central region of the cross sections (Figure 12) and longitudinal sections (Figure 13) of pure and potassium doped wires. With an increase in annealing temperature substantial microstructural modifications are observed for the pure W wires (Figure 12a and Figure 13a); continuous increase of the grain size is accompanied by the disappearance of curling structures and more equiaxed grain shape. Heat treatment at the highest

temperature of 1600°C leads to tremendous grain growth when compared to the as-received state of the material.
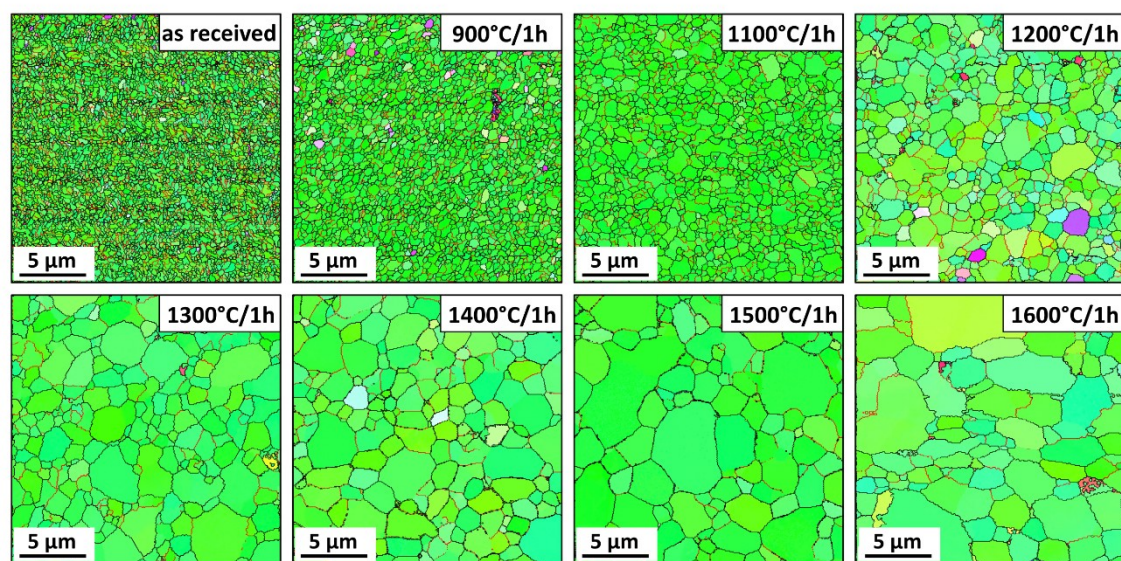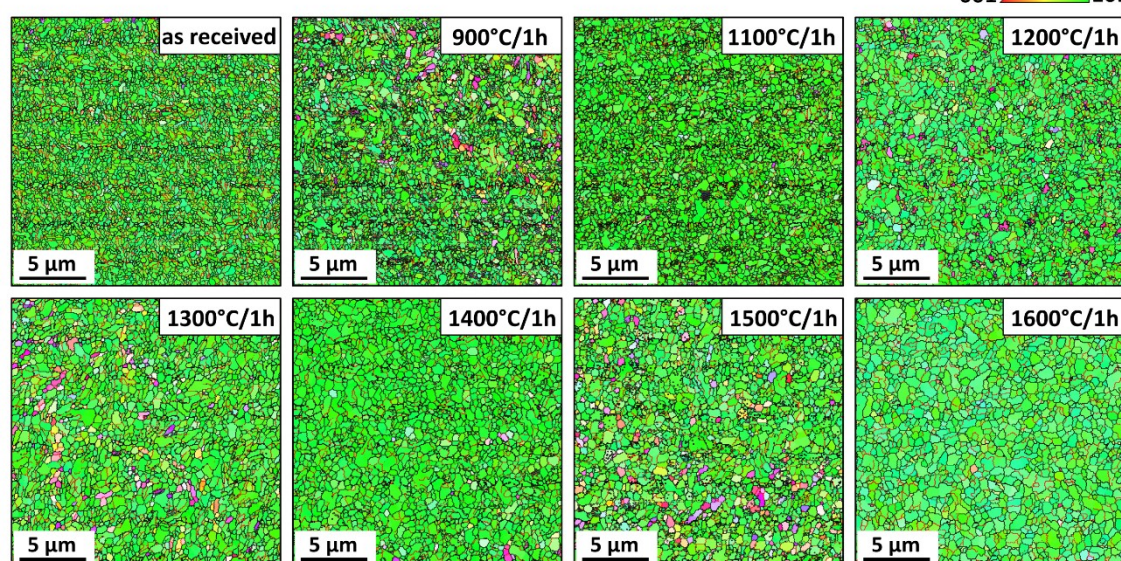
Figure 12. *EBSD orientation maps of the cross sections of a) pure tungsten and b) potassium doped tungsten wires. The evolution of the microstructure and thermal stability are investigated in respect to different annealing treatments, performed in vacuum for 1h. Colour coded unit triangle is given as well, representing <100>, <110> and <111> crystallographic directions perpendicular to the sample surface. All of the scans were taken with the same magnification.*

In contrast to these observations, K-W wires show only a mild increase in grain size and the microstructure remains rather stable over the entire temperature range (Figure 12b and Figure 13b). The noticeable uniformity of the grain colour in all the scans is an indication of a very pronounced and stable texture of the wires. Regarding the longitudinal section, the characteristic elongated

microstructure of the pure W wire is severely influence by heat treatments experiencing alternations in grain size (in both directions of the scan) already at lower temperatures of annealing. The significant coarsening eventually leads to the complete loss of fibrous appearance of the grains, where the microstructure of the final state consists of large, globular μm sized grains. Thermal stability of the K-doped wire is also observed in the longitudinal direction, where regardless of some mild growth in the size of the grains, the overall elongated microstructure is preserved, even for the highest annealing temperatures.
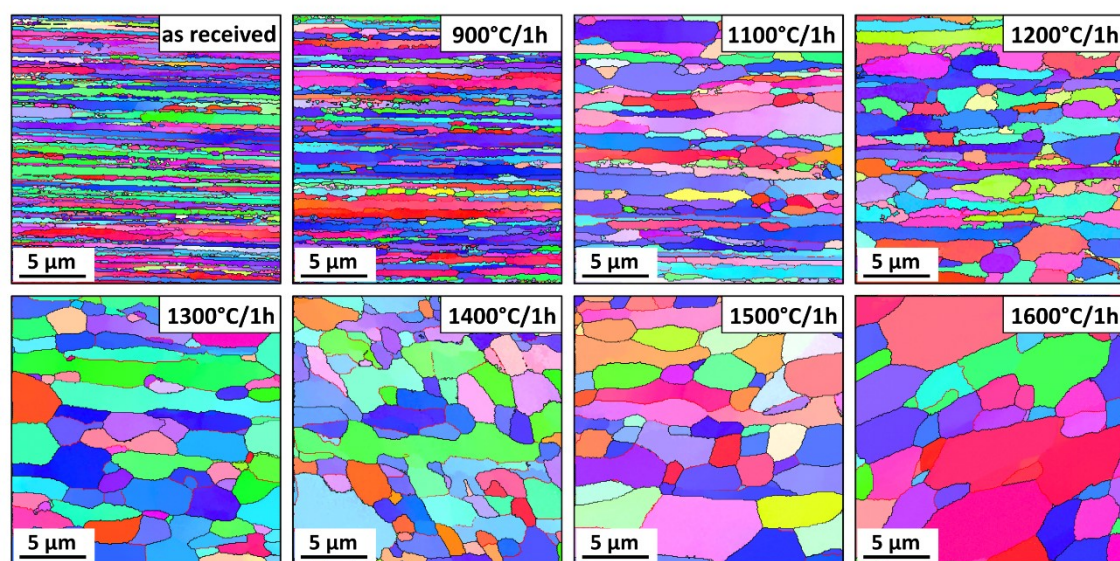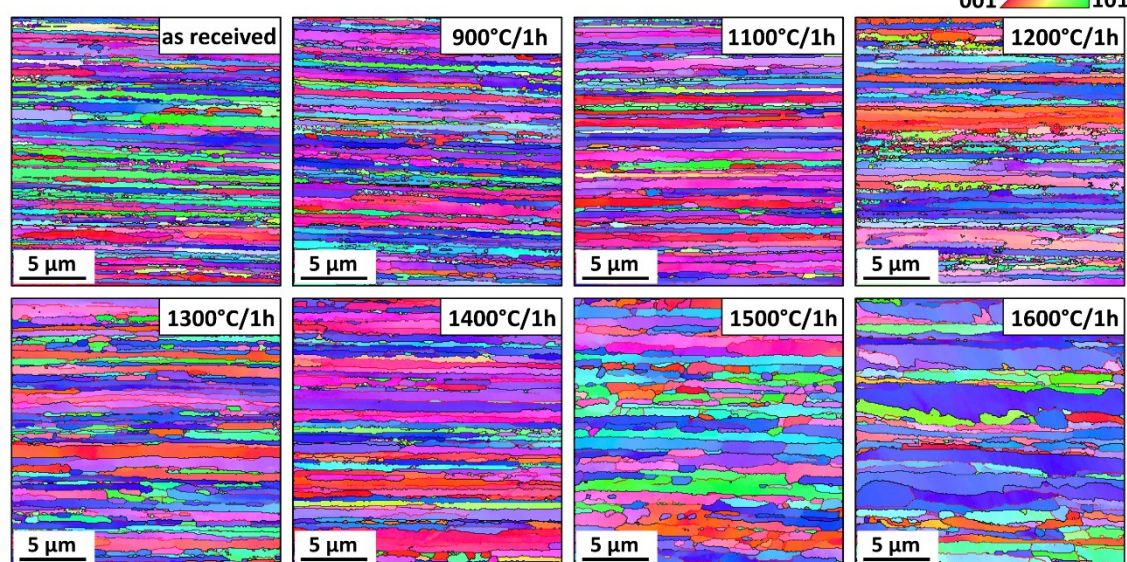
Figure 13. *EBSD orientation maps of the longitudinal section of a) pure tungsten and b) potassium doped tungsten wires. The evolution of the microstructure and thermal stability are investigated in respect to different annealing treatments, performed in vacuum for 1h. Colour coded unit triangle is given as well, representing <100>, <110> and <111> crystallographic directions perpendicular to the sample surface. All of the scans were taken with the same magnification.*

Summary of the results

From the presented orientation maps, the quantitative analyses of the grain size as a function of different annealing conditions was performed. The obtained results, as well as the comparison of different methods of grain size evaluation can be found in Publication C. Furthermore, the nature of grain boundaries was studied and due to their importance for the dislocation motion and related annealing phenomena, the misorientation angles were analysed by their frequency, from which the total GB length, as well as the individual contributions of LAGB and HAGB were acquired. All the relevant details can be found in the appended publication.

Understanding the observed modification in the grain structure of the wires, alongside with changes of other microstructural features, is inevitably related to the discussion of the main three annealing phenomena: recovery, recrystallization and grain growth [88], [89]. The driving force of the recovery is the stored energy in the deformation structure due to point and line defects. This stored energy of the material is lowered during annealing by dislocation movement through the annihilation of dislocations and the rearrangement of dislocations into lower energy configurations (polygonization and low angle grain boundaries). Recrystallization in general is a thermally activated process in which new dislocation-free grains are formed within the deformed or recovered structure and grow into it; the driving force arises from the elimination of the dislocations introduced during deformation and is characterized by the movement of high-angle grain boundaries. The driving process of this subsequent grain growth is the reduction in stored energy of the material in the form of grain boundaries. The obtained data were analysed and interpreted in regards to the respective processes as following: the recovery process is mostly determined through an increase in the fraction of LAGB; the recrystallization process is related to the temperature range where distinctive changes occur in the grain structure (in terms of size and shape) accompanied by pronounced softening of the material and variations in the amount and type of dominant grain boundaries; and lastly further substantial increase in grain size of the recrystallized structure is classified as grain growth.

Analysis of pure, undoped tungsten wires annealed in the range below 1100°C shows that the grain structure exhibited a greater degree of homogenous fine scale coarsening in the cross sections, followed by a limited grain boundary migration and increased ratio of LAGB, which is all an indication of a recovery process taking place. Annealing temperature of 1100°C seems to be the onset of the recrystallization as the first appearance of some isolated grains, which had grown more than neighbouring grains, is seen. Moreover, grain boundary movement is more pronounced and the total amount of boundaries is significantly reduced at this temperature. The recrystallization process seems to be complete after heat treatments up to 1400-1500°C as the grain boundary movement progressed to the point that the initial overall elongated structure in the longitudinal directions is eliminated leading to the relatively equiaxed structure of the grains. This coarsening process seems to be induced by a radial movement of grain boundaries. However, it can also be explained by the movement of the triple grain boundary junction of the small grains [89]. The majority of the boundaries present at this stage of recrystallization process are predominately high-angle grain boundaries. After heat treatments at the highest temperature, pure tungsten wire undergoes subsequent grain growth, where the initially fibrous microstructure is completely altered forming large, equiaxed grains with an increase in average grain size by an order of magnitude. The outlined results are in agreement with the previous studies of

properties of annealed, pure tungsten wires [90], as well as with the typically reported recrystallization temperature of tungsten (1300-1500°C) [91]–[93].

In contrast to annealing properties of pure tungsten, the potassium doped wire experiences significantly milder structural changes in the range of investigated temperatures. Below annealing temperature of 1400°C the fibrous structure is completely conserved with slight amount of apparent radial movement of grain boundaries. At higher annealing temperatures, the migration of short lengths of longitudinal boundaries of all misorientations became more pronounced, leading to the increase of grain width in the longitudinal direction. Nevertheless, an extensive grain boundary movement is successfully inhibited, while the recrystallization is shifted to even higher temperatures. The overall appearance of the elongated structure is preserved with slightly lower aspect ratios of the grains and an increase in the amount of low-angle grain boundaries; this fits pretty well with the process of polygonization, which is related to the rearrangement of dislocations in the LAGB. The annealing behaviour and recrystallization mechanism of K-W wires is closely related to the presence of the dispersed second phase, namely potassium used as a dopant element [94]. The potassium is entrapped in pores during sintering of the tungsten ingot, which are further elongated by subsequent swaging and drawing, forming long tubes with a very high aspect ratio [95]. The areas of elongated potassium are precursors of the bubbles, which are arranged in parallel rows and all aligned in the drawing direction of the wire. Upon heating of the wire to higher temperatures, the elongated tubes divide into rows formed by individual well shaped spherical bubbles [96]. An example of such a formation can be seen in Figure14. The undoubtedly important role of potassium bubbles is seen through their grain boundary pinning effect, inhibiting mostly longitudinal grain boundary motion (may hinder triple junction motion as well) and controlling the shape and growth of the grains.
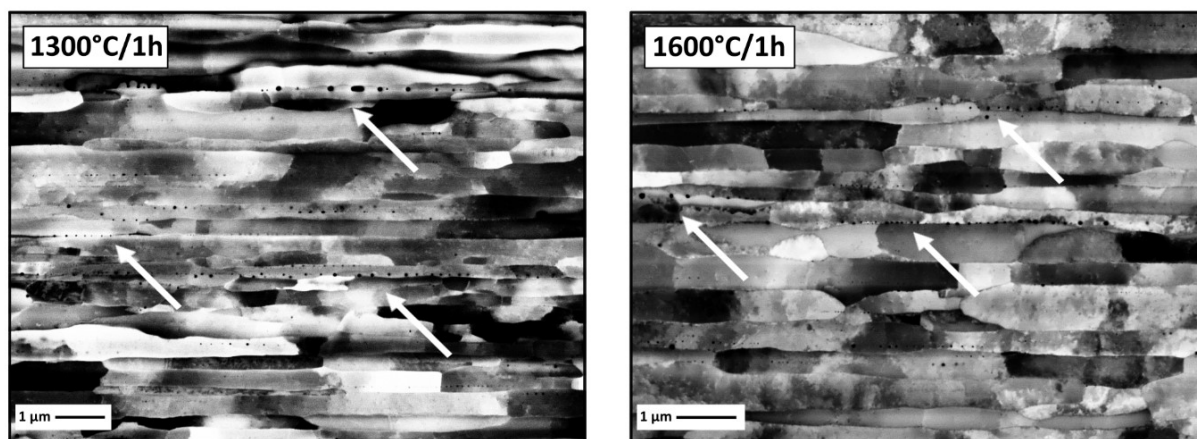
Figure 14. Scanning electron micrographs of the annealed, K-doped tungsten wires showing finely distributed rows of potassium bubbles which act as pinning sites and thus prevent grain boundary migration. The images are taken across the longitudinal sections in the BSE mode, while the dopants are indicated with white arrows.

Furthermore, microhardness measurements were conducted enabling a fast determination of the changes of the mechanical properties in respect to different heat treatments through a correlation between the strength of the material and its grain size. Thus, the loss in hardness i.e. softening of the

material occurring during annealing, complements observed alternation of the microstructure and helps identification of the recovery and recrystallization. Figure 15a shows the results of Vickers microhardness measurements (HV0.5) as a function of the isochronal annealing temperature of the longitudinal sections for both pure and potassium doped tungsten wires. The observed variation of the microhardness and the stability in case of K-W wires are in excellent correlation to the evolution of the microstructure with different annealing treatments (Figures 12 and 13). In such a way, a link can be made with the grain size, which is related to the strength of the material by the well-known Hall-Petch relation [97], [98]. This can be validated by plotting the hardness results of the samples in different annealing states against reciprocal square root of corresponding grain sizes, given as $d^{-1/2}$ (Figure 15b).
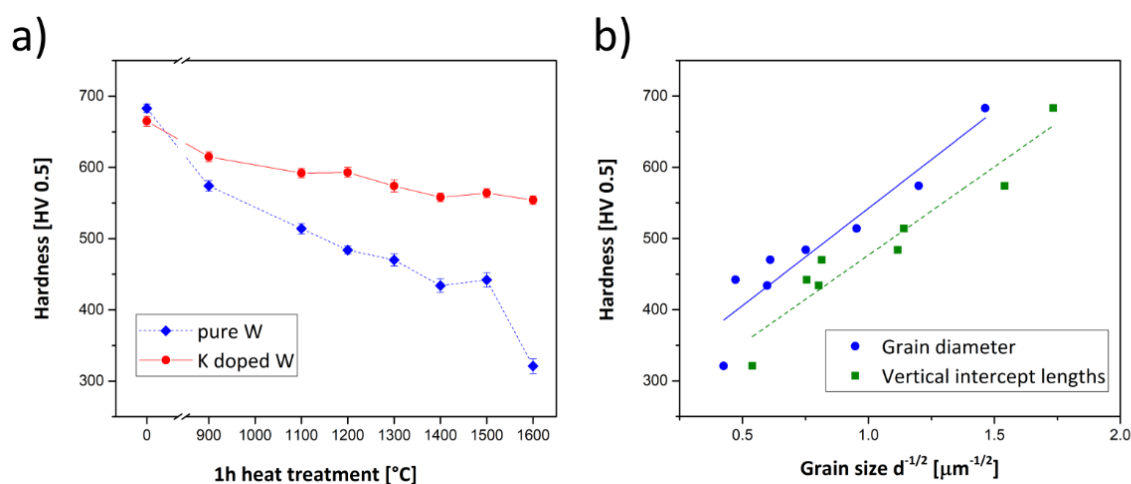
Figure 15. *a) Vickers hardness (HV0.5) results of the pure and potassium doped W wires after annealing at different temperatures for 1 h. b) The relationship of the hardness data of a pure tungsten wire is established in respect to the grain size, given as $d^{-1/2}$ and expressed in terms of grain diameters and vertical intercept lengths. The linear relationship is accentuated by a linear fit function.*

3.2.2. Room temperature fracture behaviour

The fracture toughness of pre-cracked wire samples was evaluated as a critical value of the stress intensity factor for a material subjected to tensile, mode I loading conditions. An overview of all the obtained results from both type of materials, where the apparent fracture toughness K is plotted against performed heat treatments, is given in Figure 16, with the associated values shown in Table 2. The measured room temperature values of the as-received samples for pure and K-doped tungsten are (33.4±6.4)MPa·m$^{1/2}$ and (31.9±7.2)MPa·m$^{1/2}$, respectively. A rather high standard deviation is related to a scatter of K data, which is associated with the occurence of either a brittle or a ductile fracture mode. In the case of pure tungsten wire, measured fracture toughness is in the range from 25.9MPa·m$^{1/2}$ (the lowest obtained value of a brittle appearance) to 43.3MPa·m$^{1/2}$ (the highest obtained value of a ductile appearance). The results of doped wires show a similar variation of K going from 22.7MPa·m$^{1/2}$ to 44.5MPa·m$^{1/2}$. The existence of the scatter of measured fracture toughness data under the same testing conditions strongly indicates that the testing temperature (in this case room

temperature) is in the range where a transition from a brittle to a ductile failure mode takes place. The two distinct cases of material's response in a test, namely ductile and brittle behaviour, are also reflected in the obtained load-displacement curves. In both cases specimens show nearly pure linear elastic loading at the beginning. After a maxium load is reached, a brittle sample fails catastrophically without showing any signs of plastic behaviour with the force abruptly dropping to zero. In contrast to this, a ductile sample sustains a higher maximum load and shows a certain non-linearity in a test record, where the force decreases steadily before final failure occurs. The respective curves can be seen in the Publication D.
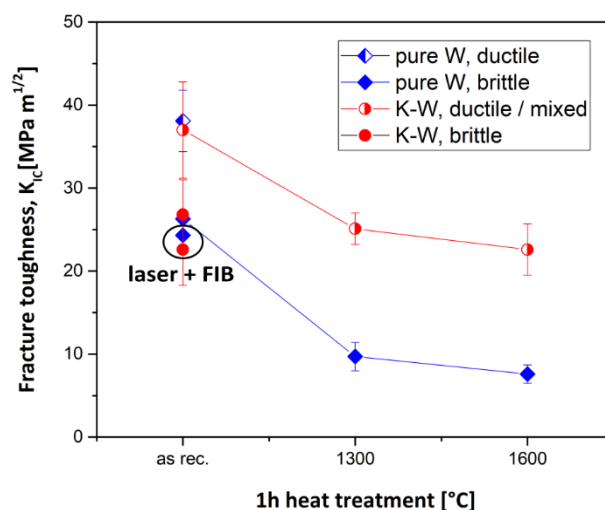
Figure 16. *Apparent fracture toughness of pure and K-doped tungsten wires as a function of annealing temperature. The occurring failure mode, being a brittle, a ductile or a mixed one, is indicated as well. The influence of different notch fabrication methods is investigated for the as-received materials.*

Additional sharpening of the conventionally processed notches by a FIB can have a very strong influence on the measured toughness values, as a result of changed stress state ahead of the crack tip. In order to elucidate whether such a notch effect takes place for wires, an additional set of as-received samples was investigated, where beside the fs-laser notch, a sharp pre-crack was introduced by means of a FIB. The results indicate that the additional refining of the notch does not have a significant influence on the resulting fracture process (a higher tendency of a brittle mode is perceived though).

Fracture properties of the heat treated samples show a substantial difference of the two investigated materials. The measurements of apparent fracture toughness of wires annealed at 1300°C yield values of (9.7 ± 1.7)MPa·m$^{1/2}$ and (25.1 ± 1.9)MPa·m$^{1/2}$ for pure and K-doped tungsten, respectively. The pronounce drop of K, in particular in the case of pure W, is further enhanced for the samples heat treated at 1600°C. In this case, measured fracture toughness is only (7.6 ± 1.1)MPa·m$^{1/2}$ for pure and (22.6 ± 3.1)MPa·m$^{1/2}$ for K-doped wire. With an increase in annealing temperature the pure tungsten wire shows a significant reduction in toughness as a result of embrittlement by annealing. The influence of heat treatments is significantly milder in the case of K-doped material, as the decrease in fracture toughness, even after annealing at 1600°C is not as pronounced.

Summary of the results

Table 2. *Overview of the apparent fracture toughness results of a pure and K-doped tungsten wires. Comparison is made between different notch techniques, material behaviour as well as annealing conditions of the samples (as-received, 1300°C and 1600°C state of the wire). The majority of the results represents an estimated lower limit of fracture toughness, which is indicated with a "greater than" sign. The bolded results outline a real mode I fracture toughness.*

Material state, notch technique	Fracture toughness [MPa(m)$^{1/2}$]	
	Pure W	**K-doped W**
as received, laser, mean value	> 33.4 ± 6.4	> 31.9 ± 7.2
as received, laser, ductile	> 38.1 ± 3.7	> 37.0 ± 5.8
as received, laser, brittle	> 26.3 ± 0.5	> 26.8 ± 4.2
as received, laser + FIB, brittle	> 24.3 ± 1.6	> 22.6 ± 4.3
1300°C/1h, laser	**9.7 ± 1.7**	> 25.1 ± 1.9
1600°C/1h, laser	**7.6 ± 1.1**	> 22.6 ± 3.1

In Publication D several critical remarks regarding the accuracy of the obtained fracture toughness results are discussed, implicating an underestimation of the determined failure resistance of the wires. The reader is referred to the publication for detailed description of the considered criteria. However, it can be stated that the obtained results should be regarded as an apparent crack resistance of the tungsten wire, representing a lower bound value for the real mode I fracture toughness. The extent of underestimation of the obtained results in respect to material's true crack resistance can be estimated from the CTOD measurements which deliver fracture toughness value of ductile materials in the elastic-plastic regime. The sample analyzed in Publication D was a K-doped wire with a measured K value of 44.5MPa·m$^{1/2}$. An estimation of the CTOD parameter yields a fracture toughness of about 80.5MPa·m$^{1/2}$. Thus, the true fracture toughness is higher by at least a factor of two in the ductile failure behaviour.

3.2.3. Fractographic evolution

Fractographic analyses of the failed samples are an essential part in studying fracture behaviour of a material, in particular when it comes to establishing a relationship between the underlying microstructure and the characteristics of the fracture process. As outlined in previous chapters, as-received wires behave in different ways at RT, corresponding to lower or higher values of fracture toughness, which is associated with the brittle or ductile failure mode, respectively. Typical fracture morphologies of both failure modes are shown in Figure 17. A unique feature occurring in all of the as-received samples, regardless of the type of failure mode, is a pronounced crack deflection by about 90°. Such a deviation from an anticipated mode I crack path occurs at the beginning of the fracture event and results in propagation along the drawing direction of the wire for a certain length, before a

final fracture surface is formed. This distinct fracture feature occurs as a consequence of the elongated microstructure of heavily drawn wires and is a strong indication of a very prominent anisotropy in fracture toughness. Such a strong anisotropy of fracture behaviour induced by microstructural orientation can also be seen in other materials, for example in the case of cold drawn steel wires [99], [100].
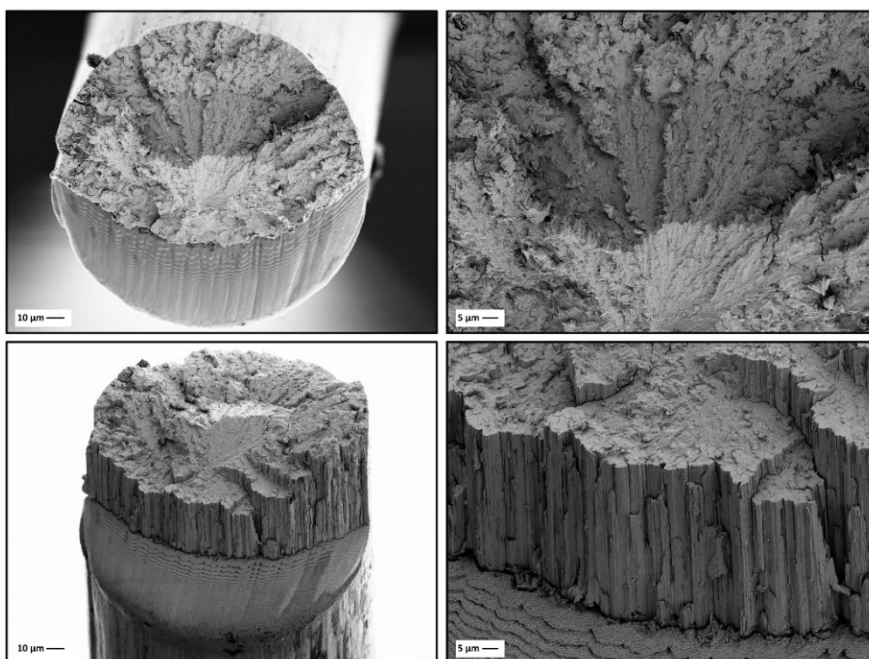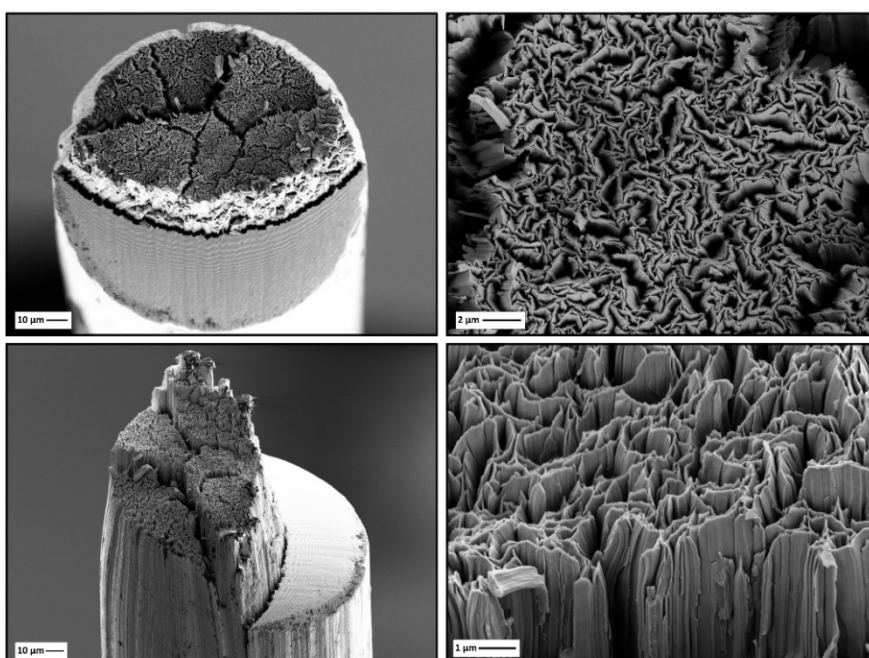
Figure 17. *Scanning electron micrographs of as-received tungsten wires showing a) a brittle, cleavage dominated and b) a ductile, knife-edge necking dominated fracture behaviour. Fracture surfaces are studied in a top and side views of the wire in respect to the laser notch. The characteristic features of the fracture process are shown in the magnified images.*

Summary of the results

Predominant micromechanisms of the as-received samples failing in a brittle manner are transcrystalline cleavage across the diameter of the wire, accompanied with the absence of necking. After the initial deflection of the crack, a mixed, predominately mode II fracture appears along the grain boundaries and the resulting final fracture surface is inclined in respect to the initial laser notch plane. The origin of the transgranular cleavage is situated in the central area of the wire with the crack propagating radially outwards and forming characteristic river patterns. Besides this, small colonies of grains with a cleavage surface roughly perpendicular to the wire axis can be seen, which are related to the {110} cleavage plane and arise as a consequence of the <110> fibre texture.

Fracture appearance of the as-received samples failing in a ductile manner is designated as knife-edge failure mode and after crack deflection it is characterized by distinct necking of the entire wire, followed by longitudinal cracking and necking of individual grains to almost 100 % reduction in area. A direct influence of the curled grains, observed in the cross sections of the untested wire, can be seen from the fractographs taken in the top view, revealing that the fracture surface consists of intertwined, convoluted ribbons. Knife-edge necking of individual grains, occurs within these ribbons and results from their intrinsic plane strain elongation [101], which is a consequence of the {110} fibre texture. Further peculiar features of the fracture surfaces are deep crevices running in the radial direction of the wire and are often referred to as delaminations. They occur by a decohesion of the grains along their longitudinal grain boundaries and thus propagate along the wire drawing direction, indicating that these boundaries are too weak to support tensile stresses generated during necking, which is also an indication that the interfibre fracture toughness is significantly lower. Furthermore, the existence of the grain boundary delaminations is closely related to the reduction in the stress triaxiality which leads to the increased crack growth resistance. Observed features of ductile as well as brittle fracture modes are very similar to the ones already reported for heavily deformed tungsten wires [101]–[103].

Influence of heat treatments on the resulting fracture morphologies can be seen in Figure 18, where a comparison is made between the pure and potassium doped tungsten wires. A tremendous difference in the micromechanisms controlling the fracture process can be observed already at the lower annealing temperature of 1300°C for 1h (Figure 18a). The failure mode of the undoped wire is characterized as a brittle, mixed one being composed of both cleavage and intergranular fracture. The most distinctive feature in this case is the absence of the crack deflection, with the fracture surface being mostly flat in respect to the wire axis. Thus, for this material state the crack path does not deviate from its designated mode I propagation direction. Annealed K-doped wires have a very similar failure appearance as in the as-received state, with the fracture surface including longitudinal cracks and knife-edge necking of the individual grains.

Influence of heat treatments at even higher temperatures (1600°C for 1h) on the resulting fracture morphologies is shown in Figure 18b. Pure W shows a very similar appearance of mixed, brittle fracture as the samples annealed at 1300°C: besides the cleavage planes with typical river lines, brittle intergranular grain boundary fractures are also occurring in between. Furthermore, the crack propagation direction remains in the same plane of the initial pre-crack with a decrease of the overall roughness of the fracture surface. The intergranular failure mode seems to dominate at the edge region of the wire which can be related to the heterogeneity of the stress state across the diameter [104], [105],

occurring as a direct consequence of the drawing process. Such a correlation of the radial position and the resulting failure mode was anticipated from the observations of the localized variations in crystallographic orientation and the texture analyses, which were conducted in the Publication C. The reader is referred to the Figure C.7, where the microstructural evolution across the entire wire diameter is investigated by a sequence of orientation maps.

a) 1300°C

pure W

K-W

b) 1600°C

pure W

K-W
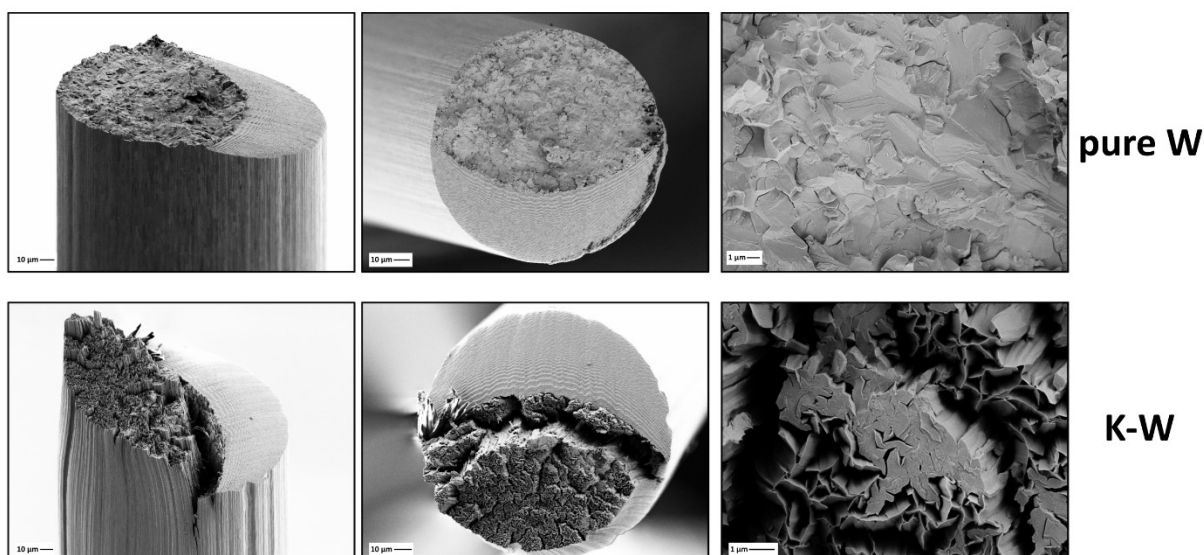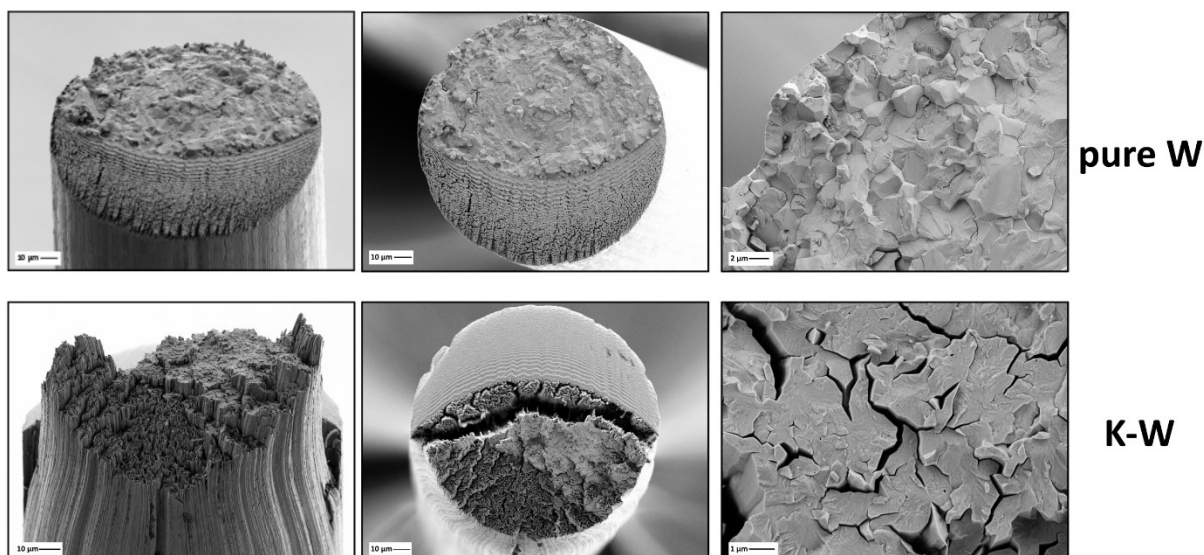
Figure 18. Scanning electron micrographs of tungsten wires annealed for 1h in vacuum at a) 1300°C and b) 1600°C. The influence of annealing temperature is studied through the evolution of dominating micromechanisms which control the fracture process. A comparison is made between pure and potassium doped wires.

Summary of the results

An increase in annealing temperature leads to a more noticeable variation of the micromechanism controlling the fracture process in the case of K-doped tungsten wire. An increase in the area of brittle, cleaved grains is observed, which can be associated with the observed decrease in fracture toughness. These cleaved grains are roughly perpendicular in respect to the wire axis, with small longitudinal cracks occurring between the convoluted colonies of grains. Nevertheless, regardless of the existence of brittle regime, the presence of an extensive necking of the wire diameter accompanied by a wide range of knife-edge fractured individual grains underlines the remarkable fracture properties of a doped wire upon annealing.

Based on the shown results it can be stated that the modifications of the initial microstructure by different heat treatments are directly reflected by the occurring failure mode in the case of heavily drawn tungsten wires. In the case of pure tungsten, annealing already at 1300°C leads to a complete loss of the elongated microstructure and a formation of large, equiaxed grains, which further increase in size by annealing at higher temperatures (Figure 12). The influence of the thermal history is seen through a tremendous decrease in fracture toughness accompanied with a major change of the failure mode, which mostly can be related to the pronounced decrease in grain boundaries aligned to the drawing direction. In the initial state of the wire, the weakness of the longitudinal grain boundaries is clearly seen through the occurrence of a strong crack deflection and the longitudinal, mode II cracking, while the transverse boundaries are widely separated and most likely not the preferred crack path. However, elevated thermal exposures above the recrystallization temperature can cause the formation of transverse boundaries enabling the crack to propagate more easily from one grain boundary facet to another without deviating from the initial crack propagating direction leading to the intergranular appearance of the fracture surface (Figure 18). In contrast to this, the K-doped wire shows remarkable fracture toughness even after the heat treatments, which is ascribed to the preservation of the fibrous, elongated microstructure and is seen through predominately knife-edge fracture mode, even for the highest annealing temperature. Investigated heat treatments and annealing temperatures of 1300°C to 1600°C lead to a small degree of broadening of the fibers, which is related to an increase in the amount of transverse grain boundaries. If there are more boundaries of this type in the same plane at the initial crack, the probability of providing a nucleation site for cleavage rises, resulting in a reduced fracture toughness and larger amount of cleaved grains in the fracture surface. However, more substantial microstructural changes are prevented by finely dispersed rows of ultrafine sized potassium bubbles which act as pinning sites and were shown in Figure 14. As already outlined, the grain boundary migration is restricted by potassium bubbles resulting in a suppressed microstructural coarsening and a shift of the recrystallization to even higher temperatures than in the case of pure tungsten.

The main conclusion of the work performed on drawn tungsten wires is that the full recrystallization and grain growth in tungsten wires can successfully be shifted to temperatures higher than 1600°C by addition of potassium as a doping element. From a microstructural point of view, the application of K-doped wire for structural parts of fusion reactors, as it is the case for W_f/W composites, is strongly advised. The systematic study of the influence of heat treatments on the evolution of the grain morphology for both type of materials is crucial for the assessment of the fracture toughness of the wire, as the grain size and more importantly grain shape have a tremendous influence on the

micromechanisms controlling the fracture process. Pure, annealed tungsten wires experience a tremendous deterioration of the fracture toughness with a very prominent transition of the failure mode. The observed embrittlement by annealing can be related to the loss of the fibrous, elongated microstructure. In contrast to this, the results of the annealed, doped wires demonstrate that the microstructural stability and preservation of the initial, beneficial grain structure is directly reflected in the crack resistance of the material. Predominately ductile behaviour, with characteristic knife-edge necking, is seen even after annealing at 1600°C.

Finally, it should be noted that a further reduction in the wire diameter (increase in the degree of deformation) is expected to further enhance the fracture toughness. This topic, alongside with the investigation of the anisotropic fracture properties, will be addressed in the future research.

3.3. Thin film tungsten alloys

The third part of the thesis is focused on a preliminary study of binary W alloy thin films. Magnetron sputter co-deposition techniques enable a production of the multinary alloy systems in the form of continuous composition spreads [106] allowing efficient high-throughput investigations. Therefore, this approach was used to investigate the influence of different alloying elements and their changing concentrations on the properties of W thin films. A major advantage of this method is that it produces a large variety of W alloys that are identical in the preparation technique, hence leading to very similar purity levels and directly comparable microstructures. In previous chapters, the tremendous influence of the microstructure was already elaborated. As the first step of the study, combinatorial co-sputtering, from separate high purity elemental sputter targets, was applied in order to produce three binary thin film alloy systems: W-Fe, W-Ir and W-Ti. A detailed chemical, morphological and microstructural analysis was performed, revealing whether the produced films are applicable (in terms of density and roughness) for further mechanical investigations.

Using pairs of elemental sputter targets, all the binary W alloy systems were successfully deposited on oxidized Si and bulk W substrates, with film thickness of 1-2.5µm. The sputter parameters were adjusted to achieve the following well-defined, continuous composition gradients: W-Fe (0-7at.%), W-Ti (0-15at.%) and W-Ir (0-12at.%). Binary W-alloy thin films show this gradient across the substrate due to the geometrical arrangement of the sputtering cathodes. Right after the deposition process was finished using oxidized Si substrates, a coarse compositional mapping was done. The maps were obtained to confirm the desired alloying range and were used as a guideline throughout the following analyses. Figure 19 shows composition maps of the materials libraries: the gradient direction reflects the position of the sputter targets, where the red arrow indicates the centre-to-centre line from the W to the alloy element cathodes. The composition ranges for each alloy element were chosen based on estimates of thermodynamically-stable low temperature solubility limits. The binary W alloys deposited on Si substrates were used for already mentioned coarse EDX mapping and thickness measurements. Detailed chemical quantification of particular regions of interest, and following morphological and microstructural characterizations were performed on thin films deposited on W substrates. The reader

is referred to the Publication E for a comprehensive and detailed overview of the obtained results, while the following paragraphs will only briefly outline the main findings.
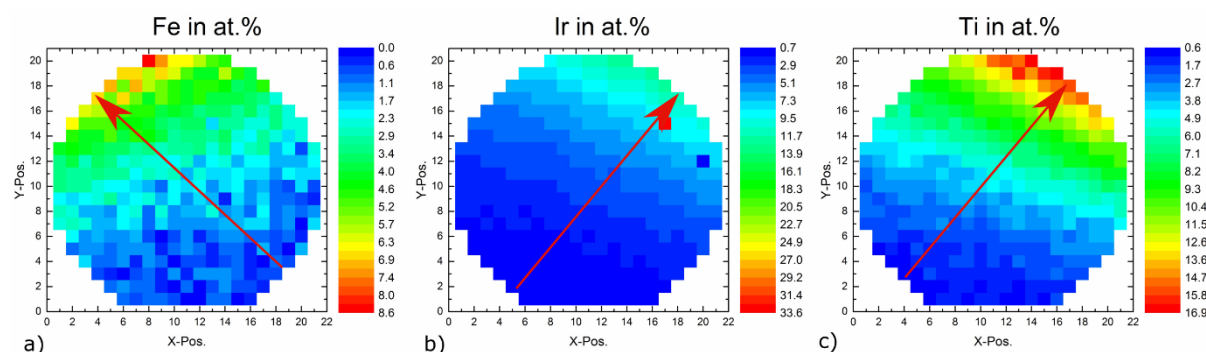
Figure 19. *EDX maps of W-X thin films on Si substrates showing the compositional gradient of the alloying element in atomic percent. a) W-Fe alloy with 0-7at.% Fe, b) W-Ir alloy with 0-12at.% Ir and c) W-Ti alloy with 0-15at.% Ti.*

The structure of sputtered thin films shows a large variety in terms of size, morphology and orientation of grains, which are in direct correlation with various deposition parameters. The morphology of the films with high added-element compositions consists of columnar structures of inverted cone-like units having domed tops and separated by voided boundaries. There is a strong correlation of the observed microstructural appearance and the alloying content - with a decrease of the content of the alloying element, flattening of surface areas occurs while the boundaries contain considerably less voids. Such a behaviour was evident for all three deposited alloys. The development of the tapered structures separated by voids seems to be mainly governed by a very low adatom surface mobility that is insufficient to overcome the effects of shadowing.

EBSD orientation imaging maps of W-Fe films reveal that the microstructure consists of uniformly distributed grains with an average size going from 401nm to 330nm with an increase in Fe content; the texture exhibits a small variation. The EBSD grain size analysis of the W-Ir alloy showed an increase in grain size with a decrease in at.% of Ir. The average grain diameters are 149nm and 239nm at 13.1at.%Ir and 5.8at.% Ir, respectively with no change in the {101} plane orientation texture. In the case of the W-Ti alloy, grains are slightly elongated perpendicular to the reference direction, having an average diameter of 139±20nm for W-5.3at.% Ti and 162±25nm for W-14.6at.%Ti. The texture remains stable having a peak in the {101} plane orientation with respect to the surface normal. Comparison of films on polished W and thermally oxidized (100) Si indicates that the substrate does not affect the generated structure, however surface quality is reflected in the film meso-roughness.

The underlying motivation of the conducted work was to study the exact influence of a single alloying element on a particular mechanical property and determine potential beneficial effects of a specific alloying element on W materials. This can be achieved by micromechanical experiments if the necessary microstructural requirements are fulfilled and optimization of the deposition parameter is performed. Many micromechanical techniques are available to characterize the mechanical properties of materials where one, two, or all three dimensions are in the micro regime: nanoindentation, micro pillar experiments, micro tension, micro bending, micro fatigue and micro fracture mechanical tests [107]–[109]. Due to the high defect density, especially in the highly alloyed regimes of the films, micro

tension and micro bending are not applicable to the films in this study. For such tests, significant improvement of the density of the films is required. Only in the lowest alloyed regimes micro pillars or nanoindentation might deliver useful data. An analysis of temperature dependence or rate dependence of the plastic deformation would permit study of the detail of deformation processes (for example to analyse whether the Re effect [64] with respect to plastic deformation takes place or not). A requirement for the nanoindentation experiment is a flat surface, hence such experiments could only be performed in-situ in the SEM, in order to select a sufficiently flat, defect-free location. Surface roughness, as a component of surface morphology, was found to significantly influence both the measured nanohardness and elastic modulus of rough thin films; these properties were lower, in comparison to smooth films, by 40 and 66%, respectively [110]. In general, the reason for the development of roughness during the deposition process is inherent in the interactions between the film-forming species, process conditions and the substrate, so it would be ideal to have perfectly prepared, homogeneous, mirror-polished substrates before deposition. Furthermore, the mechanical properties are not solely affected by the chemical composition and surface quality, as the microstructure is equally important; hence heat treatments (above 1000°C) or deformation (dislocation generation and refinement of the microstructure) of the film and the substrate are necessary. This is the main reason why W is required as a substrate material, otherwise the annealing conditions are extremely limited and residual stresses are unavoidable. However, the requirements for the substrate mentioned above are very difficult to fulfil.

As a final conclusion, it can be stated that the investigated tungsten binary alloys show a great potential for the high-throughput micromechanical characterization, given that the issues of density/porosity and roughness are overcome. Further research needs to be performed in order to determine the exact influence of the alloying elements and give a gradient of micromechanical properties over the wide range of compositional concentrations.

Summary of the results

4

Conclusions

The main objective pursued during the development of this thesis was to achieve a complete fracture toughness evaluation of heavily deformed tungsten materials - foils and wires. An important topic, also addressed in the performed work, was the question of microstructural stability of the investigated materials upon annealing. Crack resistance of pure and potassium doped, ultrafine grained 100µm tungsten foils was investigated as a function of temperature in the range from -196°C to 800°C, while the influence of anisotropic microstructure was evaluated by studying three different crack orientation systems. The purpose of the work regarding drawn tungsten wires was to perform a systematic study on the effect of heat treatments and investigate how microstructural and fracture properties develop upon annealing, with a special focus on the relationship between the investigated features. A comprehensive microstructural characterization of the 150µm pure and potassium doped tungsten wires was performed through detailed analyses of the evolution of different aspects of the microstructure (nature of grain boundaries, grain shape and size, texture). Annealing in the temperature range from 900-1600°C enabled the investigation of the microstructural stability of the two materials and arising annealing phenomena - recovery, recrystallization and grain growth. Room temperature fracture toughness measurements of the wires were conducted with the emphasis on the evolution of the fracture micromechanisms in respect to different heat treatments.

Based on presented results regarding ultrafine grained tungsten foil, it can be concluded that a deformation induced grain refinement and a formation of a beneficial microstructure of thin, elongated grains is a successful recipe for obtaining a tungsten material with exceptional fracture properties - extraordinary high values of fracture toughness and reduced DBTT to about room temperature. Fracture toughness in ultrafine grained materials can be enhanced by the mechanism of delamination toughening, which is mainly controlled by features of anisotropic microstructure: small grain size in SD direction, the elongated grain shape and the <110> rotated cube deformation texture. Furthermore, fracture surface investigations reveal distinctive behaviour with an increase in temperature. The pronounced transition in failure mode was observed going from brittle, transcrystalline fracture at -196°C towards pronounced delamination at intermediate temperatures and to ductile failure at highest temperatures.

The main conclusion of the work performed on drawn tungsten wires is that the full recrystallization and grain growth in tungsten wires can successfully be shifted to temperatures higher than 1600°C by addition of potassium as a doping element. The systematic study of the influence of heat treatments on

the evolution of the grain morphology for both type of materials is crucial for the assessment of the fracture toughness of the wire, as the grain size and more importantly grain shape have a tremendous influence on the micromechanisms controlling the fracture process. The occurrence of either a brittle or a ductile response in the as-received state of both materials is a strong indication that the ductile-to-brittle transition temperature is around room temperature. Pure, annealed tungsten wires experience a tremendous deterioration of the fracture toughness with a very prominent transition of the failure mode. The observed embrittlement by annealing can be related to the loss of the fibrous, elongated microstructure. In contrast to this, the results of the annealed, doped wires demonstrate that the microstructural stability and preservation of the initial, beneficial grain structure is directly reflected in the crack resistance of the material. Predominately ductile behaviour, with characteristic knife-edge necking, is seen even after annealing at 1600°C.

In addition, a preliminary study on binary tungsten thin film alloys, produced by combinatorial magnetron co-sputtering, was conducted. The prospects of performing a high-throughput study in a wide range of compositions and determining the exact influence of a particular alloying element on the resulting properties was explored. As a final conclusion, it can be stated that the investigated tungsten binary alloys show a great potential for the micromechanical characterization, given that the necessary microstructural requirements for valuable micromechanical tests are satisfied. Further research on thin film alloys is needed for giving definitive answers regarding potential enhancements of mechanical properties by solid solutions.

The scientific research conducted within this thesis, helped to clarify that the tungsten-related problems of poor fracture resistance at low temperatures and high DBTT can be overcome by a proper microstructural design and by engineering the grain shape and size. The investigated heavily deformed ultrafine grained tungsten materials are the key structural components of the fibre-reinforced and laminated composites, which are the leading and very promising toughening strategies of tungsten-based materials. Hence, a comprehensive understanding of the fundamentals of fracture properties of foils and wires acquired in this work is an essential and very important step in the progress and success of using tungsten for structural components. As a final remark regarding the use of tungsten materials for nuclear fusion structural applications, it can be stated that future R&D activities have to be pursued towards an advantageous, purpose-designed and stabilized microstructures (the application of potassium doped tungsten material is strongly recommended).

5

Bibliography

[1]   J. P. Freidberg, *Plasma physcis and fusion energy*, Cambridge University Press, 2010.

[2]   J. Wesson, *Tokamaks*, Oxford Science Publications, 2011.

[3]   M. A. Abdou, E. L. Vold, C. Y. Gung, M. Z. Youssef and K. Shin, "Deuterium-Tritium Fuel Self-Sufficiency in Fusion Reactors", *Fusion Technol.*, vol. 9, no. 2, pp. 250–285, 1986.

[4]   J. D. Lawson, "Some Criteria for a Power Producing Thermonuclear Reactor", vol. 6, pp. 5–10, 1957.

[5]   J. Ongena, R. Koch, R. Wolf and H. Zohm, "Magnetic-confinement fusion", *Nat. Phys.*, vol. 12, no. 5, pp. 398–410, 2016.

[6]   V. Bychkov, M. Modestov and C. K. Law, "Combustion phenomena in modern physics: I. Inertial confinement fusion", *Prog. Energy Combust. Sci.*, vol. 47, pp. 32–59, 2015.

[7]   E. I. Moses, "Advances in inertial confinement fusion at the National Ignition Facility (NIF)", *Fusion Eng. Des.*, vol. 85, no. 7–9, pp. 983–986, 2010.

[8]   L. A. El-Guebaly, "Fifty years of magnetic fusion research (1958-2008): Brief historical overview and discussion of future trends", *Energies*, vol. 3, no. 6, pp. 1067–1086, 2010.

[9]   IAEA, "ITER Final Design Report", 2001.

[10]   www.iter.org, "ITER", *accessed date 2018-08-01*.

[11]   L. Bertalot *et al.*, "Fusion Power Measurement at ITER", vol. 63, no. 3, pp. 1682–1687, 2016.

[12]   G. Federici *et al.*, "Overview of EU DEMO design and R&D activities", *Fusion Eng. Des.*, vol. 89, no. 7–8, pp. 882–889, 2014.

[13]   D. Maisonnier, "European DEMO design and maintenance strategy", *Fusion Eng. Des.*, vol. 83, no. 7–9, pp. 858–864, 2008.

[14]   G. Federici *et al.*, "Plasma-material interactions in current tokamaks and their implications for next step fusion reactors", *Nucl. Fusion*, vol. 41, pp. 1967–2137, 2001.

[15]   W. Hofer and J. Roth, "Physical Processes of the Interaction of Fusion Plasmas with Solids", Elsevier Science Publishing Co Inc, p. 1996, 384AD.

[16]   I. P. E. G. on Divertor, I. P. E. G. on D. Database and I. P. B. Editors, "Chapter 4: Power and particle control", *Nucl. Fusion*, vol. 39, no. 12, pp. 2391–2469, 2002.

[17]   F. Arbeiter *et al.*, "Planned material irradiation capabilities of IFMIF-DONES", *Nucl. Mater. Energy*, vol. 16, no. July, pp. 245–248, 2018.

[18]   J. Knaster *et al.*, "IFMIF, a fusion relevant neutron source for material irradiation current status",

J. Nucl. Mater., vol. 453, no. 1–3, pp. 115–119, 2014.

[19]   M. Pérez, "The engineering design evolution of IFMIF: From CDR to EDA phase", *Fusion Eng. Des.*, vol. 96–97, pp. 325–328, 2015.

[20]   L. El-Guebaly, V. Massaut, K. Tobita and L. Cadwallader, "Evaluation of Recent Scenarios for Managing Fusion Activated Materials: Recycling and Clearance, Avoiding Disposal", vol. 2007, no. September 2007, 2007.

[21]   D. L. Smith, M. C. Billone and K. Natesan, "Vanadium-base alloys for fusion first-wall / blanket applications", *Int. J. Refract. Metals Hard Mater.*, vol. 18, no. September 2000, pp. 213–224, 2000.

[22]   S. J. Zinkle, "Advanced materials for fusion technology", *Fusion Eng. Des.*, vol. 74, no. 1–4, pp. 31–40, 2005.

[23]   S. J. Zinkle, "Challenges in Developing Materials for Fusion Technology - Past , Present and Future", vol. 1055, no. May, 2017.

[24]   S. J. Zinkle and J. T. Busby, "Structural materials for fission & fusion energy", *Mater. Today*, vol. 12, no. 11, pp. 12–19, 2009.

[25]   H. Bolt *et al.*, "Plasma facing and high heat flux materials - Needs for ITER and beyond", *J. Nucl. Mater.*, vol. 307–311, no. 1 Suppl., pp. 43–52, 2002.

[26]   M. Merola *et al.*, "ITER plasma-facing components", *Fusion Eng. Des.*, vol. 85, no. 10–12, pp. 2312–2322, 2010.

[27]   R. A. Pitts *et al.*, "A full tungsten divertor for ITER : Physics issues and design status", *J. Nucl. Mater.*, vol. 438, pp. S48–S56, 2013.

[28]   G. Janeschitz, "Plasma-wall interaction issues in ITER", *J. Nucl. Mater.*, vol. 290–293, pp. 1–11, 2001.

[29]   R. Tivey, M. Akiba, D. Driemeyer, I. Mazul, M. Merola and M. Ulrickson, "ITER R & D: Vacuum vessel and in-vessel components: Divertor Cassette", *Fusion Eng. Des.*, vol. 55, no. 2–3, pp. 219–229, 2001.

[30]   R. Wenninger *et al.*, "DEMO Exhaust Challenges Beyond ITER", in *42nd EPS conference on plasma physic*, 2015.

[31]   M. Rieth *et al.*, "Recent progress in research on tungsten materials for nuclear fusion applications in Europe", *J. Nucl. Mater.*, vol. 432, no. 1–3, pp. 482–500, 2013.

[32]   S. Wurster *et al.*, "Recent progress in R&D on tungsten alloys for divertor structural and plasma facing materials", *J. Nucl. Mater.*, vol. 442, no. 1–3, pp. 181–189, 2013.

[33]   S. V. Nagender Naigu and P. Rama Rao, *Phase Diagrams of Binary Tungsten Alloys*, Asm Intl, 1991.

[34]   E. Lassner and W.D. Schubert, *Tungsten - Properties, Chemistry, Technology of the Element, Alloys and Chemical Compounds*, New York: Kluwer Academic/Plenum Publishers, 1999.

[35]   V. Philipps, "Tungsten as material for plasma-facing components in fusion devices", *J. Nucl. Mater.*, vol. 415, no. 1, pp. S2–S9, 2011.

[36]   T. Noda, F. Abe, Y. Hiraoka, H. Araki, T. Fujii and M. Okada, "Low activation first wall materials for fusion reactors", *Fusion Eng. Des.*, vol. 10, no. C, pp. 463–467, 1989.

[37] D. Stork *et al.*, "Materials R&D for a timely DEMO: Key findings and recommendations of the EU Roadmap Materials Assessment Group", *Fusion Eng. Des.*, vol. 89, no. 7–8, pp. 1586–1594, 2014.

[38] V. P. Budaev *et al.*, "Tungsten recrystallization and cracking under ITER-relevant heat loads", *J. Nucl. Mater.*, vol. 463, pp. 237–240, 2015.

[39] G. Pintsuk, S. Antusch, T. Weingaertner and M. Wirtz, "Recrystallization and composition dependent thermal fatigue response of different tungsten grades", *Int. J. Refract. Met. Hard Mater.*, vol. 72, no. September 2017, pp. 97–103, 2018.

[40] S. J. Zinkle and N. M. Ghoniem, "Operating temperature windows for fusion reactor structural materials", *Fusion Eng. Des.*, vol. 51–52, pp. 55–71, 2000.

[41] J. Riedle, P. Gumbsch, and H. F. Fischmeister, "Fracture Studies of Tungsten Single Crystals", *Mater. Lett.*, vol. 20, pp. 311–317, 1994.

[42] J. Riedle, P. Gumbsch, and H. F. Fischmeister, "Cleavage Anisotropy in Tungsten Single Crystals," *Phys. Rev. Lett.*, vol. 76, no. 19, pp. 3594–3597, 1996.

[43] P. Gumbsch, J. Riedle, A. Hartmaier, and H. F. Fischmeister, "Controlling factors for the brittle-to-ductile transition in tungsten single crystals", *Science 80*, vol. 282, no. November, pp. 1293–1295, 1998.

[44] P. Gumbsch, "Brittle fracture and the brittle-to-ductile transition of tungsten", *J. Nucl. Mater.*, vol. 323, no. 2–3, pp. 304–312, 2003.

[45] A. Giannattasio and S. G. Roberts, "Strain-rate dependence of the brittle-to-ductile transition temperature in tungsten", *Philos. Mag.*, vol. 87, no. 17, pp. 2589–2598, 2007.

[46] E. Tarleton and S. G. Roberts, "Dislocation dynamic modelling of the brittle-ductile transition in tungsten", *Philos. Mag.*, vol. 89, no. 31, pp. 2759–2769, 2009.

[47] M. Rieth and A. Hoffmann, "Influence of microstructure and notch fabrication on impact bending properties of tungsten materials", *Int. J. Refract. Met. Hard Mater.*, vol. 28, no. 6, pp. 679–686, 2010.

[48] D. Rupp and S. M. Weygand, "Loading rate dependence of the fracture toughness of polycrystalline tungsten", *J. Nucl. Mater.*, vol. 417, no. 1–3, pp. 477–480, 2011.

[49] Q. Yan, X. Zhang, T. Wang, C. Yang and C. Ge, "Effect of hot working process on the mechanical properties of tungsten materials", *J. Nucl. Mater.*, vol. 442, no. 1–3, pp. S233–S236, 2013.

[50] B. Gludovatz, S. Wurster, A. Hoffmann and R. Pippan, "Fracture toughness of polycrystalline tungsten alloys", *Int. J. Refract. Met. Hard Mater.*, vol. 28, no. 6, pp. 674–678, 2010.

[51] D. Rupp and S. M. Weygand, "Anisotropic fracture behaviour and brittle-to-ductile transition of polycrystalline tungsten", *Philos. Mag.*, vol. 90, no. 30, pp. 4055–4069, 2010.

[52] C. Ren, Z. Z. Fang, M. Koopman, B. Butler, J. Paramore and S. Middlemas, "Methods for improving ductility of tungsten - A review", *Int. J. Refract. Met. Hard Mater.*, vol. 75, no. January, pp. 170–183, 2018.

[53] G. A. Geach and J. E. Hughes, "The alloys of rhenium with molybdenum or with tungsten and having good high temperature properties", in *Proceedings of the 2nd Plansee Seminar, Reutte*, 1955, pp. 245–253.

[54] R. I. Jaffee, C. T. Sims and J. . Harwood, "The effect of rhenium on the fabricability and ductility of molybdenum and tungsten", in *Proceedings of the 3rd Plansee Seminar, Reutte*, 1958, pp. 380–411.

[55] P. L. Raffo, "Yielding and Fracture in tungsten and tungsten rhenium alloys", *J. Less-Common Met.*, vol. 17, pp. 133 – 149, 1969.

[56] Y. Mutoh, K. Ichikawa and M. Takeuchi, "Effect of rhenium addition on fracture toughness of tungsten at elevated temperatures", *J. Mater. Sci.*, vol. 30, pp. 770–775, 1995.

[57] J. G. Booth, R. I. Jaffee and E. I. Salkovitz, "The mechanisms of the rhenium alloying effect in group VI-A Metals", in *Proceedings of the 5th Plansee Seminar, Reutte*, 1964, pp. 547 – 570.

[58] A. Gilbert, "A fractographic study of tungsten and dilute tungsten-rhenium alloys", *J. Less-Common Met.*, vol. 10, pp. 328–343, 1966.

[59] S. Wurster, B. Gludovatz and R. Pippan, "High temperature fracture experiments on tungsten-rhenium alloys", *Int. J. Refract. Met. Hard Mater.*, vol. 28, no. 6, pp. 692–697, 2010.

[60] A. Luo, D. L. Jacobson and K. S. Shin, "Solution softening mechanism of iridium and rhenium in tungsten at room temperature", *Int. J. Refract. Met. Hard Mater.*, vol. 10, no. 2, pp. 107–114, 1991.

[61] A. Luo, K. S. Shin and D. L. Jacobson, "Ultrahigh temperature tensile properties of arc-melted tungsten and tungsten-iridium alloys", *Scr. Metall. Mater.*, vol. 25, pp. 2411–2414, 1991.

[62] S. Wurster, B. Gludovatz, A. Hoffmann and R. Pippan, "Fracture behaviour of tungsten-vanadium and tungsten-tantalum alloys and composites", *J. Nucl. Mater.*, vol. 413, no. 3, pp. 166–176, 2011.

[63] M. Faleschini, H. Kreuzer, D. Kiener and R. Pippan, "Fracture toughness investigations of tungsten alloys and SPD tungsten alloys", *J. Nucl. Mater.*, vol. 367–370 A, pp. 800–805, 2007.

[64] L. Romaner, C. Ambrosch-Draxl and R. Pippan, "Effect of rhenium on the dislocation core structure in tungsten", *Phys. Rev. Lett.*, vol. 104, no. 19, pp. 1–5, 2010.

[65] R. Gröger, A. G. Bailey and V. Vitek, "Multiscale modeling of plastic deformation of molybdenum and tungsten: I. Atomistic studies of the core structure and glide of 1/2<111> screw dislocations at 0 K", *Acta Mater.*, vol. 56, no. 19, pp. 5401–5411, 2008.

[66] H. Li, S. Wurster, C. Motz, L. Romaner, C. Ambrosch-Draxl and R. Pippan, "Dislocation-core symmetry and slip planes in tungsten alloys: Ab initio calculations and microcantilever bending experiments", *Acta Mater.*, vol. 60, no. 2, pp. 748–758, 2012.

[67] L. El-Guebaly, R. Kurtz, M. Rieth, H. Kurishita and A. Robinson, "W-Based Alloys for Advanced Divertor Designs: Options and Environmental Impact of State-of-the-Art Alloys", *Fusion Sci. Technol.*, vol. 60, no. 1, pp. 185–189, 2011.

[68] Q. Wei *et al.*, "Mechanical behavior and dynamic failure of high-strength ultrafine grained tungsten under uniaxial compression", *Acta Mater.*, vol. 54, no. 1, pp. 77–87, 2006.

[69] Q. Wei and L. J. Kecskes, "Effect of low-temperature rolling on the tensile behavior of commercially pure tungsten", *Mater. Sci. Eng. A*, vol. 491, no. 1–2, pp. 62–69, 2008.

[70] J. Reiser, M. Rieth, B. Dafferner, S. Baumgärtner, R. Ziegler and A. Hoffmann, "Deep drawing of tungsten plates for structural divertor applications in future fusion devices", *Fusion Eng. Des.*,

vol. 86, no. 12, pp. 2949–2953, 2011.

[71]　J. Reiser *et al.*, "Tungsten foil laminate for structural divertor applications – Tensile test properties of tungsten foil", *J. Nucl. Mater.*, vol. 434, pp. 357–366, 2013.

[72]　J. Reiser *et al.*, "Tungsten (W) Laminate Pipes for Innovative High Temperature Energy Conversion Systems ", *Adv. Eng. Mater.*, vol. 7, no. 4, pp. 1–11, 2014.

[73]　J. Reiser, M. Rieth, B. Dafferner and A. Hoffmann, "Tungsten foil laminate for structural divertor applications – Basics and outlook", *J. Nucl. Mater.*, vol. 423, no. 1–3, pp. 1–8, 2012.

[74]　J. Reiser and M. Rieth, "Optimization and limitations of known DEMO divertor concepts", *Fusion Eng. Des.*, vol. 87, no. 5–6, pp. 718–721, 2012.

[75]　R. Neu *et al.*, "Tungsten fibre-reinforced composites for advanced plasma facing components", *Nucl. Mater. Energy*, vol. 12, pp. 1308–1313, 2017.

[76]　B. Jasper *et al.*, "Behavior of tungsten fiber-reinforced tungsten based on single fiber push-out study", *Nucl. Mater. Energy*, vol. 9, pp. 416–421, 2016.

[77]　J. Riesch *et al.*, "Chemically deposited tungsten fibre-reinforced tungsten – The way to a mock-up for divertor applications", *Nucl. Mater. Energy*, vol. 9, pp. 75–83, 2016.

[78]　J. Riesch, T. Höschen, C. Linsmeier, S. Wurster and J. H. You, "Enhanced toughness and stable crack propagation in a novel tungsten fibre-reinforced tungsten composite produced by chemical vapour infiltration", *Phys. Scr.*, vol. T159, no. 14031, pp. 1–7, 2014.

[79]　J. Neges, B. Ortner, G. Leichtfried and H. P. Stüwe, "On the 45° embrittlement of tungsten sheets", *Mater. Sci. Eng. A*, vol. 196, no. 1–2, pp. 129–133, 1995.

[80]　"ASTM E399-90, Standard test method for plane-strain fracture toughness of metallic materials", in *Annual Book of ASTM Standards*, Philadelphia (PA):American Society of Testing and Materials, 1997.

[81]　A. Hohenwarter, C. Kammerhofer and R. Pippan, "The ductile to brittle transition of ultrafine-grained Armco iron: An experimental study", *J. Mater. Sci.*, vol. 45, no. 17, pp. 4805–4812, 2010.

[82]　J. Reiser, M. Rieth, B. Dafferner and A. Hoffmann, "Charpy impact properties of pure tungsten plate material in as-received and recrystallized condition (1 h at 2000°C (2273K))", *J. Nucl. Mater.*, vol. 442, no. 1–3, pp. S204–S207, 2013.

[83]　J. Stampfl, S. Scherer, M. Berchthaler, M. Gruber and O. Kolednik, "Determination of the fracture toughness by automatic image processing", *Int. J. Fract.*, vol. 78, pp. 35–44, 1996.

[84]　J. Stampfl, S. Scherer, M. Gruber and O. Kolednik, "Reconstruction of surface topographies by scanning electron microscopy for application in fracture research", *Appl. Phys. A Mater. Sci. Process.*, vol. 63, no. 4, pp. 341–346, 1996.

[85]　S. Suwas, R. K. Ray and R. K. R. Satyam Suwas, *Crystallographic Texture of Materials*, 2014.

[86]　M. R. Ripoll and J. Očenášek, "Microstructure and texture evolution during the drawing of tungsten wires", *Eng. Fract. Mech.*, vol. 76, no. 10, pp. 1485–1499, 2009.

[87]　W. F. J. Hosford, "Microstructural changes during deformation of [011] fiber textured metals", *Trans. Metall. Soc. AIME*, vol. 230, pp. 12–15, 1964.

[88]　F. J. Humphreys and M. Hatherly, *Recrystallization and related annealing phenomena*, Elsevier Ltd, 2004.

[89]   N. Hansen and R. A. Vandermeer, "Recovery, Recrystallization, and Grain Growth", *Encycl. Condens. Matter Phys.*, pp. 116–124, 2005.

[90]   D. B. Snow, "The recrystallization of commercially pure and doped tungsten wire drawn to high strain", *Metall. Trans. A*, vol. 10, no. 7, pp. 815–821, 1979.

[91]   O. Horacsek, "Properties and failure modes of incandescent tungsten filaments", *IEE Proc. A Physical Sci. Meas. Instrumentation, Manag. Educ. Rev.*, vol. 127, no. 3, pp. 134–141, 1980.

[92]   S. N. Mathaudhu, A. J. deRosset, K. T. Hartwig and L. J. Kecskes, "Microstructures and recrystallization behavior of severely hot-deformed tungsten", *Mater. Sci. Eng. A*, vol. 503, no. 1–2, pp. 28–31, 2009.

[93]   A. Alfonso, D. Juul Jensen, G. N. Luo and W. Pantleon, "Recrystallization kinetics of warm-rolled tungsten in the temperature range 1150-1350 °C", *J. Nucl. Mater.*, vol. 455, no. 1, pp. 591–594, 2014.

[94]   E. Pink and L. Bartha, *The metallurgy of doped/non-sag tungsten*. Elsevier Science Publishers, 1989.

[95]   C. L. Briant, "On the Formation of Potassium Bubbles in Tungsten Rod", vol. 20, no. January, pp. 179–184, 1989.

[96]   C. L. Briant, "Potassium bubbles in tungsten wire", *Metall. Trans. A*, vol. 24, no. 5, pp. 1073–1084, 1993.

[97]   E. O. Hall, "The deformation and aging of mild steel. III: Discussion of results", *Proc. Phys. Soc. Lond. B*, vol. 64, pp. 747–753, 1951.

[98]   N. J. Petch, "The Cleavage Strength of Polycrystals", *J. Iron Steel Inst.*, vol. 174, pp. 25–28, 1953.

[99]   J. Toribio and F. J. Ayaso, "Anisotropic fracture behaviour of cold drawn steel : a materials science approach", *Mater. Sci. Eng.*, vol. 343, pp. 265–272, 2003.

[100]   A. Hohenwarter *et al.*, "Ultra-strong and damage tolerant metallic bulk materials: A lesson from nanostructured pearlitic steel wires", *Sci. Rep.*, vol. 6, no. May, pp. 1–10, 2016.

[101]   S. Leber, J. Tavernelli, D. D. White and R. F. Hehemann, "Fracture modes in tungsten wire", *J. Less-Common Met.*, vol. 48, no. 1, pp. 119–133, 1976.

[102]   P. Schade, "Wire drawing failures and tungsten fracture phenomena", *Int. J. Refract. Met. Hard Mater.*, vol. 24, no. 4, pp. 332–337, 2006.

[103]   P. Zhao *et al.*, "Microstructure, mechanical behaviour and fracture of pure tungsten wire after different heat treatments", *Int. J. Refract. Met. Hard Mater.*, vol. 68, no. June, pp. 29–40, 2017.

[104]   M. R. Ripoll, S. M. Weygand and H. Riedel, "Reduction of tensile residual stresses during the drawing process of tungsten wires", *Mater. Sci. Eng. A*, vol. 527, no. 13–14, pp. 3064–3072, 2010.

[105]   J. G. Sevillano and D. González, "Heterogeneous Deformation and Internal Stresses Developed in BCC Wires by Axisymmetric Elongation", vol. 550, pp. 75–84, 2007.

[106]   A. Ludwig, R. Zarnetta, S. Hamann, A. Savan and S. Thienhaus, "High-Throughput Experimentation Methods", *Int. J. Mat. Res.*, vol. 99, no. November, pp. 1144–1149, 2008.

[107]   V. Maier, K. Durst, J. Mueller, B. Backes, H. Höppel and M. Göken, "Nanoindentation strain-rate

jump tests for determining the local strain-rate sensitivity in nanocrystalline Ni and ultrafine-grained Al", *J. Mater. Res.*, vol. 26, no. 11, pp. 1421–1430, 2011.

[108] C. Motz, T. Schöberl and R. Pippan, "Mechanical properties of micro-sized copper bending beams machined by the focused ion beam technique", *Acta Mater.*, vol. 53, no. 15, pp. 4269–4279, Sep. 2005.

[109] S. Wurster, C. Motz and R. Pippan, "Characterization of the fracture toughness of micro-sized tungsten single crystal notched specimens", *Philos. Mag.*, vol. 92, no. 14, pp. 1803–1825, 2012.

[110] W. G. Jiang, J. J. Su and X. Q. Feng, "Effect of surface roughness on nanoindentation test of thin films", *Eng. Fract. Mech.*, vol. 75, no. 17, pp. 4965–4972, 2008.

Bibliography

6

List of appended publications

Publication A
V. Nikolić, S. Wurster, D. Firneis, R. Pippan
Improved fracture behaviour and microstructural characterization of thin tungsten foils
Nuclear Materials and Energy 9 (2016) 181-188

Publication B
V. Nikolić, S. Wurster, D. Firneis, R. Pippan
Fracture toughness evaluation of UFG tungsten foil
International Journal of Refractory Metals and Hard Materials 76 (2018) 214-225

Publication C
V. Nikolić, J. Riesch, R. Pippan
The effect of heat treatments on pure and potassium doped drawn tungsten wires: Part I – Microstructural characterization
Accepted for publication in Materials Science and Engineering A (2018),
DOI: 10.1016/j.msea.2018.09.027

Publication D
V. Nikolić, J. Riesch, M.J. Pfeifenberger, R. Pippan
The effect of heat treatments on pure and potassium doped drawn tungsten wires: Part II – Fracture properties
Accepted for publication in Materials Science and Engineering A (2018),
DOI: 10.1016/j.msea.2018.09.029

Publication E
V. Nikolić, S. Wurster, A. Savan, A. Ludwig, R. Pippan
High-throughput study of binary thin film tungsten alloys
International Journal of Refractory Metals and Hard Materials 69 (2017) 40-48

Publication F
V. Nikolić, S. Wurster, R. Pippan
*Capabilities and limitations of tungsten-based materials (*as a chapter of a review paper *Development of advanced high heat flux and plasma-facing materials)*
Nuclear Fusion 57 (2017) 092007 (60pp)

Remark

In the appended papers, I, Vladica Nikolić, performed all experiments, data analyses and was primary author with the following exceptions:

- Daniel Firneis and Stefan Wurster supported the construction of the experimental setup and conduction of fracture experiments for Publications A and B.
- Stefan Wurster contributed to Publications A, B and F with helpful advices regarding analysis and interpretation of the results.
- Daniel Firneis performed the hardness measurements for Publications A and C.
- Manuel Pfeifenberger performed the pre-crack introduction by femtosecond laser for preparation of the samples used in Publication D.
- Alan Savan from the Institute for Materials at Ruhr University produced the binary tungsten film alloys, which were studied in Publication E.
- Reinhard Pippan is acknowledged for his expert guidance and contribution to all papers by providing basic ideas for publications along with helpful discussions and support during their preparation.

A

Improved fracture behaviour and microstructural characterization of thin tungsten foils

Vladica Nikolić [a], Stefan Wurster[b], Daniel Firneis[a], Reinhard Pippan[a]

[a] Erich Schmid Institute of Materials Science of the Austrian Academy of Sciences, Leoben, Austria

[b] Department of Materials Physics, Montanuniversität Leoben, Leoben, Austria

Abstract

This study is focused towards the development of the technique for investigating the fracture behaviour of 100 µm thick rolled tungsten foils, with a purity of 99.97 %. Electron backscatter diffraction (EBSD) scans reveal that the grains are elongated along the rolling direction of the foil, which has a very strong {100}<011> texture. The test specimens were fabricated by electrical discharge machining (EDM) and cracks were initiated by consecutively using a diamond wire saw, a razor blade and a focused ion beam (FIB) workstation. Fracture experiments were performed at temperatures from -196 °C to 800 °C. The investigation of fracture appearance shows an improved behaviour and significantly higher values of conditional fracture toughness K_q compared to bulk W-materials, which can be related to a higher degree of deformation during the production process. A high toughness at room temperature (RT) and 200 °C, slowly decreases when approaching the highest testing temperature of 800 °C. The most significant result reveals that the ductile to brittle transition temperature (DBTT) is around RT, which is an extraordinary result for any tungsten material. The fracture surfaces, investigated with a scanning electron microscope (SEM), show a transition from cleavage fracture at liquid nitrogen temperature, through pronounced delamination within the foil plane at ambient temperatures to ductile fracture at the highest testing temperatures.

Keywords: Thin tungsten foil, Fracture toughness, High and low temperature fracture experiments, LEFM, EBSD analysis, SEM analysis

A.1. Introduction

Tungsten (W) is a metal with an excellent combination of high temperature properties, such as high erosion resistance, low vapour pressure and high strength at elevated temperatures. It also has the highest melting point of all metals (T_m=3422°C) and other superior thermal properties: good thermal shock resistance and high thermal conductivity. These exceptional qualities qualify this metal for many high temperature applications, like e.g. in a future fusion reactor. Extensive research on divertor design concepts is directed towards the use of various tungsten materials and its composites for different divertor applications, making tungsten one of the main armour and heat sink materials candidates [1], [2]. A divertor is one of the key in – vessel components of a fusion reactor, responsible for power exhaust and cleaning the plasma from He and impurities i.e. various particles coming from the first wall. Therefore, these reactor parts will be subjected to a very high heat flux loads: in a normal scenario 10MW/m^2 is expected, having peaks of up to 20MW/m^2 in off normal events, as a consequence of different plasma instabilities [3,4]. For such a challenging and extreme thermal application, tungsten was a natural choice as a candidate material.

When thinking of using tungsten as a structural part for the divertor region, its main disadvantage – inherent brittleness - plays a decisive role. Tungsten shows low fracture toughness at low temperature and like other body cantered cubic (bcc) metals, it has a transition from brittle fracture at low temperatures to ductile and tough behaviour at high temperatures. The problem is that the transition temperature is relatively high (well above ambient temperatures), additionally complicating the machining at room temperature (RT). Several ductilization strategies have been proposed in the attempt of overcoming the main problem of tungsten and improving its fracture behaviour, including toughening tungsten by synthesis of i) solid solutions, ii) nanostructured materials and iii) various tungsten composites. Tungsten laminates synthesized of ultra – fine grained tungsten foil [5,6] is an approach towards making tungsten – based materials more ductile and expanding its application from armour to structural materials. Some divertor concepts being currently investigated might use He as a coolant and would require the use of W in form of cooling pipes, which will be exposed to 600°C and 100bar [7]. Typical manufacturing processes like extrusion or drilling of holes in rods are challenging and additionally, in this way, the alignment of elongated grains i.e. the preferred crack propagation path would be coinciding with the expected fracture direction of the pressurized pipe. Therefore, the option of synthesizing the structural tungsten pipe by rolling up and joining of tungsten foils seems to be very promising, since the best case scenario of microstructural design, where the direction of low fracture toughness follows the contour of the pipe, can be obtained. The 100μm thick foil used for forming of pipes shows some extraordinary mechanical properties, extending the foil's RT ductility to a ductile bulk material [8].

The fracture behaviour of tungsten materials has been studied for decades, but full understanding of underlying fracture processes, greatly influenced by different parameters, such as microstructure, has not been completely realized. Extensive studies of the fracture resistance of tungsten single crystals were performed in the nineties [9,10], revealing that {100} planes are primary cleavage planes with <110> being the preferred crack propagation directions. In addition, the strong loading rate dependence

of the ductile to brittle transition temperature (DBTT), in particular at elevated temperatures, confirms that the transition is controlled by dislocation mobility [9]. In contrast to the good descriptions of fracture processes in single crystals, the comprehensive experimental study of tungsten materials with more complex microstructures i.e. industrially produced polycrystalline W is still not complete. However, this could be essential in order to identify ways of improvement and to develop microstructural design concepts with optimized fracture properties.

In the case of tungsten, factors like microstructure, grain size, grain shape, texture, etc. greatly influence the resulting mechanical properties. It has been shown that there is a strong correlation between manufacturing history (sintering, rolling, swaging, hot/cold work...) and the resulting material's microstructure and mechanical properties [11]. Among various parameters affecting the fracture toughness, the established microstructure during production steps plays a decisive role for the resulting failure mode, leading to the anisotropic behaviour of deformed (worked) tungsten [12,13]. A pancake – like microstructure of tungsten plate materials is favourable for good toughness in two out of three possible testing directions and when decreasing the thickness of the material, a shift of DBTT to lower temperatures is also observed [14]. Furthermore, it was shown that low temperature rolling of commercially pure tungsten enhances its strength and ductility [15]. This leads to the conclusion that a thinner plate, which experienced a higher degree of cold work has a more beneficial microstructure, having smaller grains and higher amount of mobile edge dislocations.

So questions that need to be answered are: "How do fracture properties change if tungsten plate material is submitted to even higher degrees of rolling (deformation) resulting in commercially available 100 µm thin tungsten foil? Are the values of fracture toughness higher in comparison to other tungsten materials? What happens to the DBTT in case of such highly deformed foils?" It has already been shown that such a material behaves ductile in a tensile experiment at RT and when synthesized in laminated plates and tested with Charpy impact test, the DBTT can be reduced by 300°C [8]. As mentioned in previous paragraphs, in some He – cooled divertor concepts the use of structural, pressurized W cooling pipe is being investigated where a ductile laminated pipe can be made of 100µm ultra – fine grained W foil [7]. Therefore, from a materials design aspect, it is extremely important to determine fracture toughness values and investigate the effect of various testing conditions on the variation of fracture behaviour of such a tungsten foil used as a base material in laminated tungsten composites. The aim of this work was to develop a testing procedure for evaluating fracture toughness on a 100µm thin tungsten foil, investigating how variation of testing temperature affects the resulting fracture process.

A.2. Materials and Microstructure

The fracture mechanical testing was performed on a 100µm thin unalloyed tungsten foil, a standard material that is commercially available and produced by Plansee SE, Reutte, Austria. The tungsten plate is manufactured via the powder metallurgical route and after sintering, it is submitted to hot and cold rolling processes. As a result, a thin foil is obtained having elongated grains along the rolling direction. The dimension of grains in foil thickness direction is in ultra – fine grained regime having average grain diameter of less than half of micron. Production details regarding degree of deformation,

temperatures of hot and cold rolling and stress relieve annealing conditions are not provided by the manufacturer. The guaranteed purity of the material is 99,97% and impurities content information can be found elsewhere [16].
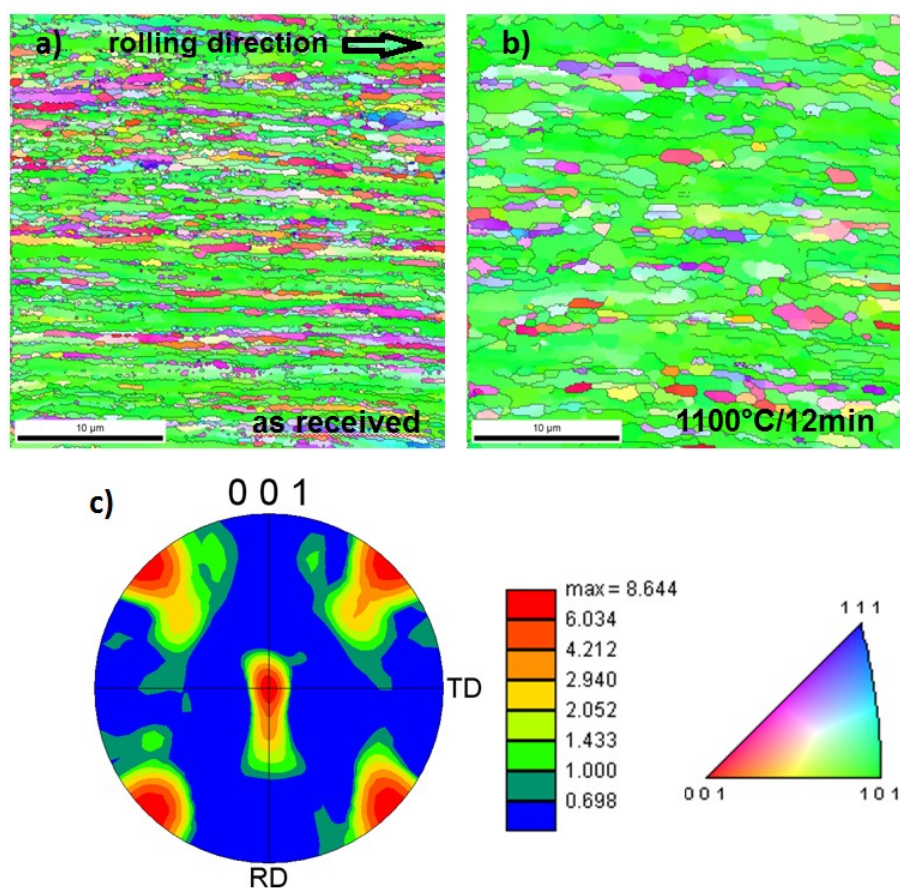
Figure A.1. *a) Inverse Pole Figures (IPF) of pure 0.1mm tungsten foil in as received condition. "Stack of pancake" microstructure is seen, with elongated grains along the rolling direction (from left to right). High angle grain boundaries with a misorientation >15° are plotted in black. b) IPF of a foil annealed at 1080°C for 12minutes (chapter 4.1.) c) Pole Figure (PF) calculated from a) showing orientation of {001} planes with respect to the sample reference frame (RD is the reference direction of the EBSD – scan and the rolling direction; TD is the transverse direction of both EBSD – scan and the rolling process); Colour scale bar quantifies the strength of the shown texture. Colour coded unit triangle representing <100>, <110> and <111> crystallographic directions.*

In order to evaluate the microstructure and texture of the foil, a scanning electron microscope (SEM) (Leo 1525, Zeiss) with an electron backscatter diffraction (EBSD) detector was used. During preparation of the tungsten foil for EBSD analysis by embedding in hard compound and mechanical grinding and polishing, delamination along the grain boundaries occurs. To prevent this, ion polishing (Hitachi E-3500 Cross Section Polisher) of the desired cross section was performed. Resulting smooth surfaces across the entire thickness of the sample were suitable for following SEM/EBSD analyses. Evaluation of the obtained scans was made with Orientation Imaging Microscopy (OIM) software.

EBSD orientation imaging map of a pure W foil in as – received condition can be seen in Figure A.1.a, with distinctive elongated grains going along the rolling direction (from left to right) forming a

typical ''pancake'' like microstructure. Such an appearance is a direct consequence of a high degree of deformation during production steps. Average grain size given by the ASTM number, calculated by enforcing the average grain area, is 19,6. The aspect ratio, one of the measures of the grain shape, is defined as ratio of the length of the minor axis divided by the length of the major axis. In the case of as received materials, average aspect ratio of grains is 0,45. Microstructure of a W foil after being exposed to 1080°C for 12 minutes is shown in the scan in Figure A.1.b and will be further discussed in Chapter 4.1. The results of the EBSD scans can be presented in Pole Figures (PF) shown in Figure A.1.c. It can be seen that a 0.1mm tungsten foil has a very strong texture in {100} <011>, indicating that the preferred cleavage planes {100} form an angle of 45° with the rolling direction. This result corresponds to other investigations [17] and such a texture established, during cold work by grain rotation, defines a saturation condition, meaning it does not change by further deformation [18].

A.3. Experimental Procedure

A.3.1. Sample Preparation

In this study, the main goal was to determine fracture toughness of a 0.1mm thin foil, which at the initial stage required designing and manufacturing a suitable experimental setup. Since the thickness of the foil and its geometry are not the standard one as e.g. given in ASTM E399 [19], optimization of sample preparation, crack initiation and brazing process had to be performed. The preparation procedure can be summed in the following three steps:

- **Cutting**
  The test specimens were fabricated out of the commercially available tungsten sheet with dimensions of 180x100x0.1mm^3 with the rolling direction being parallel to the 100mm side of the sheet. Electrical discharge machining (EDM) was used for cutting and the specimen size is 20x5x0.1mm^3. In order to examine the influence of the microstructure on the anisotropy of mechanical properties, it is important to know the direction of cutting in respect to the rolling direction of the sheet i.e. the resulting direction of the pre-crack. After cutting, all the samples were washed in isopropanol and acetone using ultrasonic bath. To facilitate proper mounting and testing, samples need to be joined to steel holders, which will then be attached to the testing device. EDM was once again used for cutting the holders in the size of 15x15x3mm^3, with a 5mm slit for brazing the samples into the holders.

- **Crack Initiation**
  In order to perform fracture mechanical testing, it is necessary to produce a sharp pre-crack at the tip of a machined notch. An attempt of fatigue pre-cracking was made by means of cyclic loading, but this standard method did not lead to successful results. Therefore, following three step procedure was performed on a 100μm foil. Initially, a very blunt notch made by a *diamond wire saw* (the wire diameter is 0.3mm) was further *razor blade* refined where the thickness of the

razor blade is about 0.1mm. In the end, a sharp pre-crack was initiated with a *Focused Ion Beam* workstation (Leo 1540, Zeiss), with the following settings: A coarse line cut was made across the whole foil thickness with 20nA for 45min. The resulting length of a FIB pre - crack, measured from the notch root, is of ~20 μm. FIB pre-cracking is a crucial step so that the length of the introduced crack is in the size regime of the notch root radius. Satisfying this requirement ensures that the pre – crack is sharp enough to determine true materials fracture properties. In Figure A.2., SEM images show the distinctive regions of mentioned steps indicated by different colours (green – wire cut, blue – razor blade refinement, red – FIB pre-crack). The final length of the pre-crack was between 25-45% of the width of the foil. In the results presented here, all the samples were produced with the pre-cracks being normal in respect to the rolling direction of the tungsten sheet.

- **Brazing**

  Joining of the pre-cracked foil to the steel holders was done in a brazing process i.e. by melting the metallic interlayer between them. It is very important to choose an appropriate interlayer so that the formation of brittle intermetallic compounds is avoided. Copper (T_m=1085°C) and silver (T_m=960°C) are good options having excellent wettability on the tungsten foil, with no diffusion into the tungsten [20]. Additional advantages are relatively low melting temperatures, ensuring that the tungsten foil remains in nearly as received microstructural state and that no recrystallization occurs during the brazing process. The time of the highest temperature should be kept as low as possible. The influence of the sample preparation on the microstructure (and therefore resulting mechanical properties) of the tungsten foil will be addressed in chapter 4.1.

The steel holders were cut from one side (5mm slit) where the tungsten foil was placed between 2 brazing foils. The pre-brazed sample was then fixed onto specially designed brazing holder and then placed in the vacuum chamber of the furnace. Brazing process was performed in high vacuum (<10^{-4}mbar) using two different brazing materials, with a thickness of 100μm each:

- ***Eutectic silver copper foil*** (72wt% Ag and 28wt% Cu): brazing took place at 780°C, for 20min with subsequent furnace cooling and produced samples were used for testing at -196°C, RT and 200°C.

- ***Pure copper foil***: brazing took place at 1080°C, for 12min with subsequent furnace cooling and produced samples were used for testing at 400°C, 600°C and 800°C.

The final appearance of a prepared sample can be seen in Figure A.3.
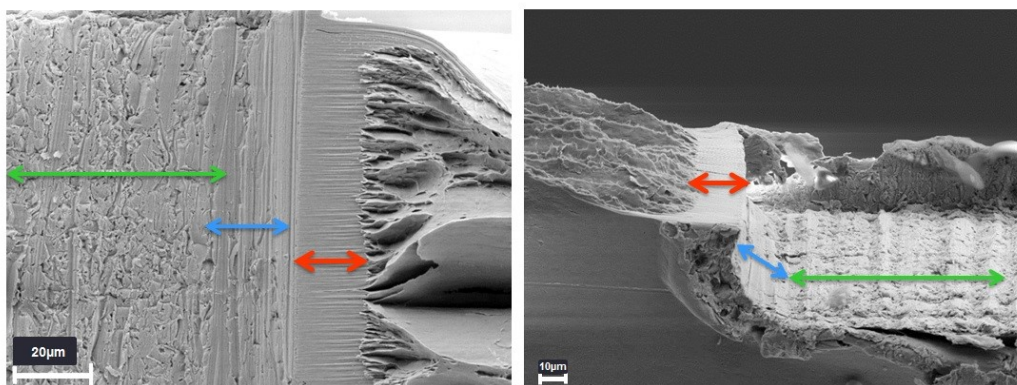
Figure A.2. *SEM images of fracture surfaces showing introduced cracks with diamond wire saw cut (green), razor blade sharpening (blue) and FIB cut (red), a) top view of fracture surface b) an inclined view of the fracture surface.*

Figure A.3. *Fracture experiment sample, tungsten foil pre – cracked with diamond wire saw, razor blade and FIB and then brazed between two steel holders.*

A.3.2. Mechanical Testing

Fracture mechanical tests were performed on a universal tensile testing device (Zwick), which is furnace and vacuum chamber equipped. Experiments were done in atmosphere at -196°C (liquid nitrogen), room temperature and 200°C and for all elevated temperatures (up to 800°C) the vacuum chamber was used. Pressures of 10^{-5} mbar can be reached, ensuring that oxidation of the material is avoided at high temperatures. During heating, pressure increases but does not exceed 10^{-3} mbar. The crosshead speed of the device was constant for all experiments and set to 0.4mm min^{-1}. Along with the temperature, measured with thermocouples placed in the vicinity of the crack tip, force and time were recorded during the experiment.

In general, conditional fracture toughness is calculated with conditional load P_q which is obtained from the load displacement curve in the following way: a 5% secant line is constructed from the origin with the slope equal to 95% of the initial linear part of the load displacement record and the P_q is identified from the intersection point. P_q is equal to the maximum load that the specimen could sustain P_{max} only if the brittle fracture occurred in linear load – displacement regime. In other words, in this case specimen fails completely before achieving 5% nonlinearity.

From the maximum applied load P_{max} and the measured crack length a, conditional fracture toughness K_q can be calculated according to the following equation for a single edge notched tension specimen [21]:

$$K_q = \frac{P_{max}}{A}\sqrt{\pi a} \cdot (1.12 - 0.231\frac{a}{W} + 10.55\left(\frac{a}{W}\right)^2 - 21.72\left(\frac{a}{W}\right)^3 + 30.39\left(\frac{a}{W}\right)^4)$$

In order to determine a valid value of K_q certain requirements need to be fulfilled. According to ASTM E − 399 [19], the size of the sample is critical and the condition is given by a, B and (W-a) > 2.5(K_{IC}/σ_{Ys})^2, where σ_{Ys} is the 0,2% offset yield strength of the material for the temperature of the test, *B* is the thickness of the sample, *a* is the notch length and *(W-a)* is the ligament length. In addition to requirements related to dimension of the specimen, the ratio P_{max}/P_q should not exceed 1.10. The validity of the measured fracture toughness values will be further addressed in chapter 4.2.

A.4. Results and Discussion

A.4.1. Influence of the sample preparation

It is well known that fine grained materials are very sensitive to annealing and recrystallization phenomena. Due to the high amount of stored energy in the material, which is present in the form of grain boundaries and dislocations, the microstructure tends to change. Once a beneficial microstructure is obtained, it is crucial to stabilize it at elevated temperatures. Thermal treatments affect the underlying microstructure, leading to recovery and subsequent recrystallization of the material, which would have an enormous effect on the resulting mechanical properties. For tungsten materials in fusion application it is very important to precisely know at what temperature recrystallization happens, as the material properties deteriorate and this sets the higher temperature operating limit [22]. Recovery refers to changes in material's microstructure prior to recrystallization and it easily occurs in worked materials having high concentration of defects. During this process, the stored energy of the material is lowered by e.g. the movement and arrangement of dislocations. Recovery happens gradually, with no clear beginning or end, leading to homogeneous microstructural appearance. In contrast to that, recrystallization involves the formation of new grains, which might be unevenly distributed over the specimen separating the microstructure into recrystallized and not recrystallized part. New grains formed during recrystallization have individual lattice orientation, which is independent of the one resulting from the cold work during the manufacturing process. Even though brazing of the test samples was done at temperatures below $T_{rec.}$ for tungsten (0.4*T_{melt} ~1200°C), it is important to check whether the short exposure of the material to elevated temperatures had an impact on its microstructure and resulting mechanical properties. Microhardness measurements were performed on the brazed foil and microstructure was evaluated with the means of EBSD.

Vickers hardness measurements, with an applied load of 4,9N, were performed on a W foil in the as

received state and after brazing at 780°C (for 20min) and 1080°C (for 12min). Under the same conditions, 10 indentations were made for each material in all the different investigated states. The unbrazed foil has a hardness of (598±5,7) HV0.5 and after being heated at 780°C, the value is nearly constant with microhardness of (590±5,4) HV0.5. The lower temperature brazing with AgCu foil is too short to have an impact on the microstructure, which can be observed in nearly constant value of the microhardness.12 minutes of brazing at 1080°C influences the hardness and a slight decrease down to (515±8,8) HV0.5 is observed. It is therefore important to examine and compare the microstructure of these materials, to establish if significant changes of grains occurred which might have an influence on the resulting fracture toughness.

In Figure A.1a and b, a comparison between EBSD scans of tungsten foil in as received state and after the 1080°C brazing can be seen. The typical microstructure with elongated grains along the rolling direction is clearly seen in both scans and high angle grain boundaries with a misorientation >15° are indicated with black lines. The measured decrease in hardness values can be related to certain microstructural changes for example by recovery. Brazing at 1080°C for 12minutes is linked to rounding of the grains and their growth in foil thickness direction, the typical pancake like microstructure is still existent but less pronounced. The number of grains across the foil thickness reduces, having average grain diameter of 1 micron. In comparison to the as received material, average grain size given by the ASTM number decreases to 17,3 and aspect ratio is 0,4. So, it can be noted that even the short temperature exposure during brazing exhibits some microstructural alterations, but mostly related to minor size and shape changes. Brazing at these temperatures did not lead to recrystallization process, which would have a noteworthy impact on the resulting fracture behaviour. Additionally, it was shown that for a more prominent decrease of microhardness [23] and significant effect on the mechanical properties, annealing at these temperatures has to take place for at least 1h.

A.4.2. Fracture toughness

Figure A.4 shows the determined fracture toughness as a function of the testing temperature for a crack system where the introduced notch is perpendicular to the rolling direction of the foil. Each symbol corresponds to one experiment at particular temperature. Samples tested at liquid nitrogen failed in a brittle manner with the conditional fracture toughness K_q= 10 MPam$^{1/2}$, which is the lowest obtained value in these experiments. At ambient temperatures, the same material tested under the same conditions shows different fracture behaviour, with values of fracture toughness in a range between 20-110 MPam$^{1/2}$. Such a scatter of data (observed only at this temperature) as well as a rapid increase of fracture toughness with temperature is an indication of a transition between different fracture regimes. The ductile to brittle transition temperature (DBTT) was defined here as the temperature where a large increase in fracture toughness and a change of the fracture surface (no transcrystalline fracture anymore) takes place. Apart from substantial difference in critical maximum load that sample could sustain before failure (and therefore the resulting fracture toughness), no significant differences in the load displacement curves were observed for RT experiments. In both cases of low and high values of K_q, a catastrophic failure occurred sudden without previous stable crack growth. With a further increase

in testing temperature, K_q initially increases but for experiments performed at elevated temperatures, 200°C and above, the values of fracture toughness slowly decrease. Performing experiments on samples with the crack introduced within the foil plane, should clarify whether a general trend of decrease of K_q can be related with an increase in in–foil toughness at elevated temperatures.
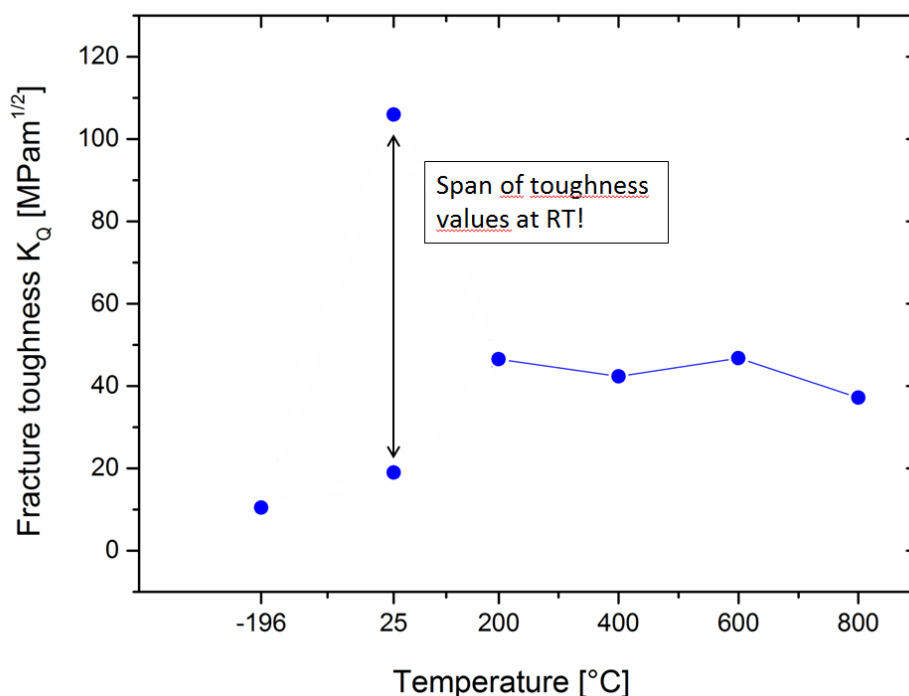

Figure A.4. *Conditional fracture toughness as a function of testing temperature for samples with crack orientation perpendicular to the rolling direction. Conditional fracture toughness K_q was calculated from the maximal applied force when pronounced crack growth occurred. Scatter of data observed around RT and the change in the fracture behaviour, from transcrystalline to lamellar fracture, indicates the existence of DBTT at around RT.*

In addition to the thin foils fracture investigation, an attempt of a study of a standard tungsten plate material with 100μm thick dimensions was made. Initial idea was to use the same experimental technique on a tungsten plate material and identify whether obtained high values of fracture toughness of a tungsten foil are indeed representing a true materials property. A plate material was chosen (over a rod) since it shows good toughness in two out of three possible testing directions [12,13]. From a bulk tungsten material, with a pancake – like microstructure, specimens with a size of $20x5x0.5mm^3$ were cut with EDM. Final thickness of 100μm was achieved with polishing, resulting in the same sample size and geometry as the thin foil specimens. The next step of notching and introducing a pre – crack was unsuccessful and all the samples failed during this process. 100μm thick tungsten plate is too brittle at room temperature, resulting in cracking under small loads applied during sample handling. Therefore, testing such a material was not possible and an exact value of K_q was not obtained. However, sample failing during preparation procedure can be linked to weak fracture behaviour which is in a correspondence with analysed fracture surfaces of cracked samples (Figure A.5). In the case of all failed samples, transcrystalline cleavage is observed which can be related to low values of K_q. In comparison with the microstructure of tungsten foil, grains of the plate material are significantly larger.

All of the observations in regards to tungsten plate material are an indication of extraordinary fracture properties of tungsten foils.
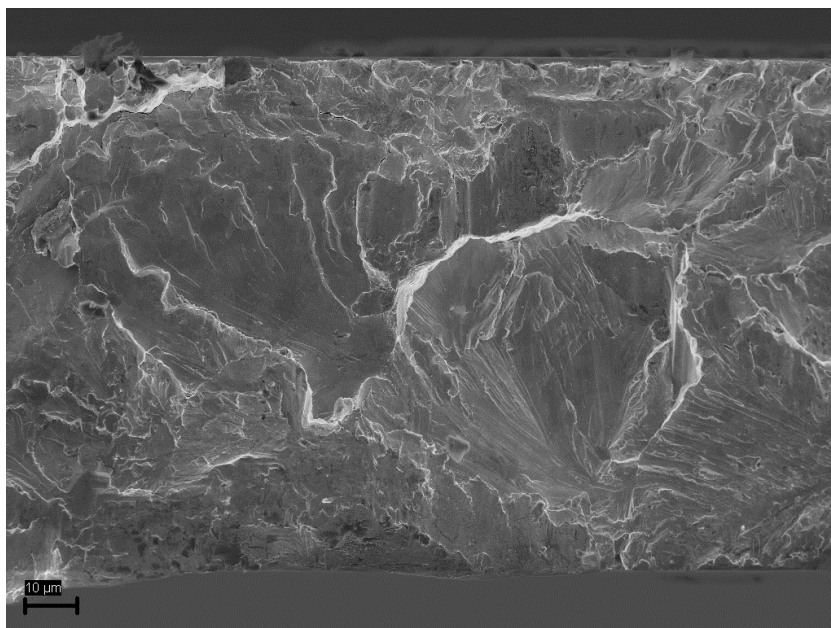

Figure A.5. *Top view of scanning electron micrograph of fracture surface of tungsten plate material polished to thickness of 100µm and failed during sample preparation. Brittle transcrystalline fracture surface can be seen.*

The investigation of the fracture behaviour of 100µm thin W foils shows an improved behaviour and higher values of K_q compared to bulk W-materials, which can be related to a higher degree of deformation. The resulting pancake – like microstructure, strong texture and small grain size in thickness direction greatly influence resulting fracture properties. As reported before, crystallographic and grain shape anisotropy play a decisive role in the fracture process of polycrystalline tungsten [24]. Therefore, it is necessary to determine whether similar anisotropic behaviour can be observed in the case of tungsten foils. Does a difference in the amount of grain boundaries in front of a propagating crack for different testing direction affect the resulting fracture behaviour? This issue will be referred in a following publication where the influence of the crack initiation direction – in respect to rolling direction, will be taken into account.

According to linear elastic fracture mechanics (LEFM), in order to obtain a valid value of fracture toughness K_{IC}, there are certain requirements regarding the thickness of the sample, ligament and crack length. Since K_{IC} loses validity with increased tough behaviour, it is very important to determine the limit of validity. The yield strength for the following calculations was taken from [8], where tensile properties of the same foil were investigated at RT (σ_{Ys}=2000MPa) and 600°C (σ_{Ys}=1100MPa). Based on these results, yield stresses for all the other temperatures were linearly extrapolated. K_q values of the samples tested in liquid nitrogen and room temperature fulfil the above mentioned criterion and represent a valid $K_{IC.}$ In case of 200°C and high toughness room temperature experiments, validity requirement is fulfilled in respect to ligament and crack length, but not the thickness. In this way, calculated K_q is thickness dependent fracture toughness. With an increase in testing temperature, the specimens are too small to accommodate the plane strain conditions and requirements of LEFM are not satisfied. Nevertheless,

calculated conditional fracture toughness values K_q given above give a lower limit. The open question of true value of fracture toughness in the tough region will be addressed in the upcoming work, where a more geometry independent value of toughness will be determined, based on crack tip opening displacement (CTOD) analyses. In addition to requirements related to dimension of the specimen, the ratio P_{max}/P_q should not exceed 1.10. This condition was met for the tests performed up to 200°C.

A.4.3. Fractographic analysis

A scanning electron microscope was used in the evaluation of the fracture surfaces of every tested sample. A comparison of various fracture appearances can be seen in Figure A.6, where a top view of a cracked surface is shown with respect to different testing temperatures. The foil tested in liquid nitrogen (-196°C) shows a classical transcrystalline fracture, the aligned grains are visible as horizontal lines (Figure A.6a). So, at low temperatures the sample fractures in a classical brittle manner which corresponds to a low value of K_{Ic} (see 4.2). With an increase in testing temperature the fracture mode changes significantly and for the test performed at 200°C the sample has strongly delaminated surfaces with a lot of small crack openings (Figure A.6b). Such a fan – out topography is a direct consequence of the characteristic microstructure – ''flat stack of pancakes''.

Equivalent to the RT scatter of data, the fracture surfaces also vary. In some cases, the samples had a fracture surface showing cleavage fracture (low K_q) and sometimes a very strong delamination was observed, which matches with higher values of fracture toughness. For temperatures higher than 200°C, the delamination is getting less pronounced and finally the resulting fracture surfaces show ductile fracture with a large crack tip opening, which clearly indicates that the calculated K_q values are only a lower limit value and K_{Ic} should be significantly larger. An example of such a fracture surface is given in Figure A.6c) for a sample tested at 800°C, where the fracture surface exhibit certain necking and development of a large crack tip opening displacement before failure. One of the open questions is if the decreasing amount of delamination and thus a lower toughness for the investigated crack system at higher temperatures can be attributed to an improvement of in – plane toughness.
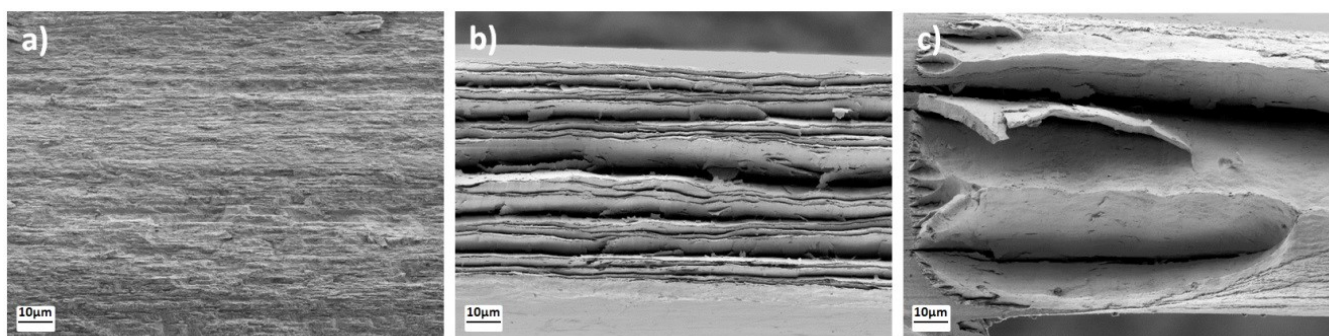

Figure A.6. *Top view of scanning electron micrographs of fracture surfaces of 100µm tungsten foil tested at a) -196 °C, b) 200 °C and c) 800 °C*

In relation to the samples shown in Figure A.6, a comparison of the recorded load vs. time curves is presented in Figure A.7. In the case of lowest testing temperature, a catastrophic failure occurred at minor loads leading to brittle fracture. With the increase of the temperature, the specimens did not fail catastrophically but in a stable manner. As it can be seen from the figure, a significant load drop occurs, for 200°C and 800°C, followed by stable crack growth before the final failure. The large load drops on the curves were accompanied by audible clicks.
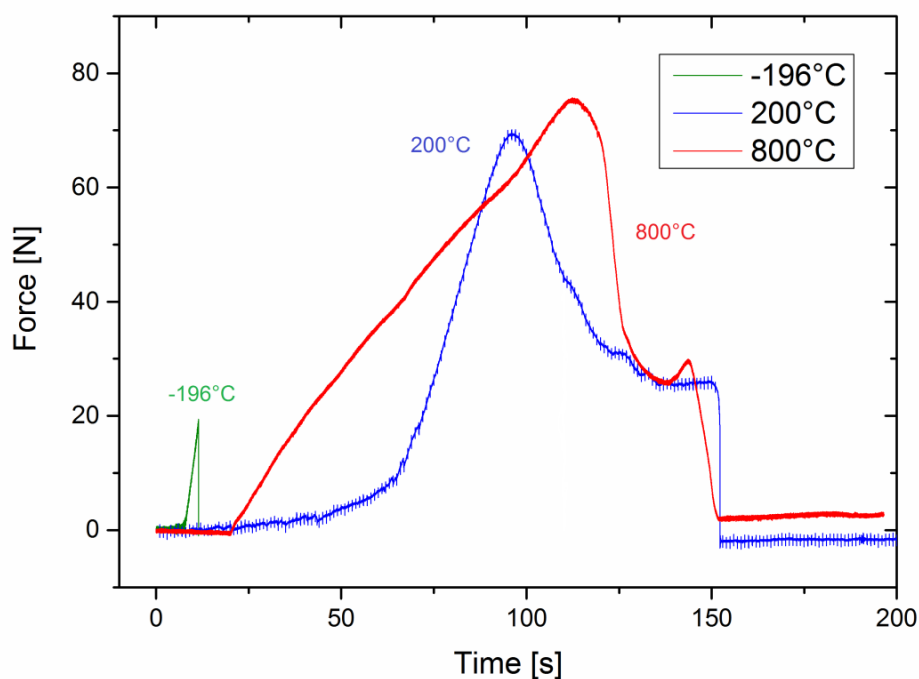
Figure A.7. Comparison of recorded load vs. time diagrams for samples tested in liquid nitrogen, at 200°C and 800°C. Curves are shifted for a better visualization.

A.5. Summary

The main purpose of the investigation discussed in this paper, was the evaluation of the fracture behaviour of 100 µm W foils. Since, the thickness of the samples and its geometry are not the standard one and in order to get appropriate specimens for fracture experiments, optimization of sample design and preparation, crack initiation and brazing was performed. The test specimens were fabricated by electrical discharge machining (EDM) and cracks were initiated by consecutively using a diamond wire saw, a razor blade and a focused ion beam (FIB) workstation. Joining of the pre-cracked foils to the steel holders was done in a brazing process performed in high vacuum, with silver – copper and pure copper brazing foils. Fracture experiments were made with a Zwick universal test machine in the temperature range from -196°C to 800°C, with the pre – crack introduced perpendicular to the rolling direction of the foil. The investigation shows an improved behaviour and significantly higher values of K_q compared to bulk W materials, which can be related to a higher degree of deformation of the foil during the production process and the resulting microstructure. A high toughness at RT, slowly decreases when approaching the highest testing temperature of 800°C. The most significant result

reveals that the ductile to brittle transition temperature (DBTT) is around room temperature, which is an extraordinary result for a tungsten material.

The microstructure of the tested materials was evaluated with the means of EBSD analysis, showing that, as a result of a high degree of deformation during production, grains are elongated along the rolling direction. The dimension of grains in foil thickness direction is very small – below 1µm and the foil has a very pronounced rotated cubic texture. Fracture surfaces of every tested specimen were analysed with an SEM. At low temperatures, the samples fractured in a brittle transcrystalline manner which corresponds to a low value of K_{IC}. Equivalent to the RT scatter of data, the fracture surfaces also vary. In some cases, the samples had a fracture surface showing cleavage fracture (low K_{IC}) and sometimes a very strong delamination was observed, which matches with high values of fracture toughness. With an increase in testing temperature, at 200°C all the samples have strongly delaminated fracture surfaces with a lot of small crack openings. For even higher temperatures, the delamination becomes less pronounced and finally the resulting fracture surfaces show ductile fracture with large crack tip openings.

The open questions, which will be addressed in a following publication, are related to the potential anisotropy of the fracture toughness, which will be analysed in respect to different crack initiation direction. In addition, going from LEFM to CTOD measurements is an important step in understanding the underlying fracture mechanisms controlling the fracture toughness in the regime of increased ductility.

Disclaimer

A.6. References

[1] M. Rieth *et al.*, "Recent progress in research on tungsten materials for nuclear fusion applications in Europe," *J. Nucl. Mater.*, vol. 432, no. 1–3, pp. 482–500, 2013.

[2] S. Wurster *et al.*, "Recent progress in R&D on tungsten alloys for divertor structural and plasma facing materials," *J. Nucl. Mater.*, vol. 442, no. 1–3, pp. 181–189, 2013.

[3] J. H. You *et al.*, "Conceptual design studies for the European DEMO divertor: Rationale and first results," *Fusion Eng. Des.*, vol. 109–111, no. PartB, pp. 1598–1603, 2016.

[4] R. A. Pitts *et al.*, "A full tungsten divertor for ITER : Physics issues and design status," *J. Nucl. Mater.*, vol. 438, pp. S48–S56, 2013.

[5] J. Reiser, M. Rieth, B. Dafferner, and A. Hoffmann, "Tungsten foil laminate for structural divertor applications – Basics and outlook," *J. Nucl. Mater.*, vol. 423, no. 1–3, pp. 1–8, 2012.

[6] J. Reiser *et al.*, "Tungsten (W) Laminate Pipes for Innovative High Temperature Energy Conversion Systems **," *Adv. Eng. Mater.*, vol. 7, no. 4, pp. 1–11, 2014.

[7] J. Reiser and M. Rieth, "Optimization and limitations of known DEMO divertor concepts," *Fusion Eng. Des.*, vol. 87, no. 5–6, pp. 718–721, 2012.

[8] J. Reiser *et al.*, "Tungsten foil laminate for structural divertor applications – Tensile test properties of tungsten foil," *J. Nucl. Mater.*, vol. 434, pp. 357–366, 2013.

[9] P. Gumbsch, J. Riedle, A. Hartmaier, and H. F. Fischmeister, "Controlling Factors for the Brittle-to-Ductile Transition in Tungsten Single Crystals," *Science (80-.).*, vol. 282, pp. 1293–1295, 1998.

[10] P. Gumbsch, "Brittle fracture and the brittle-to-ductile transition of tungsten," *J. Nucl. Mater.*, vol. 323, no. 2–3, pp. 304–312, 2003.

[11] Q. Yan, X. Zhang, T. Wang, C. Yang, and C. Ge, "Effect of hot working process on the mechanical properties of tungsten materials," *J. Nucl. Mater.*, vol. 442, no. 1–3, pp. S233–S236, 2013.

[12] D. Rupp and S. M. Weygand, "Experimental investigation of the fracture toughness of polycrystalline tungsten in the brittle and semi-brittle regime," *J. Nucl. Mater.*, vol. 386–388, pp. 591–593, 2009.

[13] D. Rupp, R. Mönig, P. Gruber, and S. M. Weygand, "Fracture toughness and microstructural characterization of polycrystalline rolled tungsten," *Int. J. Refract. Met. Hard Mater.*, vol. 28, no. 6, pp. 669–673, 2010.

[14] J. Reiser, M. Rieth, B. Dafferner, S. Baumgärtner, R. Ziegler, and A. Hoffmann, "Deep drawing of tungsten plates for structural divertor applications in future fusion devices," *Fusion Eng. Des.*, vol. 86, no. 12, pp. 2949–2953, 2011.

[15] Q. Wei and L. J. Kecskes, "Effect of low-temperature rolling on the tensile behavior of commercially pure tungsten," *Mater. Sci. Eng. A*, vol. 491, no. 1–2, pp. 62–69, 2008.

[16] Plansee, "www.plansee.com/de/werkstoffe/wolfram.html," *accessed date 2015-11-01*. .

[17] J. Neges, B. Ortner, G. Leichtfried, and H. P. Stüwe, "On the 45° embrittlement of tungsten sheets," *Mater. Sci. Eng. A*, vol. 196, no. 1–2, pp. 129–133, 1995.

[18] J. Reiser, M. Rieth, B. Dafferner, A. Hoffmann, X. Yi, and D. E. J. A. C, "Tungsten foil laminate

for structural divertor applications – Analyses and characterisation of tungsten foil," *J. Nucl. Mater.*, vol. 424, pp. 197–203, 2012.

[19] "ASTM E399-90, Standard test method for plane-strain fracture toughness of metallic materials.," in *Annual Book of ASTM Standards*, Philadelphia (PA):American Society of Testing and Materials, 1997.

[20] J. Reiser *et al.*, "Tungsten foil laminate for structural divertor applications – Joining of tungsten foils," *J. Nucl. Mater.*, vol. 436, no. 1–3, pp. 47–55, 2013.

[21] Y. Murakami, *Stress Intensity Factors Handbook*. Pergamon, 1987.

[22] S. J. Zinkle and N. M. Ghoniem, "Operating temperature windows for fusion reactor structural materials," *Fusion Eng. Des.*, vol. 51–52, pp. 55–71, 2000.

[23] T. Palacios, J. Reiser, J. Hoffmann, M. Rieth, A. Hoffmann, and J. Y. Pastor, "Microstructural and mechanical characterization of annealed tungsten (W) and potassium-doped tungsten foils," *Int. J. Refract. Met. Hard Mater.*, vol. 48, pp. 145–149, 2015.

[24] D. Rupp and S. M. Weygand, "Anisotropic fracture behaviour and brittle-to-ductile transition of polycrystalline tungsten," *Philos. Mag.*, vol. 90, no. 30, pp. 4055–4069, 2010.

B

Fracture toughness evaluation of UFG tungsten foils

Vladica Nikolić [a], Stefan Wurster[b], Daniel Firneis[a], Reinhard Pippan[a]

[a] Erich Schmid Institute of Materials Science of the Austrian Academy of Sciences, Leoben, Austria

[b] Department of Materials Physics, Montanuniversität Leoben, Leoben, Austria

Abstract

The fracture behaviour of pure, ultrafine grained 100 μm tungsten foil was investigated as a function of testing direction and temperature in the range from -196°C to 800°C. To study the influence of the anisotropic microstructure on the fracture process, the single-edge-notched specimens were extracted in three different crack orientations relative to the rolling direction. This thorough investigation shows the positive impact of deformation induced grain refinement through extraordinary values of fracture toughness and a reduction of the ductile-to-brittle transition temperature to about room temperature. Furthermore, it was demonstrated that the grain shape anisotropy and a strong rotated cubic texture are decisive factors for anisotropic fracture properties. Fracture surface investigations reveal distinctive behaviour with an increase in temperature. The pronounced transition in failure mode was observed going from brittle, transcrystalline fracture at -196°C towards pronounced delamination at intermediate temperatures and to ductile failure at highest temperatures. The measurement of the crack tip opening displacement for specimen fracturing in a completely ductile manner enables the determination of more accurate fracture toughness in the elastic plastic regime.

Keywords: Thin tungsten foil, Fracture toughness, High and low temperature fracture experiments, LEFM, EBSD analysis, SEM analysis

B.1. Introduction

Tungsten (W) belongs to the group of refractory metals and is known for its outstanding mechanical and physical properties in the high temperature environment such as high temperature strength, good thermal conductivity and creep resistance [1]. In addition, the highest melting point of all the metals (T_m=3422°C) and thermal stability against recrystallization make W a very prominent material in high-temperature applications, for example in future energy systems like a fusion reactor. Nevertheless, its fabrication and processing as well as its applicability as a high-performance structural material are somewhat limited due to its typically brittle character at low temperatures and rather high ductile-to-brittle transition temperature (DBTT). Recently, an extensive research on the ductility enhancement of tungsten at lower temperatures was conducted [2], [3] with the three main toughening strategies being alloying (e.g. with Re [4], [5] or Ir [6]), formation of W composite materials (e.g. tungsten-fibre reinforced tungsten [7]) and modification of the microstructure. The third approach enables alternation of the microstructure to an ultrafine grain (UFG) size through various methods of severe plastic deformation such as equal channel angular pressing (ECAP) [8], high pressure torsion (HPT) [9] or heavily rolling [10]. In such a way, a deformation induced grain refinement can lead to a development of a beneficial UFG microstructure of pure tungsten having enhanced both strength and ductility.

The fracture behaviour and the underlying deformation mechanisms of tungsten single crystals have been extensively studied in the past [11], [12], revealing that the fracture process in the brittle regime occurs by cleavage on the preferred {100} and {110} crack planes, while the increase of fracture toughness with temperature in the semi-brittle regime is related to the increased crack tip plasticity [13]. Furthermore, the strong dependence of the DBTT and fracture toughness on the loading rate is an indication that the dislocation availability and/or mobility at the crack tip is controlling the transition process. In contrast to the deep understanding of the fracture process and controlling mechanisms in tungsten single crystals, the comprehensive experimental study of tungsten materials with more complex microstructure i.e. polycrystalline W is still not complete. In the case of W, established microstructure during the production steps has a tremendous effect on the resulting fracture properties and factors like grain size, grain shape and texture play a decisive role for the resulting failure mode, leading to the anisotropic fracture behaviour of the deformed tungsten materials [14], [15]. The cold rolling of tungsten plate results in pancake-shaped layered microstructure parallel to the rolling direction. This elongated microstructural feature is favourable for good toughness in two out of three principal loading directions and with the decrease in thickness, the DBTT is shifted to lower temperatures [16]. Tungsten material in a form of thin foils, having an ultrafine-grained, elongated microstructure is obtained by substantial grain refinement through even higher degrees of deformation (rolling). Such a tungsten material shows an exceptional toughness and substantial decrease in DBTT [17]–[19], highlighting the potential of using tungsten as a structural component. However, a systematic study and thorough fracture mechanics investigation of ultrafine-grained tungsten foils are still lacking.

In the present paper, results of a fracture mechanical assessment of 100μm thin UFG tungsten foil, in a wide range of testing temperatures and different testing directions, is presented. The significantly lowered DBTT will be discussed and possible mechanisms controlling the process will be outlined.

Furthermore, the question of the effect of the aligned, anisotropic microstructure on the resulting fracture properties is addressed. Special focus is devoted on evaluating the relationship between the underlying microstructure and the resulting failure characteristics depending on the crack orientation.

B.2. Material and experimental methods

The material investigated in this study is a technically pure tungsten foil (>99.97 wt.% W), which is commercialy available and obtained from Plansee SE, Reutte, Austria. The standard fabrication of a tungsten base material is via powder metallurgical route and after sintering, it is submitted to hot and cold rolling. The final nominal thickness of the investigated foil was 100 μm. Production details regarding temperatures of rolling and degree of deformation are not provided by the manufacturer, however typical and guaranteed impurity concentrations are available and can be found elsewhere [20]. Due to the rolling processes, the tungsten foil is submitted to a very high degree of deformation which has a decisive effect on the developed microstructure.

The microstructural characterization, determined by electron backscatter diffraction (EBSD) in the scanning electron microscope (SEM), is consisting of a qualitative description of grain shape, analyses of grain size distribution and an evaluation of the developed texture. Smooth surfaces across the entire thickness of the sample, suitable for SEM/EBSD analyses, were prepared by a Hitachi E-3500 Ion Polisher. Orientation Imaging Microscopy (OIM) software was used to evaluate the obtained EBSD scans. Post-processing was carried out by removing points with a confidence index lower than 0.1. Grain shape maps were acquired in three principal directions of a rolled plate: RD-view (long transverse view; along longitudinal, rolling direction), TD-view (perpendicular to and in plane with the rolling direction) and SD-view (short transverse direction). In order to provide a better representation of the microstructure, EBSD images from the 100 μm W foil with different viewing directions are projected on a cuboid in Figure B.1a. As it can be perceived the long, very thin grains are elongated in the direction of rolling (with the shortest grain lengths parallel to the SD) forming a characteristic pancake-like microstructure. The investigated foil has a pronounced rotated-cube crystallographic texture, which is commonly observed in bcc metals [21], with a most dominant {001} <110> orientation, giving in addition to the anisotropic microstructure, orientation dependent mechanical properties.

Single-edge notched tension (SENT) specimens were cut from the tungsten sheet by electrical discharge machining (EDM), with a specimen size of 20x5x0.1 mm^3. Notches introduced by a diamond wire saw were further sharpened by a razor blade polishing [22]. A Focused Ion Beam workstation (FIB, Leo 1540, Zeiss) was used to create a final, sharp pre-crack with a length, measured from the notch root, of about 10-20 μm. For the analysis of the influence of the microstructure on the anisotropy of fracture properties, samples were taken with three different orientations of the pre-crack in respect to the rolling direction: parallel to the RD (∥ system), perpendicular to the RD (⊥ system) and with 45° angle (45° system) as depicted in Figure B.1b. In all three specimen orientations, the crack plane is perpendicular to the foil plane. In comparison to the nomenclature according to the standard ASTM E-399 [23], the ∥ system corresponds to the T-L and the ⊥ system to the L-T sample orientation. The results of fracture investigations on the L-T system have been presented in a previous publication [17]

and for the sake of comparison the obtained results are outlined in chapter 3. Taking into account samples of a different crack plane to foil plane relationship (T-S, L-S, S-T and S-L) would complement the understanding of the anisotropic mechanical properties. However, due to the restrictive thickness of the foil, this is a non-trivial task and exceeds the scope of this publication. To exclude the influence of impurity content on the resulting fracture properties [24], all the samples were cut from the same tungsten sheet batch; therefore, having the same chemical composition.
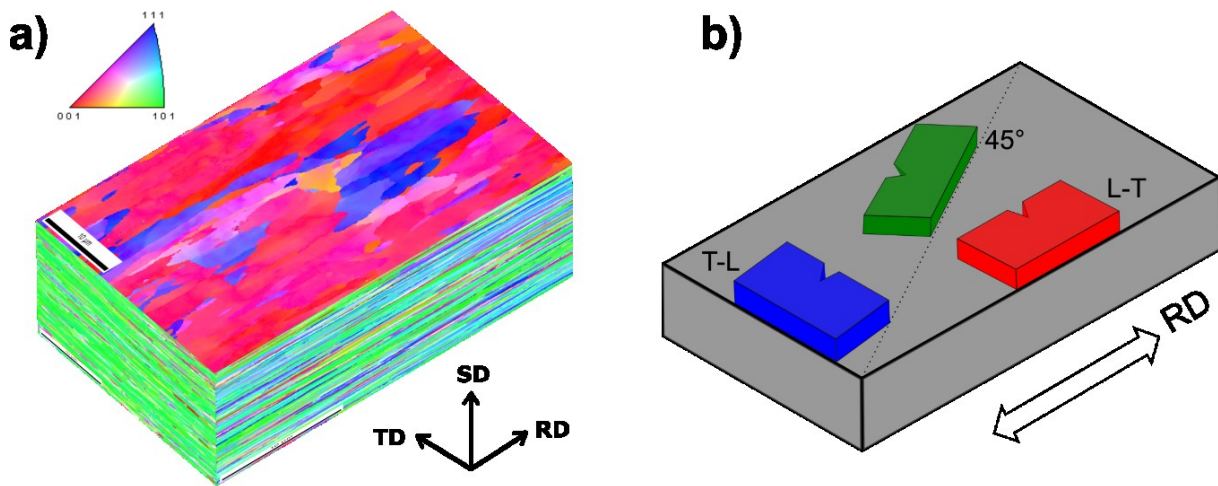

Figure B.1. a) Inverse Pole Figures (IPF) of pure 0.1mm tungsten foil in as-received condition in three principle directions of a rolled plate: RD, TD and SD. EBSD maps are projected on a cuboid to better visualize the pancake-like microstructure, with thin, elongated grains along the rolling direction. Colour coded unit triangle representing <100>, <110> and <111> crystallographic directions perpendicular to the sample surface. b) An illustration of the orientation of different SENT specimen types.

Fracture mechanical experiments were performed on a universal testing device (Zwick) in the temperature range from -196°C to 800°C. Test were done in air at -196°C (liquid nitrogen), room temperature and 200°C, while a vacuum chamber was used for the experiments at elevated temperatures, to avoid the oxidation of the foil. All the specimens were tested in crosshead displacement control at 0.4mm/min and for each testing system between one and three samples were fractured at all temperatures. A proper mounting of the samples in the testing device was enabled by brazing the pre-notched foils to two steel holders. Details of the sample preparation and brazing procedure can be found elsewhere [17]. During the experiments, the force is recorded as a function of time, while the desired temperature was kept stable throughout the measurement. The conditional fracture toughness, K_q, is calculated according to:

$$K_q = \frac{P_{max}}{A} * \sqrt{\pi * a} * f(\alpha), \text{ with } \alpha = \frac{a}{W} \tag{1}$$

where P_{max} is the maximum force measured by the load cell, A is the area of the cross section of the sample or more precisely the width W, multiplied by the thickness, B and a is the crack length. According to Murakami [25], the dimensionless function α of single-edge notched tension (SENT) specimens is:

$$f(\alpha) = 1.12 - 0.231 * \alpha + 10.55 * \alpha^2 - 21.72 * \alpha^3 + 30.39 * \alpha^4 \qquad (2)$$

After the fracture tests, fractographs of the samples were examined with a field emission gun SEM ''LEO Gemini 1525'' and the evolution of the morphology of fracture surfaces, in respect to increased temperature, was obtained. In order to determine a valid value of fracture toughness, certain size requirements need to be fulfilled so that the linear elastic fracture mechanics (LEFM) evaluations procedure is applicable and that appropriate conditions prevail. In the following sections, limits of validity and calculated fracture toughness will be discussed. Furthermore, regardless of the size requirements, in the regime of increased ductility occurring at higher temperatures LEFM loses validity. Using an automatic fracture surface analyses system (Alicona MeX), the 3D models of fracture surfaces were calculated, enabling the determination of crack tip opening displacement (CTOD) [26] representing a measure of fracture toughness of ductile materials. In principle, K_{CTOD} value represents the material's geometry independent toughness and can be correlated to determined CTOD by:

$$K_{CTOD} = \sqrt{\sigma_Y * E * m * CTOD} \qquad (3)$$

where σ_Y represents the yield strength ($\sim 600 MPa$ [27]) , E the Young's modulus ($\sim 410 GPa$ [1]) and m is a dimensionless constant that is approximately 1.0 for plane stress and 2.0 for plane strain [28] for low or non-hardening materials as used in this case.

B.3. Results

B.3.1. Fracture toughness tests

The results of the fracture experiments of the 100µm tungsten foil, for two specimen orientations (T-L and 45° system), where the conditional toughness, K_q, is plotted against the testing temperature, T are displayed in Figure B.2 with the associated values shown in Table B.1. For both systems a similar trend is seen, where the lowest K_q are obtained for experiments performed in liquid nitrogen, with the values of 13.7 MPa(m)$^{1/2}$ (T-L) and 15.4 MPa(m)$^{1/2}$ (45°). With the increase in testing temperature, as expected, values of fracture toughness increase up until room temperature or 200°C (55.5 MPa(m)$^{1/2}$ for T-L system and 77.1 MPa(m)$^{1/2}$ 45° system), after which an apparent decrease is observed. However, at elevated temperatures the samples fractured in a ductile manner and did not meet small scale yielding conditions which will be discussed in detail in 3.1.1. Consequently, the obtained values of conditional fracture toughness from Equation (1) are underestimated and can be regarded as a lower bound for the true fracture toughness. This is indicated by small arrows next to the data points and above RT an increase in fracture toughness is to be assumed.

The performed fracture investigations indicate a superior behaviour of a thin tungsten foil and extraordinarily high values of fracture toughness. For the sake of comparison, it is noted that the 200°C fracture toughness of a pure sintered tungsten material was measured as 6.1 MPa(m)$^{1/2}$ [15], which is even smaller than the lowest obtained K_q at cryogen temperatures. The fracture toughness of the same material with a crack introduced perpendicular to the rolling direction (L-T system) has been studied recently [17] and for the purpose of comparison, obtained results are also outlined in the Table B.1 and Figure B.2.
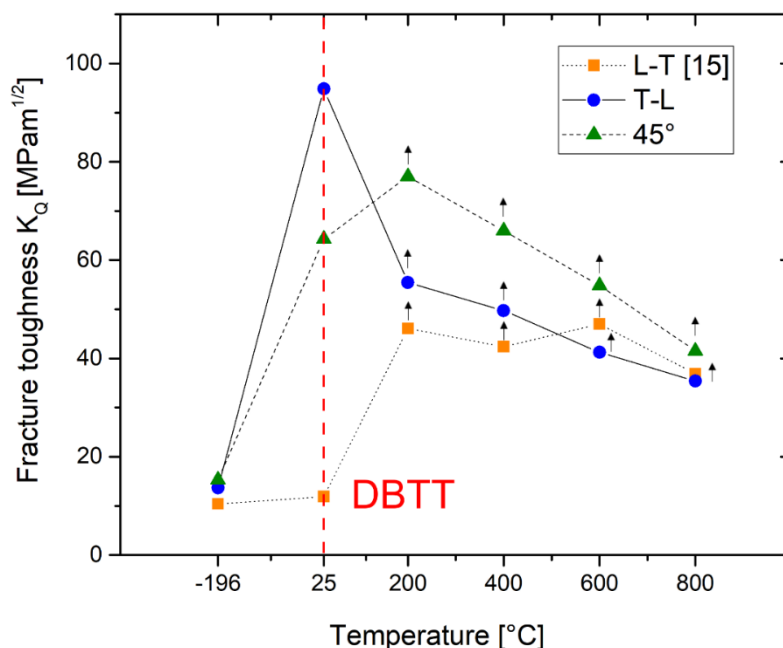
Figure B.2. *Fracture toughness K_q of the 100 µm thin tungsten foils as a function of testing temperature for three different specimen orientations.*

Table B.1. *Table of K_q values of a pure 100 µm thin tungsten foil tested in the temperature range from -196°C to 800°C; the values for different loading geometries are compared.*

Temperature [°C]	Fracture toughness [MPa(m)$^{1/2}$]		
	L-T system [17]	T-L system	45° system
-196	10.4	13.7	15.4
RT	11.9-105.9	94.8	64.3
200	46.1	55.5	77.0
400	42.4	49.8	66.7
600	47.0	41.2	54.8
800	36.9	37.9	41.6

A microstructural influence on the resulting anisotropic fracture toughness is indicated by comparison of the obtained values of K_q of all three tested systems. Except for the RT result, samples orientated at 45° show the highest fracture toughness in the entire temperature range. The most interesting is the result of the foil tested at room temperature where a large scatter of data has been observed. The example of the L-T system is outlined, where a variation of K_q goes from about 12 MPa(m)$^{1/2}$ to incredible 106 MPa(m)$^{1/2}$ [17]. Such a spread of data is in good accordance with the fracture surface observations indicating the transition from a transcrystalline cleavage to a ductile laminate failure, demonstrating that this is the temperature region where brittle to ductile transition, for this crack front orientation, takes place. Thus, the DBTT is here defined as the temperature at which the fracture toughness value is significantly increased, associated with a scatter of data and an apparent transition in fracture mode. A clearly defined temperature of this transition cannot be given for W, as it strongly depends on various parameters (microstructure, testing method, strain rate etc.); however, it is very pronounced for both single and polycrystalline materials and can vary for several hundred °C. To give an example, Charpy impact test results of the 3 mm tungsten plate, for the T-L orientation of the samples, indicate that DBTT occurs at 500°C [29].

Figure B.3 shows recorded force – crosshead displacement curves for the two tested systems in the three temperature regimes: -196°C, 400°C and 800°C. At the lowest testing temperature, the failure occurs abruptly at low loads without a noticeable plastic deformation, corresponding to the low fracture toughness values. With increasing testing temperature samples show more plastic deformation before final failure occurs (in particular at the higher temperature), where a noticeable load drop is followed by a stable crack growth. A first insight of the expected failure modes can be gained with these load displacement curves; the fractographic evolution is studied in details in the following chapters.
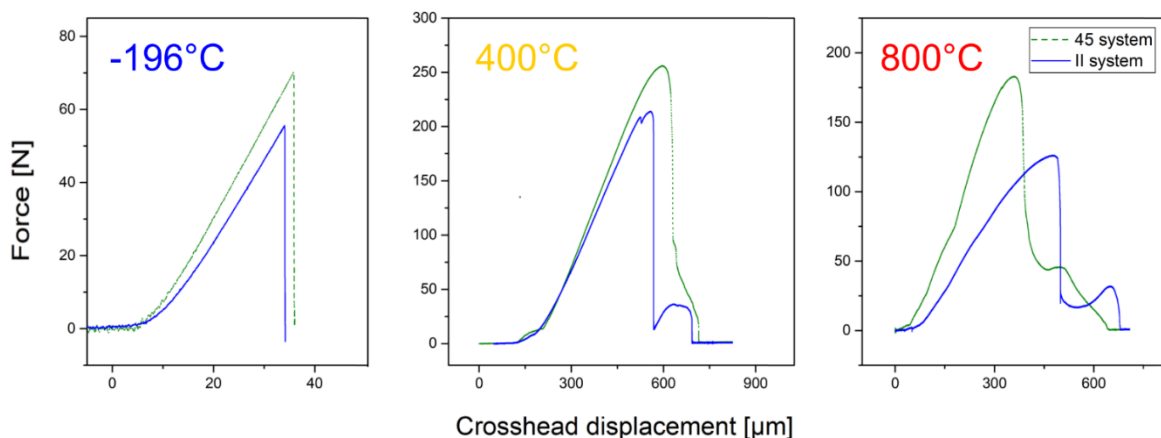

Figure B.3. A comparison of force – crosshead displacement curves ($v = 0.4mm/\min$) of 45° and T-L systems at different testing temperatures: -196°C, 400°C and 800°C with a distinctive difference in the amount of plastic deformation prior to the final failure.

B.3.1.1. LEFM – conditions and limits of validity

The standard method for fracture toughness testing given by the ASTM E399 procedure [23] ensures that LEFM conditions are met by setting certain sample size requirements. When a sample, being large enough, behaves in a linear elastic manner prior to the failure, the obtained stress intensity factor corresponds to the plane strain fracture toughness K_{IC} parameter. The method used in testing thin tungsten foil is based on this standard, however due to the sample size restrictions, especially regarding thickness, it is necessary to outline critical remarks regarding the limits of validity.

Conditional fracture toughness K_q can be considered a valid K_{IC} result when the crack length *a*, sample thickness *B* and the ligament length *(W-a)* meet the criteria given by

$$a, \ B, \ W - a \ \geq 2.5 * (\frac{K_q}{\sigma_{Ys}})^2 \qquad\qquad (4)$$

where σ_{Ys} is the 0.2% offset yield strength of the material for the temperature of the test. In addition, the ratio of maximum P_{max} and conditional load P_q should not exceed 1.10. Conditional load is equal to the maximum load in the case when specimen fails completely before achieving 5% nonlinearity.

The majority of the results determined for the thin tungsten foils (except for the lowest testing temperature) do not meet all the validity requirements and can be considered as a lower estimate of the fracture toughness. The yield strength data necessary for calculating validity criteria are taken from [27], where the tensile properties of the same tungsten material are analysed. In general, the performed tests in our study are in violation of the thickness requirement so that the plane stain conditions are not fulfilled. For the determination of the validity of measured fracture toughness values in terms of critical stress intensity factors one has to distinguish between different cases when 1) small scale yielding *and* the plane strain conditions are fulfilled (i.e. Equation 4 is fulfilled for all the variables as in the case at 77K) and 2) when the crack length and ligament size fulfilled Equation 4, but the thickness criterion does not fit. In the case of microductile fracture the apparent critical stress intensity factor increases with decreasing thickness, due to the increase of the plane stress dominated fracture regime. This increase takes place up to a maximum value where then the fracture toughness decreases, which is typical in ductile thin foils.

In the investigated W-foils in the temperatures region between room temperature and 400°C a strong delamination takes place, which realizes a plane stress state next to the crack tip. Such fracture phenomenon would take place also in thick samples with the same microstructure hence a significant thickness effect on the fracture toughness is not expected. Due to the strong temperature dependence of the yield stress [27], the small scale yielding criterion is not fulfilled for temperatures larger than 200°C. In such case the calculated critical stress intensity values can be considered as a lower limit, because in an elastic plastic evaluation of the fracture toughness the elastic part of the J-integral and the plastic part of the J-integral have to be taken into account (for calculation of K_q the later part has not been taken into account). At 600°C and especially at 800°C a complete necking takes place hence the fracture toughness values in terms of K_c, J_c or critical CTOD of such W microstructure will always be

thickness dependent i.e. the values are only valid for a specific thickness, in this case for 100µm. The measurement of the CTOD for specimens fracturing in completely ductile manner gives a geometry independent fracture toughness value as long as $CTOD_c < \frac{1}{10} B$. That is not the case at 600°C and 800°C, but the Equation (3) can be used to estimate the fracture toughness and indicate the extend of the underestimation of conditional fracture toughness results.

B.3.2. Fractographic evolution

The SEM investigation of the fracture surfaces reveals distinctive behaviour for different testing temperature regimes, with a very pronounced evolution of fracture modes over the entire temperature range (-196°C to 800°C). Results for low and intermediate temperatures, detailed analyses of RT sample and high testing temperatures are shown in Figure B.4 – Figure B.6, respectively. Displayed fractographs correspond to the samples of the 45° system (Figure B.4 and B.6) and L-T system (Figure B.5), where different magnification allows the SEM analyses across the entire thickness of the foil, as well as studying the selected areas of interest with greater detail.

At liquid nitrogen temperature (-196°C), all the samples fracture in classical brittle, transcrystalline manner associated with the lowest values of fracture toughness. The sample of the 45° system has a crack plane straight along the ligament plane, while in the case of L-T and T-L samples an immediate 45° kink takes place as a result of typical weak cleavage planes [21], which is in good agreement with the measured texture. In the obtained fracture surfaces, aligned grains can be perceived as horizontal lines. At these temperatures, no significant plastic deformation within the pancake like grains takes place and due to the applied stress, cracking occurs by separating individual grains by cleavage (as a result of crack propagation along the specific crystallographic planes).

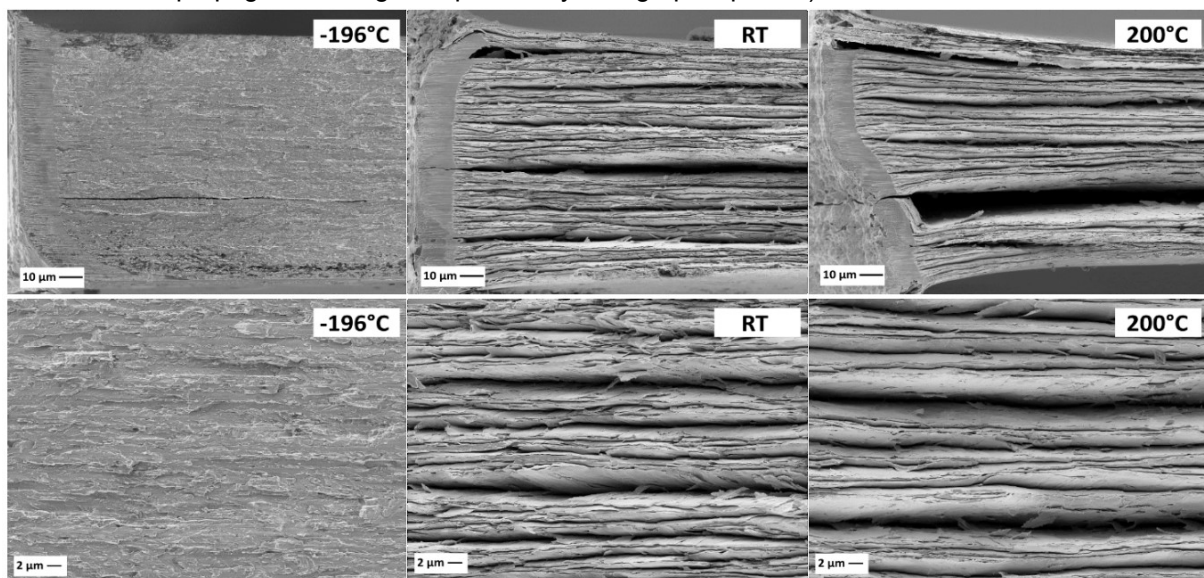***Figure B.4.*** *Fracture surface micrographs of the 100 μm thin pure tungsten foils tested 45° in respect to the RD in the low and intermediate temperature range. A sample tested at -196°C shows a typical brittle, transcrystalline fracture, whereas for samples at RT and 200°C pronounced delaminations can be perceived. In some of the micrographs the FIB induced defect is clearly visible on the left side.*

In the intermediate temperature range (RT and 200°C) the situation differs significantly with fracture surfaces showing pronounced delamination with a significant amount of small crack openings within the foil plane. Such a fan-out topography is a direct consequence of the characteristic microstructure and the weak adherence of the elongated grains. The anisotropy of the grain shape and the ability of the individual grains to deform plastically allow the delamination process to take place. Under the applied load, the delaminated grains are elongated and the small openings are formed near the notch root. With further deformation small cracks propagate along the large sides of pancake-like grains, while the conjunct ligaments are further elongated and thinned out until the fracture takes place. With an increase in temperature to 200°C the delamination takes place somewhat less frequent followed by a larger crack opening. Less frequent delamination might be attributed to an increased in-plane toughness, which could be demonstrated with S-T or S-L crack plane orientations.

Additionally, it has to be noted that the scatter of fracture toughness values at RT is consistent with the obtained fracture surfaces, indicating that at this temperature BDT really occurs. Samples that fractured in a brittle mode (cleavage) correspond to the low value of K_{IQ}, while pronounced delamination is related to higher values of fracture toughness. A more detailed SEM analysis of one of the sample tested at RT (Figure B.5) reveals two distinctive regions in the fracture surface. The first part, starting at the notch root, is characterized by pronounced delamination which is observed until the transition takes place. In this transition zone, fracture surface changes from lamellar structure to a typical brittle fracture similar to those observed for liquid nitrogen temperature. A side view of the specimen reveals that the transition region corresponds to a very pronounced geometrical deflection of the crack (by 45° in respect to the RD) to facilitate propagation along the weaker planes.
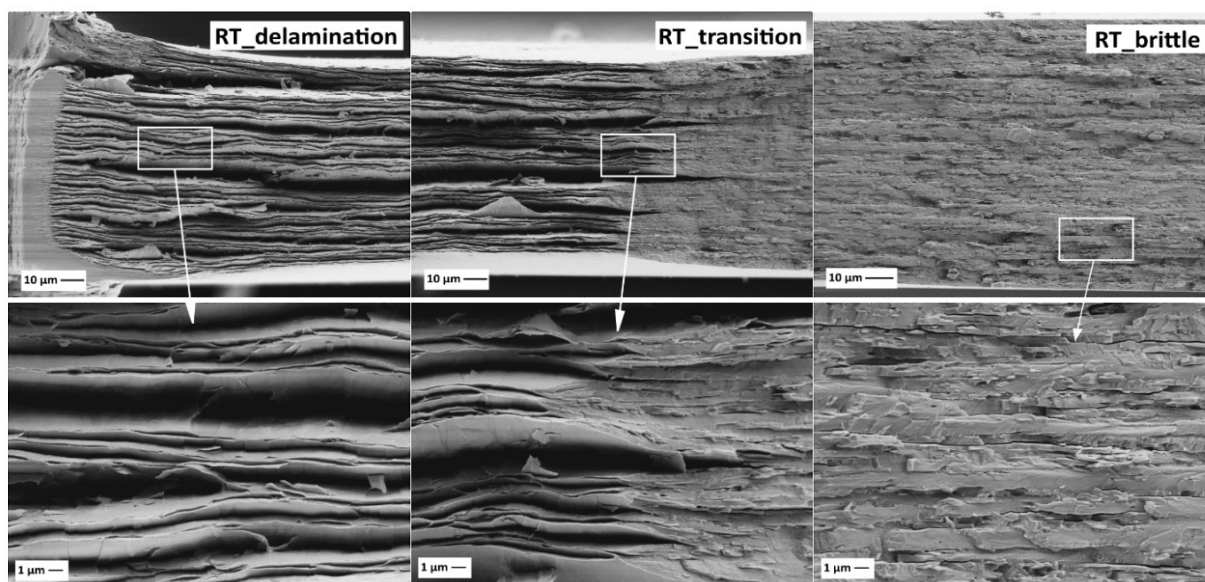

Figure B.5. *Fracture surface micrographs of the 100 µm thin pure tungsten foils tested at RT (L-T system). When progressing from the starting crack along the former ligament length, an evolution of the fracture mode is observed with a transition from strong delamination to the typical, transcrystalline brittle fracture.*

With a further increase of testing temperature, a transition of fracture surfaces continues towards a more ductile behaviour. The highest number of single lamellas is at room temperature and with increasing temperature this number decreases. Already at 400°C strong delamination is less pronounced with a significantly smaller amount of individual lamellae (Figure B.6). From a microstructural point of view, conjunct grains in a form of thicker ligaments show increased plasticity and certain amount of necking, before they break ductile, as can be seen in the inner region of the sample tested at 600°C. The distinctly different fracture surface is observed for the 800°C sample where a more usual ductile fracture appearance occurs. In this case, increased plastic deformation is indicated by pronounced necking and thinning out of the entire ligament.

The observed anisotropy of the fracture toughness values is not reflected in different failure modes observed in SEM images. All three testing systems show a very similar fractographic transition from transgranular cleavage to a ductile behaviour, with a very pronounced delamination for intermediate temperatures and thus not all fractographs for all temperatures and testing directions are shown. The only distinction comes from the 45° system, where complete necking is observed at 800°C with sample fracturing without in-plane crack openings. This is an indication that certain amount of plastic deformation takes place in front of the crack tip which enables the estimation of the crack tip opening displacement for the determination of fracture toughness of the foil.
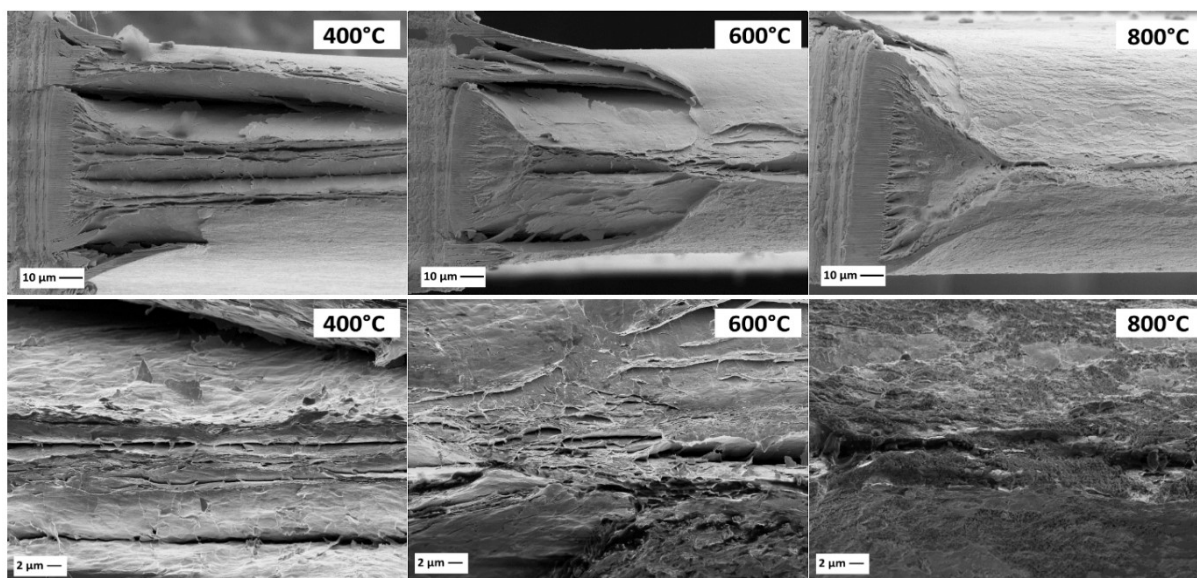
Figure B.6. *Fracture surface micrographs of the 100 µm thin pure tungsten foils tested 45° in respect to the RD in the high temperature range. Increasing the temperature from 400°C to 800°C, surfaces evolve from a coarse delamination to a ductile fracture.*

B.3.3. Crack tip opening displacement

The expected increase of fracture toughness with temperature, associated with an increase in crack tip plasticity, is not reflected by the LEFM estimated fracture toughness values. Since high temperature

results are associated with increased ductility of the tungsten foil, LEFM becomes invalid. However, blunting of the crack tip before the crack starts to propagate can be related to the fracture toughness K$_{CTOD}$ through the crack tip opening displacement parameter (CTOD). These values are geometry independent as long as $B > 10CTOD$ and becomes thickness dependent when $B < 10CTOD$. This parameter can be obtained by stereophotogrammetric reconstruction of fracture surfaces [30], [31] and an example of the procedure is presented for the 45° system sample tested at 800°C (Figure B.7). For this specimen the lower band value of K$_q$ yields 41.6 MPa(m)$^{1/2}$, so calculating K$_{CTOD}$ can reveal the extent of underestimation of the high temperature results.
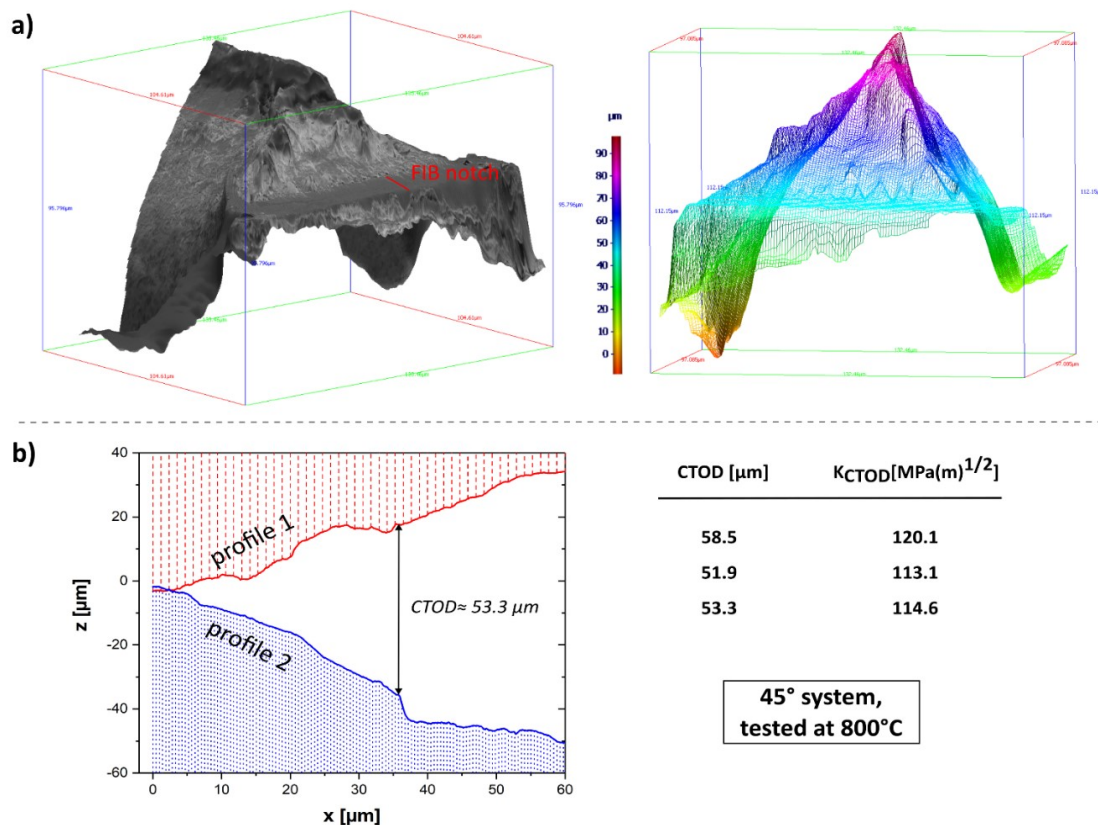
Figure B.7. *An example of the CTOD determination procedure of a 45°system sample tested at 800°C. a) Digital elevation models (DEM) representing a 3D topography reconstruction of the two fractured halves, represented in optical image and pseudocolour view. The viewing direction is along the crack propagation direction with the blue "mountain" showing the plastically deformed ligament. Colour code indicates height in µm. b) Shows two corresponding surface profiles for an evaluation of the CTOD.*

To reconstruct the depth information from the SEM fractographs, stereophotogrammetric methods are applied. Stereo-image pairs of both halves of the fractured sample are obtained from SEM images of the tilted and untitled specimen. These anaglyph pictures are further processed with an automatic image system which allows the generation of the digital elevation models (DEM) of the investigated surfaces (Figure B.7a). Hence, the obtained 3D information is used to retrieve the microscopic topography of the fracture surfaces. The degree of local plastic deformation can be calculated from DEMs as the misfit of the surfaces by finding homologue points in the two surface projections of the

specimen [30]. In the case of the characterized tungsten foil, three surface height profiles were extracted from the generated DEMs and the CTOD is quantified from the vertical distance between the profiles. The biggest challenge associated with the method is identification of the corresponding points in the two halves. An example of one crack path profile is given in Figure B.7b with associated values of CTOD and K_{CTOD} according to Equation (3) for all three profiles. The results show an average value of CTOD of 54.6 ± 3.5 µm, with relating average fracture toughness of 115.9 ± 3.7 MPa(m)$^{1/2}$. A difference of K_{CTOD} and K_q by nearly a factor of three emphasizes the importance of determining a more accurate value of fracture toughness in the elastic-plastic regime.

B.3.4. Influence of annealing

The extraordinary fracture behaviour of the analysed tungsten foil can be related to the beneficial ultrafine grained and nearly lamellar microstructure developed during the rolling process. Since fine grain materials are very sensitive to annealing and recrystallization phenomena, it is very important to look into the effect of heat treatments on the microstructural stability and whether this leads to deterioration of the obtained mechanical properties.

The influence of annealing on the microstructure was estimated through the identification of changes of the grain shape and size, analyses of the grain boundaries and evolution of the developed texture. Comparison is made between EBSD data acquired in two principal directions: TD view (Figure B.8a) and RD view (Figure B.8b), for as-received and annealed foil (1400°C in vacuum for 1h). As stated before, IPF maps reveal that the material in as-received condition has long, thin grains elongated in the direction of rolling (with the shortest grain lengths parallel to SD) forming a characteristic pancake-like microstructure having a small aspect ratio. The average grain size can be calculated from the obtained maps by a line intercepts length method. The grain size in TD and RD are denoted as length of the grain with the average calculated values of 1.19 µm and 0.97 µm, respectively. The most significant grain refinement through rolling processes occurs in SD direction, leading to the considerably smaller grain dimensions. Grain size in SD, designated as the grain width, reaches the ultrafine grained regime with the calculated average of 336 nm (TD view) and 404 nm (RD view). Heat treatments considerably affect the thin foil microstructure through a complete loss of elongated grain shape and onset of significant grain coarsening. The large, quasi-symmetric, globular µm sized grains can be seen in Figure B.8. In accordance to the shape alterations, aspect ratio is tremendously changed.

As received rolled material contains a significant combination of both low-angle grain boundaries (LAGB, misorientations between 5° and 15°) and high-angle grain boundaries (HAGB, misorientations between 15° and 65°), with a higher fraction of HAGB. Analyses of the amount of grain boundaries in the two viewing direction (RD, TD) reveal that in the TD view there is a higher number of GB which will have a significant influence on the anisotropy of fracture toughness. Simultaneously with grain growth during the heat treatments, the grain boundary area is tremendously reduced, consisting almost exclusively of HAGB. Figure B.8 illustrates this results in the grain boundary maps where LAGB are highlighted in red and HAGB are highlighted in black. The EBSD results also show a strong, preferential orientation of the grains in {001}<110> direction, which is a dominant orientation for rolled bcc metals

defined as rotated cube texture. Annealing at 1400°C shows very little influence on the lattice orientation, as the texture remains the same. These findings are in accordance with other EBSD investigations [32] and the texture developed during rolling seems to become even more pronounced at higher annealing temperatures [33].
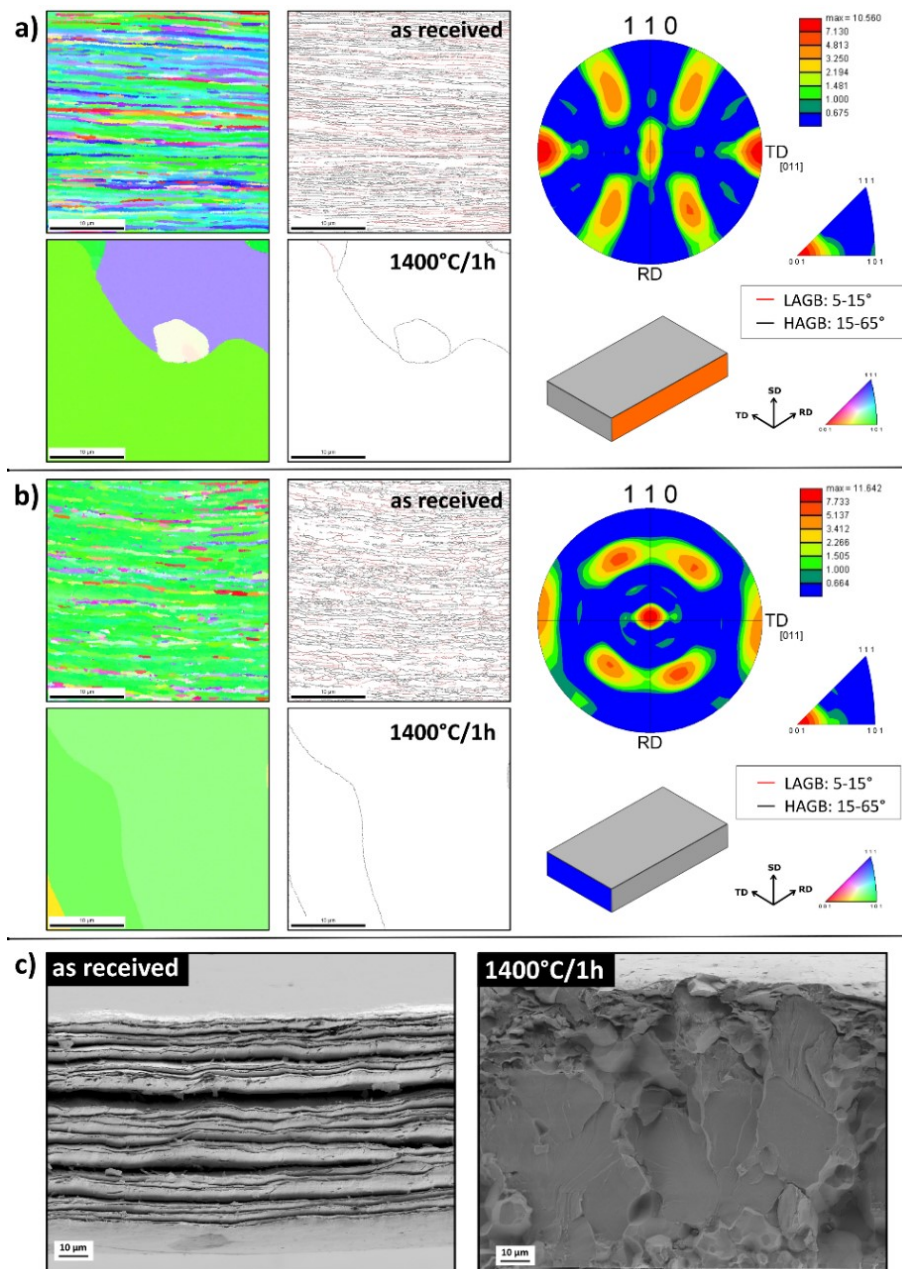
Figure B.8. *Inverse Pole Figures (IPF) maps, grain boundary maps and texture analyses of pure 0.1mm tungsten foil in as received and annealed condition (1400°C/1h) in two principle directions of a rolled plate: a) TD view (along transverse direction) and b) RD view (along longitudinal, rolling direction). c) Comparison of fractured surfaces of the sample tested at 200°C for as received foil showing strong delamination (left) and annealed foil failed by a mixed transgranular/intergranular failure mode (right).*

The first impression of the impact of annealing on the resulting fracture behaviour can be seen in Figure B.8c, where fractographs of the foils in as-received and annealed condition are compared. Tests

were done at 200°C and in the case of heat treated foil a decrease in fracture toughness from 46.5 MPa(m)$^{1/2}$ to 38.6 MPa(m)$^{1/2}$ is detected. Test curves reveal a noteworthy increase in plasticity which is in accordance to a very large plastic strain of up to 45% in a tensile test at 600°C of the same foil, related to the movement of dislocations to the surface [34]. The grain coarsening during annealing induces a significant reduction in yield stress, which permits the development of a plane stress dominated plastic zone which then induces the relatively high fracture toughness despite the brittle appearance of the fracture. Comparing SEM fractographs of the two samples, a substantial transition in failure modes can be seen. Delamination only occurs for the foil in as-received state, while the annealed foil fails in a brittle, mixed fracture mode (trans and intercrystalline mode). A closer look on its fracture surface reveals that the specimen fails predominately by transgranular cleavage on significantly enlarged grains and only a small amount of intergranular fracture morphology can be seen near the edges. This is an indication that for the annealed foil, the ductile to brittle transition temperature is shifted to significantly higher temperatures even for such thin foils (at least above 200°C). The beneficial elongated, fine grained microstructure leading to the improved fracture properties of the tungsten foil should be preserved at higher temperatures and processes like grain growth and recrystallization should be avoided at any circumstance.

B.4. Discussion

B.4.1. The role of the microstructure

The inherent brittleness of tungsten typically excludes its use as a structural material due to the absence of the necessary fracture resistance. Strengthening mechanisms by grain refinement to the ultrafine-grained (UFG) and nanocrystalline (NC) region, are very efficient methods but usually lead to a loss in ductility, brittle behaviour and poor toughness [35]. However, with proper microstructural design strategies it is possible to develop high-strength tungsten materials with exceptionally high fracture toughness. The tested 100µm tungsten foil is an example where an extraordinary combination of increased strength and high fracture resistance can be achieved. The key reason for these exceptional mechanical properties lies within a deformation induced grain refinement and development of a beneficial microstructure of thin elongated grains.

Applying high degree of plastic deformation results in grain size decrease which affects the mechanical behavior of the material. The yields stress, for example, is significantly influenced and can be linked to the grain size by the well-known Hall-Petch relation [36], [37]. Additionally, mechanisms of plastic deformation are expected to be a function of grain size. In the case of polycrystalline metals, the grain size dependence of ductile fracture toughness is related to the effect of grain boundaries on the local plastic deformation. An increase in fracture toughness will occur when grain boundary zones are preferred sites for plastic deformation [38]. A critical aspect of increased toughness is the ability of material to plastically deform, which is mostly associated with motion of dislocations. As a result, a local reduction of high stresses is enabled which would otherwise cause material to fracture. Bonk et al.

showed that alternation of the microstructure of the tungsten foil towards the ultrafine-grain sizes results in increased strength and evolution of RT ductility with a very narrow hardening region in the stress-strain curve [27].

Looking into the micromechanisms controlling the fracture process, distinction is made between a micro-ductile crack propagation and a crack propagation by de-cohesion process (transgranular or intergranular). Both are associated with local plastic deformation and represent the dominant fracture mechanism in different grain size regimes. However, the difference associated with further grain refinement is related to the enlargement of the potential places for the formation of pores and nanocracks by an increase in density of GBs, GB triple junctions and arrangement of dislocations in the vicinity of GB [39]. The enhanced fracture toughness obtained for ultrafine-grained tungsten foil is attributed to the mechanism of delamination toughening, which will be further addressed in following sections.

Pronounced alignment and elongation of the microstructure in the principal deformation direction is the second essential microstructural feature which controls the fracture process of the investigated foil. Such a distinctive grain shape inevitably leads to the anisotropic mechanical properties. As a result of such a grain geometry, the formation of exceptionally tough materials in one or two testing directions can be achieved. A complete characterization of fracture toughness of the foil would require investigating the following three specimen configuration: crack delamination, crack arrester and crack divider configuration [40], which are dependent on the external loading orientation and the arrangement of the crack. Due to the foil thickness restrictions within this study, the chosen sample orientation corresponds to the crack divider configuration where the grains are orientated with their long axes perpendicular to the crack propagation direction. Within this configuration, as outlined in chapter 2, fracture behavior is investigated in three pre-crack direction systems: T-L, L-T and 45°.

The observed variation of the fracture toughness values within different systems can be attributed to two aspects of the elongated microstructure: a) strong <110> rotated cubic texture and b) the grain shape anisotropy along the rolling direction. The crack orientation dependence is related to the spatial distribution of weak sites (such as cleavage planes) and boundaries of elongated grains. The samples with a crack at 45° in respect to RD, to our surprise, show the highest fracture toughness values in almost entire temperature range. This noticeable behaviour might be attributed to the texture of the foil which allows the main slip direction of bcc metals, the <111> direction, to be congruent to the maximum shear stress. Additionally, this is the system showing the highest plastic strain in a tensile test [34]. Fracture properties of samples with crack propagating perpendicular and parallel to the RD are in similar range, with the T-L system having slightly higher toughness. A very fine grained microstructure provides a higher density of the elongated grain boundaries lying normal to the initial crack orientation constitute a barrier against crack propagation. Variance in fracture toughness of L-T and T-L systems is related to the difference in the amount of grain boundaries appearing in the crack propagation direction. The grain shape and orientation effect might not be as influential when the failure is in the ductile regime or when it fails completely brittle, as the fracture toughness anisotropy is less pronounced at these temperatures. The difference in material response could also be attributed to the geometrical arrangement of areas with low and high fracture toughness with respect to the crack system. Anisotropic

distribution can be a result of different contributions from the grain boundary toughness, K^{gb} and toughness of the grains, K^{grains}.

B.4.2. Delamination toughening mechanism

Alongside with studying the origin of the high fracture toughness and its dependence on the loading direction and testing temperature, it is very important to determine deformation characteristics and micromechanisms controlling the fracture process by analysing the obtained fractographs. The results show that for all the three tested systems, the fracture toughness is lowest at -196°C with the occurrence of the transcrystalline fracture mode. In this case, the micromechanisms controlling the fracture toughness is de-cohesion process by cleavage of the individual crystal grains along certain crystallographic planes. The crack easily propagates in the designated crack growth direction yielding low K values. Combined with a noticeable increase of toughness, the ductile to brittle transition temperature is identified at ambient temperatures by the pronounced transition from a transcrystalline cleavage to a ductile laminate failure mode influenced by the underlying microstructure. In the transition regime, elongated, pancake-shaped grains lead to the enhanced toughness through the mechanism of delamination toughening. This mechanism leads to the characteristic appearance because of the secondary microscopic crack systems propagating perpendicular to the primary crack growing plane. As a consequence of the formation of the microscopic delamination cracks, a sample is locally divided into many thin sheet ligaments which deform plastically in a nearly plane stress state. Following delamination cracking, thin ligaments as the remaining areas between the delaminations will further stretch and eventually fail in a ductile manner. The deformation prior to final fracture by shearing of the thin ligaments is accompanied with formation of some pores and their coalescence. The origin of the micro delamination is connected to weak crack planes of low fracture toughness parallel to the foil plane, so that the splitting between grain boundaries can easily occur.

It is well-known that the constraint to plastic deformation is maximized in thick samples, so that the fracture energy is reduced in comparison to thin sample subjected to plane stress conditions [28]. The introduction of delamination leads to a drastic change in the stress state from plane strain to a plane stress dominated one (see schematic Figure B.9). Delamination of the interfaces, which are perpendicular to the crack plane, relaxes the stress component in thickness direction, σ_{zz}, which further results in the reduction of tensile triaxiality. This stress component can also be called the through-thickness stress. So, when delamination occurs, the effective thickness of the sample is reduced and at each ligament the σ_{zz} stress goes to nearly zero, reaching plane stress condition which will result in higher toughness. Consequently, the sample behaves like a stack of even thinner foils instead of one thick sample. So, the extend of fracture toughness is determined by the stress state at the crack tip and it increases with decreasing tensile triaxiality. The controlling factor of the increase in fracture toughness is the number of introduced weak boundaries in the specimen: the more interfaces will lead to the thinner ligaments which will have a higher tendency towards plane stress condition. With an increase in temperature above 200°C, less delamination i.e. larger sheet-like laminate regions, which can sustain a significant plastic deformation before and during the crack propagation, can be seen and the

conditional fracture toughness decreases.

Fracture toughness in ultrafine grained materials can be enhanced by this mechanism which is mainly controlled by features of anisotropic microstructure: small grain size in SD direction, the elongated grain shape and the <110> rotated cube deformation texture. The mechanism of delamination toughening has been known to lead to improved toughness in a wide variety of materials, for example in ceramics [41], carbon [42], fine-grained steels [43]–[45] and some bcc metals [46]–[48]. This effect has also been observed in the case of deformed tungsten products: rods [14] and plates [49].
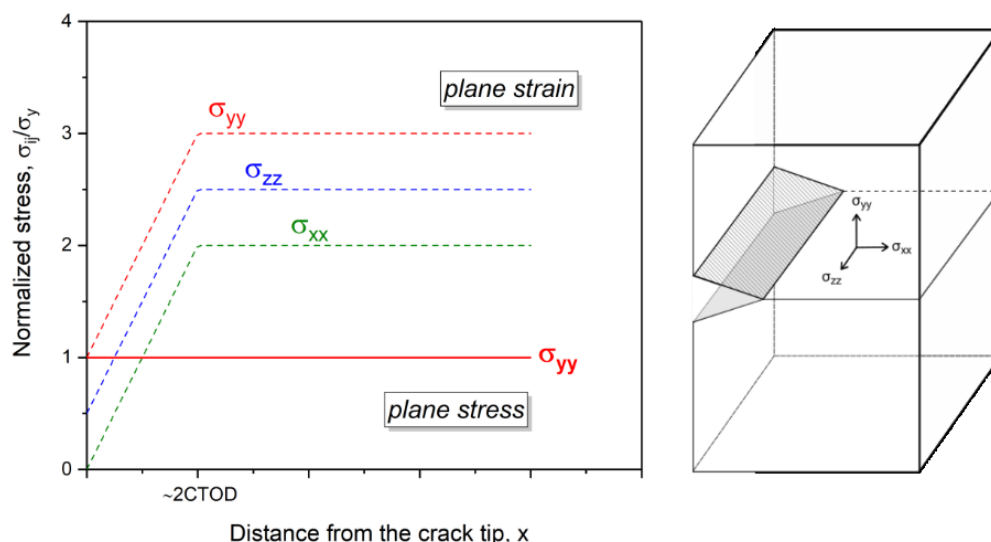

Figure B.9. Comparison of a normalized stress distribution ahead of a crack tip in the case of plane strain and plane stress state; σ_y is the plane stress. Geometry of a notch and directions of the σ_{xx}, σ_{yy} and σ_{zz} stresses can be seen as well.

B.4.3. The origin of the room temperature DBT

The anisotropic fracture properties discussed in previous chapters are linked with underlying ultrafine-grained microstructure, which also could manifest in the strong anisotropy of DBTT. Considering there is a wide temperature range between the lowest testing temperature of liquid nitrogen and RT, it is unclear whether DBTT for the investigated crack systems is affected by different crack initiation directions. Nevertheless, the fact that for ultrafine-grained tungsten foil this distinctive transition occurs at ambient temperatures represent an incredible result for a tungsten material.

The nature of ductile to brittle transition was a subject of extensive research in the past, where identification of potential mechanisms is linked with understanding crack tip plasticity [11], [50]. Emission of dislocations at the crack tip has two toughening effects: an effective shielding of the crack from the applied load and blunting of the crack tip which increases the load necessary to propagate the crack. The dislocation emission occurs in two steps through the nucleation of dislocations followed by dislocation glide. Attributed to this, two main study directions were followed considering DBTT mainly dominated by either dislocation nucleation or dislocation mobility. Models describing the DBTT as a

nucleation-controlled event assume that a sufficient amount of dislocations cannot be emitted due to the lack of active dislocation sources; thus effective shielding is not provided at low temperatures [51], [52]. Models describing the DBTT as a mobility-controlled event assume that instantaneous nucleation of further dislocations is inhibited by a large number of dislocations that cannot leave the crack tip region fast enough [53], [54]. A definite conclusion of the mechanisms limiting plastic deformation of the crack tip region is still not made.

A lot of effort has been made in experimental and theoretical studies of tungsten single crystal [11], [50], with the main conclusion from Giannattasio and Roberts stating that the DBTT is controlled by the glide of screw dislocations [12]. In the case of materials with a unique grain structure, such as polycrystalline ultrafine-grained foil, different microstructural features need to be taken into account. A decrease in grain size leads to the confinement of the plastic zone by grain boundaries as dislocations are piled up at the boundaries. The shielding dislocation pile-up closest to the crack tip, will cause high stresses in the neighbouring grain. Activation of the DBTT in such case could be related to the dislocation-grain-boundary interaction energy [55]. Evaluating the nature of the DBTT for annealing coarse-grained and as received UFG tungsten foil, Nemeth et al. concluded that the glide of the non-screw dislocations is responsible deformation mechanism for heavily deformed tungsten [18]. In contrast to that, for the same tested material Reiser et al. relates the decrease in DBTT to the availability of dislocation sources and the glide of screw dislocations [56]. Additionally, it was shown that the DBTT temperature in tungsten scales with Hall-Petch like equation, according to which grain refinement leads to the decrease in transition temperature.

At this point we would like to address to the work of Bonnekoh et al. where the change in temperature of the DB transition is studied through increasing degree of rolling. In the same way as in our study, fracture tests based on the K-concept were performed and for the most heavily deformed tungsten plate i.e. 100μm tungsten foils, the DBTT was found to be at -65°C [19]. Obtained values of fracture toughness are somewhat higher in comparison to our findings which could arise from the absence of a sharp pre-crack in the samples tested by Bonnekoh, which would lead to the enhancements of the stress level ahead of the tip, resulting in higher apparent toughness values and lower DBTT. However, we believe that the introduction of the atomically-sharp worst-case flaw in the material i.e. the pre-cracking of the test sample is an essential step in the fracture mechanical description of toughness.

Connection between grain size reduction and lowering of the DBTT can moreover be understood from the Yoffee diagram, an idealized representation of the relative likelihood of ductile or brittle fracture at the tip of a pre-existing crack [57]. The ductile-to-brittle transition in bcc metals is accompanied with a transition in the fracture mechanisms which is often interpreted as a result of a competition between the brittle fracture stress σ_F (cleavage resistance stress) and the crack tip stress σ_T. The crack tip stress is defined as the peak tensile stress in the process zone of the crack tip in the elastic-plastic material and it scales with the yield stress σ_y. On the basis of this diagram, the DBTT will occur when the σ_T exceeds the σ_F or in other words as long as the crack tip stress is below the cleavage resistance stress, the materials yields before cleavage and the material behaviour is ductile [44]. Grain refinement through rolling processes successfully enhances the yield stress (grain boundary hardening, dislocation hardening). However, fracture stresses also increase with a reduction in the average grain size and

since this grain-size dependence is higher than the grain-size dependence of a yield stress, the ductile to brittle transition temperature decreases [57]. Occurrence of the delaminations reduces the stresses in addition.

Alongside with the effect of grain refinement, the shift of the DBTT is largely attributed to the delamination toughening mechanism. In the work from Kim and Brozzo [58], [59], increased fracture toughness in the transition region is related to the cleavage crack initiation and propagation. The cleavage fracture unit, defined as the length of a cleavage between the two neighbouring breakthrough points in its propagation direction, is reduced by grain refinement. The formation of cleavage facets and the emission of crack tip dislocations are interrupted by grain boundaries, as the crack progresses through several grains. If the cleavage crack moves across HAGB, the crack front must be branched and together with the separation of the grain boundary between the breakthrough points, additional portion (plastic shearing or formation of crack bridging regime and deformation failure of the bridges) of fracture work is created. As thoroughly discussed in previous chapter, this effect of branching of the main crack along the weak boundary sites parallel to the longitudinal direction, is associated with a relaxation of the triaxial stress state towards a state of biaxial tension. Occurrence of delamination is often linked to the elongated grains and is therefore attributed to the ultrafine grain structures of the examined tungsten foil.

B.5. Conclusions

In this work, the fracture mechanical assessment of 100μm thin UFG tungsten foil was performed in a temperature range from -196°C to 800°C. In order to study the influence of the elongated microstructure and texture on the resulting fracture toughness, tests were conducted in three specimen orientations. The main conclusions can be summarized as following:

- W in form of thin foils has a pancake-shaped layered microstructure parallel to the rolling direction. The EBSD analyses reveal that substantial grain refinement occurs in SD direction reaching the ultrafine grained regime.
- The investigated foil has a pronounced rotated-cube crystallographic texture, with a most dominant {001}<110> orientation.
- The performed fracture investigations indicate a superior behavior of a thin foil, high values of fracture toughness and a reduction of the DBTT to about RT. The extraordinary fracture properties can be related to the beneficial ultrafine grained and elongated microstructure.
- The SEM investigation of the fracture surfaces reveals distinctive behavior for different testing temperature regimes, with a very pronounced evolution of fracture modes over the entire temperature range:
  - ✓ At -196°C samples fracture in classical brittle, transcrystalline manner associated with the lowest values of K_q. The controlling micromechanism is de-cohesion process by cleavage of the individual crystal grains predominately along (100) crystallographic planes.

- ✓ In the intermediate temperature range (RT and 200°C) fracture surfaces show pronounced delaminations; significantly enhanced toughness is attributed to the reduction of tensile triaxiality and drastic change in the stress state in front of the crack tip.
- ✓ With increasing testing temperature samples show more plastic deformation before final ductile failure occurs. The apparent decrease of K_q is mainly related to the limits of LEFM validity and violation of the small scale yielding criterion; thus calculated critical stress intensity values can be considered as lower limit.

- 3D topography reconstruction of the fractured surfaces of a sample of the 45° system tested at 800°C was completed, enabling the determination of the CTOD as a parameter of fracture toughness of a ductile material. The obtained difference of K_{CTOD} and K_q by a factor of three emphasizes the importance of determining the degree of underestimation of the fracture toughness values in the elastic-plastic regime.

- The observed variation of the fracture toughness values within different systems can be attributed to two aspects of the elongated microstructure: a) strong <110> rotated cubic texture and b) the grain shape anisotropy along the rolling direction. The spatial distribution of weak sites (such as cleavage planes) and boundaries of elongated grains play an additional role.

- Annealing at 1400°C for 1h in vacuum shows that heat treatments considerably affect the thin foil microstructure through a complete loss of elongated grain shape, onset of significant grain coarsening and a substantial reduction of the grain boundary area. As a result, annealed foils show lower fracture toughness values and a transition in failure mode towards a brittle, mixed fracture surface.

Based on these results, it can be concluded that a deformation induced grain refinement and a formation of beneficial microstructure of thin, elongated grains is a successful recipe for obtaining a W material with exceptional fracture properties. As demonstrated in the case of thin foil, the tungsten-related problems of poor fracture resistance at low temperatures and high DBTT can be overcome, thus potentially extending the use of W as a structural component.

Acknowledgments

B.6. References

[1]   E. Lassner and W.-D. Schubert, *Tungsten - Properties, Chemistry, Technology of the Element, Alloys and Chemical Compounds*. New York: Kluwer Academic/Plenum Publishers, 1999.

[2]   M. Rieth *et al.*, "Recent progress in research on tungsten materials for nuclear fusion applications in Europe," *J. Nucl. Mater.*, vol. 432, no. 1–3, pp. 482–500, 2013.

[3]   S. Wurster *et al.*, "Recent progress in R&D on tungsten alloys for divertor structural and plasma facing materials," *J. Nucl. Mater.*, vol. 442, no. 1–3, pp. 181–189, 2013.

[4]   P. L. Raffo, "Yielding and Fracture in tungsten and tungsten rhenium alloys," *J. Less-Common Met.*, vol. 17, pp. 133 – 149, 1969.

[5]   S. Wurster, B. Gludovatz, and R. Pippan, "High temperature fracture experiments on tungsten-rhenium alloys," *Int. J. Refract. Met. Hard Mater.*, vol. 28, no. 6, pp. 692–697, 2010.

[6]   A. Luo, D. L. Jacobson, and K. S. Shin, "Solution softening mechanism of iridium and rhenium in tungsten at room temperature," *Int. J. Refract. Met. Hard Mater.*, vol. 10, no. 2, pp. 107–114, 1991.

[7]   J. Riesch *et al.*, "In situ synchrotron tomography estimation of toughening effect by semi-ductile fibre reinforcement in a tungsten-fibre-reinforced tungsten composite system," *Acta Mater.*, vol. 61, no. 19, pp. 7060–7071, 2013.

[8]   Q. Wei *et al.*, "Mechanical behavior and dynamic failure of high-strength ultrafine grained tungsten under uniaxial compression," *Acta Mater.*, vol. 54, no. 1, pp. 77–87, 2006.

[9]   M. Faleschini, H. Kreuzer, D. Kiener, and R. Pippan, "Fracture toughness investigations of tungsten alloys and SPD tungsten alloys," *J. Nucl. Mater.*, vol. 367–370 A, pp. 800–805, 2007.

[10]   Q. Wei and L. J. Kecskes, "Effect of low-temperature rolling on the tensile behavior of commercially pure tungsten," *Mater. Sci. Eng. A*, vol. 491, no. 1–2, pp. 62–69, 2008.

[11]   P. Gumbsch, J. Riedle, A. Hartmaier, and H. F. Fischmeister, "Controlling factors for the brittle-to-ductile transition in tungsten single crystals," *Science (80-.).*, vol. 282, no. November, pp. 1293–1295, 1998.

[12]   A. Giannattasio and S. G. Roberts, "Strain-rate dependence of the brittle-to-ductile transition temperature in tungsten," *Philos. Mag.*, vol. 87, no. 17, pp. 2589–2598, 2007.

[13]   P. Gumbsch, "Brittle fracture and the brittle-to-ductile transition of tungsten," *J. Nucl. Mater.*, vol. 323, no. 2–3, pp. 304–312, 2003.

[14]   D. Rupp and S. M. Weygand, "Anisotropic fracture behaviour and brittle-to-ductile transition of polycrystalline tungsten," *Philos. Mag.*, vol. 90, no. 30, pp. 4055–4069, 2010.

[15]   B. Gludovatz, S. Wurster, A. Hoffmann, and R. Pippan, "Fracture toughness of polycrystalline tungsten alloys," *Int. J. Refract. Met. Hard Mater.*, vol. 28, no. 6, pp. 674–678, 2010.

[16]   J. Reiser, M. Rieth, B. Dafferner, S. Baumgärtner, R. Ziegler, and A. Hoffmann, "Deep drawing of tungsten plates for structural divertor applications in future fusion devices," *Fusion Eng. Des.*, vol. 86, no. 12, pp. 2949–2953, 2011.

[17]   V. Nikolic, S. Wurster, D. Firneis, and R. Pippan, "Improved fracture behavior and microstructural

characterization of thin tungsten foils," *Nucl. Mater. Energy*, vol. 9, pp. 181–188, 2016.

[18] A. A. N. Nemeth, J. Reiser, D. E. J. Armstrong, and M. Rieth, "The nature of the brittle-to-ductile transition of ultra fine grained tungsten (W) foil," *Int. J. Refract. Met. Hard Mater.*, vol. 50, pp. 9–15, 2015.

[19] C. Bonnekoh, A. Hoffmann, and J. Reiser, "The brittle-to-ductile transition in cold rolled tungsten: On the decrease of the brittle-to-ductile transition by 600 K to − 65 °C," *Int. J. Refract. Met. Hard Mater.*, vol. 71, pp. 181–189, 2018.

[20] Plansee, "www.plansee.com/de/werkstoffe/wolfram.html," *accessed date 2015-11-01.* .

[21] J. Neges, B. Ortner, G. Leichtfried, and H. P. Stüwe, "On the 45° embrittlement of tungsten sheets," *Mater. Sci. Eng. A*, vol. 196, no. 1–2, pp. 129–133, 1995.

[22] B. Tabernig and R. Pippan, "Determination of the length dependence of the threshold for the fatigue crack propagation," *Eng. Fract. Mech.*, vol. 69, no. 8, pp. 899–907, 2002.

[23] "ASTM E399-90, Standard test method for plane-strain fracture toughness of metallic materials.," in *Annual Book of ASTM Standards*, Philadelphia (PA):American Society of Testing and Materials, 1997.

[24] B. Gludovatz, S. Wurster, T. Weingärtner, a. Hoffmann, and R. Pippan, "Influence of impurities on the fracture behaviour of tungsten," *Philos. Mag.*, vol. 91, no. 22, pp. 3006–3020, 2011.

[25] Y. Murakami, *Stress Intensity Factors Handbook*. Pergamon, 1987.

[26] O. Kolednik and H. P. Stüwe, "The stereophotogrammetric determination of the critical crack tip opening displacement," *Eng. Fract. Mech.*, vol. 21, no. 1, pp. 145–155, 1985.

[27] S. Bonk, J. Hoffmann, A. Hoffmann, and J. Reiser, "Cold rolled tungsten (W) plates and foils: Evolution of the tensile properties and their indication towards deformation mechanisms," *Int. J. Refract. Met. Hard Mater.*, vol. 70, no. September 2017, pp. 124–133, 2018.

[28] T. L. Anderson, *Fracture mechanics : fundamentals and applications*. 2004.

[29] J. Reiser, M. Rieth, B. Dafferner, and A. Hoffmann, "Charpy impact properties of pure tungsten plate material in as-received and recrystallized condition (1 h at 2000 °C (2273 K))," *J. Nucl. Mater.*, vol. 442, no. 1–3, pp. S204–S207, 2013.

[30] J. Stampfl, S. Scherer, M. Berchthaler, M. Gruber, and O. Kolednik, "Determination of the fracture toughness by automatic image processing," *Int. J. Fract.*, vol. 78, pp. 35–44, 1996.

[31] J. Stampfl, S. Scherer, M. Gruber, and O. Kolednik, "Reconstruction of surface topographies by scanning electron microscopy for application in fracture research," *Appl. Phys. A Mater. Sci. Process.*, vol. 63, no. 4, pp. 341–346, 1996.

[32] S. Bonk, J. Reiser, J. Hoffmann, and A. Hoffmann, "Cold rolled tungsten(W) plates and foils: Evolution of the microstructure," *Int. J. Refract. Met. Hard Mater.*, vol. 60, pp. 92–98, 2016.

[33] J. Reiser, M. Rieth, B. Dafferner, A. Hoffmann, X. Yi, and D. E. J. A. C, "Tungsten foil laminate for structural divertor applications – Analyses and characterisation of tungsten foil," *J. Nucl. Mater.*, vol. 424, pp. 197–203, 2012.

[34] J. Reiser *et al.*, "Tungsten foil laminate for structural divertor applications – Tensile test properties of tungsten foil," *J. Nucl. Mater.*, vol. 434, pp. 357–366, 2013.

[35] A. Hohenwarter, C. Kammerhofer, and R. Pippan, "The ductile to brittle transition of ultrafine-

grained Armco iron: An experimental study," *J. Mater. Sci.*, vol. 45, no. 17, pp. 4805–4812, 2010.

[36]   E. O. Hall, "The deformation and aging of mild steel. III: Discussion of results," *Proc. Phys. Soc. Lond. B*, vol. 64, pp. 747–753, 1951.

[37]   N. J. Petch, "The Cleavage Strength of Polycrystals," *J. Iron Steel Inst.*, vol. 174, pp. 25–28, 1953.

[38]   Z. Fan, "The grain size dependence of ductile fracture toughness of polycrystalline metals and alloys," *Mater. Sci. Eng. A*, vol. 191, no. 1–2, pp. 73–83, 1995.

[39]   R. Pippan and A. Hohenwarter, "The importance of fracture toughness in ultrafine and nanocrystalline bulk materials," *Mater. Res. Lett.*, vol. 4, no. 3, pp. 127–136, 2016.

[40]   J. L. H. Richard W. Hertzberg, Richard P. Vinci, *Deformation and Fracture Mechanics of Engineering Materials*, 5th Editio. Wiley, 2012.

[41]   W. J. Clegg, K. Kendall, N. M. Alford, T. W. Button, and J. D. Birchall, "A simple way to make tough ceramics," *Nature*, vol. 347, no. 6292, pp. 455–457, 1990.

[42]   M. Sakai, R. C. Bradt, and D. B. Fischbach, "Fracture toughness anisotropy of a pyrolytic carbon," *J. Mater. Sci.*, vol. 21, no. 5, pp. 1491–1501, 1986.

[43]   Y. Kimura, T. Inoue, F. Yin, and K. Tsuzaki, "Inverse Temperature Dependence of Toughness in an Ultrafine Grain-Structure Steel," *Science (80-.).*, vol. 320, no. 5879, pp. 1057–1060, 2008.

[44]   T. Inoue, F. Yin, Y. Kimura, K. Tsuzaki, and S. Ochiai, "Delamination effect on impact properties of ultrafine-grained low-carbon steel processed by warm caliber rolling," *Metall. Mater. Trans. A Phys. Metall. Mater. Sci.*, vol. 41, no. 2, pp. 341–355, 2010.

[45]   R. Song, D. Ponge, and D. Raabe, "Mechanical properties of an ultrafine grained C-Mn steel processed by warm deformation and annealing," *Acta Mater.*, vol. 53, no. 18, pp. 4881–4892, 2005.

[46]   A. Hohenwarter and R. Pippan, "Fracture of ECAP-deformed iron and the role of extrinsic toughening mechanisms," *Acta Mater.*, vol. 61, no. 8, pp. 2973–2983, 2013.

[47]   K. Babinsky, S. Primig, W. Knabl, A. Lorich, R. Stickler, and H. Clemens, "Fracture Behavior and Delamination Toughening of Molybdenum in Charpy Impact Tests," *Jom*, vol. 68, no. 11, pp. 2854–2863, 2016.

[48]   B. V. Cockeram, "The role of stress state on the fracture toughness and toughening mechanisms of wrought molybdenum and molybdenum alloys," *Mater. Sci. Eng. A*, vol. 528, no. 1, pp. 288–308, 2010.

[49]   M. Rieth and A. Hoffmann, "Influence of microstructure and notch fabrication on impact bending properties of tungsten materials," *Int. J. Refract. Met. Hard Mater.*, vol. 28, no. 6, pp. 679–686, 2010.

[50]   S. G. Roberts, P. B. Hirsch, A. S. Booth, F. C. Serbena, and M. Ellis, "Dislocations, cracks and brittleness in single crystals," *Phys. Scr.*, vol. 1993, no. T49B, pp. 420–426, 1993.

[51]   J. R. Rice and R. Thomson, "Ductile versus brittle behaviour of crystals," *Philos. Mag.*, vol. 29, no. 1, pp. 73–97, 1974.

[52]   M. Khantha, D. P. Pope, and V. Vitek, "Dislocation screening and the brittle-to-ductile transition: A Kosterlitz-Thouless type instability," *Phys. Rev. Lett.*, vol. 73, no. 5, pp. 684–687, 1994.

[53]   S. G. Roberts, "Modelling the brittle to ductile transition in single crystals," in *Computer simulation in materials science*, 1996, pp. 409–433.

[54]   P. B. Hirsch, S. G. Roberts, and J. Samuels, "The Brittle-Ductile Transition in Silicon. II. Interpretation," *Proc. R. Soc. A Math. Phys. Eng. Sci.*, vol. 421, no. 1860, pp. 25–53, 1989.

[55]   X. H. Zeng and A. Hartmaier, "Modeling size effects on fracture toughness by dislocation dynamics," *Acta Mater.*, vol. 58, no. 1, pp. 301–310, 2010.

[56]   J. Reiser *et al.*, "Ductilisation of tungsten (W): On the shift of the brittle-to-ductile transition (BDT) to lower temperatures through cold rolling," *Int. J. Refract. Met. Hard Mater.*, vol. 54, pp. 351–369, 2016.

[57]   J. W. Morris Jr., "Materials Science: Stronger, Tougher Steels," *Science (80-.).*, vol. 320, no. 5879, pp. 1022–1023, 2008.

[58]   S. Kim, Y. R. Im, S. Lee, H. C. Lee, Y. J. Oh, and J. H. Hong, "Effects of alloying elements on mechanical and fracture properties of base metals and simulated heat-affected zones of SA 508 steels," *Metall. Mater. Trans. A Phys. Metall. Mater. Sci.*, vol. 32, no. 4, pp. 903–911, 2001.

[59]   P. Brozzo, G. Buzzichelli, A. Mascanzoni, and M. Mirabile, "Microstructure and cleavage resistance of low-carbon bainitic steels," *Met. Sci.*, vol. 11, no. 4, pp. 123–130, 1977.

Publication B

C

The effect of heat treatments on pure and potassium doped drawn tungsten wires: Part I – Microstructural characterization

Vladica Nikolić [a], Johann Riesch[b], Reinhard Pippan[a]

[a] Erich Schmid Institute of Materials Science of the Austrian Academy of Sciences, Leoben, Austria
[b] Max Planck Institute for Plasma Physics, Garching, Germany

Abstract

Advanced tungsten fiber-reinforced composites (W_f/W), showing pseudo ductile behaviour even at room temperature, are a promising option for future fusion reactors as the intrinsic brittleness of tungsten can be mitigated effectively. The drawn tungsten wires used as reinforcements are the key components of the composites, thus their mechanical properties and thermal stability define the allowed operation / fabrication temperature of the composite material itself. In this work, a comprehensive characterization of the pure and potassium doped tungsten wires was performed, focusing on the influence of various heat treatments on different microstructural features (nature of grain boundaries, grain shape and size, texture analyses) and mechanical properties. Annealing in the temperature range from 900 to 1600 °C enables the investigation of the microstructural stability of the two materials and arising annealing phenomena – recovery, recrystallization and grain growth. The results demonstrate that the pure tungsten recrystallizes fully in the temperature range 1300-1500 °C accompanied with tremendous coarsening and a complete loss of the initial fibrous, elongated grain structure. In contrast to this, potassium doped wire shows superior high temperature properties, where the performed heat treatments cause only milder microstructural changes, consequently suppressing recrystallization and grain growth to temperatures well above the investigated ones. Furthermore, hardness measurements and observed softening complement the discussion of the grain morphology evolution.

C.1. Introduction

The realization of commercial fusion energy systems is closely related to the development of the advanced materials capable of sustaining the harsh and challenging environment of a reactor device. This so called plasma facing components (PFC) are exposed to enormous particle fluxes, which impose extreme heat loads on the materials in use [1,2]. Tungsten (W) stands out as the most promising candidate for the first wall and divertor material [3,4] due to the highest melting point of all metals (thus allowing operation at elevated temperatures), good thermal conductivity, low tritium retention and low erosion [5]. However, as other bcc metals, tungsten features an intrinsic brittleness below the ductile-to-brittle transition temperature, which is rather high, being typically around 200 – 300 °C for a standard bulk tungsten and moreover increased upon annealing [6,7]. Additional challenges associated with the use of W are further operational embrittlement caused by neutron irradiation [8] and/or recrystallization by overheating [9,10]. Thus, a successful design of the next generation of fusion reactors will greatly depend on the availability of the novel options of the tungsten based materials.

Tungsten fibre-reinforced composites (W_f/W) are extensively investigated as a potential material for advanced plasma facing components [11]. This composite structure is obtained by embedding commercially available drawn tungsten wires in a tungsten matrix which is produced either by powder metallurgy [12] or by a chemical deposition process [13]. The advantage of W_f/W is in its pseudo ductile behavior and thereby increased toughness as a consequence of extrinsic toughening mechanism such as crack bridging by intact fibres, fibre pull-out, crack deflection and ductile deformation of fibres [14]. In such a way, the brittleness problem of W can be mitigated, making W_f/W composite a feasible PFC alternative. The drawn tungsten wires used as reinforcements are the key structural component of W_f/W composite, which sets the requirement of investigating their mechanical and microstructural properties.

The research on W wires was rather extensive in the past century as this type of material has been used in the light bulb industry as a filament element [15]. The initial efforts were directed towards improving the production and processing routes while mainly using pure tungsten wire. However, embrittlement of pure tungsten as a result of recrystallization, grain growth and thermal fatigue arose as the main issue, which directly influenced lifetime performance of the lamps. The big breakthrough, which determined the course of wire research in the next few decades, was the discovery of the advantageous effect of the doping of tungsten by potassium (K). K bubbles strengthen the grain boundaries by acting as pinning sites and in such way suppress the grain growth to higher temperatures. Thus, the initial advantageous, elongated grain structure can be preserved for a longer operational time. An improved potassium bubble strengthened non-sag tungsten wire was of great importance for the incandescent lamps due to its increased creep resistance at very high temperatures and excellent coiling properties at room temperature [16]. Following years were mostly dedicated to the investigation of topics regarding the potassium bubbles such as their formation and evolution during production [17–19], size modifications during operation [20], mechanisms of reshaping the bubbles during the deformation [21,22], just to name a few.

The potential application of tungsten based composites as structural components for a fusion reactor increased the interest in studying W wires with respect to mechanical properties and recently set off

series of investigations. Both, pure and K-doped tungsten wires show exceptional ductility [23] and significant strength (due to the Hall-Petch effect) [24] at room temperature, properties important for facilitating toughening mechanisms of W_f/W through the crack bridging effect as well as the fibre deformation effect [25]. Furthermore, studies regarding the mechanical response and plastic deformation at elevated temperatures showed that the wire can keep its valuable properties [26,27]. Additionally, some investigations dealt with the question of the effect of annealing on tensile properties of pure [28] and potassium doped tungsten wires [29], interconnecting in such a way general microscopic features to different material responses occurring in the experiment.

Despite a rather wide-ranging body of research on tungsten wires, there are still open questions where a deeper microscopic understanding of the main, important properties is needed. In this context of using tungsten wires as a reinforcement material, performing fracture toughness experiments and investigating the underlying mechanisms that control the fracture process is of great importance. This holds true for the as-fabricated condition, as well as for different states after annealing. The evolution of the different microstructural features as a result of annealing is very important as it is strongly related to the macroscopic materials response and in particular to the fracture behaviour.

The purpose of this work is to perform a systematic study on the effect of heat treatments in the broad range of annealing temperatures and investigate how microstructural and fracture properties develop upon annealing, with the special focus on the relationship between the investigated features. The study is divided into two parts. Here, in the first contribution, a comparison of the microstructural evolution is made between pure and potassium doped tungsten wires; hence, addressing the question of recrystallization phenomena and preservation of the grain structure by addition of doping elements. The use of advanced microscopy tools allows the detailed analyses of the evolution of different aspects of the microstructure (nature of grain boundaries, grain shape and size, texture) enabling the assessment of the different stages of occurring annealing phenomena. The second paper concentrates on the fracture toughness assessment and investigates embrittlement by annealing [30].

C.2. Materials and experimental methods

The materials investigated within this study are drawn pure and potassium doped (K-W, 60 ppm) tungsten wires, commercially available and provided by the OSRAM GmbH, Schwabmünchen. The standard fabrication of a tungsten based material is via the powder metallurgical route by sintering and swaging; subsequent drawing process enables obtaining the final, desired diameter of the wire. The nominal diameter of the investigated material for both types was 150 µm. Besides the as-received wires, series of heat treated samples were produced from both materials. In order to thoroughly study the influence of annealing on the microstructure, heat treatments were conducted at following temperatures: 900 °C, 1100 °C, 1200 °C, 1300 °C, 1400 °C, 1500 °C and 1600 °C. In each case, the holding time was 1 h with subsequent cooling in the furnace until room temperature. The oxidation was avoided by annealing in a tungsten based vacuum furnace (Leybold Heraeus PD 1000) at a pressure < 10^{-5} mbar. To exclude the influence of the composition, all the samples were cut from the same two

spools of pure and K-doped tungsten wires, respectively; therefore, each having the same chemical composition and identical production process.

The preparation of samples suitable for further analyses was conducted by embedding the wire pieces in hard resin, followed by standard polishing steps resulting in the necessary smooth surfaces. For each material and annealing condition, samples were prepared in two principal viewing directions: longitudinal section (plane parallel to the drawing axis) and cross section (plane perpendicular to the drawing axis), as shown in the schematic drawing in Figure C.1. The investigation of the microstructure was performed in a Zeiss Leo 1525 field-emission-gun scanning electron microscope (SEM) with an electron backscatter diffraction (EBSD) detector. The analysis was done using an acceleration voltage of 20 kV and approximately 10 nA probe current. For each kind of wire in both longitudinal and cross sections, an area of 25 x 25 µm^2 was acquired with a step size of 100 nm. As a verification of the performed analyses, both smaller and larger additional scans were collected, showing very similar trends in the microstructural evolution. The presented 25 x 25 µm^2 area was chosen, as it enables making a nice comparison of occurring structural variations at different heat treatments, in both cross and longitudinal sections. Orientation Imaging Microscopy (OIM) software was used to evaluate the obtained EBSD scans. Post-processing was carried out by removing points with a confidence index lower than 0.1. The evaluation of the acquired orientation maps allows the identification of the grain size distribution, qualitative description of the grain shape and studying the nature of the grain boundaries. Misorientations between 5° and 15° are considered as low-angle grain boundaries (LAGB) and high-angle grain boundaries (HAGB) are defined for misorientations between 15° and 65°. Pole figures, determined from the orientation information of the EBSD scans, enable studying the evolution of the texture.

To give the first impression of a correlation between the microstructure and mechanical properties, Vickers hardness measurements were performed for both wires in the as-received and all annealed states. A load of 500 g was applied (4.5N, HV0.5), with a dwell time of 15 s. With these conditions, microhardness was measured in the central area of the longitudinal sections of the wire and for each sample 12 indentations were made within a distance of about 500 µm. The reported hardness values are statistical averages, with the indicated error bars being the standard deviation of the average values.

C.3. Results

C.3.1. Microstructural analyses

The first impression of the deformed microstructure of the as-received wire can be seen from the backscatter electron (BSE) images, where the observed contrast of the image is related to different crystallographic orientations. The initial appearance of both materials is very similar; therefore, to avoid repetition, only the example of the doped tungsten wire in the longitudinal section (Figure C.1a) and cross section (Figure C.1b) is given. As a direct consequence of the drawing process of the wire, a unique microstructure is obtained consisting of extremely elongated grains along the drawing direction.

Perpendicular to the drawing axis, uniformly distributed grains have significantly smaller dimensions. The grains are not equiaxed but rather twisted forming a characteristic curled structure. The influence of annealing, investigated through a systematic microstructural characterization comprising identification of changes of the grain shape and size, analyses of the grain boundaries and evolution of the developed texture, will be addresses in the following chapters.
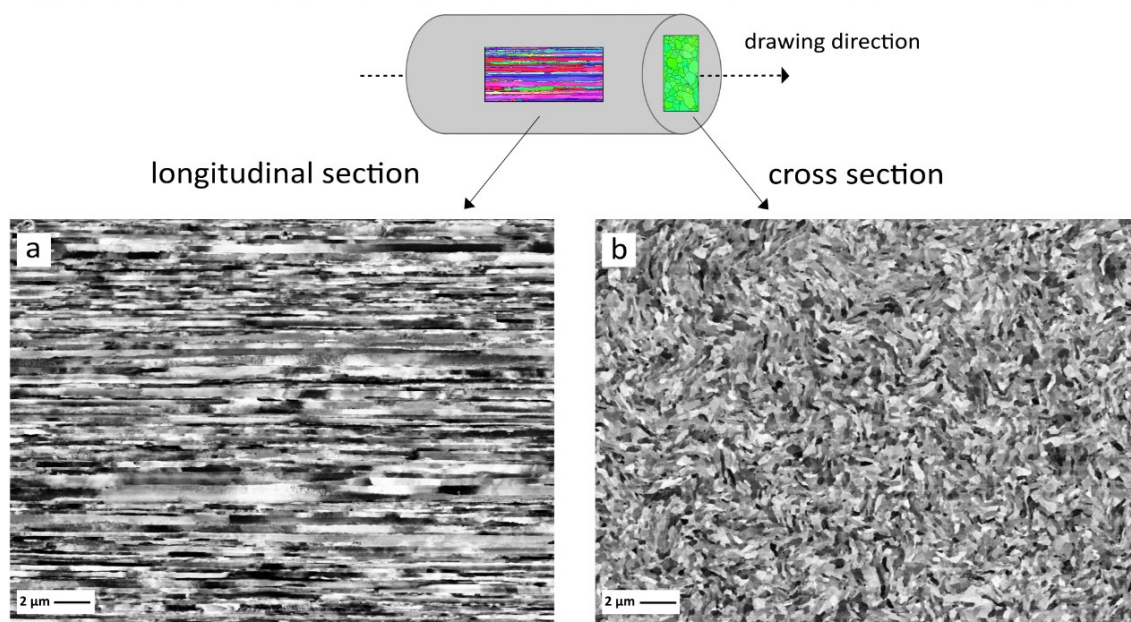

Figure C.1*. Scanning electron micrographs of the as-received potassium doped tungsten wire in the BSE mode taken in the central area across a) longitudinal section and b) cross-section. The schematic drawing on the top shows the principle direction of deformation, as well as the position of the typical scanning areas in respect to the drawing direction.*

C.3.1.1. Grain size and shape

The effect of different heat treatments on the microstructural stability was studied through series of EBSD orientation maps by making a comparison between data acquired in the central region of the cross sections (Figure C.2) and longitudinal sections (Figure C.3) of pure and potassium doped wires. Grains are identified as areas with a continuous orientation, while the low-angle grain boundaries and the high-angle grain boundaries are distinguished in the orientation maps by red and black lines, respectively. Cross sectional scans of the as-received wire reveal a microstructure of uniformly distributed fine grains and in the case of both pure and potassium doped tungsten, similar appearance can be seen. With an increase in annealing temperature substantial microstructural modifications are observed for the pure W (Figure C.2a and Figure C.3a); continuous increase of the grain size is accompanied by the disappearance of curling structures and more equiaxed grain shape. Heat treatment at the highest temperature of 1600 °C leads to tremendous grain growth when compared to the as-received state of the material. In contrast to these observations, K-W wires show only a mild increase in grain size and the microstructure remains rather stable over the entire temperature range

(Figure C.2b and Figure C.3b). The noticeable uniformity of the grain colour in all the scans is an indication of a very pronounced and stable texture of the wires; however, this topic will be treated with greater detail in the chapter 3.1.3. The orientation maps acquired across the longitudinal sections reveal that both materials in the as-received condition have long, thin grains elongated in the drawing direction, with the shortest grain lengths in radial direction of the wire. As seen in Figure C.3a, the characteristic elongated microstructure of the pure W wire is severely influence by heat treatments experiencing alternations in grain size (in both directions of the scan) already at lower temperatures of annealing. The significant coarsening eventually leads to the complete loss of fibrous appearance of the grains, where the microstructure of the final state consists of large, globular µm sized grains. Thermal stability of the K-doped wire can be observed in Figure C.3b, where regardless of some mild growth in the size of the grains, the overall elongated microstructure is preserved, even for the highest annealing temperatures.

From the orientation maps obtained by EBSD, the qualitative analyses of the grain size as a function of annealing temperature is performed. In Figure C.4a, the results extracted from the cross sectional scans can be seen, where the evolution of the area weighted grain diameter is compared for pure and K-doped W wire. The microstructural stability of K-W wire is clearly seen as the grain size increases only slightly over the entire range of annealing temperatures, going from 0.57 µm in the as-received state to the 0.73 µm for the 1600 °C treated sample. However, the heat treatments considerably affect the pure W wire through a tremendous grain coarsening with an average grain diameter changing from 0.47 µm (as-received state) to the value of 5.53 µm (1600 °C). By employing the line intersect length method in both vertical and horizontal orientation of the longitudinal orientation maps, information regarding length and width of the elongated grains can be obtained (Figure C.4b and 4c). Similar trends of the grain coarsening with an increase of annealing temperature can be observed for the pure W wire. Furthermore, the aspect ratio close to 1 is in the agreement with the complete loss of elongated grain shape. K-doped wire experiences significantly milder variations in grain size, with an increase being more pronounced for the length of the elongated grains. Nevertheless, when compared to pure wire, an overall stability of the microstructure can be observed with relatively small aspect ratio remaining rather constant.

a) pure W
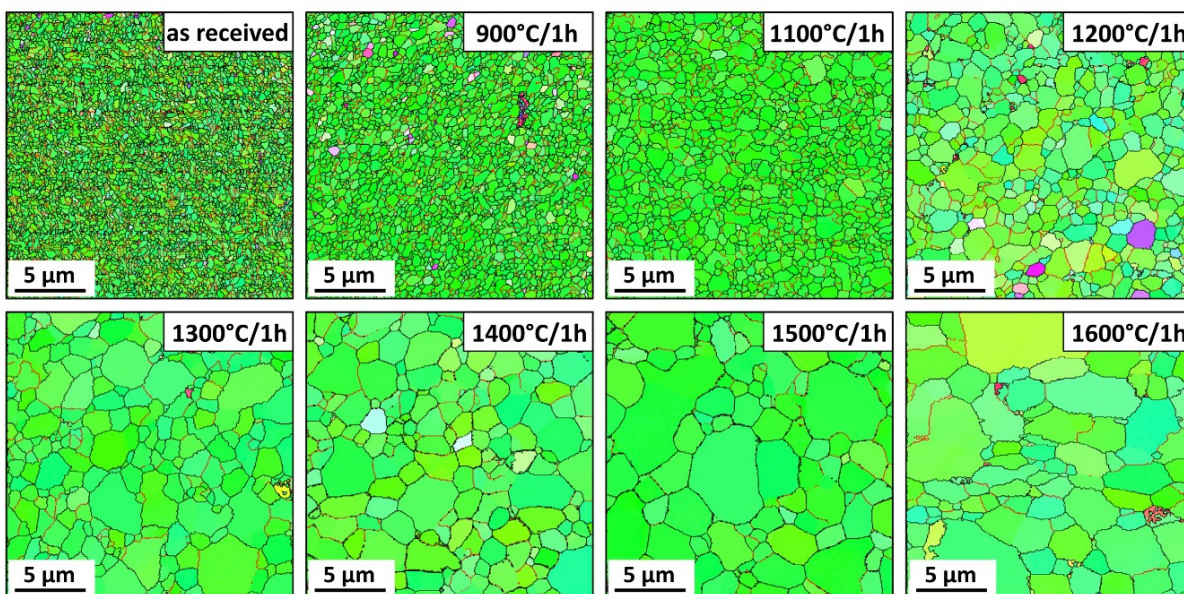
b) K doped W

Figure C.2. EBSD orientation maps of the cross sections of a) pure tungsten and b) potassium doped tungsten wires. The evolution of the microstructure and thermal stability are investigated in respect to different annealing treatments, performed in vacuum for 1h. Colour coded unit triangle is given as well, representing <100>, <110> and <111> crystallographic directions perpendicular to the sample surface. All of the scans were taken with the same magnification.
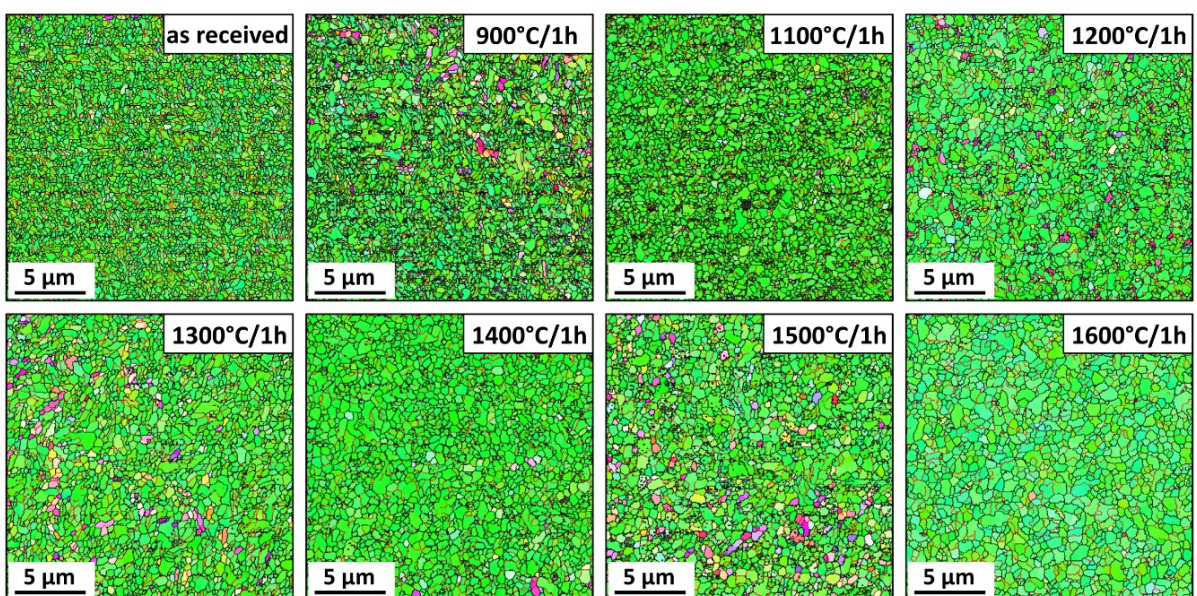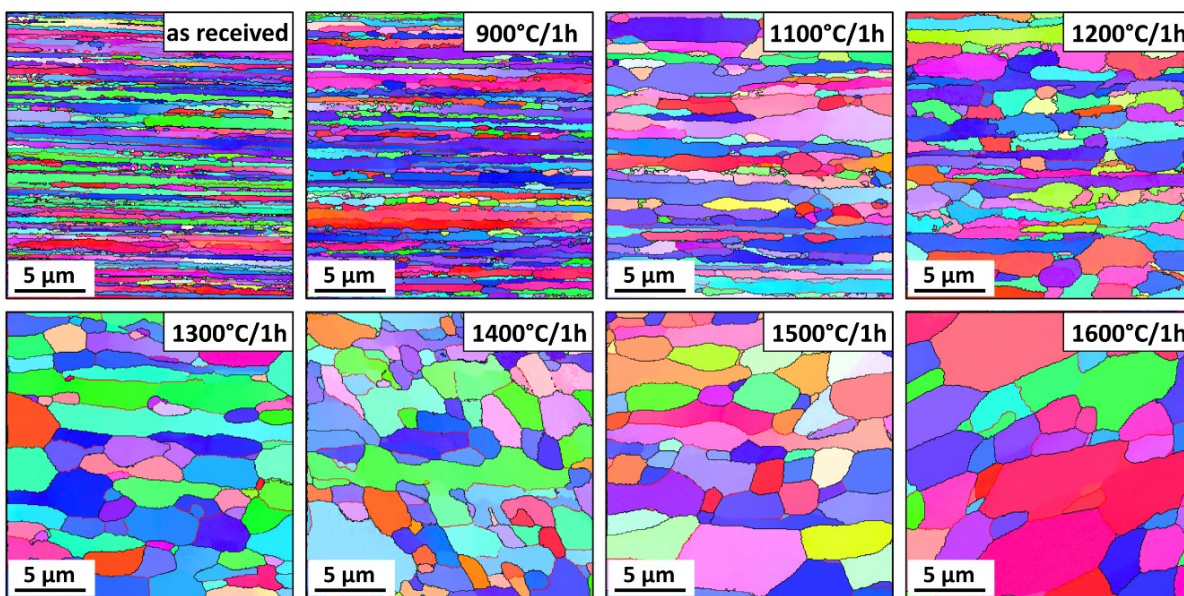
a) pure W

b) K doped W

Figure C.3. *EBSD orientation maps of the longitudinal section of a) pure tungsten and b) potassium doped tungsten wires. The evolution of the microstructure and thermal stability are investigated in respect to different annealing treatments, performed in vacuum for 1h. Colour coded unit triangle is given as well, representing <100>, <110> and <111> crystallographic directions perpendicular to the sample surface. All of the scans were taken with the same magnification.*

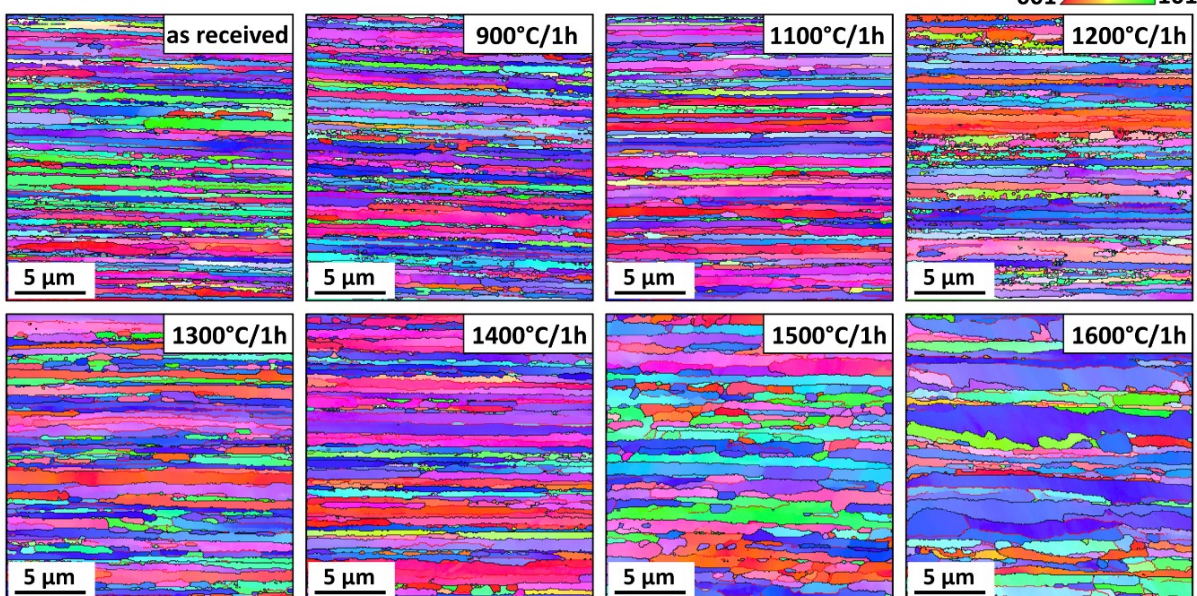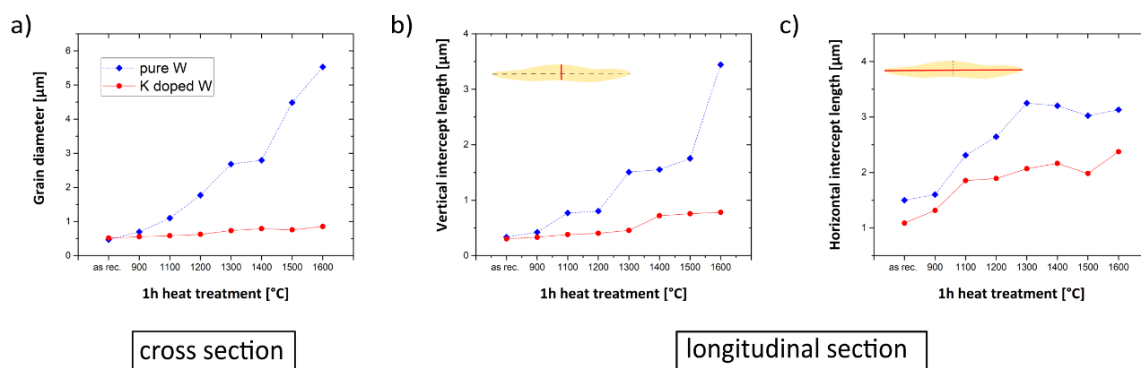Figure C.4. Evolution of the grain dimensions as a function of different annealing conditions, derived by a) area weighted grain diameters from the cross sectional EBSD maps, b) the line intersect method in the vertical direction of the longitudinal sections of the EBSD maps and c) the line intersect method in the horizontal direction of the longitudinal sections of the EBSD maps.

C.3.1.2. The nature of grain boundaries

The type of grain boundary is defined through misorientation angle between neighbouring grains and as already outlined, the low-angle grain boundaries (LAGB, 5°-15°) and the high-angle grain boundaries (HAGB, 15°-65°) are identified in the orientation maps in Figures 2 and 3 as red and black lines, respectively. In order to make these features more distinguishable from the underlying orientation maps, examplary grain boundary maps are given for pure tungsten in the as-received and 1600 °C conditions in both directions of the scanning area (Figure C.5a). Furthermore, due to the importance of grain boundaries for the dislocation motion and related annealing phenomena, the misorientation angles were analysed by their frequency from which the information regarding the total GB length, as well as the individual contributions of LAGB and HAGB can be acquired. Analyses of the total amount of GB per scanning area in respect to different heat treatments are performed from the cross sectional (Figure C.5b) as well as longitudinal orientation maps (Figure C.5c), where fractions of low-angle and high-angle grain boundaries are also shown. Furthermore, a comparison is made between the results of pure and K-doped tungsten wires.

a) GB maps

cross section   longitudinal section
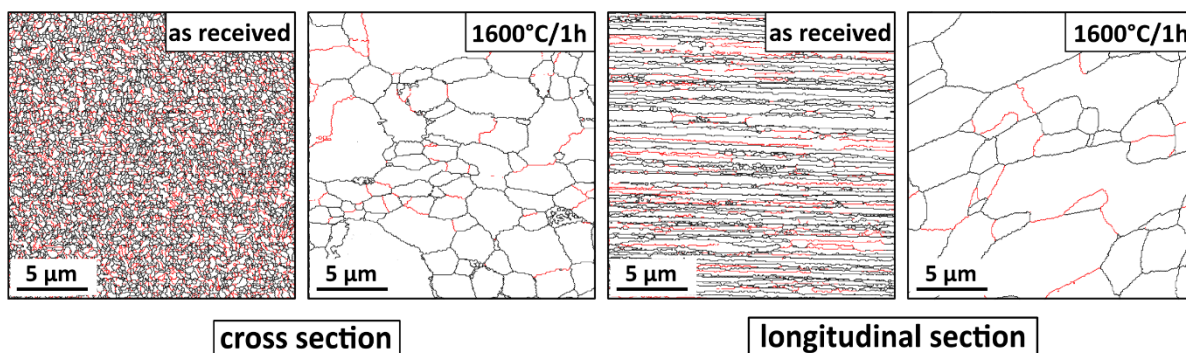
b) Total GB length per scanning area - *cross section*
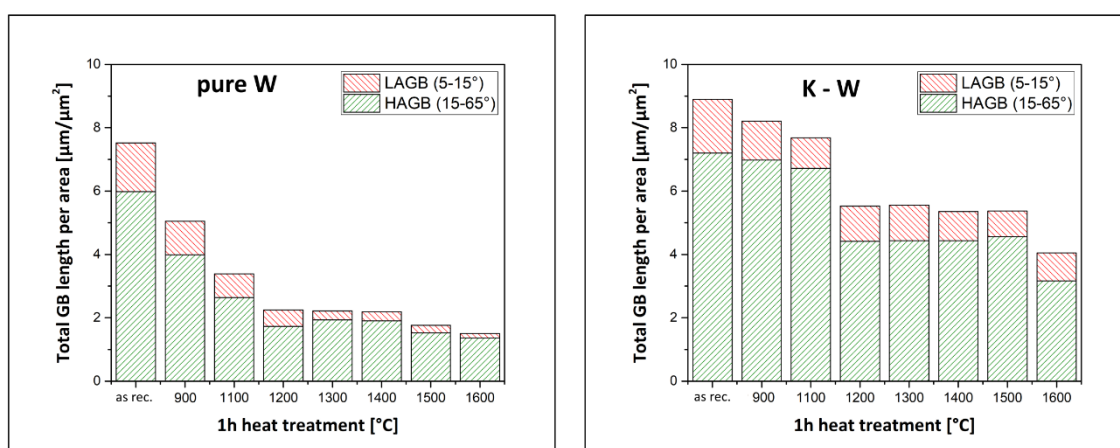
c) Total GB length per scanning area - *longitudinal section*
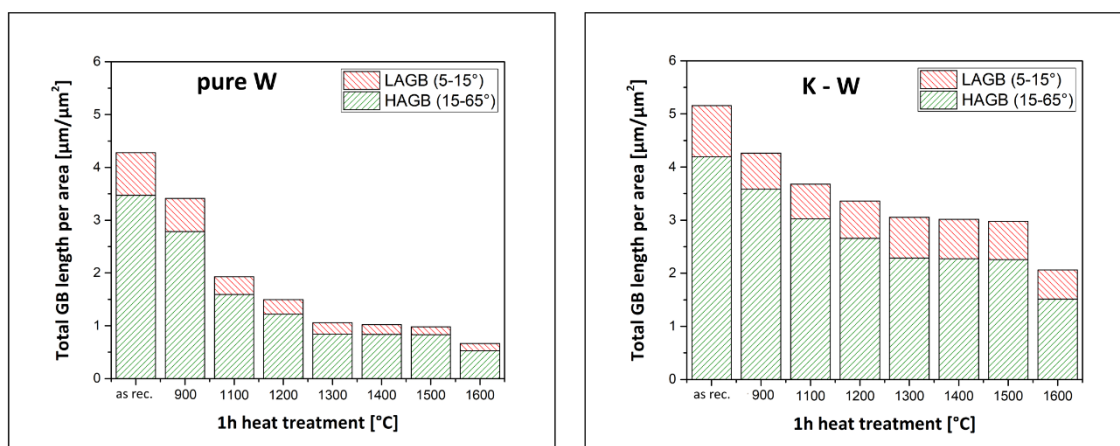
Figure C.5. *a) Grain boundary map of the as-received and 1600°C annealed pure tungsten wire, where the low-angle grain boundaries (LAGB, 5°-15°) and the high-angle grain boundaries (HAGB, 15°-65°) are identified as red and black lines, respectively. Total length of grain boundaries per scanning area of pure and potassium doped W wires is given, depending on different annealing temperatures, analysed from b) cross sectional orientation maps and c) longitudinal orientation maps. Abundance of low-angle and high-angle grain boundaries is indicated as well.*

In all the cases, the as received material shows the highest amount of GBs which consist to a large extent of high-angle boundaries. Simultaneously with initial annealing processes and increase in grain size, the length of grain boundaries reduces, with the effect being significantly pronounced for pure tungsten annealed at and above 1100 °C. At the highest annealing temperature, the total GB reduction is about 80 % and 85 % for the data obtained from the cross sectional and longitudinal maps, respectively. The K-doped material shows a similar trend, but with a significantly smaller GB reduction which is related to the stabilization of the grain structure at elevated temperatures. A correlation can be made between different heat treatments, the nature of grain boundaries and their number fraction. The misorientations histogram shows that a fraction of LAGB is about 20 % for as-received sample. In the case of pure W, the amount of low-angle grain boundaries increases from about 20 to about 30 % after annealing at 1100 °C, which can be correlated to recovery process. With the further increase in annealing temperature, LAGB are still present, but the ratio of better ordered high-angle grain boundaries significantly increases. For heat treatments above 1300 °C, many grain boundaries are annihilated due to grain growth, many of the low-angle grain boundaries disappear and are replaced by high-angle boundaries, which is an indication of the recrystallization taking place. For a sample annealed at 1600 °C, the vast majority of grains is separated by HAGB with a fraction of over 90 %. K doped wire does not show such a drastic drop in the fraction of LAGB and the analyses from the longitudinal sections show a steady increase from 18.7 % to 26.6 % for as received and 1600 °C respectively, indicating that the beginning of the recrystallization is shifted to higher temperatures.

C.3.1.3. Evolution of the texture

The analyses of the pole figures obtained from EBSD data confirm a strong, preferential orientation of the grains with the <110> direction parallel to the wire axis, which is a direct consequence of the severe plastic deformation induced during the wire drawing process. The developed texture of both materials is very similar; therefore, to avoid repetition, only an example of the pure tungsten wire in the as received (Figure C.6a) and annealed condition (Figure C.6b) is depicted. All pole figures are presented using stereographic projection showing that the centre of the pole Figure corresponds to the wire axis. Additionally, six peaks of lower intensity at approximately 60° can be observed, forming a continuous distribution of poles along a ring. The evolution of the developed texture is not influenced by the isothermal annealing treatments. Even at the highest annealing temperature of 1600 °C very little effect can be seen on the lattice orientation, as the texture remains the same with a very dominant <110> direction. The less continuous rings are related to the increase of grain size and therefore limited grain statistics. Slight weakening of the texture after recrystallization is observed as well.
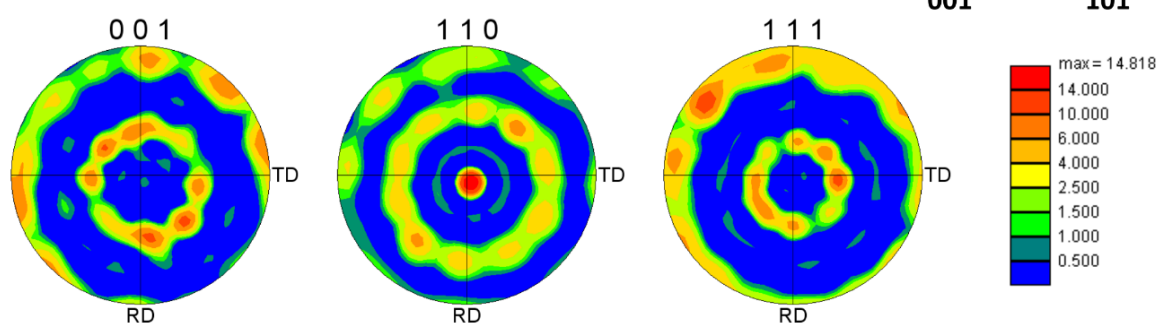
a) as received
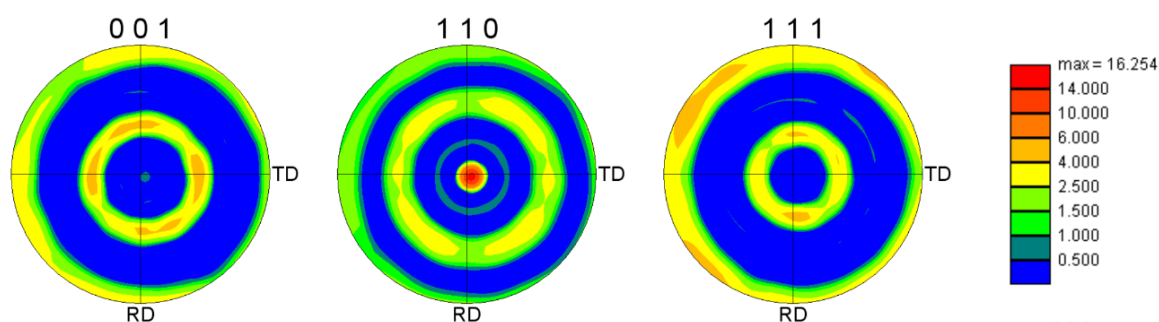
b) 1600°C/1h

Figure C.6. *{001}, {110} and {111} pole figures derived from EBSD texture analyses of the cross section of a pure tungsten wire in a) as received condition and b) after annealing for 1 h at 1600 °C.*

C.3.2. Radial microstructural investigation

During the drawing process, a wire is imposed to a great amount of plastic deformation that is inhomogeneous throughout the cross section [16]. As a result, the heterogeneity of the stress state occurs across the diameter with a higher shear stress and strain in the surface region than in the interior of the wire. Consequently, variations of microstructural features and texture could occur, which would have a noteworthy effect on mechanical properties of the materials. With that in mind, additional microstructural analyses were completed, where EBSD mapping was performed as a function of wire radius. In Figure C.7, a sequence of orientation maps of the center region of the as-received pure W wire can be seen. The microstructural evolution across the entire diameter of the wire can be investigated by connecting the obtained scans from one edge to another.

The qualitative analyses of the grain size do not reveal alternations throughout the cross section yielding an average area weighted grain diameter of (0.471 ± 0.005) µm. The grain shape, in terms of aspect ratio, is unchanged as well. However, some features of the texture in the centre and the edge region appear to be somewhat different indicating an impact of the drawing process and the resulting heterogeneity of the stress state. In the centre region, a very strong <110> fibre texture is seen with a maximum intensity in a pole Figure of 16.6. Approaching the edge of the wire, a certain grain orientation change is perceived leading to the slightly inclined <110> pole and smearing of the characteristic rings

in {001} and {111} pole figures. Furthermore, the texture is significantly weaker with a maximum intensity of only 8.9. The variation of the maximum intensity from one edge to the other is significant and can be represented with a bell shape curve.
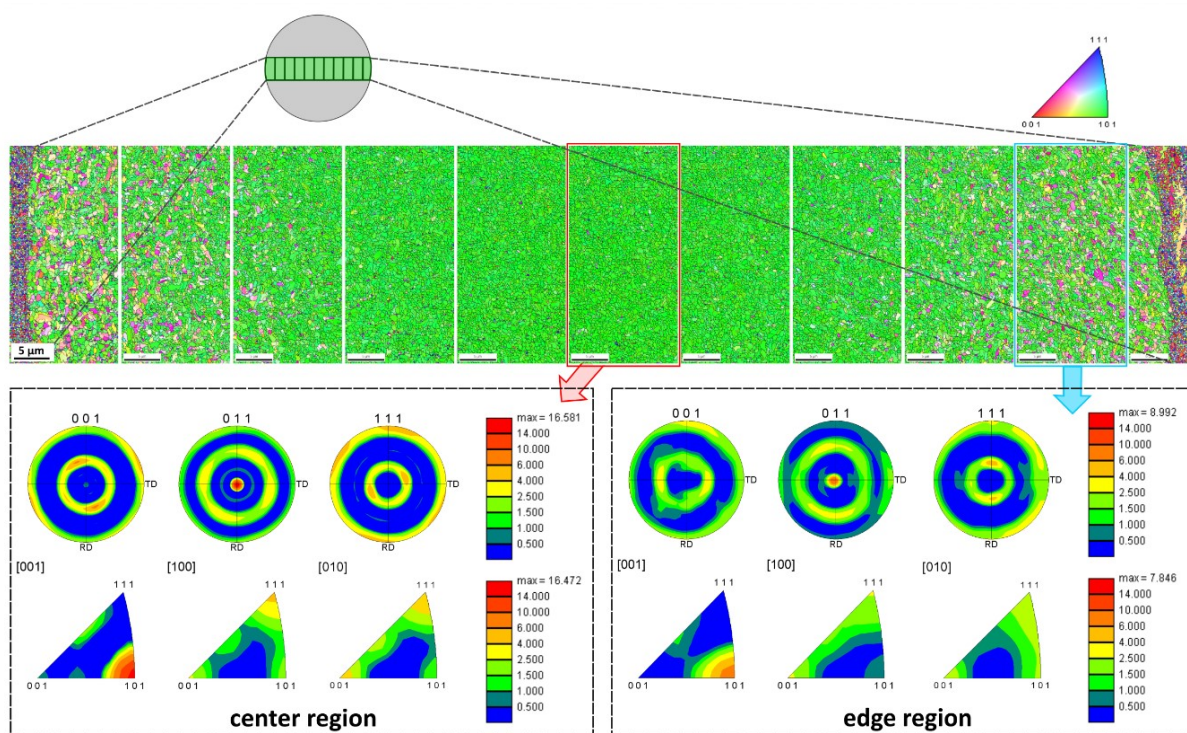
Figure C.7. *EBSD orientation maps of the cross section of the as-received, pure tungsten across the wire diameter. The evolution of the texture is investigated by analyses of the pole figures and inverse pole figures of the scans in central and edge region. Colour coded unit triangle is given as well, representing <100>, <110> and <111> crystallographic directions perpendicular to the sample surface.*

C.3.3. Microhardness measurements

Hardness measurements enable a fast determination of the changes of the mechanical properties in respect to different heat treatments through the correlation between the strength of the material and its grain size. Thus, the loss in hardness i.e. softening of the material occurring during annealing, complements observed alternation of the microstructure and helps identification of the different annealing stages – recovery and recrystallization. Figure C.8a shows the results of Vickers microhardness measurements (HV0.5) as a function of the isochronal annealing temperature of the longitudinal sections for both pure and potassium doped tungsten wires. Three areas can be distinguished:

- In the as-received condition, the hardness of a pure and K-doped W wire is 683 ± 5.8 HV0.5 and 665 ± 7.2 HV0.5, respectively. After annealing for 1 h at 900 °C, both materials experience a moderate decrease in hardness, with the effect being more pronounced for pure W.

- With the further increase in annealing temperature (above 1100 °C), a significant reduction in hardness of a pure W can be observed, reaching a value of 442 ± 10.4 HV0.5 for the sample heat treated at 1500 °C. In contrast to this, the hardness of the K-W wire only slightly changes, changing from 615 ± 7.1 HV0.5 to 564 ± 6.2 HV0.5.

- At the highest annealing temperature of 1600 °C, the pure W wire experiences a drastic drop of hardness to the lowest obtained value of 321 ± 10.4 HV0.5. Contrary to this strong softening, the hardness of the K-W wire remains nearly constant, indicating high temperature stability of the underlying microstructure. The lowest obtained microhardness value of this material yields 551 ± 6.1 HV0.5.

The observed variation of the microhardness and the stability in case of K-W wires are in excellent correlation to the evolution of the microstructure with different annealing treatments (Figures 2 and 3). In such a way, a link can be made with the grain size, which is related to the strength of the material by the well-known Hall-Petch relation [31,32]. This can be validated by plotting the hardness results of the samples in different annealing states against reciprocal square root of corresponding grain sizes, given as $d^{-1/2}$ (Figure C.8b). The presented exemplary plot is given for the pure W wire, where the dependence is shown for two values of grain size: area weighted grain diameters obtained from the cross sections (Figure C.4a) and averaged vertical intercept lengths obtained from the longitudinal sections (Figure C.4b). In both cases, the linear fit corresponds to the obtained results quite well and the same is also true for K-W wire. Additionally, the linear relationship is also seen by plotting the hardness results against square root of corresponding length of grain boundaries, given as $d^{1/2}$ (Figure C.8c), with the similar behaviour observed for lengths of HAGB, LAGB and their total amount.
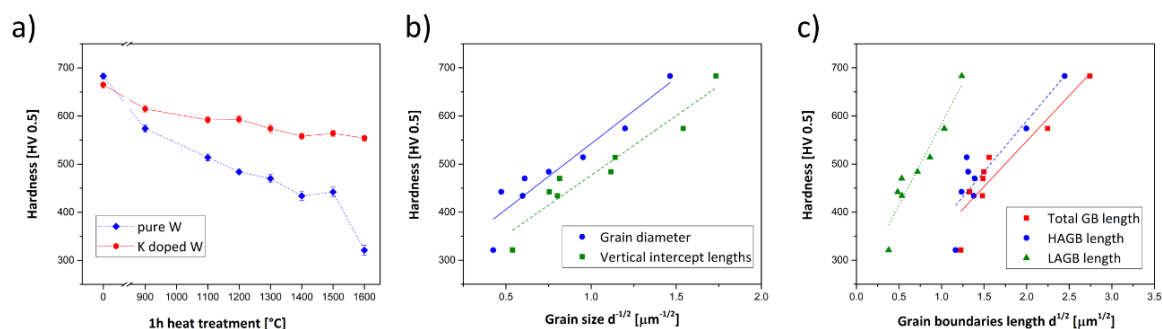
Figure C.8. *a) Vickers hardness (HV 0.5) results of the pure and potassium doped W wires after annealing at different temperatures for 1 h. The microhardness was measured in the longitudinal section of the sample. The relationship of the hardness data of a pure tungsten wire is established in respect to b) the grain size, given as $d^{-1/2}$ and expressed in terms of grain diameters and vertical intercept lengths and c) the GB lengths, given as $d^{1/2}$, where a comparison is made for the HAGB, LAGB and their total amount. The linear relationship is accentuated by a linear fit function.*

C.4. Discussion

The main characteristics of the wire microstructure in the as received state are fibrous grains elongated along the axial direction and the development of a very pronounced <110> fiber texture. Such an appearance is typically seen in heavily deformed bcc wires [33] and as expected, the results of as-received pure and K doped tungsten are very similar. Another peculiar feature observed in the cross section of the wire is a distinctive pattern known as grain curling or the so called Van Gogh sky structures [34]. The origin of the formation of such ribbon-shaped grains lies within the tendency of textured grains to deform by plane strain elongation [35]. In the course of severe plastic deformation during the drawing process, the microstructure of the wire is severely altered from the initially equiaxed grains (of the sintered ingot) to the elongated grains parallel to the axial direction and the shape change of each grain must be compatible with that of the neighbouring grains. However, with plane strain flow, this can only be accomplished by twisting of grains around each other. In such a way, grains become shaped like ribbons, curled around the wire axis establishing a very pronounced, sharp <110> fiber texture. As observed in our investigations, the developed <110> texture is conserved after heat treatments, which is in a good agreement with other investigations [28]. Furthermore, the characteristic appearance of the microstructure is conserved throughout the wire diameter with a noticeable localized variation in texture in the outer region, which is in a good correlation to other studies [36]. Such a heterogeneity can have a notable effect on the resulting failure mode in the edge region of the wire, as it will be shown in the second part of this contribution [30].

The heat treatments cause modifications in the grain structure of the wires alongside with changes of other microstructural features, as well as mechanical properties. Understanding this behaviour is inevitably related to the discussion of the main three annealing phenomena: recovery, recrystallization and grain growth [37,38]. The recovery refers to homogeneous microstructural changes in a deformed material and occurs prior to the recrystallization; the driving force of the process is the stored energy in the deformation structure due to point and line defects. This stored energy of the material is lowered during recovery by dislocation movement through two primary thermally activated mechanisms, these being the annihilation of dislocations and the rearrangement of dislocations into lower energy configurations (polygonization and low angle grain boundaries). Both processes are achieved by glide, climb and cross-slip of dislocations leading to the overall decrease in dislocation density by the end of recovery [37].

Recrystallization in general is a thermally activated process in which new dislocation-free grains are formed within the deformed or recovered structure and grow into it; the driving force arises from the elimination of the dislocations introduced during deformation and is characterized by the movement of high-angle grain boundaries. When recrystallization sets in, dislocations are almost entirely removed from the recrystallized regions by sweeping grain boundaries. After completion of this process, further growth of the recrystallized grains may occur. The driving process of this subsequent grain growth is the reduction in stored energy of the material in the form of grain boundaries [37].

Determination of different annealing phenomena that occur in the range of investigated temperatures is inevitably linked to how one defines the recrystallization process itself, which can be quite variant in

the literature. The obtained data were analysed and interpreted in regards to the respective processes as following: the recovery process is mostly determined through an increase in the fraction of LAGB; the recrystallization process is related to the temperature range where distinctive changes occur in the grain structure (in terms of size and shape) accompanied by pronounced softening of the material and variations in the amount and type of dominant grain boundaries; and lastly further substantial increase in grain size of the recrystallized structure is classified as grain growth. It should be mentioned, that the used terminology [37] has been developed for medium or heavy deformed coarse grained metals, but not for very heavy deformed materials as is the case in this study, where the grain size (thickness) has been reduced significantly below 1 µm, which is the typical order of the dislocation cell size. Hence, the used terms may not reflect exactly the same process, as in the case of not as heavy deformed materials.

The grain structure and related microstructural features of the two investigated materials appear rather different after annealing at successively increasing temperatures. Analysis of pure, undoped tungsten wire annealed in the range below 1100 °C shows that the grain structure exhibited a greater degree of homogenous fine scale coarsening in the cross sections, followed by a limited grain boundary migration and increased ratio of LAGB, which is all an indication of a recovery process taking place. Further proof is an initial rapid decrease of the Vickers hardness, which is related to the reduction of dislocation density by dislocation rearrangement and annihilation. Annealing temperature of 1100 °C seems to be the onset of the recrystallization as the first appearance of some isolated grains, which had grown more than neighbouring grains, is seen. Moreover, grain boundary movement is more pronounced and the total amount of boundaries is significantly reduced at this temperature. The recrystallization process seems to be complete after heat treatments up to 1400-1500 °C as the grain boundary movement progressed to the point that the initial overall linearity of the structure in the longitudinal directions is eliminated leading to the relatively equiaxed structure of the grains. This coarsening process seems to be induced by a radial movement of grain boundaries. However, it can also be explained by the movement of the triple grain boundary junction of the small grains [38]. The majority of the boundaries present at this stage of recrystallization process are predominately high-angle grain boundaries. Simultaneously, a noticeable reduction of hardness is observed associated with dislocation-free, recrystallized softer regions of the material, which replaced the work hardened fine, fibrous microstructure. After heat treatments at the highest temperature, pure tungsten wire undergoes subsequent grain growth process where the initially fibrous microstructure is completely altered forming large, equiaxed shaped grains with an increase in average grain size by an order of magnitude. Furthermore, tremendous softening is observed with a reduction in hardness by more than 50 % of initial value. The outlined results are in agreement with the previous studies of annealing properties of pure tungsten wires [39], as well as with the typically reported recrystallization temperature of tungsten (1300-1500 °C) [40–42]. Nevertheless, the results are not in (complete) correlation with conclusions made by Zhao [28], where it was deduced that the wire fully recrystallizes already after annealing for 3 h at 1000 °C. Such a conclusion was drawn mostly from the absence of the grain curling and the removal of the dislocation structures. However, a direct comparison to our findings is not straightforward as the interpretation of the different stages of annealing phenomena is not the same and is based on analyses of different microstructural features. Furthermore, the annealing times are not

corresponding, as the wire was heat treated three times longer than in our case, which would make an additional influence to the observed microstructural changes.

In contrast to annealing properties of pure tungsten, potassium doped wire experiences significantly milder structural changes in the range of investigated temperatures. Below annealing temperature of 1400 °C the fibrous structure is completely conserved with slight amount of apparent radial movement; the variation in grain size, aspect ratio and Vickers hardness are minor as well. At higher annealing temperatures, the migration of short lengths of longitudinal boundaries of all misorientations became more pronounced, leading to the increase of grain width in the longitudinal direction. As more sections of grain boundaries parallel to the wire axis move in radial direction, few boundaries transverse to the drawing direction are formed. Nevertheless, an extensive grain boundary movement is successfully inhibited, while the recrystallization is shifted to even higher temperatures. The overall appearance of elongated structure is preserved with slightly lower aspect ratios of the grains and an increase in the amount of low-angle grain boundaries; this fits pretty well with the process of polygonization, which is related to the rearrangement of dislocations in the LAGB. In the case of heavily drawn doped tungsten, the process of polygonization is sometimes referred in literature as primary recrystallization or homogenous grain growth [43]. Furthermore, it can be seen that the microstructure of the doped wire after a 1600 °C anneal was approximately equivalent to that of the undoped material annealed at 1100 °C.

It is well known that the annealing behaviour and recrystallization mechanism of K-W wires is closely related to the presence of the dispersed second phase, namely potassium used as a dopant element [16]. The potassium is entrapped in pores during sintering of the tungsten ingot. The pores are further elongated by subsequent swaging and drawing, forming long tubes with a very high aspect ratio [44]. The areas of elongated potassium are precursors of the bubbles, which are arranged in parallel rows and all aligned in the drawing direction of the wire. Upon heating of the wire to higher temperatures, the elongated tubes divide into rows formed by individual well shaped spherical bubbles [45]. These bubble rows are the responsible mechanism for inhibiting grain boundary migration and controlling the shape and growth of the grains. The complete study of the successive annealing processes and observation of all the morphological modifications of the doped tungsten wire require performing heat treatments at significantly higher temperatures. The observed structural stabilization of the microstructure within this contribution, seems to remain an active mechanism up to 2100 °C which is the highest annealing temperature, where the uniform, fine-grained elongated structure persists [29,46]. As the wire is heated above this temperature, secondary recrystallization or exaggerated grain growth would occur, characterized by formation of large grains and predominance of the longitudinally oriented grain boundaries. The undoubtedly important role of potassium bubbles is seen through their pinning effect, inhibiting mostly longitudinal grain boundary motion and may hinder triple junction motion as well. The strings of bubbles influence the grain morphology by retarding the lateral motion of grain boundaries, while grain growth occurs unimpeded parallel to the strings and to the wire axis. In such a way long grains with interlocking boundaries of large areas can be formed [47].

C.5. Conclusions

In this work, a comprehensive characterization of the pure and potassium doped tungsten wires was performed, focusing on the influence of various heat treatments on different microstructural features and mechanical properties. Annealing in the temperature range from 900-1600 °C enabled the investigation of the microstructural stability of the two materials and arising annealing phenomena. The main findings can be summarized as following:

- The microstructure of both materials in the as-received state is very similar, consisting of fibrous grains extremely elongated along the axial direction; characteristic ribbon shaped grains curled around the wire axis can be observed in the cross sections of the both wire types.

- The grain structure of the undoped tungsten wire experiences severe modifications upon heat treatments, which can be related to sequential processes of recovery, recrystallization and grain growth. A correlation can be made between the variation in grain size / shape, the nature and abundance of particular types of grain boundaries at certain annealing temperature and softening of the material, indicating that the recrystallization process is finished in the temperature range between 1300-1500 °C for the pure material. The significant coarsening ultimately leads to the complete loss of fibrous appearance of the grains, where the microstructure of the final state consists of the large, quasi-symmetric, globular µm-sized grains.

- In contrast to the annealing properties of pure W, the K doped wire experiences significantly milder structural changes in the range of investigated temperatures. The most pronounced changes occur above 1400 °C, where the migration of shorts lengths of longitudinal boundaries of all misorientations became more noticeable alongside with an increase in the amount of low-angle grain boundaries, indicating that the process of polygonization took place. Nevertheless, an extensive grain boundary movement is successfully inhibited by the dispersed second phase preserving the overall elongated microstructure, even for the highest annealing temperature.

- Hardness measurements are in a good correlation with different stages of observed annealing phenomena. Pronounced softening can be seen for the pure W with a tremendous drop in microhardness, going from 683 ± 5.8 HV0.5 (as-received) to 321 ± 10.4 HV0.5 (1600 °C). In contrast, the doped wire experiences significantly milder changes. Furthermore, a linear relationship between hardness data and grain size / GB length was shown, corresponding to the well-known Hall-Petch relation.

- As a direct consequence of the drawing process, a very sharp <110> fiber texture is developed by deformation induced grain rotation. The texture is slightly less prominent at the surface of the wire. Such a pronounced preferential orientation of the grains remains unaltered for both materials, even upon heat treatments at the highest annealing temperature of 1600 °C.

The main conclusion of the work is that the full recrystallization and grain growth in tungsten wire can be successfully shifted to temperatures higher than 1600 °C by addition of potassium as a doping element. From a microstructural point of view, the application of K-doped wire for a structural parts of fusion reactors, as it is the case for W_f/W composites, is strongly advised. The performed systematic

study of the influence of heat treatments on the evolution of the grain morphology for both type of materials is crucial for the assessment of the fracture toughness of the wire. The grain size and more importantly grain shape have a tremendous influence on the micromechanisms controlling the fracture process. Deeper insights, however, will be gained from fracture tests on non-annealed, as well as annealed wires. With the help of the results presented here, it is possible to investigate the correlation of the observed microstructural features to fracture properties and embrittlement by annealing [30]. These topics are treated in details within the second part of the contribution.

Acknowledgments

C.6. References

[1]   H. Zohm, "Assessment of DEMO challenges in technology and physics," *Fusion Eng. Des.*, vol. 88, no. 6–8, pp. 428–433, 2013.

[2]   D. Stork *et al.*, "Developing structural, high-heat flux and plasma facing materials for a near-term DEMO fusion power plant: The EU assessment," *J. Nucl. Mater.*, vol. 455, no. 1–3, pp. 277–291, 2014.

[3]   M. Rieth *et al.*, "Recent progress in research on tungsten materials for nuclear fusion applications in Europe," *J. Nucl. Mater.*, vol. 432, no. 1–3, pp. 482–500, 2013.

[4]   C. Linsmeier *et al.*, "Development of advanced high heat flux and plasma-facing materials," *Nucl. Fusion*, vol. 57, no. 92007, pp. 1–60, 2017.

[5]   V. Philipps, "Tungsten as material for plasma-facing components in fusion devices," *J. Nucl. Mater.*, vol. 415, no. 1, pp. S2–S9, 2011.

[6]   E. Lassner and W.-D. Schubert, *Tungsten - Properties, Chemistry, Technology of the Element, Alloys and Chemical Compounds*. New York: Kluwer Academic/Plenum Publishers, 1999.

[7]   J. Reiser, M. Rieth, B. Dafferner, and A. Hoffmann, "Charpy impact properties of pure tungsten plate material in as-received and recrystallized condition (1 h at 2000 °C (2273 K))," *J. Nucl. Mater.*, vol. 442, no. 1–3, pp. S204–S207, 2013.

[8]   V. Barabash, G. Federici, M. Rödig, L. L. Snead, and C. H. Wu, "Neutron irradiation effects on plasma facing materials," *J. Nucl. Mater.*, vol. 283–287, no. I, pp. 138–146, 2000.

[9]   Y. Yuan, J. Du, M. Wirtz, G. N. Luo, G. H. Lu, and W. Liu, "Surface damage and structure evolution of recrystallized tungsten exposed to ELM-like transient loads," *Nucl. Fusion*, vol. 56, no. 3, pp. 1–8, 2016.

[10]   G. Pintsuk, S. Antusch, T. Weingaertner, and M. Wirtz, "Recrystallization and composition dependent thermal fatigue response of different tungsten grades," *Int. J. Refract. Met. Hard Mater.*, vol. 72, no. September 2017, pp. 97–103, 2018.

[11]   R. Neu *et al.*, "Tungsten fibre-reinforced composites for advanced plasma facing components," *Nucl. Mater. Energy*, vol. 12, pp. 1308–1313, 2017.

[12]   B. Jasper *et al.*, "Behavior of tungsten fiber-reinforced tungsten based on single fiber push-out study," *Nucl. Mater. Energy*, vol. 9, pp. 416–421, 2016.

[13]   J. Riesch *et al.*, "Chemically deposited tungsten fibre-reinforced tungsten – The way to a mock-up for divertor applications," *Nucl. Mater. Energy*, vol. 9, pp. 75–83, 2016.

[14]   J. Riesch, T. Höschen, C. Linsmeier, S. Wurster, and J. H. You, "Enhanced toughness and stable crack propagation in a novel tungsten fibre-reinforced tungsten composite produced by chemical vapour infiltration," *Phys. Scr.*, vol. T159, no. 14031, pp. 1–7, 2014.

[15]   P. Schade, "100 years of doped tungsten wire," *Int. J. Refract. Met. Hard Mater.*, vol. 28, no. 6, pp. 648–660, 2010.

[16]   E. Pink and L. Bartha, *The metallurgy of doped/non-sag tungsten*. Elsevier Science Publishers, 1989.

[17]   B. P. Bewlay, N. Lewis, and K. A. Lou, "Observations on the evolution of potassium bubbles in tungsten ingots during sintering," *Metall. Trans. A*, vol. 23, no. 1, pp. 121–133, 1992.

[18]   W. D. Schubert, B. Lux, and B. Zeiler, "Formation and incorporation of dopant phases during technical reduction of NS-doped tungsten blue oxide," *Int. J. Refract. Met. Hard Mater.*, vol. 13, no. 1–3, pp. 119–135, 1995.

[19]   D. M. Moon and R. C. Koo, "Mechanism and kinetics of bubble formation in doped tungsten," *Metall. Mater. Trans. B*, vol. 2, no. 8, pp. 2115–2122, 1971.

[20]   P. Schade, "Potassium bubble growth in doped tungsten," *Int. J. Refract. Met. Hard Mater.*, vol. 16, no. 1, pp. 77–87, 1998.

[21]   B. P. Bewlay and C. L. Briant, "The formation and the role of potassium bubbles in NS-doped tungsten," *Int. J. Refract. Met. Hard Mater.*, vol. 13, no. 1–3, pp. 137–159, 1995.

[22]   O. Horacsek and L. Bartha, "Development of the bubble structure from selectively deforming potassium-pores in doped tungsten wires," *Int. J. Refract. Met. Hard Mater.*, vol. 22, no. 1, pp. 9–15, 2004.

[23]   J. Riesch *et al.*, "Properties of drawn W wire used as high performance fibre in tungsten fibre-reinforced tungsten composite," *IOP Conf. Ser. Mater. Sci. Eng.*, vol. 139, no. 12043, pp. 1–9, 2016.

[24]   J. Riesch *et al.*, "Tensile behaviour of drawn tungsten wire used in tungsten fibre-reinforced tungsten composites," *Phys. Scr.*, vol. T170, no. 14032, p. 7, 2017.

[25]   J. Riesch *et al.*, "In situ synchrotron tomography estimation of toughening effect by semi-ductile fibre reinforcement in a tungsten-fibre-reinforced tungsten composite system," *Acta Mater.*, vol. 61, no. 19, pp. 7060–7071, 2013.

[26]   D. Terentyev, J. Riesch, S. Lebediev, A. Bakaeva, and J. W. Coenen, "Mechanical properties of as-fabricated and 2300°C annealed tungsten wire tested up to 600°C," *Int. J. Refract. Met. Hard Mater.*, vol. 66, no. March, pp. 127–134, 2017.

[27]   D. Terentyev *et al.*, "Plastic deformation of recrystallized tungsten-potassium wires Constitutive deformation law in the temperature range 22–600 °C," *Int. J. Refract. Met. Hard Mater.*, vol. 73, pp. 38–45, 2018.

[28]   P. Zhao *et al.*, "Microstructure, mechanical behaviour and fracture of pure tungsten wire after different heat treatments," *Int. J. Refract. Met. Hard Mater.*, vol. 68, no. June, pp. 29–40, 2017.

[29]   J. Riesch *et al.*, "Development of tungsten fibre-reinforced tungsten composites towards their use in DEMO - Potassium doped tungsten wire," *Phys. Scr.*, vol. T167, no. 14006, p. 8, 2016.

[30]   V. Nikolić, J. Riesch, M. J. Pfeifenberger, and R. Pippan, "The effect of heat treatments on pure and potassium doped drawn tungsten wires : Part II - Fracture properties," *Mater. Sci. Eng. A*, submitted, 2018.

[31]   E. O. Hall, "The deformation and aging of mild steel. III: Discussion of results," *Proc. Phys. Soc. Lond. B*, vol. 64, pp. 747–753, 1951.

[32]   N. J. Petch, "The Cleavage Strength of Polycrystals," *J. Iron Steel Inst.*, vol. 174, pp. 25–28, 1953.

[33]   S. Suwas, R. K. Ray, and R. K. R. Satyam Suwas, *Crystallographic Texture of Materials*. 2014.

[34]   M. R. Ripoll and J. Očenášek, "Microstructure and texture evolution during the drawing of tungsten wires," *Eng. Fract. Mech.*, vol. 76, no. 10, pp. 1485–1499, 2009.

[35]   W. F. J. Hosford, "Microstructural changes during deformation of [011] fiber textured metals," *Trans. Metall. Soc. AIME*, vol. 230, pp. 12–15, 1964.

[36]   P. F. Browning, C. L. Briant, K. Rajan, and B. A. Knudsen, "An analysis of splitting failures during the drawing of tungsten wire," *Eng. Fail. Anal.*, vol. 2, no. 2, pp. 105–115, 1995.

[37]   F. J. Humphreys and M. Hatherly, *Recrystallization and related annealing phenomena*. Elsevier Ltd, 2004.

[38]   N. Hansen and R. A. Vandermeer, "Recovery, Recrystallization, and Grain Growth," *Encycl. Condens. Matter Phys.*, pp. 116–124, 2005.

[39]   D. B. Snow, "The recrystallization of commercially pure and doped tungsten wire drawn to high strain," *Metall. Trans. A*, vol. 10, no. 7, pp. 815–821, 1979.

[40]   O. Horacsek, "Properties and failure modes of incandescent tungsten filaments," *IEE Proc. A (Physical Sci. Meas.* Instrumentation*, Manag. Educ. Rev.*, vol. 127, no. 3, pp. 134–141, 1980.

[41]   S. N. Mathaudhu, A. J. deRosset, K. T. Hartwig, and L. J. Kecskes, "Microstructures and recrystallization behavior of severely hot-deformed tungsten," *Mater. Sci. Eng. A*, vol. 503, no. 1–2, pp. 28–31, 2009.

[42]   A. Alfonso, D. Juul Jensen, G. N. Luo, and W. Pantleon, "Recrystallization kinetics of warm-rolled tungsten in the temperature range 1150-1350 °c," *J. Nucl. Mater.*, vol. 455, no. 1, pp. 591–594, 2014.

[43]   C. L. Briant, O. Horacsek, and K. Horacsek, "The effect of wire history on the coarsened substructure and secondary recrystallization of doped tungsten," *Metall. Trans. A*, vol. 24, no. 4, pp. 843–851, 1993.

[44]   C. L. Briant, "On the Formation of Potassium Bubbles in Tungsten Rod," vol. 20, no. January, pp. 179–184, 1989.

[45]   C. L. Briant, "Potassium bubbles in tungsten wire," *Metall. Trans. A*, vol. 24, no. 5, pp. 1073–1084, 1993.

[46]   D. B. Snow, "The recrystallization of heavily-drawn doped tungsten wire," *Metall. Trans. A*, vol. 7, no. 6, pp. 783–794, 1976.

[47]   J. L. Walter and C. L. Briant, "Tungsten wire for incandescent lamps," *J. Mater. Res.*, vol. 5, no. 9, pp. 2004–2022, 1990.

D

The effect of heat treatments on pure and potassium doped drawn tungsten wires: Part I – Fracture properties

Vladica Nikolić [a], Johann Riesch[b], Manuel J. Pfeifenberger[a], Reinhard Pippan[a]

[a] Erich Schmid Institute of Materials Science of the Austrian Academy of Sciences, Leoben, Austria
[b] Max Planck Institute for Plasma Physics, Garching, Germany

Abstract

Advanced tungsten fibre-reinforced composites (W_f/W), showing pseudo ductile behaviour even at room temperature, are a promising option for future fusion reactors as the intrinsic brittleness of tungsten can be mitigated effectively. The drawn tungsten wires used as reinforcements are the key components of the composites, thus their mechanical properties and thermal stability define the allowed operation / fabrication temperature of the composite material itself. In this work, the room temperature fracture behaviour of the pure and potassium doped tungsten wires was investigated, focusing on the evolution of the fracture micromechanisms in respect to annealing. Single-edge-notched specimens were used, with the crack growth direction perpendicular to the drawing axis of the wire. The occurrence of either a fractographic brittle or a ductile response in the as-received state of both materials is a strong indication that the ductile-to-brittle transition temperature is about room temperature. Pure, annealed tungsten wires experience a tremendous deterioration of the fracture toughness with a very prominent transition of the failure mode. The observed embrittlement by annealing can be related to the loss of the fibrous, elongated microstructure. In contrast to this, the results of the annealed, doped wires demonstrate that the microstructural stability and preservation of the initial, beneficial grain structure is directly reflected in the crack resistance of the material. Predominately ductile behaviour, with characteristic knife-edge necking, is seen even after annealing at 1600 °C.

D.1. Introduction

The progress of the next generation of fusion reactors is strongly associated with the development of advanced high heat flux and plasma-facing materials, capable of enduring the challenging environment imposed by extreme operating conditions [1,2]. An extensive research regarding the first wall and divertor materials was conducted in recent years [3] leading to the choice of tungsten based materials as the most prominent candidates for these reactor parts [4,5]. Besides many advantageous properties of this refractory metal, the challenges associated with the use of tungsten (W) in high-temperature applications are its typically brittle nature and relatively high ductile-to-brittle transition temperature (DBTT) [6]. Further operational embrittlement is expected as a result of tremendous amount of neutron irradiation [7] and/or by annealing through recrystallization and grain growth [8,9]. Thus, one of the main goals in the development of the novel tungsten based material options is overcoming the problem of brittleness.

The broad range of conducted studies on the ductility and toughness enhancement of tungsten at lower temperatures led to the three main strategies being alloying (e.g. with Re [10,11] or Ir [12]), nanostructuring [13,14] and synthesizing composite materials. The third approach is a very promising option, in particular when thinking of tungsten fibre-reinforced tungsten composites (W_f/W) [15], where brittleness is mitigated by utilizing extrinsic toughening mechanisms [16]. W_f/W composites consist of commercially available drawn tungsten wires which are embedded in a tungsten matrix, either by a chemical deposition process [17] or by powder metallurgy [18]. Thus, key components which determine the structural integrity of these advanced plasma facing composites are the tungsten wires used as fibres, which sets the requirement of their exceptional properties and brings an interest in studying them.

Drawn tungsten wire was of great importance in the past century as it was originally developed for the illumination industry and used as the main filament element for light bulbs [19]. Initial studies were mostly focused on the production process and creep resistance at very high temperatures, which led to the discovery of the exceptional influence of doping of tungsten by a small amount of potassium (K) [20]. In such a way, the embrittlement of pure tungsten as a result of recrystallization, grain growth and thermal fatigue, which directly influenced lifetime performance of the lamps, was successfully mitigated. The advantageous effect of doping was correlated to the formation of K bubbles at the grain boundaries, which suppress the secondary recrystallization to higher temperatures and keep the initial, beneficial microstructure for a longer timespan [21]. The research in the following years was mostly dedicated to the optimization of the manufacturing process and the high temperature stability of the microstructure.

When used as reinforcement element in the composite materials, the performance of the tungsten wire and in particular its crack resistance properties at moderate temperatures are of fundamental importance. Investigations dealing with the fracture behaviour of W wire conducted over the past decades, focused on a wide range of different topics such as the typical failure modes occurring during the drawing process [22], complex mechanisms of lamp filaments deterioration [23], analyses of the wire splitting as a result of bending, stretching or coiling [24,25], just to name a few. Furthermore, several studies were addressing the influence of the microstructure on the occurrence of different fracture

modes [26,27], as well as discussing the effect of grain structure of recrystallized wires [28].

However, despite the existing significant body of research on tungsten wires, there are still some open questions and gaps in the scientific knowledge, where a deeper microscopic understanding of the important properties is needed. This is particularly true for the crack resistance of the wire, where more comprehensive information regarding the fracture mechanisms, as well as correlation to the underlying microstructure is of the utmost importance. This holds true for both the as-received, as well as the annealed state of the wire.

Determination of the relationship between the microstructural features and the resulting fracture mechanical properties is one of the main goals of the performed work, as the variations in the grain structure are strongly reflected in the materials fracture behaviour. This contribution is the second part of the study conducted on pure and potassium doped wires. In the first part, the question of recrystallization phenomena and microstructural stability was addressed [29], through detailed analyses of the evolution of various aspects of the microstructure with annealing temperature. The main scope of this part of the study is the room temperature (RT) fracture toughness assessment of tungsten wires and the investigation of the evolution of the fracture mechanisms in respect to different heat treatments.

D.2. Materials and experimental methods

The investigated materials are commercially available drawn pure and potassium doped (K-W, 60 ppm) tungsten wires, with a diameter of 150 µm, which were provided by the OSRAM GmbH, Schwabmünchen. The typical production steps of tungsten-based materials involve a powder metallurgical process of sintering and swaging, while the final, small dimension of the wire is obtained by series of subsequent drawing steps.

In order to study the effect of heat treatments and annealing phenomena on the resulting fracture behavior, the experiments were performed on both as-received and annealed samples. Based on the microstructural characterization conducted in the first part of the publication, two annealing temperatures were chosen for this study: 1300 °C and 1600 °C. The results indicate that the pure tungsten wire recrystallizes when annealed for 1 h at 1300 °C, while the highest temperature of 1600 °C induces substantial grain growth. In contrast, the elongated microstructure of the doped wire remains mostly preserved throughout the heat treatments. In such a way, selected temperatures enable investigating the relation between the microstructural evolution and the embrittlement by annealing and/or ductility conservation. The oxidation of the wires during heat treatments was prevented by using a tungsten based vacuum furnace (Leybold Heraeus PD 1000). The annealing was done at a pressure $< 10^{-5}$ mbar with the holding time of 1 h with subsequent furnace cooling. All the samples are assumed to have identical chemical composition, as they were cut from the same two spools of wires. Thus, the influence of the composition on the resulting properties can be excluded.

Single-edge notched tension (SENT) specimens were used for studying the damage tolerance of the investigated materials. Hence, the fracture experiments were conducted in one principal testing direction with the crack growth directions perpendicular to the drawing axis of the wires. The notches

were introduced by a femtosecond (fs) laser (Origami 10 XP, Onefive GmbH), which is attached to the focused ion beam / scanning electron microscope (FIB/SEM, Auriga) workstation, enabling a precise positioning of the laser cuts. It has a pulse duration of about 500 fs and a focused spot size diameter of about 25 µm. Further details on the laser system can be found elsewhere [30]. The processing of the notches was performed under vacuum conditions with a fluence of 0.6 J/cm^2 and a pulse repetition rate of 100 kHz. The laser beam is guided across the sample surface by a galvanometer scanner. It was scanned repeatedly 14 times with a speed of 1 mm/s along a line, sufficient to cover the whole diameter of a wire. Hence, the time required for the processing of a single notch is below 4 seconds making laser cutting a very fast and therefore advantageous notch fabrication technique. Due to the ultrashort pulse duration, the heat influence on the material is negligible in the ideal case [31]. The typical sample length of the wire was about 20 mm with the notch depth being about one third of the wire diameter. Furthermore, in order to investigate the influence of a nearly atomically-sharp flaw in a material, some of the as-received samples also contained a pre-crack like notch introduced by a FIB workstation (FIB, Leo 1540, Zeiss). A crack-like structure, with the length of 50 µm, was milled in the centre of the laser notch using an ion current of 5 nA for 30 min. An example of a top view of a laser notch (perpendicular to the drawing axis) as well as the position of the FIB cut can be seen in Figure D.1a.

Fracture mechanical experiments were performed on a small scale tensile testing machine provided from Kammrath and Weiss, with a maximum load capacity of 200 N. All the tests were displacement controlled at the rate of 1 µm/s and were done at room temperature in air. Number of tested samples containing only a laser notch for the as-received and all annealed states were six and three, respectively. An additional four tested samples, in the as-received state, had a FIB pre-crack as well. This was the same for both pure and K-doped wires. Thus, the reported fracture toughness values are statistical averages, with the indicated error bars being the standard deviation of the average values. During the experiments, the load-displacement curves were recorded which were used in evaluating the critical stress intensity factor K. K as a measure of fracture toughness of the SENT specimen subjected to tensile loading conditions was evaluated according to [32]:

$$K = \sigma * \sqrt{\pi * a} * f\left(\frac{a}{D}\right) \tag{1}$$

where σ is the applied stress of the round bar given by $\sigma = 4F/\pi D^2$, F is the force, D the diameter of the wire and a the length of the transverse semi-elliptical surface crack. A minimal length of a crack is taken for all the calculations, which is determined from fracture surfaces by a straight line parallel to the end of a notch, as shown in Figure D.1b. In each test, the K is calculated with the maximum recorded load. The dimensionless geometry factor $f\left(\frac{a}{D}\right)$ can be obtained numerically by the finite element method [33] and for a straight-fronted edge crack is given as:

$$f\left(\frac{a}{D}\right) = 1.4408 - 3.6364\left(\frac{a}{D}\right) + 19.3500\left(\frac{a}{D}\right)^2 - 34.7849\left(\frac{a}{D}\right)^3 + 36.8446\left(\frac{a}{D}\right)^4 \tag{2}$$

The fracture surfaces of the samples were investigated with a scanning electron microscope (SEM, LEO Gemini 1525) equipped with a field emission gun and the evolution of the morphology of fracture surfaces was obtained in respect to different annealing conditions and material states. Additionally, a backscatter electron (BSE) detector was used to examine the initial microstructure across the longitudinal and cross sections of the as-received and heat treated wires. The preparation of samples suitable for these analyses was conducted by embedding the wire pieces in hard resin, followed by standard polishing steps resulting in the necessary smooth surfaces.
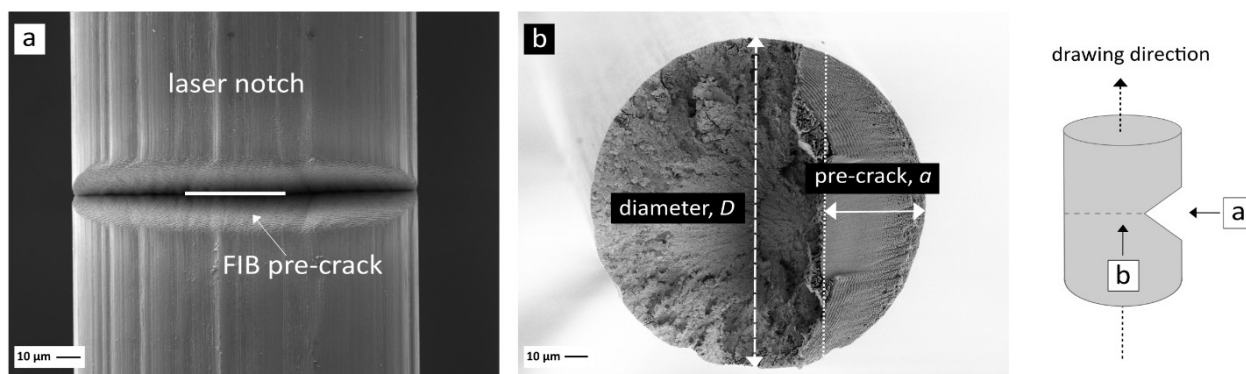

Figure D.1. *Scanning electron micrographs of a) a top view of a laser notch with designated position of a FIB cut and b) an exemplary fracture surface showing how a minimal length of a pre-crack was measured. The schematic drawing on the right illustrates a characteristic SENT specimen with indicated viewing directions.*

D.3. Results and discussion

D.3.1. Microstructure

In order to determine the role of the underlying microstructure in the resulting fracture process and failure mode, it is very important to investigate the grain structure of the studied materials prior to fracture experiments. BSE images can be used as a suitable representation of the microstructure as the contrast of the image, related to different crystallographic orientations, gives a very good impression of the grain size and shape. An overview of the pure and potassium doped material is seen in the two principal viewing directions: longitudinal section - plane parallel to the drawing axis (Figure D.2a) and cross section - plane perpendicular to the drawing axis (Figure D.2b). Furthermore, comparison between as-received, 1300 °C and 1600 °C annealing states enable studying the effect of heat treatments and annealing phenomena on the resulting fracture behaviour.

The initial appearance of the both materials is very similar, which is directly influenced by the severe plastic deformation imposed on the wire during the drawing process. In such a way, a unique microstructure is obtained consisting of thin, fibrous grains elongated along the axial direction, as clearly
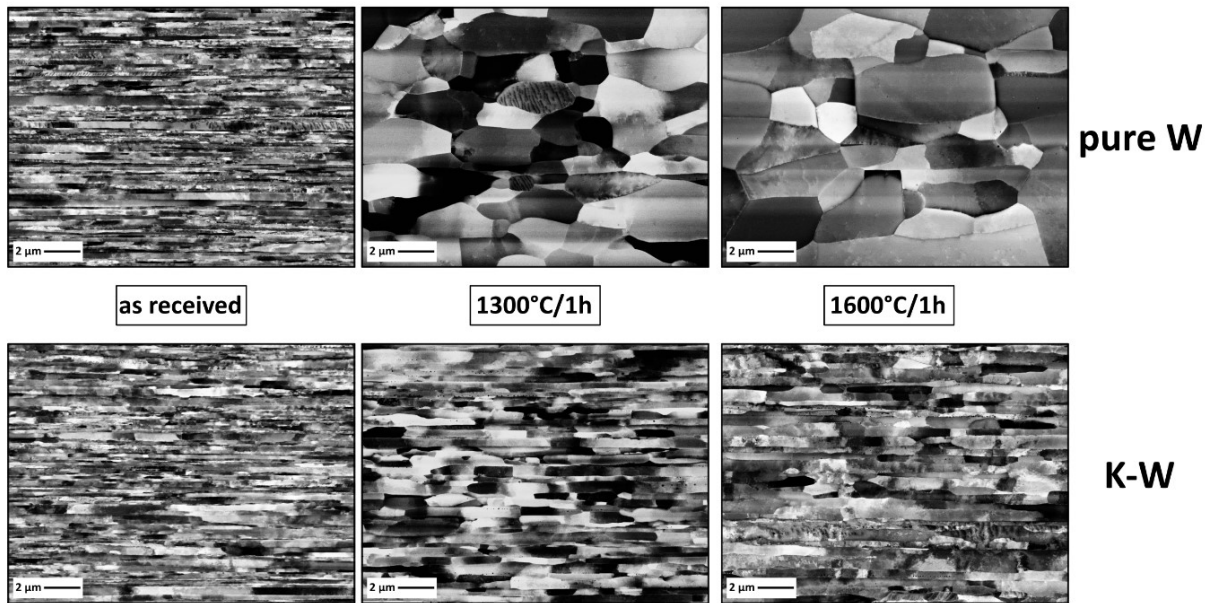
seen in the longitudinal sections. The BSE images of the cross sections reveal uniformly distributed grains twisted around each other and thus forming a characteristic pattern known as grain curling or the so called Van Gogh sky structures [34]. This unique microstructural feature is related to the tendency of grains to deform by plane strain elongation [35] and in such a way they become shaped like ribbons curled around the wire axis. Such an appearance is typically seen in heavily deformed tungsten wire and has been reported by other researchers [36,37].

The grain structure and related microstructural features of the two investigated materials appear rather different after annealing at successively increasing temperatures. In the case of the pure, undoped W wire substantial microstructural modifications occur. As seen in Figure D.2a, the characteristic elongated structure is severely influenced already after annealing at 1300 °C, experiencing increase in the grain size in both horizontal and vertical directions. Significant grain growth leads to the complete loss of fibrous appearance, where the microstructure of the final state consists of large, quasi-symmetric, globular µm sized grains. Furthermore, cross sectional examinations reveal the complete disappearance of curling structures, the tremendous grain growth and a formation of large, equiaxed shaped grains.

In contrast to annealing properties of pure tungsten, the overall elongated microstructure of the K-doped W wire is preserved even for the highest annealing temperatures, indicating a very pronounced thermal stability of the material. Minor structural changes occurring in the range of the investigated temperatures are related to the small amount of radial boundary movement leading to an increase of grain width in the longitudinal direction. The effect of heat treatments observed in the plane perpendicular to the drawing direction, is seen through rounding of the grains and their slight increase in size. Furthermore, the disappearance of the grain curling is seen as well.

A comprehensive microstructural characterization and the more in-depth investigation of the influence of annealing on the pure and potassium-doped tungsten wires was already performed. Thus, for all the details regarding quantification of changes of the grain shape and size, analyses of the grain boundaries, evolution of the developed texture and influence of heat treatments on hardness, the reader is referred to [29].

a) longitudinal section

pure W

| as received | 1300°C/1h | 1600°C/1h |

K-W

b) cross section

pure W

| as received | 1300°C/1h | 1600°C/1h |

K-W

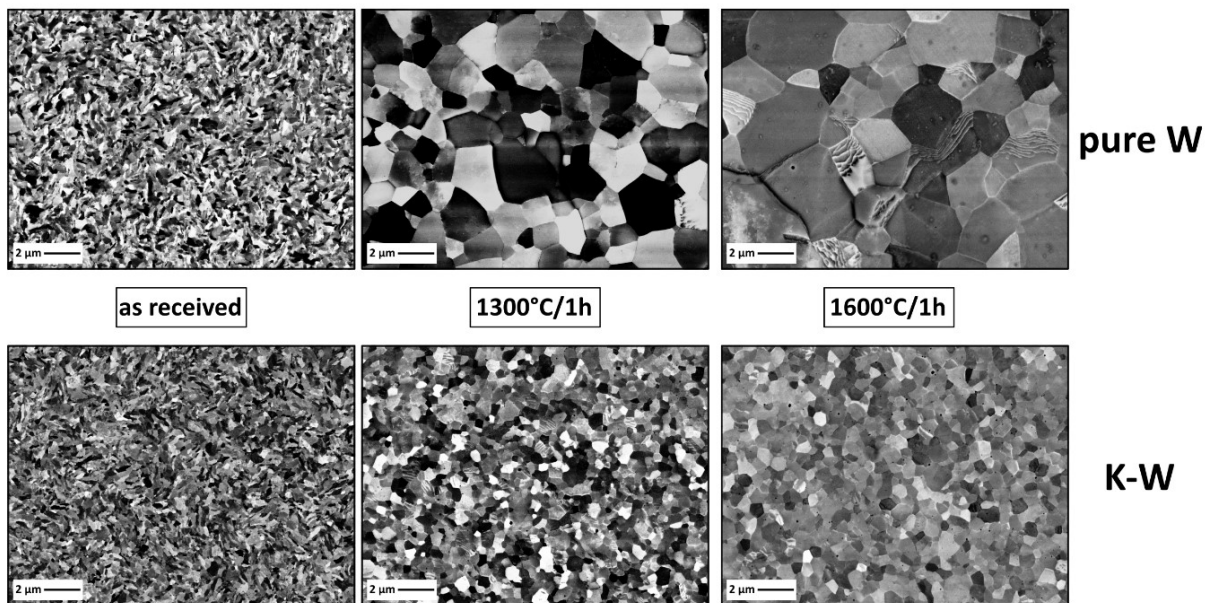**Figure D.2.** *Scanning electron micrographs, taken in the BSE mode, of the pure and K-doped tungsten wires in the as-received and annealed states (1300 °C and 1600 °C for 1h). The images are taken in the central area across a) longitudinal sections and b) cross-sections. The schematic drawings show the principle direction of deformation, as well as the position of the typical scanning areas in respect to the drawing direction.*

D.3.2. Fracture toughness

D.3.2.1. As-drawn wires

Typical load-displacement curves obtained in a fracture experiment on wires in the as-received state are shown for pure and potassium doped tungsten wires in Figure D.3a and Figure D.3b, respectively. A comparison is made between two distinct cases of material's response in a test, namely ductile and brittle failure mode, which occurred at the ratio of about 50 – 50 % of tested samples. In both examples specimens show nearly pure linear elastic loading at the beginning. After a maximum load is reached, a brittle sample fails catastrophically without showing any signs of plastic behaviour with the force abruptly dropping to zero. In contrast to this, a ductile sample sustains a higher maximum load and shows a certain non-linearity in a test record, where the force decreases steadily before a final failure occurs. This is highlighted in the magnified part of the load displacement curve of a pure W (Figure D.3a) and similar trends can be observed for both type of wires.

The critical fracture toughness K was calculated from the maximum obtained load in an experiment and based on the results of six tested samples, for each type of a material, a mean value of fracture toughness is derived. The measured values for pure and K-doped tungsten are (33.4 ± 6.4) MPa·m$^{1/2}$ and (31.9 ± 7.2) MPa·m$^{1/2}$, respectively. A rather high standard deviation is related to a scatter of K data, which is associated with the occurence of either a brittle or a ductile fracture mode. In the case of a pure tungsten wire, measured fracture toughness is in the range from 25.9 MPa·m$^{1/2}$ (the lowest obtained value of a brittle appearance) to 43.3 MPa·m$^{1/2}$ (the highest obtained value of a ductile appearance). The results of doped wires show a similar variation of K going from 22.7 MPa·m$^{1/2}$ to 44.5 MPa·m$^{1/2}$. The existence of the scatter of measured fracture toughness data under the same testing conditions strongly indicates that the testing temperature (in this case room temperature) is in the range where a transition from a brittle to a ductile failure mode takes place. Similar scatter of K data in a fracture experiment at room temperature was also observed for heavily rolled ultrafine grained tungsten foil [14].

Furthermore, in Figure D.3 an overview of characteristic fracture morphologies can be seen. The displayed fractographs represent either a brittle or a ductile failure behaviour related to low or high values of fracture toughness. However, in both cases, a crack immediately deflects along the longitudinal direction of the wire, followed by either a brittle, transcrystalline cleavage or a ductile, knife-edge failure mode accompanied with a pronounce necking. An in-depth fractographic investigation will be presented in the following chapters.
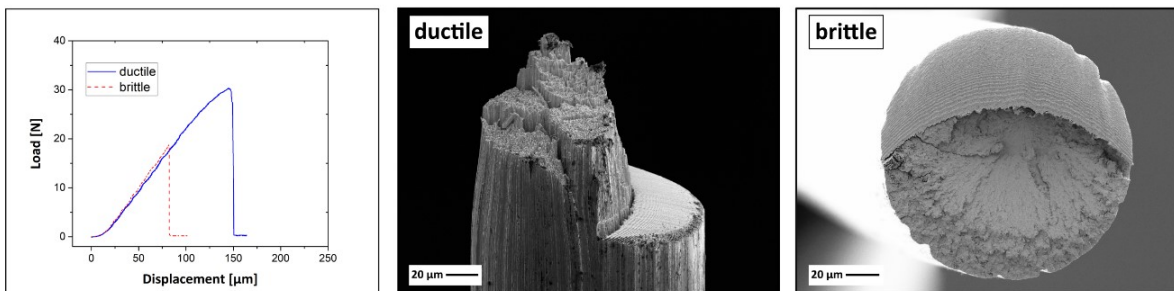
a) pure W
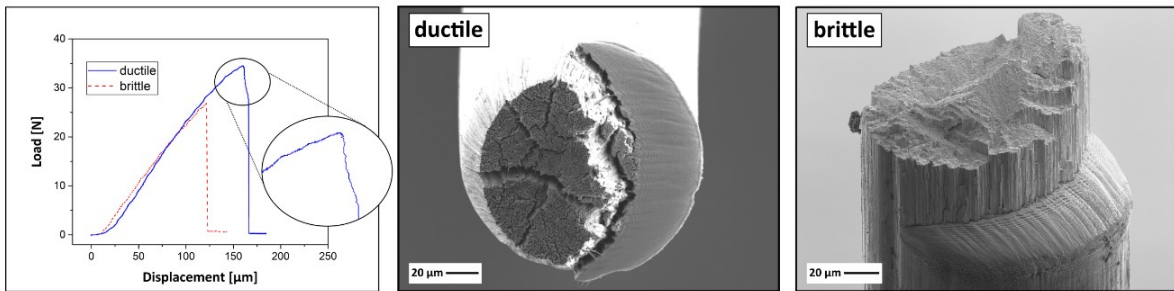
b) K doped W

Figure D.3. *The results of room temperature fracture experiments performed on a) pure tungsten and b) K-doped tungsten wires in the as-received state. The exemplary load-displacement curves and corresponding fractographs indicate the occurrence of both a brittle and a ductile materials behaviour in a test.*

The evaluation of the fracture toughness of pre-cracked wire samples, as a critical value of the stress intensity factor for this material subjected to tensile, mode I loading conditions can be used as a suitable method of measuring failure resistance of such a material. However, following critical remarks implicate an underestimation of the determined fracture toughness values and therefore they need to be discussed:

- The accuracy and/or discrepancy of the results is to some extent influenced by the measurement of the crack length a. The shape of the transverse crack in a cylindrical specimen under tension is the key parameter in numerical solutions of dimensionless geometrical factor f occurring in equation 1. Generally speaking, f is dependent on three parameters: the crack depth, the crack aspect ratio and the position of the considered point at the crack front [33]. Performing different finite element calculations on the basis of geometrical model of a crack having a different shape (the straight-fronted, semi-elliptical or semi-circular) gives several expressions of f where one, two or all three of aforementioned parameters play a role. In the case of a crack with a straight front, one-parameter K-solutions are obtained i.e. the expression of the dimensionless geometrical factor depends only on the relative crack depth $\frac{a}{D}$ [33,38]. K values determined within this study were based on the one-parameter expression approximating a curved laser produced notch to a straight one, defined by a central region of a

crack front. Determined values of fracture toughness are underestimated as the minimal crack length a_{min} was used in the calculations i.e. a longer measured crack length would yield a higher value of K.

- Further underestimation of K comes from a strong deflection of the crack i.e. a deviation of the crack path from its designated mode I propagation direction and thus approaching the direction of the wire axis. As a result, a mixed mode stress state is produced and therefore, the calculated values cannot be considered as a pure mode I fracture toughness. If a crack path and the fracture process would follow the initial plane of the pre-crack, the resulting K_{IC} would be even higher than the reported values. Therefore, the obtained results should be regarded as a lower bound value for the real mode I fracture toughness.

- Determination of the stress intensity factor in the framework of linear elastic fracture mechanics (LEFM) implies a plastic zone significantly smaller than the crack length, the ligament width and specimen thickness. In the regime of increased ductility, as can be seen in some of the tested samples, an elastic plastic evaluation of the fracture toughness would be more suitable. In this case, both the elastic part of the J-integral and the plastic part of the J-integral have to be taken into account. For calculation of K the later part has not been included, hence the calculated critical stress intensity values can only be considered as a lower limit.

Taking into account all of these considerations, the determined fracture toughness can be treated as an underestimated value. Despite some inaccuracies, in particular in the measurement of the crack length, the same procedure was followed for all of the tested samples. Therefore, when making a comparison between the investigated materials and different annealing conditions, the measured crack resistance can be used as a suitable apparent fracture toughness value.

D.3.2.2. Annealed wires

Typical load-displacement curves acquired from fracture experiments performed on annealed wires are shown for pure and K doped W wires in Figure D.4a and Figure D.4b, respectively. In this case a comparison is made between samples heat treated at 1300 °C and 1600 °C for 1h, where a substantial difference of the two investigated materials can be seen. For both annealing temperatures pure W wires show a typical brittle behaviour in the load-displacement curves with purely linear elastic loading and an abrupt decrease of force. In addition, it is evident that the maximum attained load before a failure is significantly lower than in the case of the as-received wire. In contrast to these observations, a non-linearity of the testing curves can be seen for doped wires, which is comparable to the ductile response of the as-received samples. Regardless of some decrease of the maximum load, even after annealing at the highest temperature of 1600 °C, the wire seems to preserve its good properties.

The measurements of apparent fracture toughness of wires annealed at 1300 °C yield values of (9.7 ± 1.7) MPa·m$^{1/2}$ and (25.1 ± 1.9) MPa·m$^{1/2}$ for pure and K-doped tungsten, respectively. The pronounce drop of K, in particular in the case of pure W, is further enhanced for the samples heat treated at 1600

°C. In this case, measured fracture toughness is only (7.6 ± 1.1) MPa·m$^{1/2}$ for pure and (22.6 ± 3.1) MPa·m$^{1/2}$ for K-doped wire. Such a distinctive difference of the two examined materials is also clearly reflected in the fractographic images. The doped wire fails predominately in a ductile, knife-edge failure manner having a characteristic crack deflection, while for the pure tungsten a planar crack propagation is observed with a typical brittle, mixed mode. Comprehensive evaluation of the failure process and the low fracture resistance will be given by examination of fracture surfaces in Section D.3.3.
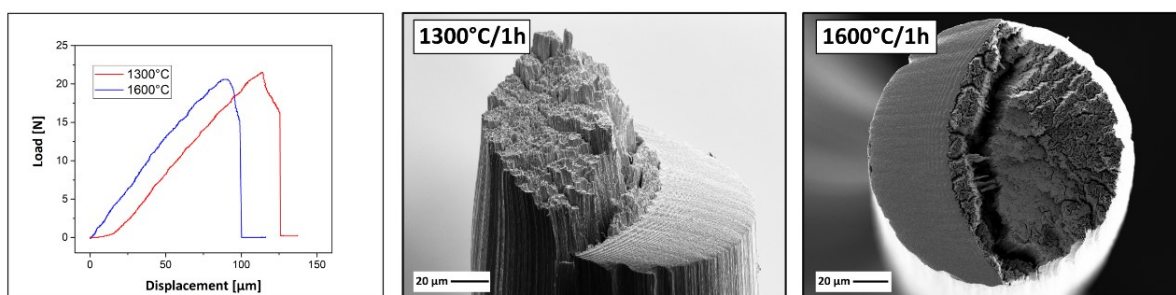
a) pure W
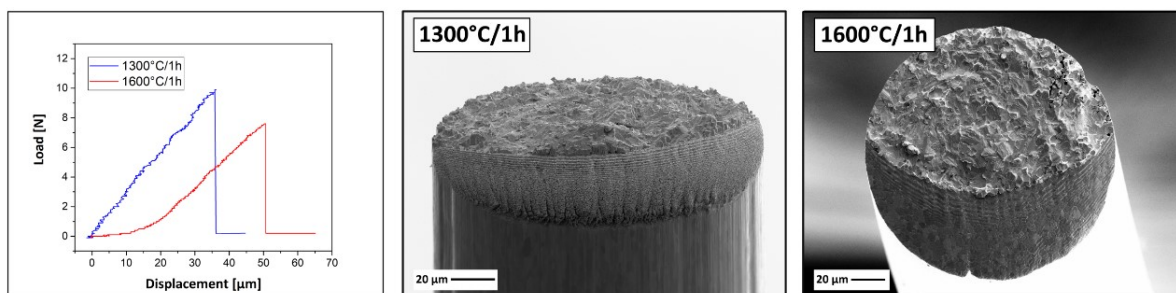
b) K doped W

Figure D.4. *The results of room temperature fracture experiments performed on a) pure tungsten and b) K-doped tungsten wires in two annealed states: 1300 °C/1h and 1600 °C/1h. The exemplary load-displacement curves and corresponding fractographs indicate the influence of different heat treatments on the resulting fracture properties.*

D.3.2.3. Influence of a pre-crack

An essential aspect of the determination of fracture toughness is the availability of a sharp notch. In terms of conventional notching methods, such as a fatigue pre-cracking, the case of tungsten is somewhat specific due to its typically brittle nature. The selection of the femtosecond laser processed notches is quite advantageous as the root radius yields between 5 and 20 nm [39], allowing fracture testing also for nanostructured tungsten alloys. A very strong influence of notch root radii on the measured fracture toughness was demonstrated, showing that blunter notches lead to an overestimation of the K values. Another beneficial characteristic is that fs-laser processing has no influence on the microstructure, as it was shown for cold rolled tungsten foils [30]. Sharpening of the conventionally processed notches additionally by a FIB showed a very strong influence on the measured toughness values of the ultrafine grain tungsten foils. A higher K$_q$ was obtained for samples

having a notch introduced only by electrical discharge machining [40] in comparison to lower fracture toughness values measured for samples having a sharper pre-crack made subsequently by a diamond wire, razor blade and FIB [41]. The absence of a nearly atomically-sharp worst-case flaw in the material produced by a FIB would lead to an enhancement of the stress level ahead of the tip, resulting in higher apparent toughness values. Furthermore, a link between the sharpness of a notch and resulting fracture behaviour was shown for cold drawn steel wires [42]. Samples having sharp notches presented a microscopically brittle behaviour (higher stress triaxiality), in contrast to ductile fracture process occurring in specimens with blunt notches.

In order to elucidate whether a similar notch effect takes place also for wires, an additional set of as-received samples was investigated, where beside the fs-laser notch, a sharp pre-crack was introduced by means of a FIB. An overview of all the obtained results from both type of materials, where the apparent fracture toughness K is plotted against performed heat treatments, is given in Figure D.5, with the associated values shown in Table D.1. As already discussed, pure tungsten shows a strong reduction in toughness with an increase of annealing temperature, with the effect being significantly milder in the case of the doped wires. Samples containing a FIB cut are compared against the fs-laser processed samples behaving in a ductile or a brittle manner. As-received samples with a sharp FIB pre-crack yield mean values of fracture toughness of (24.3 ± 1.6) MPa·m$^{1/2}$ and (22.6 ± 4.3) MPa·m$^{1/2}$ for pure and K-doped tungsten, respectively. When compared to the averaged fracture toughness of fs-laser processed samples fracturing in a ductile mode, a difference of about 15 MPa·m$^{1/2}$ is observed. However, it is very important to point out that all of the FIB samples failed in exclusively brittle or mixed mode with a pronounced 90° crack deflection followed by a transcrystalline cleavage. Thus, a comparison of the fracture toughness of the laser produced samples behaving in a brittle manner is more appropriate when discussing the notch effect. Similar K values indicate that sharpening of the notch does not lead to the change in a failure mode, which is in this case also dominated by a strong crack deflection at the initial stage of the fracture process. The reasons for the occurence of only a brittle behaviour and cleavage in the FIB samples are not obvious and will be further investigated and addressed in the following publication related to the effect of wire or grain thickness.
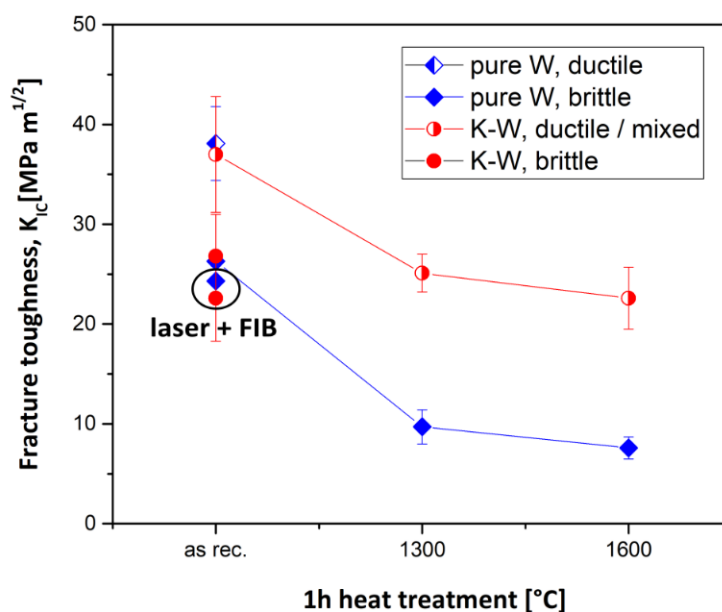
Figure D.5. *Apparent fracture toughness of pure and K-doped tungsten wires as a function of annealing temperature. The occurring failure mode, being a brittle, a ductile or a mixed one, is indicated as well. The influence of different notch fabrication methods is investigated for the as-received materials.*

Table D.1. *Overview of the apparent fracture toughness results of a pure and K-doped tungsten wire. Comparison is made between different notch techniques, material behaviour as well as annealing conditions of the samples (as-received, 1300 °C and 1600 °C state of the wire). The majority of the results represents an estimated lower limit of fracture toughness, which is indicated with a "greater than" sign. The bolded results outline a real mode I fracture toughness.*

Material state, notch technique	Fracture toughness [MPa·m$^{1/2}$]	
	Pure W	K-doped W
as received, laser, mean value	> 33.4 ± 6.4	> 31.9 ± 7.2
as received, laser, ductile	> 38.1 ± 3.7	> 37.0 ± 5.8
as received, laser, brittle	> 26.3 ± 0.5	> 26.8 ± 4.2
as received, laser + FIB, brittle	> 24.3 ± 1.6	> 22.6 ± 4.3
1300°C/1h, laser	**9.7 ± 1.7**	> 25.1 ± 1.9
1600°C/1h, laser	**7.6 ± 1.1**	> 22.6 ± 3.1

D.3.3. Fractography

D.3.3.1. As drawn wires

Fractographic analyses of the failed samples are an essential part in studying fracture behaviour of a material, in particular when it comes to establishing a relationship between the underlying microstructure and the characteristics of the fracture process. As outlined in previous chapter, as-received wires behave in different ways at RT, corresponding to lower or higher values of fracture toughness. Typical fracture morphologies are shown in Figure D.6 and Figure D.7, where detailed fractographic investigations are performed for brittle and ductile failure mode, respectively.

A unique feature occurring in all of the as-received samples, regardless of the type of failure mode, is a pronounced crack deflection (Figure D.6a and Figure D.7a). Such a deviation from an anticipated, mode I crack path occurs at the beginning of the fracture event and results in propagation along the drawing direction of the wire for a certain length, before a final fracture surface is formed. This distinct fracture feature occurs as a consequence of the elongated microstructure of heavily drawn wires and is a strong indication of a very prominent anisotropy in fracture toughness. It is implied that the crack growth resistance is significantly higher perpendicular to the aligned grains than parallel to them; consequently, crack deviates upon loading at an angle of about 90° in relation to the initial fracture plane and follows a path along a weaker crack growth direction. A magnified view of this 90° propagation step reveals this aligned, fibrous appearance of the microstructure with grains elongated along the drawing direction. So, it is energetically more favorable for a crack to propagate parallel to the wire axis generating longitudinal splitting by separation of individual grains at their weak grain boundaries than to propagate radially in pure mode I direction by breaking the grains. Such a strong anisotropy induced by microstructural orientation and appearing during fracture can also be seen in other materials, for example in the case of cold drawn steel wires [32,42].

The fractographic analyses of a sample behaving brittle (Figure D.6) reveals that the predominant micromechanisms of the final fracture process is cleavage. The shown example is a pure W wire, where magnified fracture features are seen in the side (Fig. 6a) and top view (Fig. 6b) of the wire. After the initial deflection of the crack, a mode II fracture appears at the interface between the grains and the resulting final fracture surface is inclined in respect to the initial laser notch plane. The origin of the transgranular cleavage is situated in the central area of the wire with the crack propagating radially and forming characteristic river patterns. Besides this, small colonies of grains with a cleavage surface roughly perpendicular to the wire axis can be seen (bottom magnified fractograph in Figure D.6a), which are related to the {110} cleavage plane and arise as a consequence of the <110> fiber texture. The occurrence of the {110} cleavage in heavily-drawn wires can be considered as a special case imposed by the extremely fibrous nature of the structure and a very sharp texture [27]. Moreover, the dominating brittle appearance is characterized by a missing necking of the wire diameter and a small amount of

130

longitudinal micro-crack formation, located at the edge region (bottom magnified fractograph in Figure D.6b).
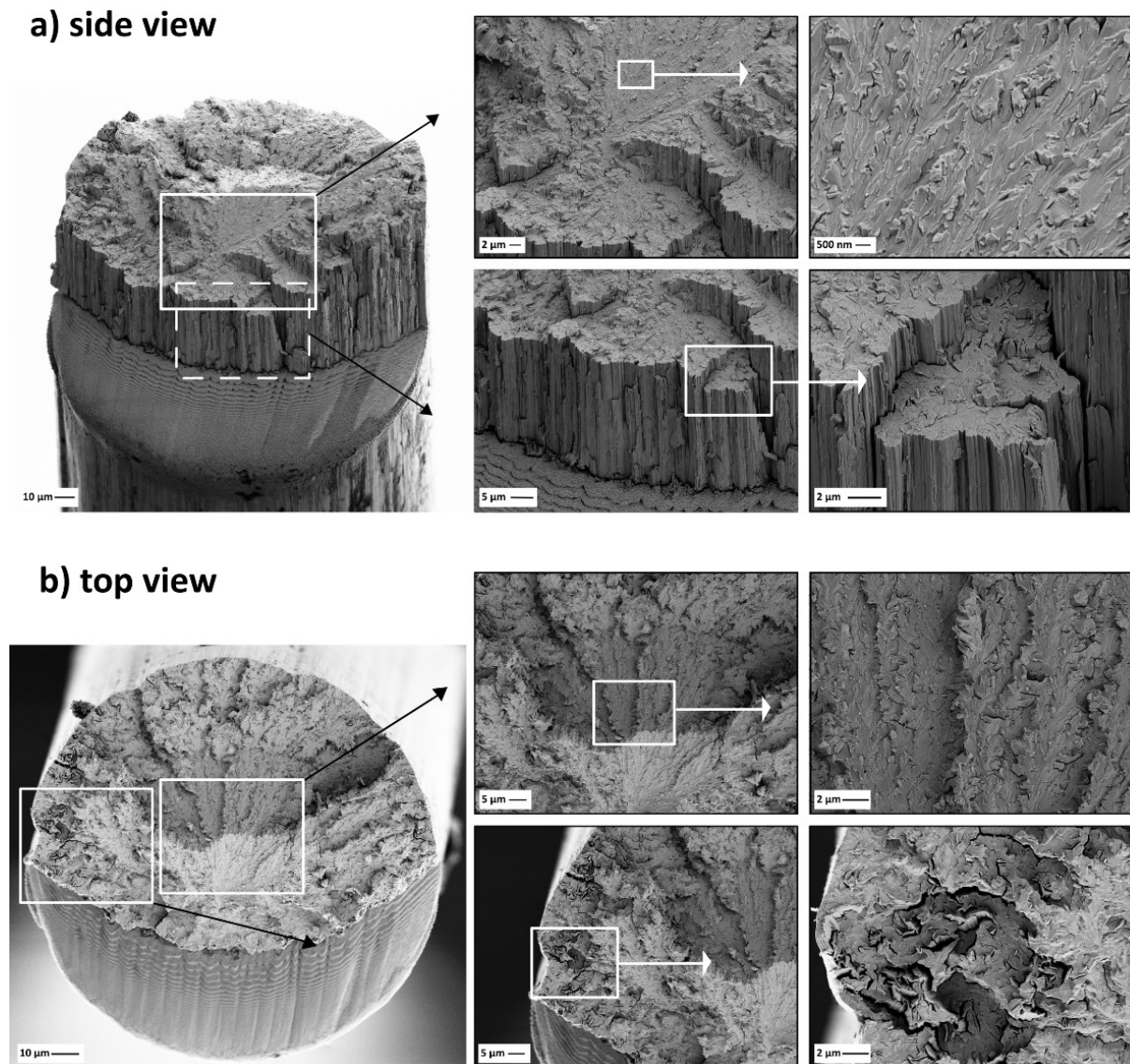
Figure D.6. *Scanning electron micrographs of a pure, as-received tungsten wire showing a typical brittle, cleavage dominated fracture behaviour. Fracture surfaces are studied in a) a side view and b) a top view of the wire in respect to a laser notch. The most characteristic features of the fracture process are shown in the magnified images.*

The fracture morphology demonstrating a ductile behaviour of the as-received wires, seen in Figure D.7, is shown for the K-doped material. This fracture appearance is typically designated as ductile, knife-edge failure mode and after crack deflection it is characterized by distinct necking of the entire wire, followed by longitudinal cracking and necking of individual grains to almost 100 % reduction in

area (bottom magnified fractograph in Figure D.7a). Significantly higher amount of plastic deformation, when compared to the sample behaving in a brittle manner, is seen through pronounced necking of the wire which is in a good correlation with the obtained load-displacement curve. A direct influence of the curled grains, observed in the cross sections of the untested wire (Figure D.2b), can be seen from the fractographs taken in the top view (Figure D.7b), revealing that the fracture surface consists of intertwined, convoluted ribbons. Knife-edge necking of individual grains, similar to the knife-edge fracture observed in a <110> tungsten single crystal, occurs within these ribbons and results from their intrinsic plane strain elongation [27], which is a consequence of the {110} fibre texture.

Further peculiar features of the fracture surfaces are deep crevices running in the radial direction of the wire and are often referred to as delaminations. Closer inspection of the magnified fractographs reveals that between large delaminations, smaller ones can be observed as well, which alongside with individual grain necking lead to the fracture surface appearing as a network of lines. Delaminations occur by a decohesion of the grains along their longitudinal grain boundaries and thus propagate along the wire drawing direction. It is a process that proceeds necking of the individual grains, indicating that these boundaries are too weak to support tensile stresses generated during necking, which is also an indication that the interfibre fracture toughness is significantly lower than the strength of the grains themselves [27]. As a result, the occurrence of delaminations permits the individual grains to act as bundled, individual wires which will be manifested through their aforementioned reduction in area. Furthermore, the existence of the grain boundary delaminations is closely related to the reduction in the stress triaxiality which leads to the increased crack growth resistance. The formation of these longitudinal cracks along the weak boundaries of the elongated grain structure gives a further hint of a strong anisotropy in the fracture properties of a heavily deformed tungsten wire. Observed features of a ductile as well as brittle fracture modes are very similar to the ones already reported for heavily deformed tungsten wires [22,27,37].
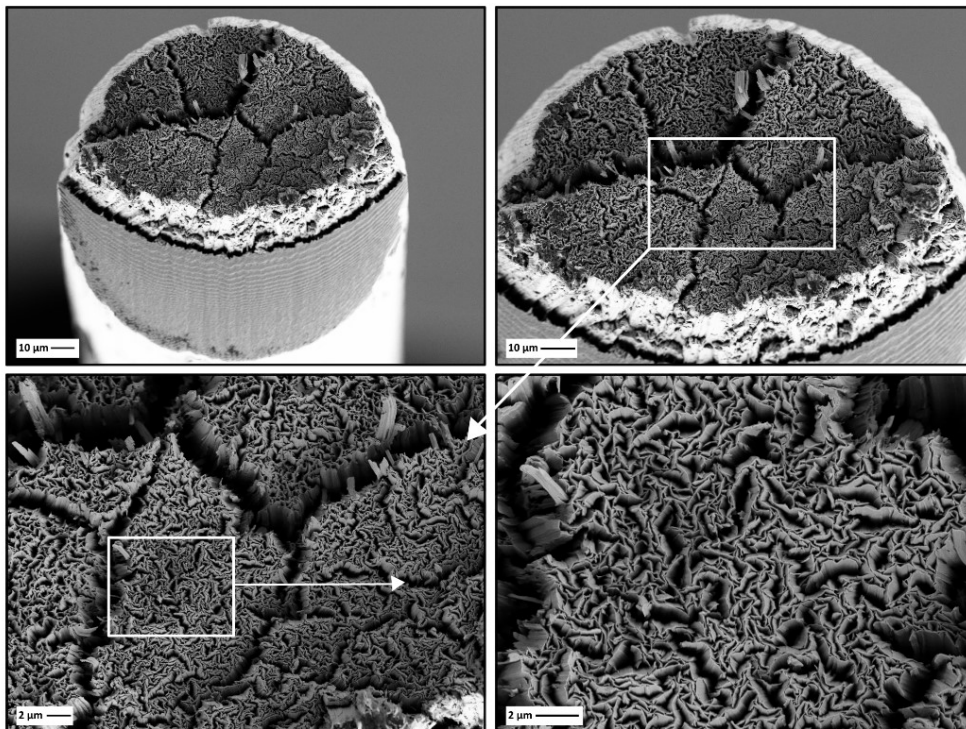
a) side view
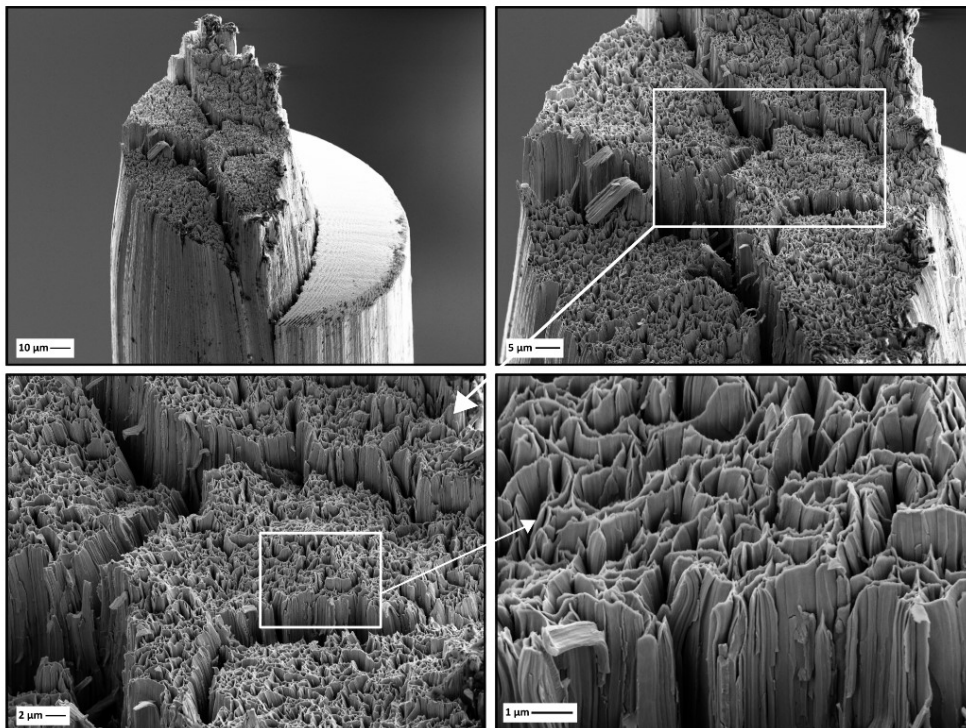
b) top view

Figure D.7. Scanning electron micrographs of a K-doped, as-received tungsten wire showing a typical ductile, knife-edge necking dominated fracture mode. Fracture surfaces are studied in a) a side view and b) a top view of the wire in respect to a laser notch. The most characteristic features of the fracture process are shown in the magnified images.

D.3.3.1. Annealed wires

Fracture surfaces of the wires heat treated at the lower annealing temperature of 1300 °C for 1h are shown in Figure D.8. A tremendous difference in the micromechanisms controlling the fracture process can be observed when comparing pure (Figure D.8a) and K-doped tungsten wires (Figure D.8b). The failure mode of the undoped wire is characterized as a brittle, mixed one being composed of both cleavage and intergranular fracture. The most distinctive feature in this case is the absence of the crack deflection, with the fracture surface being mostly flat in respect to the wire axis. Thus, for this material state the crack path does not deviate from its designated mode I propagation direction. Annealed K-doped wire has a very similar failure appearance as in the as-received state, with the fracture surface including longitudinal cracks and knife-edge necking of the individual grains. In addition, small colonies of brittle grains can be observed (shown in the magnified fractographs in Figure D.8b) with the cleavage surfaces roughly perpendicular to the longitudinal direction. However, as these areas are rather small and the knife-edge ruptures of individual fibers dominate over the fracture surface, the occurring failure mode can be considered as the predominately a ductile one.

Influence of even higher heat treatments (1600 °C for 1h) on the resulting fracture morphologies can be seen in Figure D.9, where once again comparison is made between the two types of the investigated materials. Pure W shows a very similar appearance of mixed, brittle fracture as the samples annealed at 1300 °C: besides the cleavage planes with typical river lines, brittle intergranular grain boundary fractures are also occurring in between, as shown in the magnified fractographs in Figure D.9a. The intergranular failure mode seems to dominate at the edge region of the wire which can be related to the heterogeneity of the stress state across the diameter [43,44], occurring as a direct consequence of the drawing process. Such a correlation of the radial position and the resulting failure mode was anticipated from the observations of the localized variations in crystallographic orientation and the texture analyses, which were conducted in the first part of the publication [29]. Furthermore, the crack propagation direction remains in the same plane of the initial pre-crack with a decrease of the overall roughness of the fracture surface.

Once annealed at 1600 °C, the K-doped tungsten wire shows a more noticeable variation of the micromechanisms taking place during the fracture process, as shown in Figure D.9b. In this case, an increase in the area of the cleaved grains is observed, which can be associated with the observed decrease in fracture toughness. Magnified fractographs reveal that the cleaved planes are also roughly perpendicular in respect to the wire axis, with small longitudinal cracks occurring between the convoluted colonies of grains. Nevertheless, regardless of the existence of the brittle phase, the presence of the extensive necking of the wire diameter accompanied by a wide range of the knife-edge fractured individual grains underlines the remarkable fracture properties of a doped wire upon annealing.
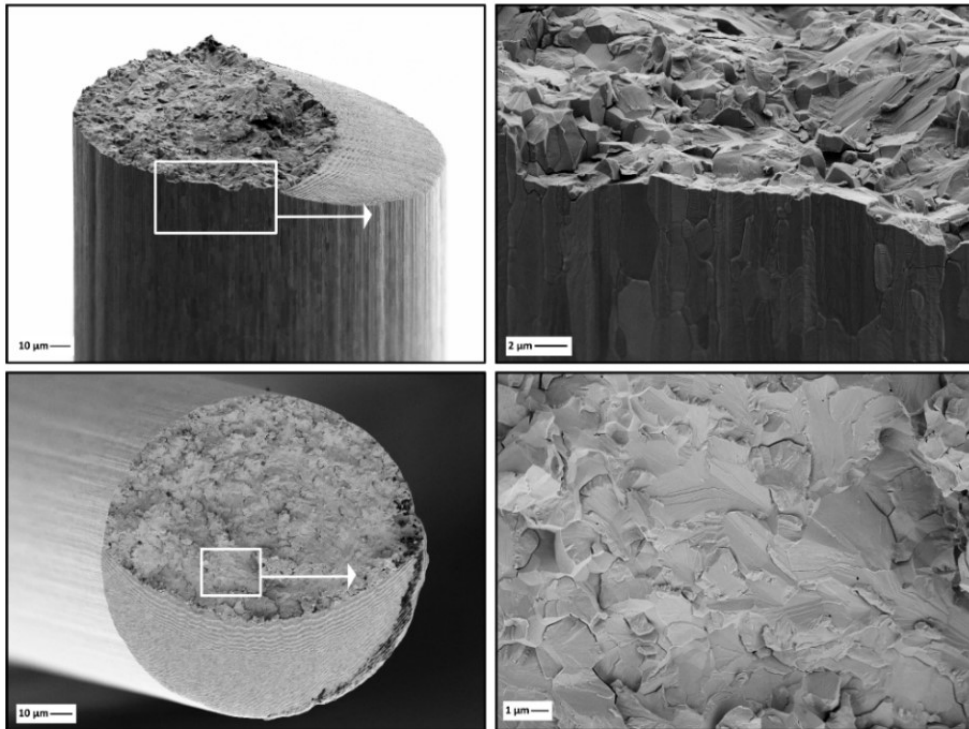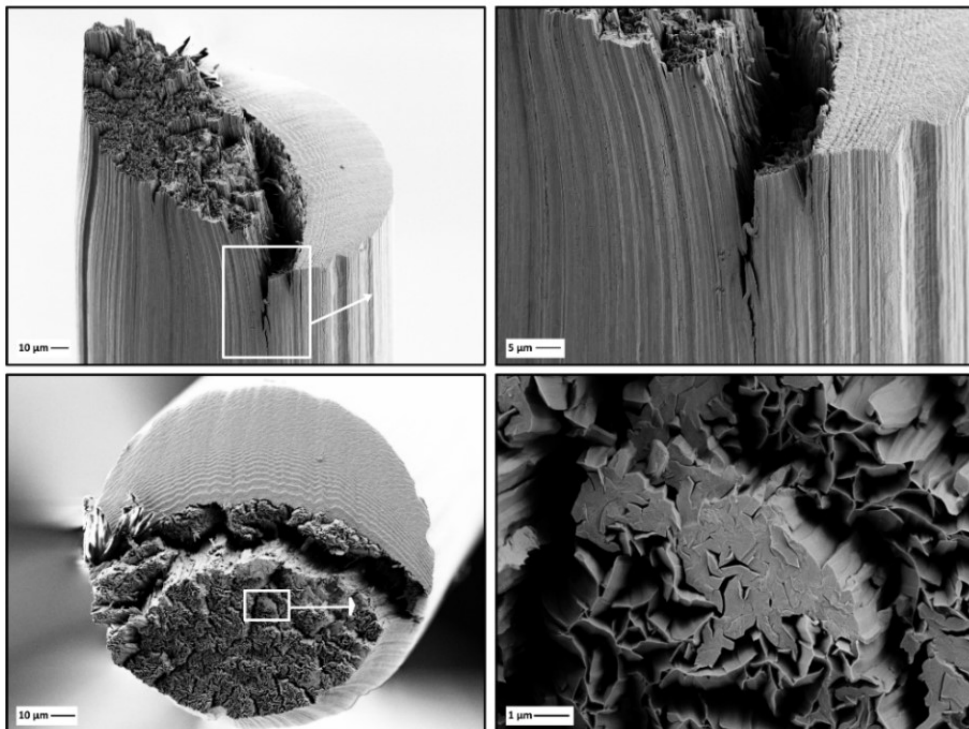
Figure D.8. *Scanning electron micrographs of tungsten wires annealed at 1300°C for 1h. A comparison is made between a) a pure W wire showing mixed, brittle failure mode consisting of both cleavage and intergranular fracture and b) a K-doped W wire showing predominately a typical ductile, knife-edge necking dominated fracture mode.*

a) pure W
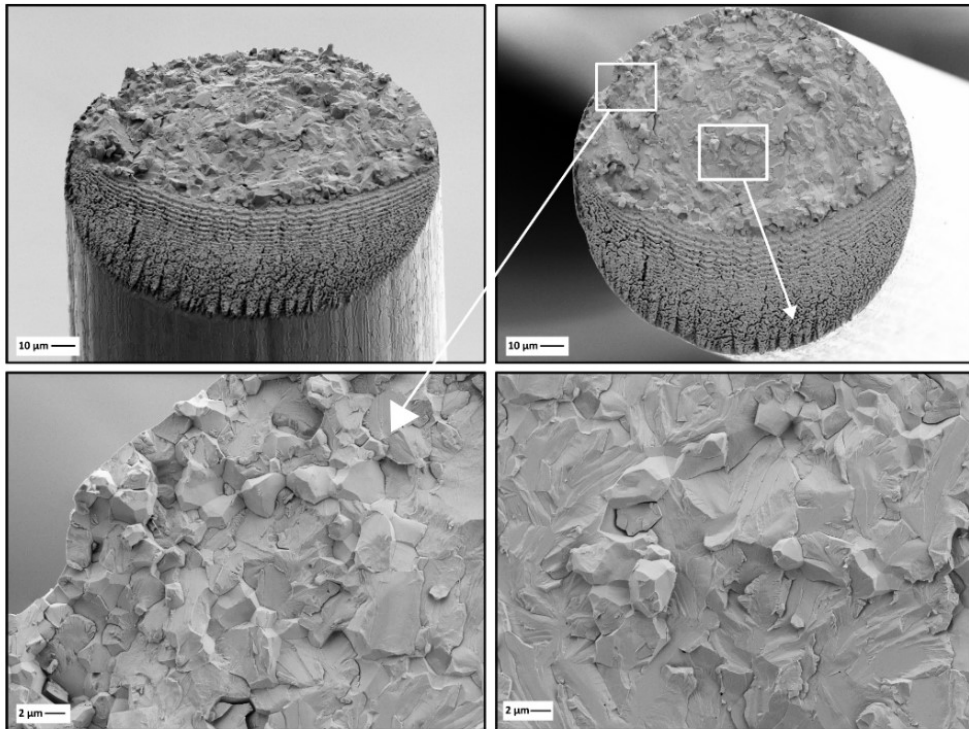
b) K doped W
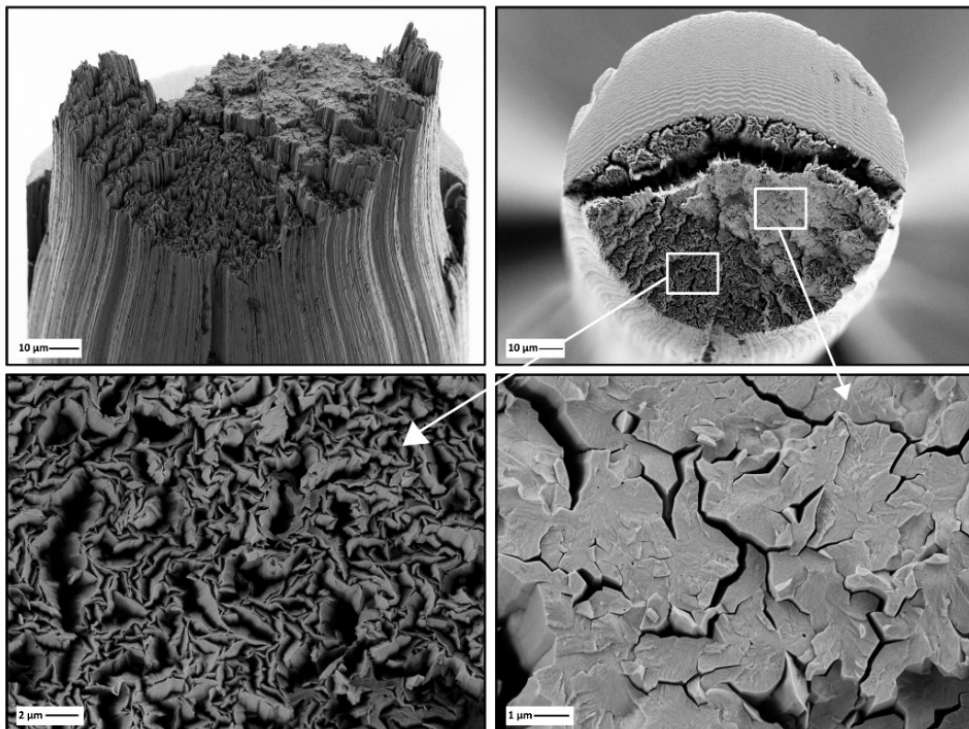
Figure D.9. *Scanning electron micrographs of tungsten wires annealed at 1600°C for 1h. A comparison is made between a) a pure W wire showing mixed, brittle failure mode consisting of both the cleavage and intergranular fracture (which is a dominant mode in the edge region) and b) a K-doped W wire showing a mixed fracture mode consisting of a typical ductile, knife-edge necking and cleavage with facets roughly perpendicular to the wire axis.*

A strong influence of fibrous, elongated grain structure with ultrafine size is clearly seen in a very ductile appearance of the respective fracture surfaces. Modifications of the initial grain structure by different heat treatments are also translated to the occurring failure mode in the case of heavily drawn tungsten wires. Thus, it is possible to find a correlation between the thermal history and micromechanisms controlling the fracture process, which is very important when discussing the beneficial influence of potassium doping. In the case of pure tungsten, annealing already at 1300 °C leads to a complete loss of elongated microstructure and a formation of large, equiaxed grains, which further increase in size by annealing at higher temperatures (Figure D.2).

The influence of the thermal history is seen through a tremendous decrease in fracture toughness accompanied with a major change of the failure mode, which mostly can be related to the pronounced decrease in grain boundaries aligned to the drawing direction. In the initial state of the wire, the weakness of the longitudinal grain boundaries is clearly seen through the occurrence of a strong crack deflection and the longitudinal cracking, while the transverse boundaries are widely separated and most likely not a preferred crack path. However, elevated thermal exposures above the recrystallization temperature can cause the formation of transverse boundaries through polygonization and by movement of a small section of the longitudinal boundaries [45]. Due to the overall changes in the grain size and shape of a pure W wire, instead of having transverse and longitudinal boundaries at approximately right angles to each other, the boundaries after annealing intersect at a variety of angles. As a result, a crack can more easily propagate from one grain boundary facet to another without deviating from the initial crack propagating direction leading to the intergranular appearance of the fracture surface. In some areas the grains are cut through, resulting in characteristic river patterns of cleavage fracture.

In contrast to this, the K-doped wire shows remarkable fracture behaviour even after the heat treatments, which is ascribed to the preservation of the fibrous, elongated microstructure and is seen through predominately knife-edge fracture mode. Investigated heat treatments and annealing temperatures of 1300 °C to 1600 °C lead to a small degree of broadening of the fibers, which is related to an increase in the amount of transverse grain boundaries. If there are more boundaries of this type in the same plane, the probability of providing a nucleation site for cleavage rises, resulting in a reduced fracture toughness and larger amount of cleaved grains in the fracture surface. However, more substantial microstructural changes are prevented by finely dispersed rows of ultrafine sized potassium bubbles which act as pinning sites and can be seen in Figure D.10. In such a way, the grain boundary migration is restricted resulting in a sluggish microstructural coarsening and a shift of the recrystallization to even higher temperatures than in the case of pure tungsten.
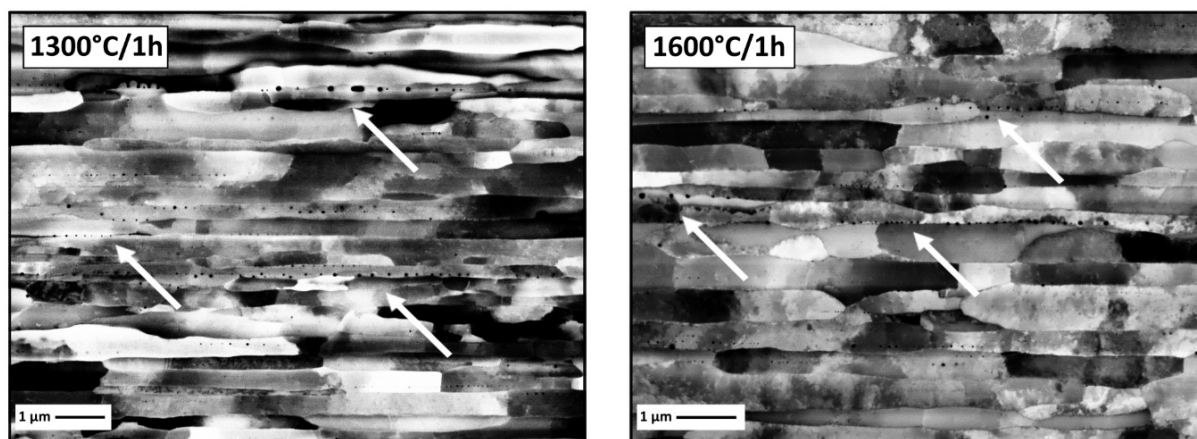
Figure D.10. Scanning electron micrographs of the annealed, K-doped tungsten wires showing finely distributed rows of potassium bubbles which act as pinning sites and thus prevent grain boundary migration. The images are taken across the longitudinal sections in the BSE mode, while the dopants are indicated with white arrows.

D.3.4. True vs. apparent fracture toughness

Taking into account different criteria of underestimation of fracture toughness discussed in Section D.3.2.1., the evaluated critical stress intensity K can only be considered as an apparent crack resistance of the investigated wires. The biggest deviation from the valid K_{IC} values, comes from the discrepancy between the designated mode I loading conditions and nearly immediate deflection of the crack propagation direction by 90°. Thus, the measured toughness and the extend of necking is influenced by a plastic limit load. In contrast to this, the experiments performed on the annealed pure tungsten wires deliver a valid K_{IC} according to the ASTM 399 standard [46], as the crack does not deviate and can easily propagate in the designated direction. This is true for pure W after both heat treatments of 1300 °C and 1600 °C, yielding fracture toughness of (9.7 ± 1.7) MPa·m$^{1/2}$ and (7.6 ± 1.1) MPa·m$^{1/2}$, respectively. These results, highlighted in Table D.1, can be considered as a valid lower limit of fracture toughness, keeping in mind approximations regarding the definition of a crack front. In all the other samples, where a pronounced crack deflection takes place followed by a brittle cleavage or a knife edge ductile failure mode, it can be assumed that the true fracture toughness is significantly higher than the calculated K values. The question is by which order of the magnitude are the obtained results underestimated in comparison to material's true crack resistance?

A convenient method of measuring fracture toughness of ductile materials in the elastic-plastic regime is by determining the critical crack tip opening displacement (CTOD), which measures a degree of blunting of a crack tip before the crack propagation takes place [47]. CTOD parameter is related to a more geometry independent toughness K_{CTOD} and can be determined by stereophotogrammetric reconstruction of fracture surfaces, where a local plastic deformation is extracted from the 3D microscopic topography [48,49]. Additional fractographic analyses of samples fracturing in a ductile manner reveal small areas of a fibrous knife-edge necking over a very small distance as a first

subcritical crack growth in mode I, followed by a strong deflection of a crack and occurrence of vertical walls of grains. The example shown in Figure D.11 is a K-doped wire with a measured K value of 44.5 MPa·m$^{1/2}$. A rough estimation of a CTOD parameter can be extracted from the dimension of this ductile area before the propagation step occurs, giving an approximate value of about 6µm. Employing the expression between CTOD and K$_{CTOD}$ given by [47] with yield strength of $\sim 2700 MPa$ [50] and the Young's modulus of $\sim 400 GPa$ [6], an estimated fracture toughness of about 80.5 MPa·m$^{1/2}$ is obtained. Therefore, experimental results yield an underestimation of a true fracture toughness of tungsten wires at least by a factor of two. Similar features in failure mode and estimations of K are seen for pure tungsten, as well as the annealed K-doped wire, where a dominant micromechanism of fracture is ductile, fibrous mode having some isolated cleavage facets indicating a locally brittle fracture.
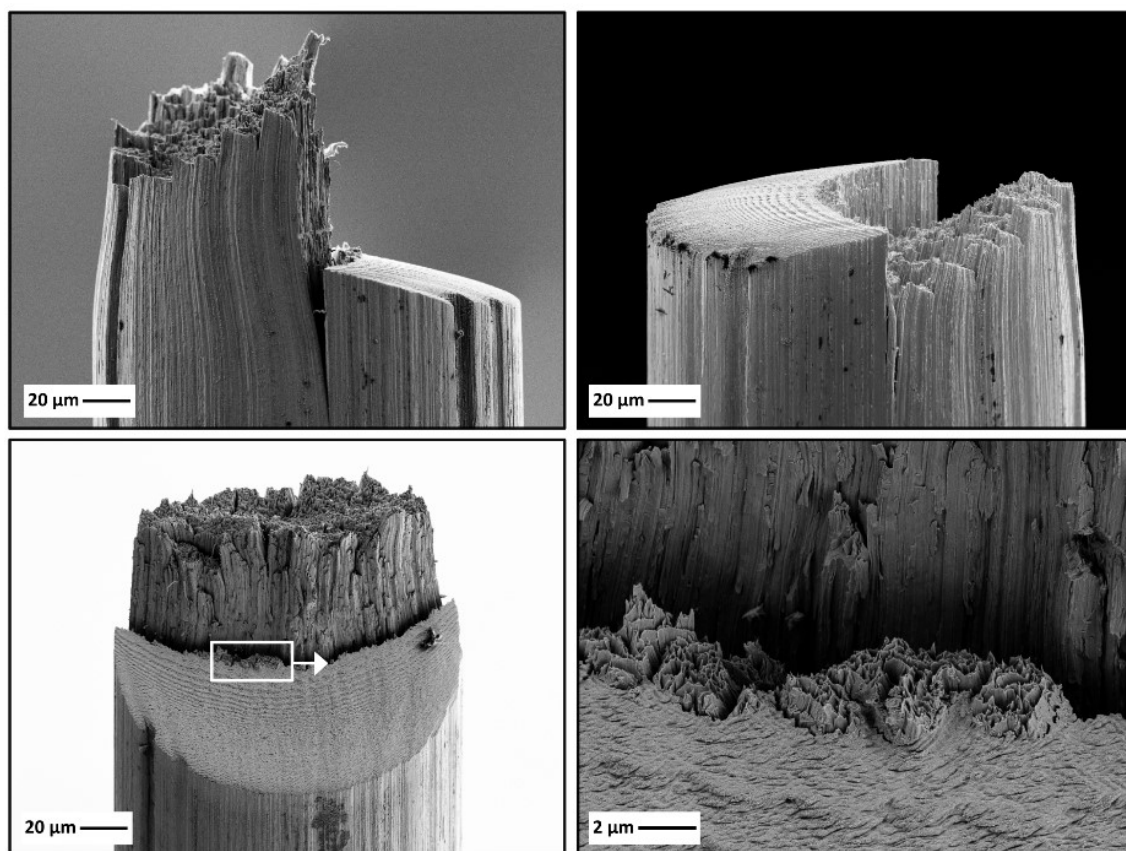
Figure D.11. Scanning electron micrographs of a K-doped tungsten wire showing a typical ductile, knife-edge necking dominated fracture mode. Top fractographs show the resulting failure mode in both halves of the fractured wire. Bottom fractographs display a side view of the sample, where a small ductile area occurring before the crack deflects by 90° is magnified. This first, fibrous subcritical crack growth in mode I is used in approximating a CTOD parameter and estimating a true fracture toughness.

D.4. Conclusions

The main scope of the study was the room temperature fracture mechanical assessment of pure and potassium doped tungsten wires with a diameter of 150 μm. The investigation was predominantly focused on the evolution of the fracture mechanisms in respect to annealing, with selected heat treatment temperatures being 1300 °C and 1600 °C. In such a way, a relationship between the microstructural features, annealing phenomena and resulting fracture properties were established. The main findings can be summarized as following:

- The fracture properties of both types of wires in the as-received state are very similar. The occurrence of either a brittle or a ductile materials response in a test is observed, which is related to either lower or higher obtained values of fracture toughness, respectively. The existence of a large scatter of measured K data is an indication that the ductile-to-brittle transition temperature is around room temperature.

- With an increase in annealing temperature the pure tungsten wire shows a significant reduction in toughness as a result of embrittlement by annealing. The influence of heat treatments is significantly milder in the case of K-doped material, as the decrease in fracture toughness, even after annealing at 1600 °C is not as pronounced.

- A comprehensive SEM investigation of the fracture surfaces reveals four dominant micromechanisms controlling the fracture process, which are summarized in schematic drawings in Figure D.12. The predominant micromechanism of the as received samples failing in a brittle manner is transcrystalline cleavage, while a ductile fracture mode is designated as a knife-edge necking. In both cases, a very prominent crack deflection by about 90° is perceived. Tremendous changes upon annealing in case of pure tungsten are seen through the absence of crack deflection, with a mixed failure mode consisting of both cleavage and intergranular fracture. In contrast, annealed doped tungsten wire shows a similar appearance as in the as-received state, having a predominately a ductile fracture mode.

- An additional sharpening of the fs-laser notch by a FIB cut does not have a significant influence on the resulting fracture process (a higher tendency of a brittle mode is perceived). Considering different criteria of underestimation, the evaluated fracture toughness can be regarded as an apparent crack resistance of the tungsten wire. The extent of underestimation can be estimated from CTOD measurements, evaluating that the true fracture toughness is higher by at least a factor of two in the ductile failure behaviour.
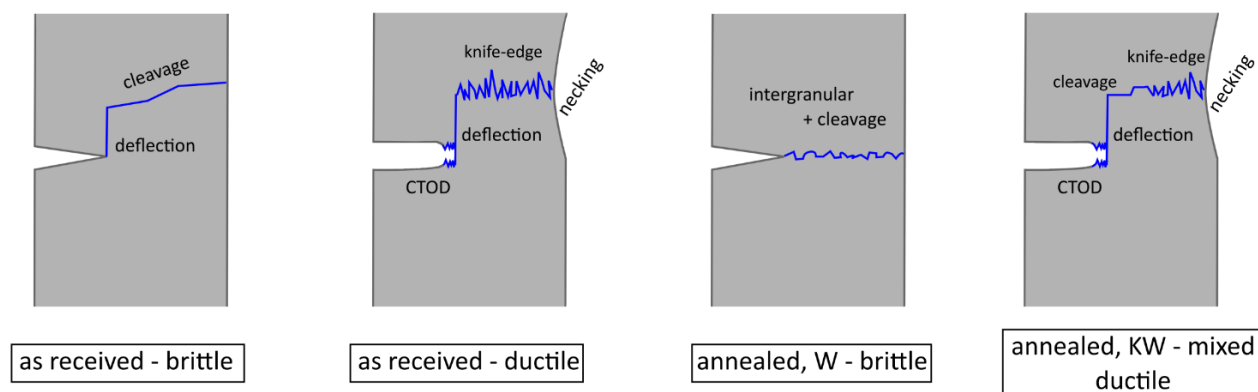
Figure D.12. *Schematic drawings displaying the main micromechanisms controlling the fracture process of the wire in the as-received and annealed state.*

The main conclusion of the work is that the underlying microstructure is the key parameter controlling the resulting fracture process. In the case of pure tungsten wires, the microstructural modifications induced by annealing are directly reflected in fractographic features and a tremendous variation of a failure mode is observed. Thus, the occurring embrittlement can be correlated to the loss of the fibrous, elongated grain structure. In contrast to that, addition of potassium as a doping element results in a restriction of the grain boundary migration and a sluggish microstructural coarsening, maintaining in such a way a ductile behaviour up to very high temperatures. Therefore, from a perspective of the investigated fracture properties, the application of K-doped tungsten wires is strongly advised for a structural part of fusion reactors, as it is the case for W_f/W composites.

Acknowledgments

D.5. References

[1] H. Zohm, "Assessment of DEMO challenges in technology and physics," *Fusion Eng. Des.*, vol. 88, no. 6–8, pp. 428–433, 2013.

[2] D. Stork *et al.*, "Developing structural, high-heat flux and plasma facing materials for a near-term DEMO fusion power plant: The EU assessment," *J. Nucl. Mater.*, vol. 455, no. 1–3, pp. 277–291, 2014.

[3] C. Linsmeier *et al.*, "Development of advanced high heat flux and plasma-facing materials," *Nucl. Fusion*, vol. 57, no. 92007, pp. 1–60, 2017.

[4] M. Rieth *et al.*, "Recent progress in research on tungsten materials for nuclear fusion applications in Europe," *J. Nucl. Mater.*, vol. 432, no. 1–3, pp. 482–500, 2013.

[5] V. Philipps, "Tungsten as material for plasma-facing components in fusion devices," *J. Nucl. Mater.*, vol. 415, no. 1, pp. S2–S9, 2011.

[6] E. Lassner and W.-D. Schubert, *Tungsten - Properties, Chemistry, Technology of the Element, Alloys and Chemical Compounds*. New York: Kluwer Academic/Plenum Publishers, 1999.

[7] V. Barabash, G. Federici, M. Rödig, L. L. Snead, and C. H. Wu, "Neutron irradiation effects on plasma facing materials," *J. Nucl. Mater.*, vol. 283–287, no. I, pp. 138–146, 2000.

[8] G. Pintsuk, S. Antusch, T. Weingaertner, and M. Wirtz, "Recrystallization and composition dependent thermal fatigue response of different tungsten grades," *Int. J. Refract. Met. Hard Mater.*, vol. 72, no. September 2017, pp. 97–103, 2018.

[9] Y. Yuan, J. Du, M. Wirtz, G. N. Luo, G. H. Lu, and W. Liu, "Surface damage and structure evolution of recrystallized tungsten exposed to ELM-like transient loads," *Nucl. Fusion*, vol. 56, no. 3, pp. 1–8, 2016.

[10] P. L. Raffo, "Yielding and Fracture in tungsten and tungsten rhenium alloys," *J. Less-Common Met.*, vol. 17, pp. 133 – 149, 1969.

[11] S. Wurster, B. Gludovatz, and R. Pippan, "High temperature fracture experiments on tungsten-rhenium alloys," *Int. J. Refract. Met. Hard Mater.*, vol. 28, no. 6, pp. 692–697, 2010.

[12] A. Luo, D. L. Jacobson, and K. S. Shin, "Solution softening mechanism of iridium and rhenium in tungsten at room temperature," *Int. J. Refract. Met. Hard Mater.*, vol. 10, no. 2, pp. 107–114, 1991.

[13] Q. Wei and L. J. Kecskes, "Effect of low-temperature rolling on the tensile behavior of commercially pure tungsten," *Mater. Sci. Eng. A*, vol. 491, no. 1–2, pp. 62–69, 2008.

[14] V. Nikolic, S. Wurster, D. Firneis, and R. Pippan, "Improved fracture behavior and microstructural characterization of thin tungsten foils," *Nucl. Mater. Energy*, vol. 9, pp. 181–188, 2016.

[15] R. Neu *et al.*, "Tungsten fibre-reinforced composites for advanced plasma facing components," *Nucl. Mater. Energy*, vol. 12, pp. 1308–1313, 2017.

[16] J. Riesch, T. Höschen, C. Linsmeier, S. Wurster, and J. H. You, "Enhanced toughness and stable crack propagation in a novel tungsten fibre-reinforced tungsten composite produced by chemical vapour infiltration," *Phys. Scr.*, vol. T159, no. 14031, pp. 1–7, 2014.

[17]   J. Riesch *et al.*, "Chemically deposited tungsten fibre-reinforced tungsten – The way to a mock-up for divertor applications," *Nucl. Mater. Energy*, vol. 9, pp. 75–83, 2016.

[18]   B. Jasper *et al.*, "Behavior of tungsten fiber-reinforced tungsten based on single fiber push-out study," *Nucl. Mater. Energy*, vol. 9, pp. 416–421, 2016.

[19]   P. Schade, "100 years of doped tungsten wire," *Int. J. Refract. Met. Hard Mater.*, vol. 28, no. 6, pp. 648–660, 2010.

[20]   C. L. Briant and B. P. Bewlay, "The Coolidge Process for Making Tungsten Ductile: The Foundation of Incandescent Lighting," *MRS Bull.*, vol. 20, no. 8, pp. 67–73, 1995.

[21]   E. Pink and L. Bartha, *The metallurgy of doped/non-sag tungsten*. Elsevier Science Publishers, 1989.

[22]   P. Schade, "Wire drawing failures and tungsten fracture phenomena," *Int. J. Refract. Met. Hard Mater.*, vol. 24, no. 4, pp. 332–337, 2006.

[23]   O. Horacsek, "Properties and failure modes of incandescent tungsten filaments," *IEE Proc. A (Physical Sci. Meas. Instrumentation, Manag. Educ. Rev.*, vol. 127, no. 3, pp. 134–141, 1980.

[24]   D. Lee, "Fracture of drawn tungsten wires," *Metall. Trans. A*, vol. 6, no. 11, pp. 2083–2088, 1975.

[25]   J. L. Walter, C. L. Briant, and E. F. Koch, "Splitting of Tungsten Wire in the Knife-Edge Compression Test.," *Metall. Trans. A, Phys. Metall. Mater. Sci.*, vol. 13 A, no. 8, pp. 1501–1510, 1982.

[26]   A. W. Funkenbusch, F. Bacon, and D. Lee, "The influence of microstructure on fracture of drawn tungsten wire," *Metall. Trans. A*, vol. 10, no. 8, pp. 1085–1091, 1979.

[27]   S. Leber, J. Tavernelli, D. D. White, and R. F. Hehemann, "Fracture modes in tungsten wire," *J. Less-Common Met.*, vol. 48, no. 1, pp. 119–133, 1976.

[28]   R. H. Forster and A. Gilbert, "The effect of grain structure on the fracture of recrystallized tungsten wire," *J. Less-Common Met.*, vol. 20, pp. 315–325, 1970.

[29]   V. Nikolić, J. Riesch, and R. Pippan, "The effect of heat treatments on pure and potassium doped drawn tungsten wires : Part I - Microstructural characterization," *Mater. Sci. Eng. A*, submitted, 2018.

[30]   M. J. Pfeifenberger *et al.*, "The use of femtosecond laser ablation as a novel tool for rapid micro-mechanical sample preparation," *Mater. Des.*, vol. 121, pp. 109–118, 2017.

[31]   B. N. Chichkov, C. Momma, S. Nolte, F. von Alvensleben, and A. Tünnermann, "Femtosecond, picosecond and nanosecond laser ablation of solids," *Appl. Phys. A Mater. Sci. Process.*, vol. 63, no. 2, pp. 109–115, 1996.

[32]   A. Hohenwarter *et al.*, "Ultra-strong and damage tolerant metallic bulk materials: A lesson from nanostructured pearlitic steel wires," *Sci. Rep.*, vol. 6, no. May, pp. 1–10, 2016.

[33]   J. Toribio, N. Álvarez, B. González, and J. C. Matos, "A critical review of stress intensity factor solutions for surface cracks in round bars subjected to tension loading," *Eng. Fail. Anal.*, vol. 16, no. 3, pp. 794–809, 2009.

[34]   M. R. Ripoll and J. Očenášek, "Microstructure and texture evolution during the drawing of tungsten wires," *Eng. Fract. Mech.*, vol. 76, no. 10, pp. 1485–1499, 2009.

[35]   W. F. J. Hosford, "Microstructural changes during deformation of [011] fiber textured metals," *Trans. Metall. Soc. AIME*, vol. 230, pp. 12–15, 1964.

[36]   D. B. Snow, "The recrystallization of commercially pure and doped tungsten wire drawn to high strain," *Metall. Trans. A*, vol. 10, no. 7, pp. 815–821, 1979.

[37]   P. Zhao *et al.*, "Microstructure, mechanical behaviour and fracture of pure tungsten wire after different heat treatments," *Int. J. Refract. Met. Hard Mater.*, vol. 68, no. June, pp. 29–40, 2017.

[38]   C. A. Valiente, "Criterios de fractura para alambres," 1980.

[39]   T. Palacios and J. Y. Pastor, "Influence of the notch root radius on the fracture toughness of brittle metals : Nanostructure tungsten alloy , a case study," *RMHM*, vol. 52, pp. 44–49, 2015.

[40]   C. Bonnekoh, A. Hoffmann, and J. Reiser, "The brittle-to-ductile transition in cold rolled tungsten: On the decrease of the brittle-to-ductile transition by 600 K to − 65 °C," *Int. J. Refract. Met. Hard Mater.*, vol. 71, pp. 181–189, 2018.

[41]   V. Nikolić, S. Wurster, D. Firneis, and R. Pippan, "Fracture toughness evaluation of UFG tungsten foil," *Int. J. Refract. Met. Hard Mater.*, vol. 76, no. June, pp. 214–225, 2018.

[42]   J. Toribio and F. J. Ayaso, "Anisotropic fracture behaviour of cold drawn steel : a materials science approach," *Mater. Sci. Eng.*, vol. 343, pp. 265–272, 2003.

[43]   M. R. Ripoll, S. M. Weygand, and H. Riedel, "Reduction of tensile residual stresses during the drawing process of tungsten wires," *Mater. Sci. Eng. A*, vol. 527, no. 13–14, pp. 3064–3072, 2010.

[44]   J. G. Sevillano and D. González, "Heterogeneous Deformation and Internal Stresses Developed in BCC Wires by Axisymmetric Elongation," vol. 550, pp. 75–84, 2007.

[45]   C. L. Briant, "Cleavage of tungsten rod," *Mater. Sci. Technol.*, vol. 7, no. 8, pp. 739–745, 1991.

[46]   "ASTM E399-90, Standard test method for plane-strain fracture toughness of metallic materials.," in *Annual Book of ASTM Standards*, Philadelphia (PA):American Society of Testing and Materials, 1997.

[47]   T. L. Anderson, *Fracture mechanics : fundamentals and applications*. 2004.

[48]   J. Stampfl, S. Scherer, M. Berchthaler, M. Gruber, and O. Kolednik, "Determination of the fracture toughness by automatic image processing," *Int. J. Fract.*, vol. 78, pp. 35–44, 1996.

[49]   J. Stampfl, S. Scherer, M. Gruber, and O. Kolednik, "Reconstruction of surface topographies by scanning electron microscopy for application in fracture research," *Appl. Phys. A Mater. Sci. Process.*, vol. 63, no. 4, pp. 341–346, 1996.

[50]   J. Riesch *et al.*, "Development of tungsten fibre-reinforced tungsten composites towards their use in DEMO - Potassium doped tungsten wire," *Phys. Scr.*, vol. T167, no. 14006, p. 8, 2016.

High-throughput study of binary thin film tungsten alloys

Vladica Nikolić [a], Stefan Wurster[b], Alan Savan[c], Alfred Ludwig[c], Reinhard Pippan[a]

[a] Erich Schmid Institute of Materials Science of the Austrian Academy of Sciences, Leoben, Austria

[b] Department of Materials Physics, Montanuniversität Leoben, Leoben, Austria

[c] Institute for Materials, Ruhr-Universität Bochum, Bochum, Germany

Abstract

Combinatorial magnetron co-sputtering from elemental sources was applied to produce W-alloy thin film composition spread materials libraries with well-defined, continuous composition gradients (film thicknesses between 1 and 2.5 μm). Three systems were studied: W-Fe (0-7 at. %), W-Ti (0-15 at. %) and W-Ir (0-12 at. %). High-throughput characterization of the materials libraries comprised of chemical, morphological and microstructural analyses. Scanning electron microscope investigations revealed that the films have a columnar structure of inverted cone-like units separated by voided boundaries, with a strong correlation to the alloying element content. Significant morphological changes occurred with an increase in the amount of the added element; W films with lower at. % of the alloying element had higher density and tighter grain boundaries, altering towards an increased amount of voids as the concentration of the alloying element increased. Electron backscatter diffraction scanning was used to determine microstructural components (grain size, grain shape, texture evolution), in dependence on the concentration of the alloying element.

Keywords: Binary tungsten alloys, thin films, magnetron co-sputtering, morphological characterization, EBSD analyses

E.1. Introduction

Tungsten (W), the refractory metal with the highest melting point (T_m=3422°C), shows outstanding properties such as excellent high temperature strength, good thermal conductivity, high creep resistance and low vapour pressure [1]. In contrast to these advantageous properties, one of its major drawbacks is its inherent brittleness at low temperatures. In addition, a characteristic transition from brittle to ductile fracture behaviour (DBTT), typical for most body-cantered cubic (bcc) metals, occurs at relatively high temperatures for W. An exact value of the transition temperature cannot be given, as this strongly depends on microstructure and testing direction [2], the strain-rate [3] and the type of mechanical test. However, when discussing the use of W in high temperature applications, this high transition temperature is an issue and it is very important to determine a way of decreasing the DBTT and increasing ductility and fracture toughness. Different strategies of ductility improvement are possible; here we investigate alloying i.e. formation of W solid solutions.

Influences of alloying on the mechanical properties of W materials are studied since the mid-1950s with the work of Geach and Jaffe [4,5], initially mainly focusing on the investigation of the influence of Re additions to W materials [6,7]. Since then, extensive research has been carried out [8–11] investigating different alloying elements [12–15], as well as performing various calculations and simulations [16–18]. Nevertheless, the effect of alloying elements on the mechanical properties of W-based materials is still not completely understood. Large datasets are available from these publications and a general trend indicating whether an alloying element is beneficial or detrimental for certain properties can be concluded. However, a thorough comparison of the obtained results is difficult. Experiments conducted over past decades were performed on different materials processed by different production techniques. Hence, microstructures and purity levels differ and it is very challenging to judge the influence of a single alloying element on important materials properties. In the case of W-based materials, the microstructure established during production has a tremendous influence on the resulting mechanical properties. For example, it was shown that an anisotropic microstructure strongly impacts deformation [19] and fracture behaviour [14,20,21], where direction of testing plays a decisive role in the resulting fracture toughness.

Magnetron sputter co-deposition techniques can generate multinary alloy systems in the form of continuous composition spreads [22] enabling efficient high-throughput investigations. Therefore, this approach was used to investigate the influence of different alloying elements and their concentrations on the properties of W thin films. A major advantage of this method is that it produces a large variety of W alloys that are *identical* in the preparation technique, hence leading to very *similar* purity levels and directly comparable microstructures. Within the scope of this study, combinatorial co-sputtering from separate high purity elemental sputter targets was applied in order to produce three binary thin film alloy systems: W-Fe, W-Ir and W-Ti. All films were deposited on oxidized Si and bulk W substrates, with film thickness of 1-2.5 µm. The sputter parameters (see below) were adjusted to achieve the desired composition gradients. A detailed chemical, morphological and microstructural analysis of the composition spread films was performed, revealing whether the produced films are applicable (in terms

of density and roughness) for further mechanical investigations.

E.2. Experimental Procedure

E.2.1. Co-deposition of W-X thin film materials libraries

W-X composition spread thin films were deposited by magnetron co-sputtering in an ultra-high vacuum system (DCA, Finland) [22] from targets of W (Ø100 mm, 99.995 %, FHR Germany) and X, where X is Ir (Ø2 inch, 99.9 %, Alfa Aesar, Germany), Ti (Ø100 mm, 99.995 % K.J. Lesker, UK) and Fe (Ø100mm, 99.9 %, MaTeck, Germany). In the deposition chamber, there are 5 cathodes regularly spaced in a confocal, sputter-down configuration. The target-to-substrate, centre-to-centre distance was approximately 185 mm. Due to this geometry, the material sputtered from each cathode deposits on a static substrate with a regular thickness gradient. Sputtering from two cathodes, located 144° apart onto a Ø100 mm substrate, resulted in combinatorial materials libraries with a continuous composition spread from the sum of the gradients. The base vacuum before sputtering was for every deposition 4.4 x 10^{-7} Pa or lower. Immediately prior to each deposition, the targets were precleaned by sputtering against closed shutters for 10 minutes, while the substrate was lightly Ar-plasma etched with a 25 Watt RF bias.

For pure W reference films and for each of the binary composition spread materials libraries, a Ø100 mm (100) Si wafer with 1.5 µm thermal oxide, and a Ø100 mm mechanically polished W disc were used as substrates. W discs were cut out from technically pure (>99.97 wt. % W) commercially available polycrystalline W plates with an average grains size of 3.9 µm. The standard fabrication of such a plate is via powder metallurgical route and after sintering it is submitted to different rolling processes. A suitable surface of the W substrate was obtained using a Buehler Phoenix 4000 sample preparation system by a grinding/polishing procedure under the following conditions: *a silicon carbide grinding paper* for 30 min (SiC 180, Struers; at 350 N), *a grinding disc* for 30 min at 300 N (Hercules S, 9 µm, Buehler; at 300 N) and *polishing cloths* (MD-Dac, Struers; at 200 N) for 20 min, (MD-Nap, Struers; at 150 N) for 10 min and (MD-Chem, Struers; at 150 N) for 5 min. Depositions were made in Ar (99.9999%) at a pressure of 0.67 Pa. Substrate temperature was at ambient values for all the deposition processes. The pure W reference film was deposited with a power of 303 W DC and a substrate rotation rate of 20 rpm, yielding a film with a uniform thickness of 1.6 µm. The binary films were co-sputtered with no substrate rotation, so that composition gradients were produced due to the geometrical arrangement described above, and a thickness in the substrate center of approximately 1.6 µm. This ensured that the deposited film thickness was at least 1 µm everywhere on the substrate. For the W-Ir composition spread materials library, the W cathode was powered with 303 W DC while the Ir cathode was powered with 98 W RF, resulting in a composition spread of Ir from approximately 0.7 to 12 at. %. In the case of W-Fe, the W cathode had 259 W DC applied while the Fe had 20 W RF, with the Fe gradient produced being approximately 0.5 to 7 at. %. For W-Ti the W and Ti cathodes had 246 W DC and 85 W RF applied

respectively. The Ti content was in the range of 0.6 to 15 at. %. The solubility of Fe in W at 1800 K is about 4 at. % and somewhat less than 1 at. % at 1000 K; Ir in W has a maximum solubility at 1800 K of about 4 at. % and about 2 at. % at 1400 K, whereas Ti is completely solvable at 1800 K, while at 1000 K and 800 K the solubility is 30 at. % and 15 at. %, respectively [23,24]. Room temperature data for the solubility are not available, but seems to be very low. It might be that only the lowest concentrations of Ir and Fe are solvable at RT. The libraries for each W alloy were deposited first on a Si wafer, sequentially followed by a deposition on a W substrate using identical recipes.

E.2.2. Thin film characterization techniques

The binary thin film W-alloys were characterized with the following techniques. Elemental composition was mapped on the oxidized Si substrates using a scanning electron microscope (SEM, Jeol 5800, Japan) equipped with an automated stage for high-throughput energy dispersive X-ray spectroscopy (EDX, INCA X-act, Oxford Instruments, U.K.) measurements, with an accuracy of about 1 at. %. However, due to the continuous and quasi-linear nature of the gradients, we denote compositional values with 0.1 at. % resolution. Elemental quantification and mapping was done on the oxidized Si substrates to preclude any interference from using W also as a substrate. The acceleration voltage was 20 kV, at a magnification of 600x and a working distance of 10 mm. The deposited film thickness was measured and mapped on photolithographically lift-off patterned Si substrates by automated stylus profilometery (Ambios XP2, California, USA).

The morphological properties of the films were investigated by scanning electron microscopy (SEM). High resolution structural observations were taken by using a Leo 1525 Zeiss system with an accelerating voltage of 5 kV and a working distance of WD ~ 6 mm. For the optimal image quality, signals between secondary electrons (SE) and in-lens detectors were combined. Cross-sectional examination of structures developed during deposition was done by a focused ion beam (FIB) workstation (Leo 1540, Zeiss), while the electron back scatter diffraction (EBSD) detector was used to map the film microstructure. For EBSD measurements, areas of 5 x 5 μm^2 were scanned, so that enough data points could be collected for a proper analysis. Evaluation of the obtained scans was made with orientation imaging microscopy (OIM) software. Grain size and texture information was recorded for the different alloy compositions.

E.3. Results and Discussion

E.3.1. Chemical composition of the W-X thin film libraries

Binary W-alloy thin films show a composition gradient across the substrate due to the geometrical arrangement of the sputtering cathodes. Right after the deposition process was finished using oxidized Si substrates, a coarse compositional mapping was done. The maps were obtained to confirm the desired alloying range and were used as a guideline throughout the following analyses. Figure E.1 shows composition maps of the materials libraries. The gradient direction reflects the position of the sputter targets (a red arrow indicates the centre-to-centre line from the W to the alloy element cathodes). The following desired composition spreads were obtained: 0-7 at. % of Fe (Figure E.1a), 0-12 at. % of Ir (Figure E.1b) and 0-15 at. % of Ti (Figure E.1c). The composition ranges for each alloy element were chosen based on estimates of thermodynamically-stable low temperature solubility limits. The binary W alloys deposited on Si substrates were used for coarse EDX mapping and thickness measurements. Detailed chemical quantification of particular regions of interest, and following morphological and microstructural characterizations were performed on thin films deposited on W substrates.
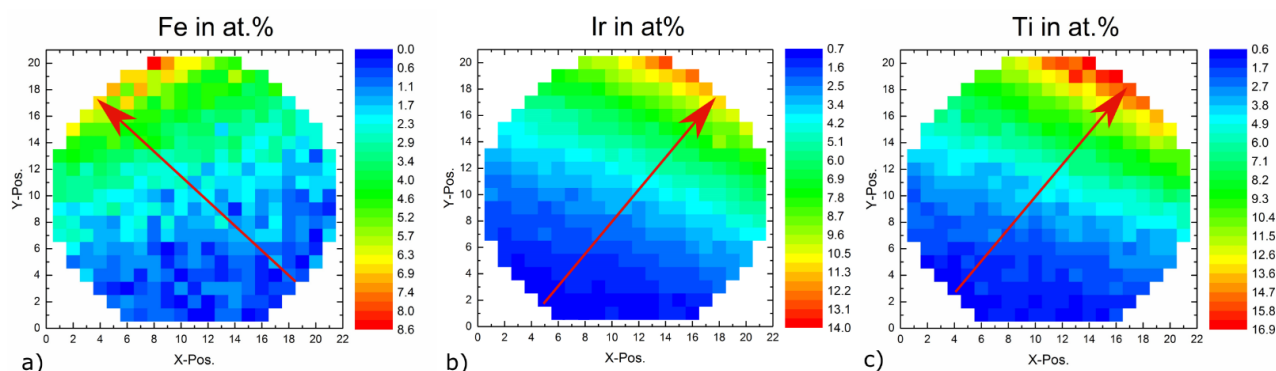
Figure E.1. EDX maps of W-X thin film libraries on Si substrates showing the compositional gradient of the alloying element in atomic percent. a) W-Fe alloy with 0-7 at. % Fe, b) W-Ir alloy with 0-12 at. % Ir and c) W-Ti alloy with 0-15 at. % Ti.

E.3.2. Film morphology

The structure of sputtered thin films shows a large variety in terms of the size, morphology and orientation of grains, which are in direct correlation with various deposition parameters. Substrate temperature, pressure, substrate bias and target power are some of the important deposition parameters in magnetron sputtering, known to influence grain growth and crystallographic texture, which affect the resulting microstructure and properties of the film [25]. All W alloys were deposited in the same atmosphere (Ar), under the same pressure and deposition temperature; in the following analyses the effect of the concentration of the single alloying element is investigated. In Figure E.2a a

top view surface of the reference W film can be seen, where needle-shaped grains are uniformly distributed over the sample. The following sequence of SEM images (Figure E.2b to i) shows the as-deposited W-Ir alloy film indicating a structural transition with a steady increase of the concentration of Ir. The samples with 1.0 at. % Ir (2b) and 1.7 at. % Ir (2c) have surfaces with flat areas and some voided boundaries are perceived. A morphological transition is visible in the samples of the medium alloying range depicted in images 2d) 2.9 at. % Ir, 2e) 3.5 at. % Ir and 2f) 5.4 at. % Ir. Flat areas of the surface decrease, irregularly shaped grains become smaller (with a certain uniformity) and the grain boundaries contain slightly more voids. For regions with the highest concentration of this alloying element, shown in 2g) 7.9 at. % Ir, 2h) 10.4 at. % Ir and 2i) 12.6 at. % Ir, a finer microstructure, consisting of quasi-uniformly distributed structures, is even more pronounced. As the grain size decreases, the amount of grain boundaries goes up, leading to the increase of the total volume of voids. With an increase of concentration, a change from flat to round tops can be observed as well.
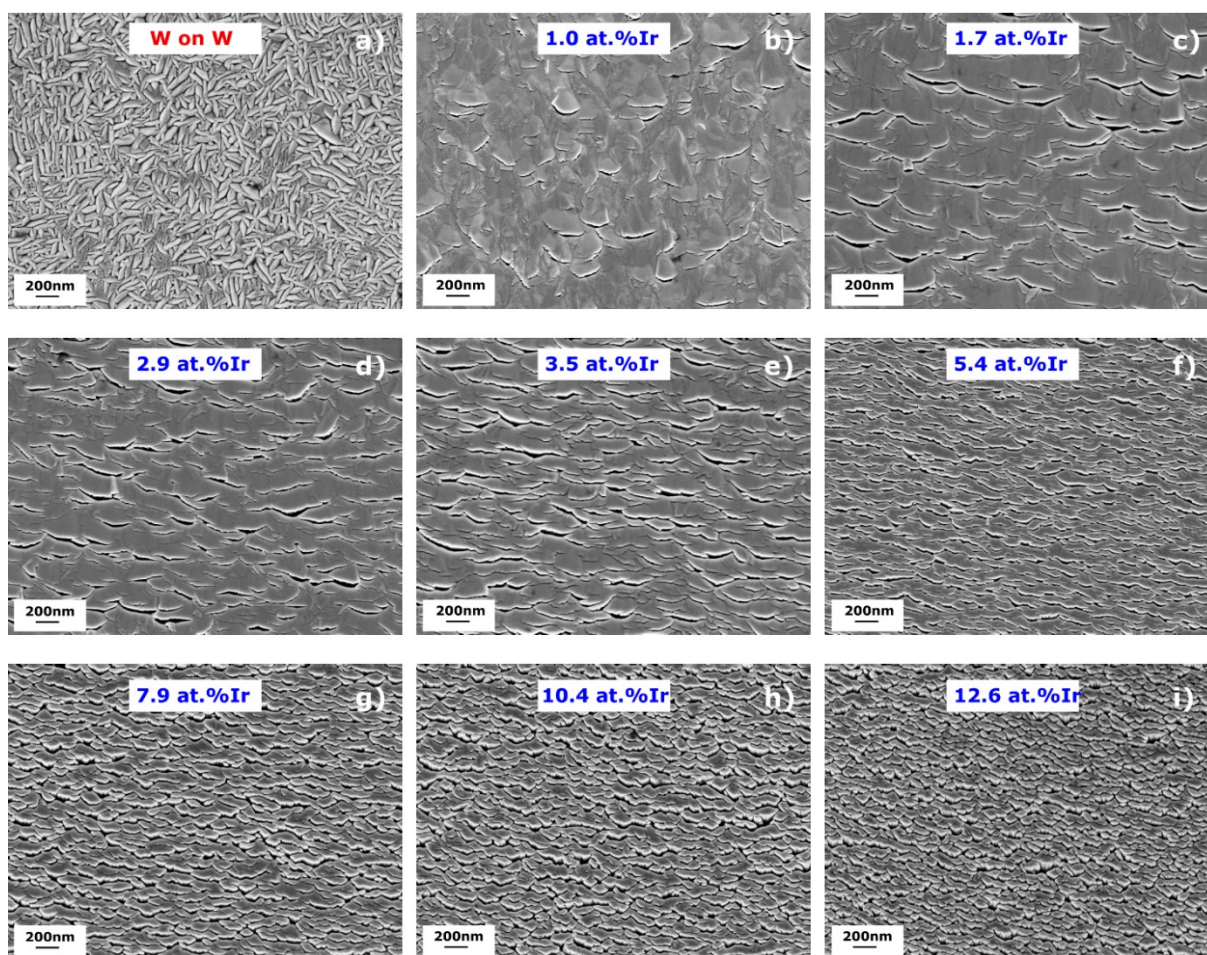

Figure E.2. SEM morphologies of the surface of a) the pure W film (deposited with rotation) and W-Ir alloys with increasing Ir content b) 1.0 at. %, c) 1.7 at. %, d) 2.9 at. %, e) 3.5 at. %, f) 5.4 at. %, g) 7.9 at. Ir, h) 10.4 at. % and i) 12.6 at. %. All films are in the as-deposited state on a W substrate.

Figure E.3 shows a comparison between three different as-deposited W alloys on polished W substrates where SEM top view surface micrographs in regions with a low (3a, d, g), medium (3b, e, h) and high (3c, f, i) alloying content are presented. Similar morphological changes are noticed for Fe, Ir and Ti additions to W, where flatter areas with larger grains (having significantly fewer, tighter grain boundaries) slowly transform into smaller, more similarly shaped structures. A network of voided boundaries separating an array of grains is pronounced in all three film types. The, alloying content influences the surface morphology and in the case of all three W-alloys, an increase in at. % of each alloying element leads to smaller surface structures.
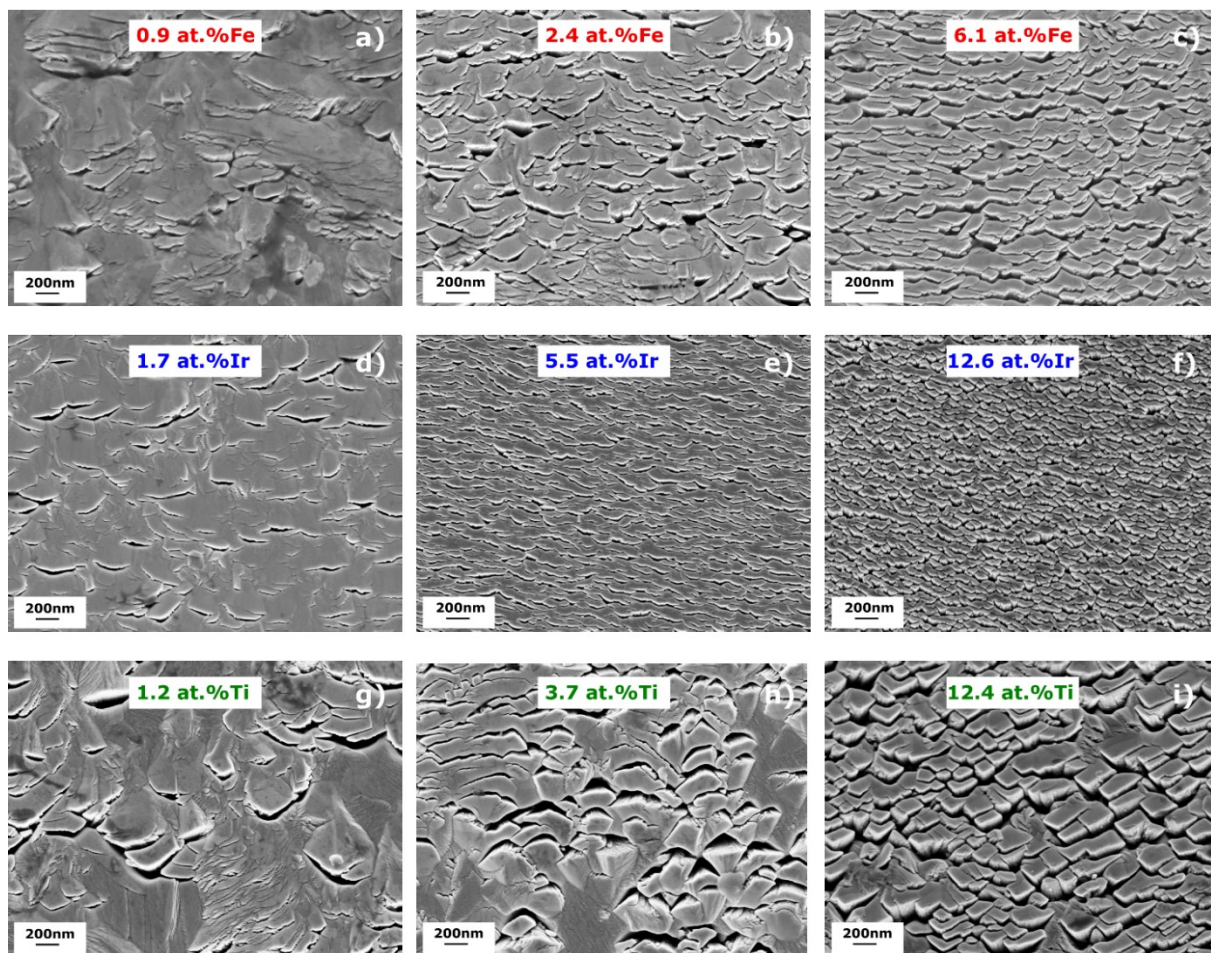
Figure E.3. Top surface view SEM images of W-Fe, W-Ti and W-Ir alloys in the as-deposited state on W substrates, at different concentrations of alloying elements. a), b) and c) W-Fe with 0.9, 2.4 and 6.1 at. % of Fe, respectively, d), e) and f) W-Ir with 1.7, 5.5 and 12.6 at. % of Ir, and g), h) and i) W-Ti with 1.2, 3.7 and 12.4 at. % of Ti, respectively.

In Figure E.4 a comparison of the SEM micrographs of the surface and cross section of the pure W and W-3 at. % Fe film is made. The deposited pure W film has a surface consisting of randomly oriented plate-like structures, uniformly distributed across the film. The cross section reveals that the platelets are elongated columnar structures with a vertical orientation relative to the substrate surface and interface (Figure E.4a). In contrast, the morphology of the W-Fe alloyed film consists of a network of

low-density material surrounding an array of directed columns of higher density. Columnar structures of inverted cone-like units having domed tops and separated by voided boundaries are seen with more detail in a magnified image on the right in Figure E.4b.
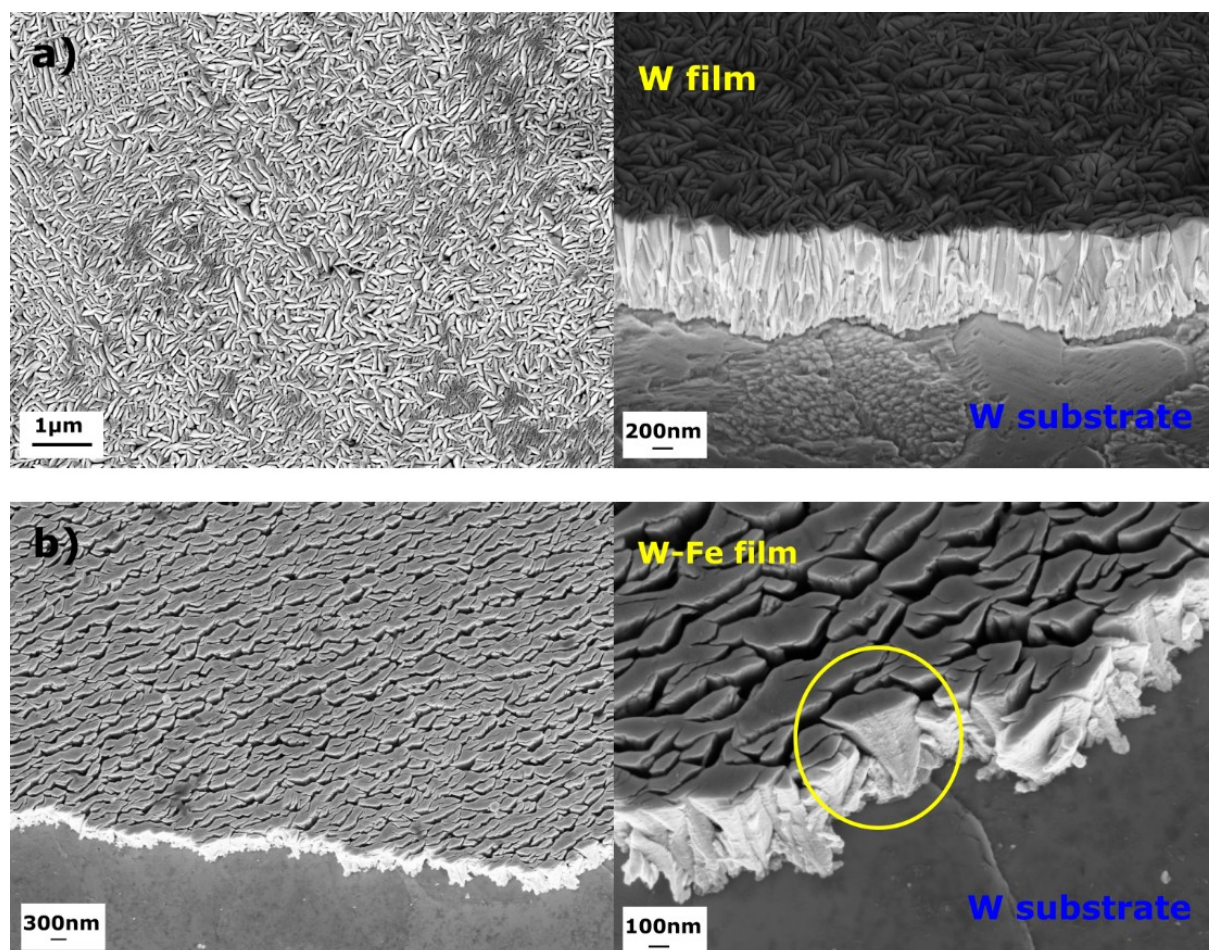
Figure E.4. SEM surface and cross sectional images of a) pure W film having compact platelet structures across the surface and b) W-3at % Fe alloy showing columnar inverted cone-like units.

Thin film microstructures and properties significantly depend on the sputter conditions. The structural zone diagrams (SZD) can give a first estimate of the microstructure which most likely will form given different deposition parameters. In the case of the W-alloys, the deposition process took place at about room temperature. Considering the very high melting point of W (T_m = 3422°C), the homologous temperature is about 0.1 indicating that the resulting film structure should always be in the range of zone I [26]. Considering the sputtering pressure and target to substrate distance used, it should be expected that energies from the particles arriving at the growth surface will not significantly change this zone I morphology [27]. The physical basis of the SZD is related to a large extent on the interplay of atomic processes: shadowing, surface diffusion, bulk diffusion and desorption [28,29]. The distinct zones that appear in the resultant coating structures are a consequence of a variation of these basic processes and effects which dominate in a particular temperature range. The morphology of the grown

film in the low temperature regime of zone I is mainly governed by atomic shadowing effects. Shadowing can be interpreted as a geometric interaction between the angular directions of arriving coating atoms and the roughness of the growing surface. In this case, adatom surface mobility is very low and insufficient to overcome the effect of shadowing. This means that the deposited atoms will adhere where they impinge, leading to the development of tapered structures separated by voids, as seen in Figures 3 and 4. Shadowing induces open boundaries because more coating flux arrives to the high points of the growing surface than to the valleys and the coating growth within this zone is mainly dominated by the set of directions of arriving species to the substrate and the transport of the coating species to the substrate. Therefore, when W substrates are used, it is very important to properly prepare and mirror polish them. The surface diffusivity can be increased by higher substrate temperature, by the increase of energy in the deposition flux, and/or by additional ion bombardment of the surface, resulting in changes in the structure of the growing film. This can lead to larger grains, denser boundaries and smoother surfaces.

Figure E.5 shows the effect of the change of Ti content on the cross sections and surfaces of different W-Ti films. Columnar structures, vertically oriented with respect to the substrate, are visible in all three samples. At low amounts of Ti, the film has columns that have tight grain boundaries, interspersed with cracks and tilted, flat surfaces. As the Ti concentration increases, the cross-section appearance remains similar but with an increased number of columns which appear to have smaller cross-section sizes. The porous columnar structure of the W-Ti films becomes even more apparent with further increase of Ti content; cone-shaped, tapered features are more pronounced while the faceted surface gradually changes into more dome-like tops. These results indicate that with an increased Ti content, there is reduced surface diffusion and therefore self-shadowing effects are more dominant, leading to the porous films and with isolated columnar structures.

Considering the SZM, a denser film structure can be promoted by an increase in temperature (so that the adatoms have enough surface diffusion to remove the effects of atomic shadowing) or by decrease in working gas pressure (so that the arriving species can reach substrate with a substantial fraction of their initial energy). Considering that the deposition of differently alloyed samples took place under the same parameters (in terms of temperature and pressure), other factors had to be a decisive cause for the resulting morphological differences. The development of a denser film in the region with the lower content of added element seems to be influenced by the existence and species of the 2nd sputtered material, geometrical arrangement of sputtering targets and relative deposition rates used to obtain the desired compositional gradients.
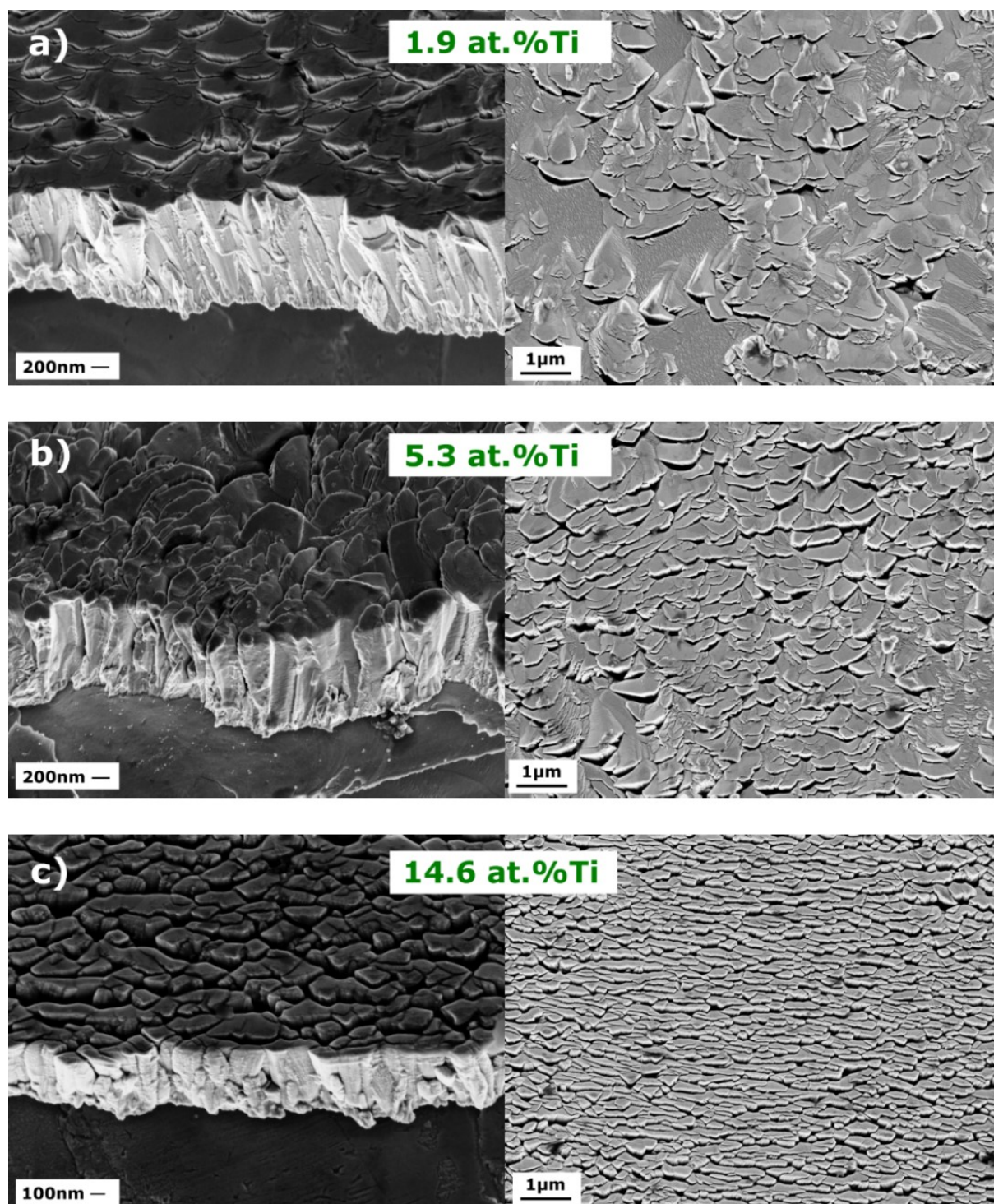
Figure E.5. SEM micrographs of the fracture cross-section and surface of W-Ti films deposited on W substrates with Ti contents of a) 1.9 at. %, b) 5.3 at. % and 14.6 at. %.

In order to investigate further the morphological changes in the films with low added element concentrations and to obtain a better structural understanding of the produced alloys, FIB cross-sections of the films were made (Fig. 6). Long, vertical grooves starting at the surface and going through

the interface and W substrate are artefacts of the ion milling and are not features of the film morphology. In Figure E.6a the W-0.5 at. % Fe film appears to be dense having tighter grain boundaries and with several gaps arising through the thickness. In contrast to that, in the case of an alloy with a high amount of the added element (Fig. 6b), the W-4.8 at. % Fe film shows a significant amount of pores which extend nearly through the entire thickness of the film. If columnar cone-like structures are formed during the early stages of film growth, with further increasing film thickness, these columns simply grow higher with some degree of competitive growth due to crystalline orientation. This is accompanied by an increase in voids size as a result of the self-shadowing effect. In a simple estimation of void volume (by measuring the surface area of pores and cracks), the increase in pores surface area, in respect to the total measured area, was from 1.27% to 21.6 %. It is observed in both alloys that voids/cracks are slanted and this tilt is a direct consequence of the substrate to cathode geometry (Figure E.1a).
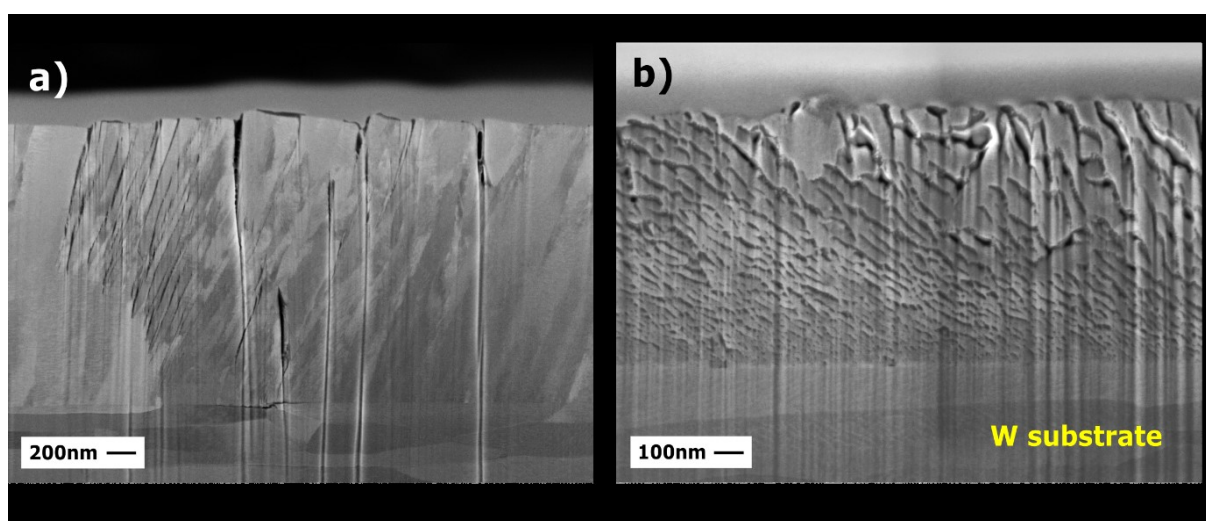
Figure E.6. SEM of the FIB cross-sections in two alloying ranges. a) W-Fe with 0.5 at. % of Fe, having voids across the film and b) W-4.8 at. % Fe, where porosity is significantly increased. A protective W layer is visible on top of the film, which was deposited by electron beam as a preparation step before FIB cutting.

E.3.3. Microstructure and texture analysis

An EBSD analysis was performed to gain a better understanding of the grain size and shape, as well as the preferred crystallographic orientation (texture) of the W-X thin films in dependence on composition. Figure E.7 shows orientation imaging maps of the surface of W-X thin films comparing low and high alloying regions. Due to the surface roughness and characteristic topography of the samples, it is impossible to obtain EBSD patterns in all the points of the selected area. Black areas are regions where a suitable pattern was not acquired. The surface maps of W-Fe, W-Ti and W-Ir show the orientation of the grains where each grain is represented by a distinct color in the color-coded unit triangle of the inverse pole Figure (IPF). Grains marked with blue are oriented along the [101] crystal direction, grains in red are [001] oriented and grains labeled green are assigned to the [111] direction.

The presence of a preferred orientation among a film's grains, relative to a certain fixed reference direction, represents the texture of the material.

Figure E.7 shows EBSD orientation maps of a) W-1.6 at. % Fe and b) W-4.8 at. % Fe films. The microstructure consists of round, uniformly distributed grains and no significant differences can be perceived for different Fe concentrations. The average grain diameter of 401±48 nm measured for film with 1.6 at. % Fe slightly decreases to an average size of 330±38 nm for W- 4.8 at. % Fe. The EBSD maps of the entire range of concentrations could not be obtained, however a further decrease in grain size is expected going from the region at low % Fe to areas of higher concentrations of Fe. The grain diameter is calculated by determining the area of a grain and assuming the grain is circular. A preferential {101} plane orientation is observed for all the analysed samples. Comparing Figure E.7a and E.7b, a slight change in the texture is observed. In addition to composition, texture evolution mechanisms in thin films are influenced by surface free energy, surface diffusivity, adatom mobility, strain energy; the influence of each varies dependent on processing parameters. The observed changes in preferred orientation might be a result of competition between strain energy and surface free energy during film growth [30]. In addition, the substrate roughness may also affect the grain growth and texture. Figures E.7c and E.7d show the microstructure of the W-Ir alloy with 5.8 at. % Ir and 13.1 at. % Ir. The texture remains relatively stable (with a very slight change in IPF in the sample with higher amount of Ir), with a peak in the {101} plane orientation on the [001] IPF. The EBSD grain size analysis showed an increase in grain size with a decrease in Ir content. The average grain diameters are 239±27 nm for W-5.8 at. % Ir and 149±16 nm for W-13.1 at. %Ir. A similar preferential orientation observation can be stated for W-Ti alloy (Figure E.7e and f). Measured grains are slightly elongated perpendicular to the reference direction (top to bottom in the scan) having an average size of 139±20 nm for W-5.3 at. % Ti and 162±25 nm for W-14.6 at. %Ti. A directionality of the grains, as a result of the path of the incoming flux of particles during deposition, is noticed.

In addition, microstructural characterization of the reference W film deposited on W substrate can be seen in Figure E.8a. The EBSD orientation map shows uniformly distributed grains with an average grain diameter of 185±19 nm. A very strong peak in the {101} plane orientation on the [001] IPF is observed. Additionally, in order to exclude the potential influence of the W substrate on the resulting microstructure and texture, a comparison of W-Ti films deposited on W substrate: W-5.3 at. % Ti (8b) and W-0.7 at. % Ti Si substrate (8c) is made. It is clearly seen that the difference in IPF figures is minimal, indicating that the obtained texture is representing preferred orientation of the deposited films, without an effect of the underlying substrate.
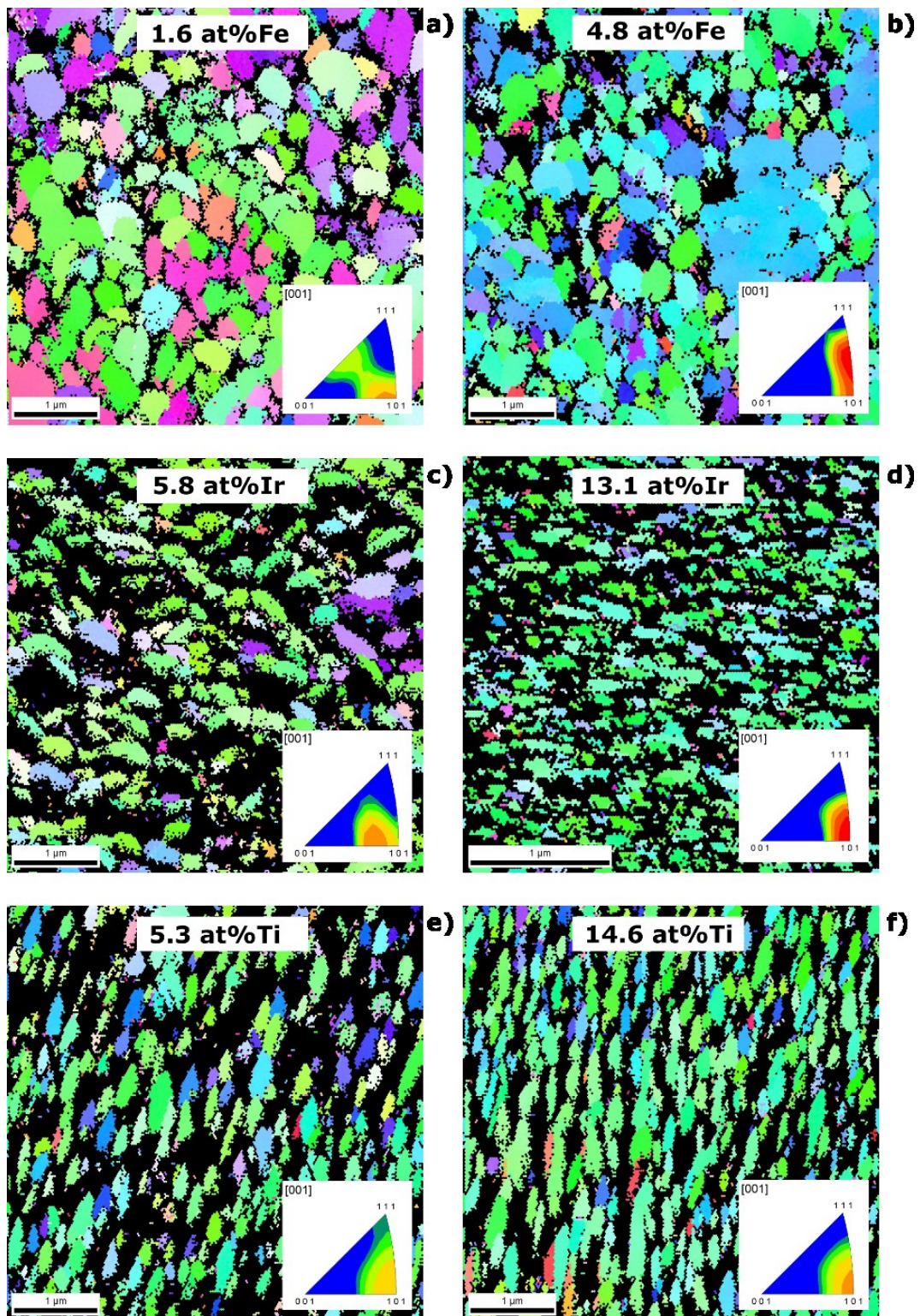
Figure E.7. Color-coded orientation maps obtained by EBSD scanning for different W alloys in high and low alloying regions: a) W-1.6 at. % Fe, b) W-4.8 at. % Fe, c) W-5.8 at. % Ir, d) W-13.1 at. % Ir, e) W-5.3 at. % Ti and f) W-14.6 at. % Ti. For each scan an IPF is designated showing the [001] direction parallel to the sample normal.
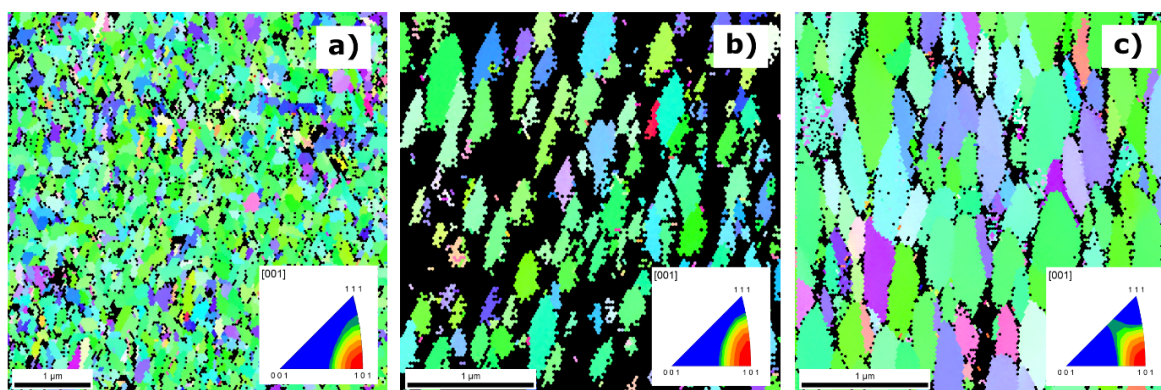
Figure E.8. EBSD orientation maps with designated IPF showing the [001] direction parallel to the sample normal of a) W film deposited on W substrate b) W-Ti alloy film deposited on W substrate and c) W-Ti alloy film deposited on Si substrate.

E.3.4. Remarks to micromechanical testing

Many micromechanical techniques are available to characterize the mechanical properties of materials where one, two, or all three dimensions are in micro regime: nanoindentation, micro pillar experiments, micro tension, micro bending, micro fatigue and micro fracture mechanical tests [31-33]. Due to the high defect density, especially in the highly alloyed regimes of the films, micro tension and micro bending (all tests where tensile properties are examined) are not applicable to the films in this study. For such tests, significant improvement of the density of the films is required. Only in the lowest alloyed regimes micro pillars or nanoindentation might deliver useful data. An analysis of temperature dependence or rate dependence of the plastic deformation would permit study of the detail of deformation processes (for example to analyse whether the Re effect [16] with respect to plastic deformation takes place or not). A requirement for the nanoindentation experiment is a flat surface, hence such experiments could only be performed in situ in the SEM, in order to select a sufficient flat, defect-free location. Surface roughness, as a component of surface morphology, was found to significantly influence both the measured nanohardness and elastic modulus of rough thin films; these properties were lower, in comparison to smooth films, by 40 and 66%, respectively [34]. In general, the reason for the development of roughness during the deposition process is inherent in the interactions between the film-forming species, process conditions and the substrate, so it would be ideal to have perfectly prepared, homogeneous, mirror-polished substrates before deposition. Furthermore, the mechanical properties are not solely affected by the chemical composition and surface quality, as the microstructure is equally important; hence heat treatments (above 1000°C) or deformation (dislocation generation and refinement of the microstructure) of the film and the substrate are necessary. This is the main reason why W is required as a substrate material, otherwise the annealing conditions are extremely limited and residual stresses are unavoidable.

E.4. Conclusions

Binary W alloy thin film composition spreads were fabricated and were analysed by chemical, morphological and microstructural methods in dependence on alloying content. The main findings can be summarized as following:

- Using pairs of elemental sputter targets, three binary W alloy systems were successfully deposited in the form of a thin film with a continuous change in alloying content. The obtained materials had the following composition ranges: 0-7 at. % of Fe, 0-12 at. % of Ir and 0-15 at. % of Ti.

- The morphology of the films with high added-element compositions consists of columnar structures of inverted cone-like units having domed tops and separated by voided boundaries. There is a strong correlation of the observed microstructural appearance and the alloying content – with a decrease of the content of the added element, flattening of surface areas occurs while the boundaries contain considerably less voids. Such a behavior was evident for all three deposited alloys.

- The development of the tapered structures separated by voids seems to be mainly governed by very low adatom surface mobility that is insufficient to overcome the effects of shadowing.

- EBSD orientation imaging maps of W-Fe films reveal that the microstructure consists of uniformly distributed grains with an average size going from 401 nm to 330 nm with an increase in Fe content; the texture exhibits a small variation. The EBSD grain size analysis of the W-Ir alloy showed an increase in grain size with a decrease in at. % of Ir. The average grain diameters are 149 nm and 239 nm at 13.1 at. %Ir and 5.8 at. % Ir, respectively with no change in the {101} plane orientation texture. In the case of the W-Ti alloy, grains are slightly elongated perpendicular to the reference direction, having an average diameter of 139±20 nm for W-5.3 at. % Ti and 162±25 nm for W-14.6 at. %Ti. The texture remains stable having a peak in the {101} plane orientation with respect to the surface normal.

- Comparison of films on polished W and thermally oxidized (100) Si indicates that the substrate does not affect the generated structure, however surface quality is reflected in the film meso-roughness.

Binary W alloys deposited in the form of thin films represent a materials library which is the basis of a high-throughput characterization of various properties as a function of alloying content. With the fulfilment of the necessary microstructural requirements and optimization of the deposition parameters, the possibility of studying the exact influence of a single alloying element by micromechanical experiments is created. This can lead to the validation of potential beneficial effects of a particular alloying element on W materials.

Disclaimer

E.5. References

[1]   E. Lassner and W.-D. Schubert, *Tungsten - Properties, Chemistry, Technology of the Element, Alloys and Chemical Compounds*. New York: Kluwer Academic/Plenum Publishers, 1999.

[2]   D. Rupp and S. M. Weygand, "Loading rate dependence of the fracture toughness of polycrystalline tungsten," *J. Nucl. Mater.*, vol. 417, no. 1–3, pp. 477–480, 2011.

[3]   A. Giannattasio and S. G. Roberts, "Strain-rate dependence of the brittle-to-ductile transition temperature in tungsten," *Philos. Mag.*, vol. 87, no. 17, pp. 2589–2598, 2007.

[4]   G. A. Geach and J. E. Hughes, "The alloys of rhenium with molybdenum or with tungsten and having good high temperature properties," in *Proceedings of the 2nd Plansee Seminar, Reutte*, 1955, pp. 245–253.

[5]   R. I. Jaffee, C. T. Sims, and J. . Harwood, "The effect of rhenium on the fabricability and ductility of molybdenum and tungsten," in *Proceedings of the 3rd Plansee Seminar, Reutte*, 1958, pp. 380–411.

[6]   P. L. Raffo, "Yielding and Fracture in tungsten and tungsten rhenium alloys," *J. Less-Common Met.*, vol. 17, pp. 133 – 149, 1969.

[7]   Y. Mutoh, K. Ichikawa, and M. Takeuchi, "Effect of rhenium addition on fracture toughness of tungsten at elevated temperatures," *J. Mater. Sci.*, vol. 30, pp. 770–775, 1995.

[8]   J. G. Booth, R. I. Jaffee, and E. I. Salkovitz, "The mechanisms of the rhenium alloying effect in group VI-A Metals," in *Proceedings of the 5th Plansee Seminar, Reutte*, 1964, pp. 547 – 570.

[9]   R. H. Forster and A. Gilbert, "The effect of grain structure on the fracture of recrystallized tungsten wire," *J. Less-Common Met.*, vol. 20, pp. 315–325, 1970.

[10]   B. Gludovatz, S. Wurster, A. Hoffmann, and R. Pippan, "Fracture toughness of polycrystalline tungsten alloys," *Int. J. Refract. Met. Hard Mater.*, vol. 28, no. 6, pp. 674–678, 2010.

[11]   S. Wurster, B. Gludovatz, and R. Pippan, "High temperature fracture experiments on tungsten-rhenium alloys," *Int. J. Refract. Met. Hard Mater.*, vol. 28, no. 6, pp. 692–697, 2010.

[12]   A. Luo, D. L. Jacobson, and K. S. Shin, "Solution softening mechanism of iridium and rhenium in tungsten at room temperature," *Int. J. Refract. Met. Hard Mater.*, vol. 10, no. 2, pp. 107–114, 1991.

[13]   A. Luo, K. S. Shin, and D. L. Jacobson, "Ultrahigh temperature tensile properties of arc-melted tungsten and tungsten-iridium alloys," *Scr. Metall. Mater.*, vol. 25, pp. 2411–2414, 1991.

[14] S. Wurster, B. Gludovatz, A. Hoffmann, and R. Pippan, "Fracture behaviour of tungsten-vanadium and tungsten-tantalum alloys and composites," *J. Nucl. Mater.*, vol. 413, no. 3, pp. 166–176, 2011.

[15] M. Faleschini, H. Kreuzer, D. Kiener, and R. Pippan, "Fracture toughness investigations of tungsten alloys and SPD tungsten alloys," *J. Nucl. Mater.*, vol. 367–370 A, pp. 800–805, 2007.

[16] L. Romaner, C. Ambrosch-Draxl, and R. Pippan, "Effect of rhenium on the dislocation core structure in tungsten," *Phys. Rev. Lett.*, vol. 104, no. 19, pp. 1–5, 2010.

[17] R. Gröger, A. G. Bailey, and V. Vitek, "Multiscale modeling of plastic deformation of molybdenum and tungsten: I. Atomistic studies of the core structure and glide of 1/2<1 1 1> screw dislocations at 0 K," *Acta Mater.*, vol. 56, no. 19, pp. 5401–5411, 2008.

[18] H. Li, S. Wurster, C. Motz, L. Romaner, C. Ambrosch-Draxl, and R. Pippan, "Dislocation-core symmetry and slip planes in tungsten alloys: Ab initio calculations and microcantilever bending experiments," *Acta Mater.*, vol. 60, no. 2, pp. 748–758, 2012.

[19] J. Reiser *et al.*, "Tungsten foil laminate for structural divertor applications – Tensile test properties of tungsten foil," *J. Nucl. Mater.*, vol. 434, pp. 357–366, 2013.

[20] D. Rupp, R. Mönig, P. Gruber, and S. M. Weygand, "Fracture toughness and microstructural characterization of polycrystalline rolled tungsten," *Int. J. Refract. Met. Hard Mater.*, vol. 28, no. 6, pp. 669–673, 2010.

[21] E. Gaganidze, D. Rupp, and J. Aktaa, "Fracture behaviour of polycrystalline tungsten," *J. Nucl. Mater.*, vol. 446, no. 1–3, pp. 240–245, 2014.

[22] A. Ludwig, R. Zarnetta, S. Hamann, A. Savan, and S. Thienhaus, "High-Throughput Experimentation Methods," *Int. J. Mat. Res.*, vol. 99, no. NOVEMBER, pp. 1144–1149, 2008.

[23] B. Predel, *Phase Equilibria, Crystallographic and Thermodynamic Data of Binary Alloys*, vol. 5. Springer, 1992.

[24] S. V. ; Nagender Naigu and P. Rama Rao, *Phase Diagrams of Binary Tungsten Alloys*. Asm Intl, 1991.

[25] P. M. Martin, *Handbook of Deposition Technologies for Films and Coatings (Third Edition)*, Third Edit., vol. 1996, no. December 2011. Elsevier Ltd., 2010.

[26] B. A. Movchanm and A. V. Demchishin, "Study of the structure and properties of thick vacuum condensates of nickel titanium tungsten aluminium-oxide and zirconium-dioxide," *Fiz Met Met.*, vol. 28, pp. 83–95, 1969.

[27] J. a. Thornton, "Influence of substrate temperature and deposition rate on structure of thick sputtered Cu coatings," *J. Vac. Sci. Technol.*, vol. 12, no. 4, p. 830, 1975.

[28] P. B. Barna and M. Adamik, "Fundamental structure forming phenomena of polycrystalline films and the structure zone models," *Thin Solid Films*, vol. 317, pp. 27–33, 1998.

[29] I. Petrov, P. B. Barna, L. Hultman, and J. E. Greene, "Microstructural evolution during film growth," *J. Vac. Sci. Technol. A*, vol. 21, p. S117, 2003.

[30] C. V. Thompson and R. Carel, "Texture development in polycrystalline thin films," *Mater. Sci. Eng. B*, vol. 32, no. 3, pp. 211–219, 1995.

[31]   V. Maier, K. Durst, J. Mueller, B. Backes, H. Höppel, and M. Göken, "Nanoindentation strain-rate jump tests for determining the local strain-rate sensitivity in nanocrystalline Ni and ultrafine-grained Al," *J. Mater. Res.*, vol. 26, no. 11, pp. 1421–1430, 2011.

[32]   C. Motz, T. Schöberl, and R. Pippan, "Mechanical properties of micro-sized copper bending beams machined by the focused ion beam technique," *Acta Mater.*, vol. 53, no. 15, pp. 4269–4279, Sep. 2005.

[33]   S. Wurster, C. Motz, and R. Pippan, "Characterization of the fracture toughness of micro-sized tungsten single crystal notched specimens," *Philos. Mag.*, vol. 92, no. 14, pp. 1803–1825, 2012.

[34]   W. G. Jiang, J. J. Su, and X. Q. Feng, "Effect of surface roughness on nanoindentation test of thin films," *Eng. Fract. Mech.*, vol. 75, no. 17, pp. 4965–4972, 2008.

F

Capabilities and limitations of tungsten based materials

Vladica Nikolić [a], Stefan Wurster[b], Reinhard Pippan[a]

[a] Erich Schmid Institute of Materials Science of the Austrian Academy of Sciences, Leoben, Austria
[b] Department of Materials Physics, Montanuniversität Leoben, Leoben, Austria

Abstract

Tungsten and tungsten based materials are considered as top candidates for various fusion applications due to their supreme high temperature properties. However, the major disadvantages and the biggest issues when dealing with these materials are their low ductility at room temperature and their high ductile-to-brittle transition temperature (DBTT). This review article discusses different ductilization and toughening strategies describing the relevant experimental results and an overall conclusion regarding the feasibility of application of tungsten based materials in the future fusion reactors. In addition, the influence of the microstructure and microstructural changes on the material's behaviour is outlined.

F.1. Introduction

Tungsten (W) and tungsten based materials have been investigated in the last years as potential candidates for divertor and plasma facing components. These materials have an interesting combination of advantageous properties such as a high melting point, a high creep resistance, a high temperature strength, a good thermal conductivity, a low vapour pressure and a good erosion resistance [1]. Due to these beneficial properties, tungsten based materials are well suitable for high temperature applications, like in a fusion reactor. However, in contrast to the excellent high-temperature properties, the main disadvantage of the proposed material is its brittleness at low temperatures. W, like most body – cantered cubic (bcc) metals, has a characteristic transition from brittle to ductile behaviour taking place at a certain temperature. An exact value of the transition temperature cannot be given, as this quantity strongly depends on the condition of the material (i.e. microstructure and testing direction) [2] and on the strain – rate [3]. Thus, problems might arise during application because the DBTT can be rather high. This is clearly seen in the results of Charpy tests [4] performed on pure, recrystallized W plate material with the crack orientated perpendicular to the rolling direction, where the transition temperature goes up to 1000°C and beyond. Further problems arise when W – based materials are exposed to the harsh irradiation environment of the reactor. The ductility degrades even more [5, 6, 7].

The successful application of W for future fusion reactor will be determined by both, a decrease in the DBTT and an increase in the ductility and the fracture toughness. Extensive research is focused on these issues [8, 9] and in principle there are three ductilization strategies: (i) the synthesis of a W solid solution - alloying, (ii) the synthesis of materials with an ultra-fine-grained (UFG) microstructure - nanostructuring, and (iii) the synthesis of W composite materials – material's design. This publication will discuss the attempts of ductility enhancement of W by alloying with various elements as well as the influence of the microstructure and microstructural changes on the material's behaviour.

Metals that show an unrestricted solid solubility in W are only V, Ta, Mo and Nb. Besides these, a few other elements such as Re, Ti and Ir exhibit a limited solubility. Their applicability is restricted to the amounts of about 27at%, 12at% and 10at%, respectively, due to the formation of different intermetallic phases [9, 10]. In order to ensure that the nuclear waste properties at the end of the lifetime of the respective components are within acceptable limits, a low activation and a rapid decay of the radiation in the case of the activated materials are mandatory. Therefore, for all of the materials in question this is one of the main requirements [11] and it can be achieved by the selection of the appropriate alloying elements and by controlling the impurities. Since it is well known that Mo and Nb transmute to very long-living radioactive isotopes, they cannot be used for fusion applications [12, 13]. W – Ti and W – Hf alloys could be a possible option, but they have not been investigated so far and very little is known about Ti and Hf as an alloying element. Furthermore, based on experimental observations, Klopp [14] listed Tc, Os and Ru as possible ductilizers for W. However, Os is too expensive to be considered for fusion applications, Tc is radioactive and does not have stable isotopes and Ru is a rare metal with a very low abundance. The possible candidates discussed in this publication, for attempts of W toughening by alloying, are Re, Ir, V and Ta. The following sections will address each of these alloys

describing the relevant experimental results and an overall conclusion regarding the feasibility of application in future fusion reactors.

F.2. Alloys

F.2.1. Tungsten – Rhenium Alloys

Re is by far the most important alloying element for W in respect to ductilization. Besides W it has the highest melting point of all metals: 3186 °C [15]. The maximum solubility of Re in W is 37at% Re at 3000°C which decreases with the decrease in temperature, reaching 27,5 at% at 1600°C. Apart from solid solutions, the existence of two intermetallic phases is observed: a tetragonal σ-phase with a broad homogeneity range and a cubic χ-phase with a narrow homogeneity range [10].

W – Re alloys gained an outstanding importance since it was shown that they exhibit a significantly lower DBTT [16] and are even stronger than pure W at high temperatures [17]. Seeing that the main shortcoming of W is its low- temperature brittleness, it is not a surprise that the interest in alloying by Re has considerably increased. Furthermore, Re additions have a beneficial impact on the reduction of the degree of recrystallization embrittlement [18], it significantly improves weldability and when compared to pure W, W – Re alloys show a superior corrosion behaviour [10].

One of the first investigations of the supreme properties of these alloys was conducted in the mid-fifties by Geach and Hughes [19]. They reported that W – Re alloys show a good temperature strength (that originates from Re) and a very high ductility that can be related neither to the pure W nor to the Re. The room temperature ductility of W alloys varies with rhenium content reaching a maximum at about 30 wt.%. Later on, Jaffe et al. indicated that the terminal solid solution is at about 24 to 25 wt.% Re. They attributed the improvement in low temperature ductility to the mechanical twinning which allows plastic deformation at low stresses, thus avoiding the increased locking of dislocations at low temperature and high strain rates [16].

A detailed fracture mechanical investigation was performed by Mutoh et al. [20] focusing on the fracture behaviour of W and its Re – alloys at elevated temperatures, as well as on the dependence of the fracture toughness on rhenium content. The materials in question were W, W-5wt%Re and W-10wt%Re alloys produced in a standard and sidegroved 3PB – specimens. The experiments were conducted at a temperature range from room temperature (RT) to 1600°C. At low temperatures (RT to 600°C) the plain strain fracture toughness values K_{IC} and for higher temperatures (up to 1600°C) the elastic- plastic fracture toughness J_{IC} were determined. The results show that for all three materials K_{IC} is about the same at RT with the values of 12 – 14 MPam$^{1/2}$ [20]. By increasing the temperature, Re – alloys tend to be tougher (higher J_{IC}) until 1000°C when a decrease is observed. It is interesting that the drop in fracture toughness for pure W occurs at 1200°C. In addition, a correlation between fracture mode and microstructure as well as hardness was investigated. Corresponding to the results of the fracture toughness values at RT, the fractographic analysis of all the materials reveals a quasi- cleavage fracture, showing brittle fracture. At 800 °C, a ductile dimple fracture is visible on the fracture surfaces

of the Re alloys indicating that the DBTT has already been exceeded. In case of pure W, the fracture surface still has a dominant quasi – cleavage fracture with no dimples. At very high temperatures, pure W experiences an embrittlement of the intergranular regions and crystal growth due to recrystallization. As a result of this intergranular fracture, the fracture toughness values decrease dramatically. However, the materials containing rhenium show no significant recrystallization and embrittlement of the grain boundaries leading to a mild reduction of toughness values. Based on the obtained results, adding Re to W has a beneficial impact on the improvement of the high temperature toughness as well as on the decrease of DBTT.

In the work of Gludovatz et al. [21], the effects of the microstructure and the production route on the fracture toughness of W based materials were investigated by the means of 3 – point bending, double cantilever beam and compact tension specimens. The tested W – Re alloys had 26wt% of Re and were tested at room temperature and at elevated temperatures (up to 600 °C). For all materials, as expected, an increase of fracture toughness was observed when raising the temperature. However, W – Re alloys show significantly higher levels of K_{IC} and a more pronounced plastic deformation in comparison with other materials. Even at room temperature, a very distinct plasticity is revealed in the Electron Back Scatter Diffraction (EBSD) scans along the crack path of the propagated crack. At higher temperatures, plasticity appears in the wider vicinity of the crack flanks (Figure F.1).
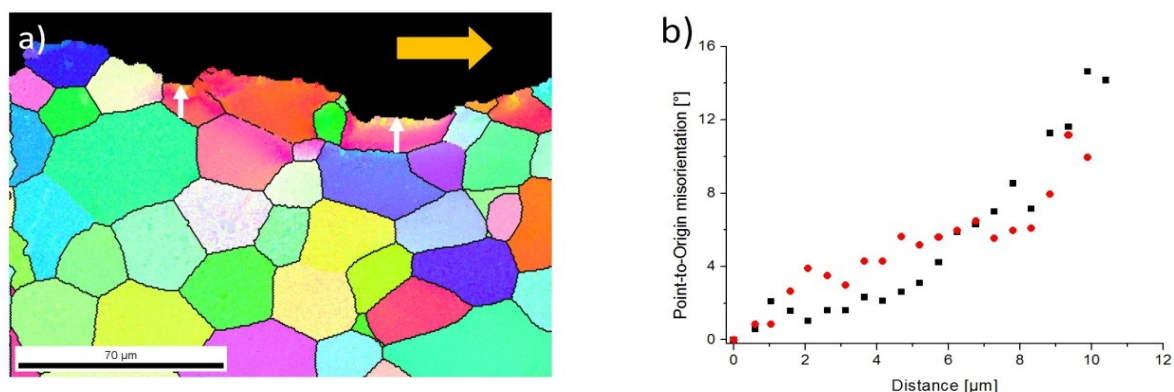
Figure F.1. a) Inverse Pole Figures compiled by an EBSD scans showing plastically deformed areas along the crack path (yellow arrow) of tungsten – rhenium CT specimens tested at 300 °C b) Misorientation of the two grains is indicated by white arrows

The main focus in [22] was the investigation of the fracture behaviour of W – 26Re alloys in a wide temperature range (between RT and 900°C). The experimental results reveal a high anisotropy of fracture toughness in the case of the as – forged material, where the conditional fracture toughness was changed almost by a factor of two, when changing the crack plane and crack propagation direction with respect to the microstructure. The materials that were subjected to a heat treatment (recrystallized samples) are less tough compared to the specimens made of rolled material; nevertheless, the fracture toughness values of recrystallized WRe are well above the ones of recrystallized pure W. A detailed fractography analysis was conducted on the samples and both intercrystalline and transcrystalline fracture surfaces were revealed. At elevated temperatures, there is a tendency towards transcrystalline

fracture for recrystallized samples. The amount of this fracture mode is in correlation with the fracture toughness of the sample, thus it is not a surprise that the samples in as – forged state, orientated in the preferential way, exhibit a larger amount of transcrystalline fracture surface.

The recrystallization that might happen in future fusion reactors completely changes the microstructure and affects the good mechanical properties and lowers the fracture toughness. However, in [22] it was shown that even though the fracture toughness is lowered by almost 50% at room temperature and 300 °C, after recrystallization, this material is still superior over pure, recrystallized tungsten, by a factor of 3.

So how can this advantageous influence of rhenium alloying to tungsten be explained? What is the mechanism(s) that enhances toughness and what kind of physical processes lay beneath this effect?

A decade after the discovery of improved properties for W – Re, but also of Mo – Re alloys, Booth et al. published a paper reviewing several possible factors that could explain this positive influence [23]. One fact is the promotion of twinning in Re – based alloys with W and Mo, with a lot of experimental results for Mo – Re but less for W – Re. Twinning was identified as a mechanism aiding deformation, e.g. by reducing stress concentrations, but it cannot be the sole criterion making these alloys tough. Not giving a proof but a hint for further mechanisms, no twins were found in the vicinity of the crack path shown in Figure F.1a).

Segregation of Re to grain boundaries was also discussed in [23]. At that time, the conclusions were rather drawn indirectly from a change in fracture morphology, going from cleavage fracture for pure materials, to grain boundary fracture for Re – alloys. However, two years later Gilbert [24] found a change from grain boundary fracture in unalloyed W to cleavage fracture for Re – alloys. One of the explanations given was a change in grain size when alloying with Re. From the authors' experience [25] it can be said that it is difficult to link the ratio of inter- to transcrystalline fracture with alloying (or impurity) content. It is influenced to a greater extend by microstructural features such as grain size and grain shape. Booth et al. also refer to older work from Jaffee et al. [16] and Gilbert et al [26], who gave first hints on a reduced strain rate sensitivity of Mo – Re and Cr – Re alloys, showing that dislocations motion in Re – alloys responds as quickly to different loading rates.

Besides the improved properties, many authors mention the solid solution softening phenomenon which can be observed at low temperatures [14, 27, 28]. When adding small amounts of rhenium, there is a significant decrease in hardness. However, this effect diminishes when increasing the Re content and the temperature; it completely disappears above a homologous temperature T_m of 0.16 [14]. The maximum rhenium concentration for a change from softening to hardening was found to be 16at% [27]. However, in [28] it was found that with an increase in testing temperature, the rhenium concentration needed for a maximized softening effect decreases and for a temperature of 730K, the softening already vanished. The phenomenon of solid solution softening is not peculiar for Re – alloys but it is a common feature of bcc materials. A list of solid solution softening materials is given in [29]. Keeping in mind that W – Re alloys also show markedly good mechanical properties at high Re contents and elevated temperatures, there have to be (at least) two mechanisms working that ductilize and toughen these alloys. So it is necessary to speak of solid solution softening (appearing for many combinations of

167

metals) and a *real* Re ductilizing effect – appearing for alloys of Re with group 6 metals. For applications, the solid solution softening is of less interest as this effect vanishes for higher temperatures. A thorough review of this effect is given by Pink and Arsenault [28]. Thus, in the next paragraphs, recent result on explaining the Re ductilizing effect – also working at elevated temperatures – is given.

What seems to promote these improved mechanical properties of W – Re alloys is assigned to the change in the dislocation properties, in particular screw dislocations of ½ <111> type. Gröger et al [30] performed computer simulations based on bond order potentials and showed that {110} glide planes are the preferred glide planes for pure W and Mo at low temperatures. An explanation of the Re ductilizing effect was then given by Romaner et al. [31] by means of the density functional theory (DFT) calculations of ½ <111> screw dislocation in W – Re alloys. It was demonstrated that alloying with Re leads to crucial changes in the interatomic bonding, therefore affecting the screw dislocation core structure. The existence of the transition from a symmetric to an asymmetric core is revealed, which causes a change in the preferred slip plane [31], which is depicted in Figure F.2. On the left side, a core structure of the relaxed dislocation can be seen, when there is no applied stress. W atoms projected on the (111) surface are represented by the empty circles and the arrows indicate two neighbouring atoms shift in the out-of-the-paper direction when a dislocation is inserted into a perfect crystal. The scheme on the right side of Figure F.2 explains the length of the arrows in greater depth. A screw dislocation, defined by the dislocation line s and the burgers vector b is inserted into a crystal. In the case shown here, both vectors are parallel to the x-axis. Due to this insertion, there appear different x-coordinates for neighbouring atoms, which would have the same coordinates in a perfect crystal. This difference d in x-coordinates for two neighbouring atoms gives the length of the arrows. Re additions influence the interatomic bonding and in the centre of the Figure F.2 a pronounced asymmetry in the <112> direction (arrows of different length) and a transition from a symmetric to an asymmetric core structure can be seen. This has a significant influence on the glide behaviour of the dislocation. Whereas the glide in pure W is uniform on one glide plane, the glide plane changes for W – Re alloys, resulting in an overall movement on {112} planes.
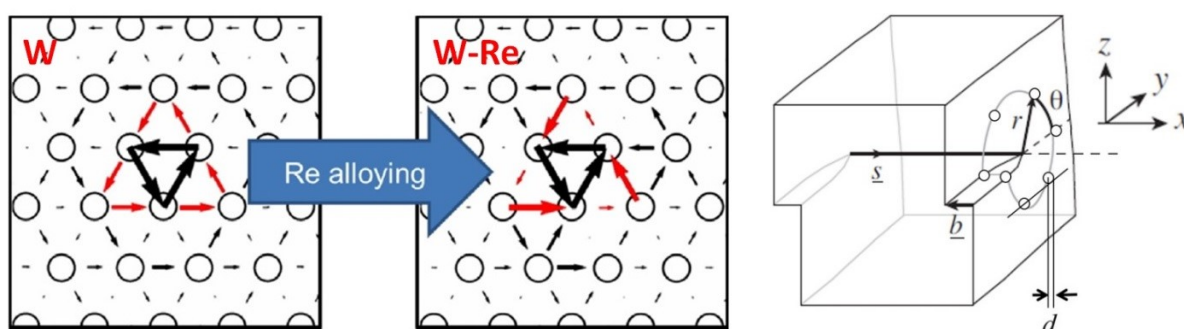

Figure F.2. Transition of dislocation – core symmetry of screw dislocations introduced by alloying tungsten with 25% Re. The scheme on the right explains how the arrows in the other two figures have to be understood. The length of the arrows depicts the magnitude of d, which is the difference of - in this case - x-coordinates of two neighbouring atoms. Taken from [9].

Additions of Re affect not only the slip plane but also the Peierls stress σ_p which is lowered. σ_p is the shear stress required to make a dislocation glide in an otherwise perfect crystal without the assistance of thermal activation. The Peierls stress depends on the nature of interatomic bonding and arises as a direct consequence of the periodic structure of the crystal lattice. In agreement to this are the results of many experiments where the plastic behaviour and the glide planes of W and different W alloys were investigated [32, 33, 34]. At room temperature for pure W, in both {110} and {112} slip systems, slip has been observed. Adding Re promotes slip at room temperature on {112} planes. The publication by Li et al. demonstrates and explains this increase in number of slip planes, combining both experimental work and computer simulations [35]. Similar simulations were performed for alloying of W with Ta and V, but no change in the screw dislocation core structure was found which is in agreement with the experimental results collected over the years.

To summarize, the ductilizing effect can be attributed to the change in core symmetry, the decrease of σ_p and the increase of the number of slip planes. Hence, the origin of this phenomenon is intrinsic and results from the filling of the $d-$ band which modifies inter $-$ atomic bonding, leading to the enhanced dislocation mobility and an improved plastic deformation.

It becomes clear that ductility and toughness enhancement of W by formation of solid solution is possible by adding Re since many experimental results show e.g. improved toughness and lower DBTT and computational results give the explanation. However, despite a big technological relevance of the Re ductilizing effect its use is limited by the fact that Re is a rare metal and therefore very expensive. For fusion energy applications, W alloying by Re has been ruled out. Nevertheless, knowledge on the effect of Re alloying is important for fusion application. W-atoms partially transmute into Re due to neutron irradiation and therefore materials properties might change with increasing neutron dosage.

F.2.2. Tungsten – Iridium Alloys

Iridium is rarely mentioned in the literature as a typical W alloying element. Nevertheless, its electronic configuration, the neighbourhood to Re in the periodic system of elements and the W − Ir phase diagram indicate some promising effects on W. The W − Ir system has a peritectic reaction occurring at 2540 °C and at 25at% Ir, resulting in the formation of a high temperature σ phase. The melting points of Ir and W are 2447°C and 3422 °C, respectively. The solubility of Ir in W decreases with decreasing temperature - the maximum of about 10at% is at the peritectic temperature (2540°C) and decreases to about 4at% at 1810°C [15].

Luo et al. were investigating the mechanical properties of W − Ir alloys, in two publications in the early nineties [36, 37]. In the first paper, the scope was the investigation of a solid solution softening mechanism of Ir in W (as well as Re in W) at room temperature [36]. The alloys in question contained 0.4 and 0.8wt% Ir. Based on the Vickers hardness measurements and tensile tests, it was deduced that even at small amounts of Ir the properties noticeably change. The concentration of 0.4% Ir corresponds to the maximum in solid solution softening, the minimum strength and the maximum ductility. In comparison to the alloy containing Re, these effects are more pronounced and the iridium is shown to

be more efficient in terms of solid solution softening. The initial material, having a coarse grained, recrystallized microstructure with an average grain size of 180 μm, dominantly fractured by transgranular cleavage at room temperature.

The explanations given in [36] for the improved room temperature ductility, like changing the d – electrons configuration and easier formation of double kinks match the ones already given in the section on Re alloys.

In the second paper of Luo et al., the investigation of the effects of Ir concentration and the test temperature on the strength and fracture behaviour of W – Ir alloys at ultrahigh temperatures was performed [37]. Iridium shows a moderate strengthening effect in the temperature range 2200 – 2600 K, but with the increase in temperature the effect decreases and finally vanishes at 2600K. The increase in tensile properties of the alloy is proportional to the concentration of added Ir (see Figure 4 in [36]). The dominant fracture mode is transgranular with a tendency of transition to intergranular either with the increase in temperature or with Ir content. Thus, the addition of Ir seems to promote the toughness of the grain interior, which is – as it can be expected – in contrast to the effect from Ta additions, as it was shown in [38] and will be explained in greater detail in one of the next sections.

As the experimental data for tungsten-iridium system are limited and very little is known, in order to make final conclusions regarding the beneficial effect of Ir addition, further investigations of mechanical properties are necessary. However, from a technical point of view i.e. fusion application, iridium is assumed to be not significant due to the fact it is a very rare metal and therefore it has a high price. Yet, if about 0.2at% would be sufficient to obtain a substantial improvement, then it might be reconsidered for applications in fusion environments.

F.2.3. Tungsten – Vanadium Alloys

The W - V system belongs to the binary isomorphic category meaning that a continuous series of solid solutions with a bcc structure occurs between pure V and pure W at all compositions [15]. Melting points of V and W are 1910 and 3422°C, respectively. They exhibit a high strength, good fabricability and a good corrosion resistance.

Experimental results of mechanical properties and the fracture behaviour of W – V alloys are scarce. Based on the data from the Charpy impact testing at different temperatures, it seems that alloying W with V is not a promising way of toughness and ductility enhancement. No improvement in the DBTT can be observed (Figure F.3) and when compared to pure tungsten, all depicted alloys are more brittle, for temperatures below 1000°C [9].
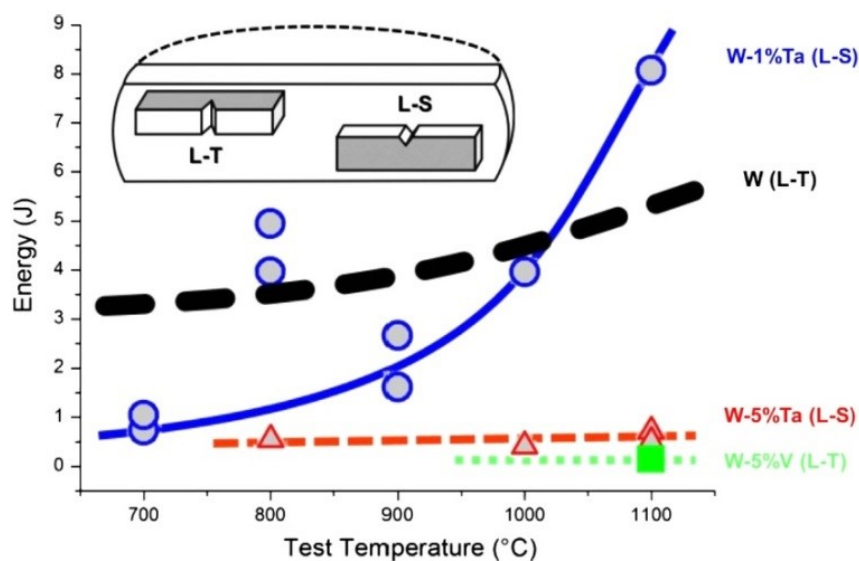
Figure F.3. Charpy results of pure W, W-Ta, and W-V alloys. The specimens were fabricated out of round, forged blanks that were forged to a height reduction of 80% [9].

Additionally, a density – functional theory (DFT) investigation on V alloying was conducted, but did not reveal any significant change in the dislocation- core symmetry [39]. Hence, using V as alloying element will not be an option for the ductilization of W.

However, the idea of using V as one of the compounds is not completely discarded. In [40] W - V composites have been explored for a possible medium temperature application for fusion technology. In the numerical analysis that was conducted, various composite microstructures were introduced: W or V particle reinforced composites, short fibre reinforced composites of random or aligned fibre orientation and unidirectional infinite fibre reinforced materials with W fibres and the vanadium phase constituting the matrix. The introduced materials show promising properties and the results reveal a distinct potential of the material. E.g., by varying the content of V, the thermal expansion coefficient can be changed over a large range. This would promote the bonding of the W-based material with other materials having a higher coefficient of thermal expansion than W.

Furthermore, the fracture behaviour of the HPT deformed ultra-fine grained (UFG) W –V material was investigated by Wurster et al. [38]. The main idea was to determine whether the appropriate microstructural design and the different chemical composition could have a beneficial impact on the fracture toughness. On the one hand W – V composite materials with UFG microstructure were fractured and then compared with the work of Hohe et al. [40], the microstructure would resemble a mixture of particle reinforced and randomly distributed short fibre – reinforced composites. The results show that the fracture behaviour is not markedly different to UFG pure tungsten with a strong anisotropy regarding testing direction [41]. The material homogenized at high temperatures show inferior fracture behaviour. With these new results available it was stated that W cannot be ductilized and toughened by V – alloying [8], composite production, for medium temperature application, seems to be the only viable option.

F.2.4. Tungsten – Tantalum Alloys

The tantalum – tungsten system is defined by the complete miscibility in both solid and liquid states, over the entire range [15]. The tantalum alloys, with a few percent of tungsten, gained a great technical significance especially for structural materials in corrosive media. Advantageous properties are due to the combination of high elasticity and good corrosion resistance of Ta, and the solid solution strengthening of W [10].

The possibility of using tantalum as a tungsten ductilizer was explored as well. If we refer to Figure F.3, the results of Charpy impact testing are not promising – the increase in the amount of Ta leads to a decrease in the fracture toughness of W – Ta alloy. The DBTT in Charpy tests seems to be even higher.

Wurster et al. [38] performed a detailed investigation of the industrially produced solid solution W – Ta alloys in as – forged condition. The examined materials were tungsten alloys with tantalum additions of 1, 5 and 10 wt.% provided by Plansee SE. Compact Tension and 3- Point Bending samples were tested from room temperature up to 600 °C in vacuum. The fracture behaviour was studied taking into account several crack propagation directions, in relation to the forging directions, i.e. in relation to the pancake – like grains. An increase of fracture toughness was observed when increasing the temperature as well as a decrease when increasing the Ta content. When the crack propagates along the forging direction, where the pancake – like grains are spread perpendicular to the propagation direction, the fracture was almost completely transcrystalline. In contrast, intercrystalline fracture was observed when the crack propagates perpendicular to the forging direction. Fracture surfaces of W – 5 Ta tested at various conditions and temperatures are presented in Figure F.4. For specimens with crack propagation parallel to the rolling direction, the observed increase in fracture toughness with temperature has a drop. This drop is related to the change in fracture behaviour where the crack deviates from along to perpendicular to the forging direction. The strong dependency of fracture mode on Ta content is evident since, for W – 10 Ta, the maximum tested temperature was not sufficient for transition from transcrystalline to intercrystalline fracture to take place. For this special testing geometry, this is a sign for an increasing grain interior embrittlement with increasing Ta content. When compared to pure tungsten, transcrystalline fracture toughness of W – Ta is significantly lower at high temperatures.

Based on these results and several other publications [8, 9], it is clear that tantalum additions lead to a decrease in fracture toughness and workability. Therefore, these alloys will not be proposed for fusion applications.
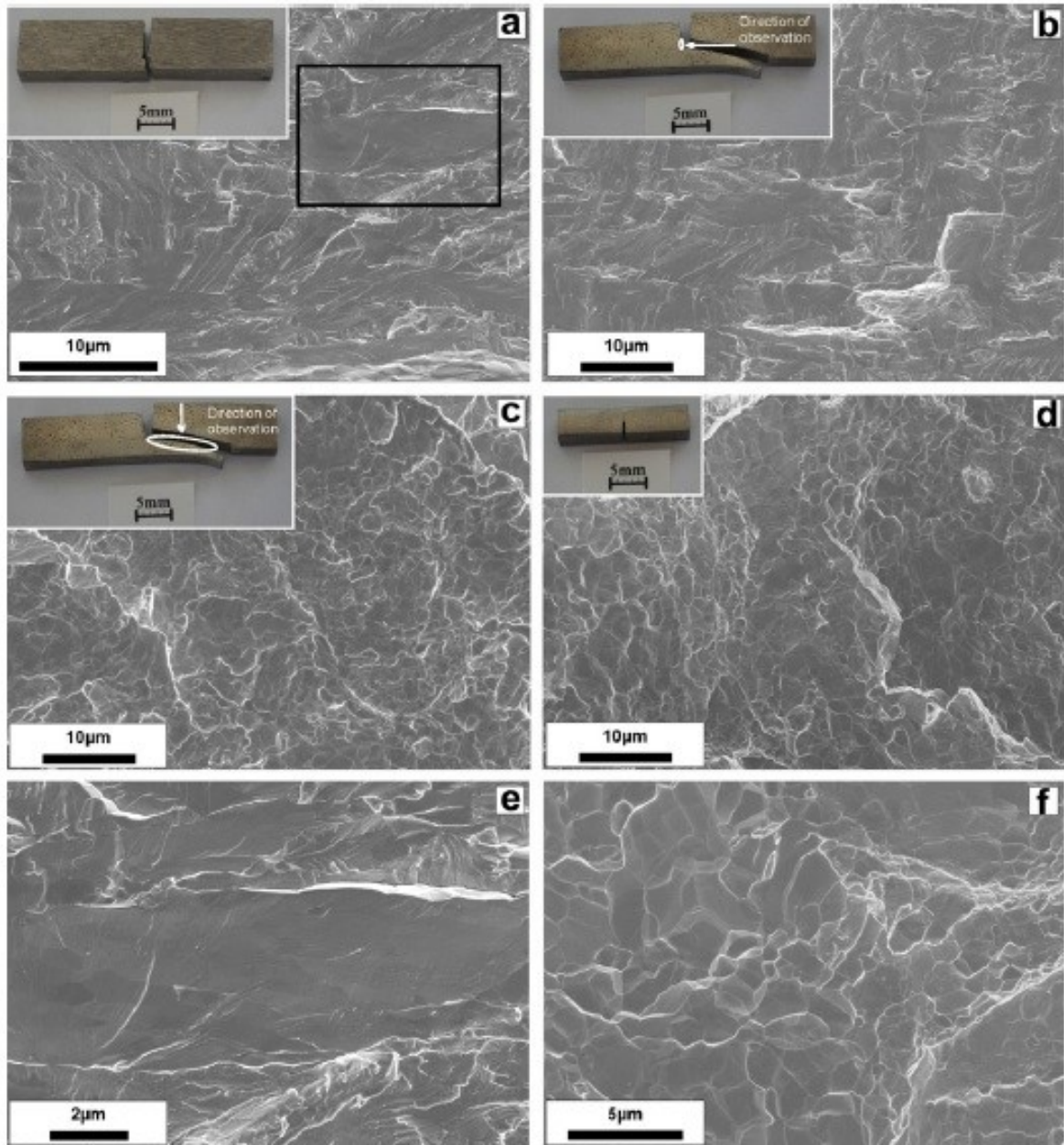
Figure F.4. Fractography analysis of the W – 5Ta (3 PB specimens) (a) Crack propagation in the forging direction, RT experiment, transcrystalline fracture; (b) Crack propagation in forging direction, 600 °C experiment, transcrystalline fracture for small crack extension. (c) The same sample as in (b) but for the area of the crack deviation from the forging direction, intercrystalline fracture. (d) Crack propagation perpendicular to the forging direction, RT experiment, intercrystalline fracture. (e) Higher magnification of the sample shown in (a). (f) Higher magnification of the sample shown in d). [38]

F.2.5. Summary on tungsten alloys

Based on experimental and computational results, it can be concluded that the ductility of tungsten can be improved by formation of solid solution when adding Re, Ir and –continuing the sequence- maybe Os. In contrast to the thorough research on the Re effect, alloying by iridium and osmium has not been investigated in detail, therefore the true extent of possible improvement of mechanical properties and the minimal needed alloying content is unknown. For a large, technical scale application like fusion reactors, these elements seem to be ruled out mainly due to their low abundance and their high price. Therefore, when treating the problem of room temperature brittleness of tungsten, solid solution approach is not an option for fusion application and other solutions need to be found.

F.3. W materials with stabilized microstructure

Another possibility in an attempt of achieving higher fracture toughness and improved ductility is by a beneficial microstructure of W. To extend this microstructure to higher operating temperatures, it should be stabilized by any measure. Grain size, grain shape and a crystallographic texture are here the main focus which can be used to improve the ductility and fracture toughness.

W single crystals exhibit a quite ductile behaviour in tensile experiments even below room temperature [42]. However, in fracture toughness experiments W – single crystals exhibit a DBTT above 300°C. In the coarse grained material, the DBTT increases to even higher temperatures. This seems to be induced by the effect that the DBTT for intercrystalline cleavage fracture is significantly larger than DBTT for transcrystalline cleavage fracture. Thus, grain boundaries in front of crack tips and aligned in the propagation direction, should be avoided as much as possible.

A change in grain shape usually results in anisotropic fracture toughness [38]. The toughness is low when vast, interconnected areas of grain boundaries are in front of the crack and parallel to the crack plane. Toughness values are found to be higher, when the crack has to deviate from its initial plane to follow the grain boundary or the grain interior has to be cleaved. Two principal versions of available semi – finished tungsten products are wires and plates/foils, both with some beneficial fracture properties. These microstructures have to be stabilized for high temperature applications. Among several possible dispersoids that can be incorporated in tungsten matrix in order to stabilize the microstructure, following chapters will focus on the tungsten materials stabilized by lanthanum oxides and potassium bubbles.

F.3.1. WL10

WL10 is a nanostructured tungsten material with 1wt% La_2O_3 particles dispersed in its metal matrix. The microstructure of the material, its texture and grain size strongly depend on the manufacturing history, thus its thermomechanical treatments. During the production steps (e.g. rolling) the initial lanthanum oxide particles which have spherical shape get elongated along the rolling direction forming needle – like structures. The final particle distribution and the size of La_2O_3 are determined by the initial particle size, the initial grain size and the degree of deformation. In a typical industrial product, rod material with a diameter of 10mm and a final hot forging step (degree of deformation > 80%), the size of the lanthanum - oxide needles is about 400nm in diameter and 20µm in length [43].

In the work done by Rieth and Dafferner [43], high energy Charpy tests on commercially available W and WL10 rod materials were performed. The initial microstructure in both materials shows a very distinct forging texture with the grains elongated along the rod axis as a result of the high level of hot working. However, it should be noted that for typical industrial application the degree of deformation is significantly larger. In order to achieve optimum Charpy properties, due to the anisotropic microstructure, testing specimens were fabricated with the long side along the rod axis and with the notch perpendicular to it. The experiments were performed up to 1100°C. The analysis was performed based on the absorbed energy vs. test temperature and from the upper – shelf energy, a DBTT can be determined. It leads to 800±50°C for pure W and an estimation of 950±50°C for WL10. The obtained transition temperatures are too high to consider these materials well suitable for structural applications in fusion technology. The fact that the already insufficient fracture characteristic of pure W is further reduced by adding La_2O_3 is even more unpromising. Additionally, it is important to point out that the chosen orientation of the specimens leads to the lowest possible transition temperatures. Therefore, the obtained DBTT are the best possible for the tested materials. Fully ductile behaviour was only observed for tungsten at 1050°C, while all the other specimens fractured in a brittle manner. Thus, the value of a DBTT for WL10 can only be estimated. Fractographic appearance is strongly dependent on the anisotropic grain shape and the crack propagates in the rod axis, which is at an angle of about 90° to the initial crack propagation direction, rather than along the bending direction. WL10 rods behave more like a uniaxial fibre – reinforced materials where the crack propagates along the needle like La_2O_3, which yields in a further rise of the DBTT compared to pure W. An additional, detailed investigation of Charpy properties was performed on pure and WL10 tungsten rod materials in order to examine the influence of microstructural characteristics like grain size, texture and anisotropy as well as the notch fabrication [44]. All of the materials exhibit brittle behaviour at temperatures below 600°C, where the weakest link in the microstructure are the grain boundaries leading to intergranular fracture. The high DBTT is also strongly influenced by an extended range of delamination, which is furthermore promoted by the dispersion of oxide particles. Additionally, the influence of different notch fabrication methods was investigated revealing that electro discharge machining produces more micro – cracks which promotes delamination. In contrast, specimens with sawed notches, having a notch root radius almost twice as large compared to the EDM fabricated samples show an improvement of the delamination –

to – ductile transition by 100°C, but DBTT seems not to be influenced by the fabrication process. The authors conclude that regardless of the beneficial impact of La_2O_3 on W materials (such as an improvement of the processability and tensile properties, the suppression of recrystallization and a slight strengthening in creep [44, 45]), fracture characteristics compared to pure tungsten are not enhanced.

However, an appropriate optimization of the production method leading to a homogenous grain distribution and a reduction in size of dispersed particles, could improve ductility to some extent. Yan et al. [46] performed a systematic investigation of the effect of working processes on the microstructure, fracture behaviour and DBTT, comparing pure W and WL10. Working processes in question, for a lanthanum – oxides doped material, were swaging, rolling and swaging + rolling. Optical micrographs reveal a uniform distribution of La_2O_3 in the W matrix, with grains of 60μm. The obtained results in [46] distinctly differ from the ones in [45] since it was found that WL10 has a lower DBTT than pure W. Impact toughness of pure tungsten can be improved by an increase in relative density since pores could act as crack initiators. Density measurements that were also performed indicate that swaging before rolling could lead to higher fracture strength by eliminating residual pores from the matrix. According to their opinion, swaging + rolling as a production method could be successful, in combination with lanthanum oxides additions, and could lead to enhanced mechanical properties of tungsten materials.

F.3.2. WVM

When discussing nanostructured and ultra – fine grained materials, it is very important to stabilize its microstructure at elevated temperatures, since beneficial mechanical properties would deteriorate if recrystallization occurs. Potassium – doped tungsten (WVM, W vacuum metallizing) is a nanostructured tungsten material doped with potassium (0,005wt %). The potassium bubbles are known to retard recrystallization [47] and therefore it is a very promising option for nuclear fusion applications. The effect of doping tungsten with potassium is well known from wire industry [48]. During processing, deforming and annealing, strings of fine, nanometre sized potassium bubbles are formed and located in grains as well as on grain boundaries effectively impeding dislocation and grain boundary movement [49].

In [44], the DBTT for WVM rod material was determined to be around 1000°C which is even higher than the value for pure tungsten. For the used materials, it was also determined that the microstructure of rod materials is more favourable compared to rolled plates, indicating that underlying microstructure has a significant influence. This matter will be addressed in greater details in the following chapter. Gludovatz et al. [21] investigated the fracture toughness of various tungsten materials (including WVM) by the means of 3 – point bending, double cantilever beam and compact tension specimens. As expected, all the materials show an increase of fracture toughness with increasing temperature and WVM even has higher values of K_q then pure tungsten, at tested temperatures of 400 and 800°C. For a sample tested at room temperatures, fracture surfaces and EBSD analysis reveal two types of fracture behaviour: intergranular and transgranular. Transgranular propagation of a crack was slightly more dominant. Faleschini et al. investigated the toughness of tungsten materials taking into account the influence of cold work [41]. Seriously depending on the degree of the deformation, the fracture

toughness was found to be improved for L – R orientation (according to ASTM E399 [50]) compared to sintered materials over the whole temperature range. Additional hot or cold work is expected to lead to an increase in toughness. For C – R orientation the toughness was comparable at low and worse at high temperatures then for sintered material. Dominant fracture for WVM is intercrystalline, with fracture occurring at grain boundaries and sintered pores. This kind of behaviour is observed at all temperature ranges.

F.3.3. Summary on W materials with stabilized microstructure

So, it is clear that toughness could be improved to some extent by dispersion-strengthened tungsten by appropriate manufacturing processes. A high degree of deformation as well as an alignment of grains along a certain contour has a considerable impact on ductility and fracture toughness of tungsten materials. This indicates that materials microstructural characteristics like grain size, anisotropy and texture play an important role in overall mechanical properties.

During processing, dispersoids like La_2O_3 or potassium bubbles affect the evolution of the microstructure and significantly increase the stabilization of the fine microstructures with improved properties. It should be pointed out that the degree of deformation for the performed mechanical tests in the literature are often quite small compared to the deformation degrees which are necessary to really obtain a good or the optimum in ductility and toughness. This is mainly due to the fact that the necessary degree of deformation is very high (about 7 or more [51]) which leads to small dimensions for mechanical testing (especially for standard impact or standard fracture mechanics experiments).

F.4. Discussion of microstructural influence on the mechanical behaviour

In order to ensure that tungsten can be used in fusion application, it is necessary to produce tougher and more ductile W based materials on an *industrial* scale. A promising way that leads to improved mechanical properties is by applying adequate manufacturing steps since setting a beneficial microstructure plays a decisive role e.g. for the fracture process and resulting fracture toughness. A detailed understanding of fracture mechanics, controlling factors affecting DBTT and their interaction with underlying microstructure are essential so that a materials design concept with optimized fracture behaviour could be developed.

Since there is a strong correlation between manufacturing history (powder mixing, pressing, sintering, rolling, forging or swaging, hot work, cold work) and resulting material's microstructure, this chapter will focus on two different and industrially relevant types of tungsten materials: rods and plates/foils, revealing how their different microstructures lead to a different crack behaviour. For tungsten rod materials, the microstructure looks like a bundle of fibres where the needle – shaped grains are elongated along the rod axis. In case of tungsten plate materials, grains are flattened parallel to the plate surface and appear like a stack of ''pancakes'' [52].

A detailed investigation on fracture toughness as a function of temperature of pure tungsten rods

was performed in [53] and [54]. In order to examine the influence of the anisotropic microstructure, different crack orientations in respect to materials texture were taken into account. Starting materials were commercially available 99,98% pure tungsten rods with a diameter of 14mm having elongated grains (aspect ratio of roughly 1:3) as a result of a break down rolling with 65% degree of deformation. It was determined that a fibre texture had formed during rolling with <110> direction parallel to the rolling direction. Three specimen types were extracted from the rod with different kinds of crack orientations: 2 transversal samples (with a continuous sequence of grain boundaries in front of the crack front) and 1 longitudinal sample (with the crack front perpendicular to the needle – shaped grains, thus grain interior being in front of the crack tip). The results indicate that there is a strong influence of the anisotropic microstructure on the values of fracture toughness as well as on the DBTT. All the samples show an increase in fracture toughness with increasing temperature. However, longitudinal samples have higher values of K_{IC} in the brittle regime, fracture almost exclusively by transgranular cleavage at RT and ductile to brittle transition occurred at lower temperatures compared to transversal specimens. In contrast to that, both transverse specimens failed by intercrystalline fracture at RT and have lower values of fracture toughness [53]. What seems to play a significant role in the fracture process of all the samples are the elongated grain boundaries parallel to the rolling direction, as they are the preferred crack paths for transverse specimens or become favourable with increasing temperature (longitudinal specimen) [54]. The latter case is associated with a kink of the crack propagation direction by about 90°. Three – point bending experiments performed above 600°C show a pronounced delamination behaviour, where the crack propagates along the rod axis i.e. parallel to the specimen's long side and perpendicular to the notch [45]. The needle like grains are orientated in the same direction. By applying a force during the experiment, the specimen is bent which generates tensile stress in front of the tip but also tensile stresses normal to the grain boundaries and intergranular fracture is most likely to appear since the grain boundaries are most likely the weakest link in the microstructure [44].

Similar anisotropic fracture behaviour of rolled WL10 was found in [55] resulting in one tough direction out of three testing directions. The main goal of the investigation was to alter the microstructure of the initial rod material by an additional rolling step and by doing so, to establish a beneficial microstructure which would result in improved mechanical properties. Due to this processing step, initial needle – like grains of the rod material got elongated perpendicular to the rolling direction, but a desired perfect pancake like structures was not reached yet; the degree of deformation was not high enough. The results for conditional fracture toughness show a pronounced dependence on the testing directions. A crack system which follows the network of grain boundaries has small values of K_I which increases relatively slowly with temperature. The system where a crack is perpendicular to the rolling direction exhibits a higher value of fracture toughness, but the crack kinks at angle of about 90° in respect to the initial crack plane, following the same direction as the samples of the first crack systems and showing grain boundary fracture surfaces. Specimens of the crack system, where the crack cannot easily kink into the brittle crack propagation direction show high values of conditional fracture toughness. As a result, the fracture surface is a mixture of transcrystalline cleavage fracture, where a crack follows a plane defined by the notch, and grain boundary fracture, where the crack deviated from the original

plane. Therefore, it can be concluded that tungsten based rod materials with a needle – like, elongated grain appearance of the microstructure, shows only one tough testing direction with a significantly higher value of fracture toughness in comparison to other crack systems.

The second promising option for fusion application is tungsten plate materials which were investigated in [52]. The material in question is a commercially available 99,97% pure tungsten plate with a thickness of 1mm. A sintered plate was additionally hot and cold rolled with a high degree of deformation leading to the characteristic microstructure of plates – a stack of ''pancakes''. Elongated grains are the reason for an anisotropic behaviour in tensile and Charpy tests properties thus the sample orientation was a key parameter in the experiments. The authors distinguish between 0°, which means tests are performed in the rolling direction, 90°, which means perpendicular to the rolling direction and 45°, which is the orientation in between. The results of tensile testing at room temperatures indicate that there is a strong influence of rolling direction and thus of the microstructure, since two testing directions (0° and 45°) have high yield strength and a high tensile strength. The specimens orientated in 0° even show ductile behaviour at room temperature. In contrast, samples oriented perpendicular to the rolling direction, fail in a brittle way. At elevated temperatures of 600°C, the anisotropic behaviour of the materials disappears and the stress - strain curves of all three specimen types are nearly identical. Fracture surfaces of high temperature tested samples show distinctive necking. Furthermore, Charpy impact testing was performed and a typical transition curve from brittle to ductile regime was obtained. The comparison of 0° and 90° samples was made, revealing that samples orientated in the rolling direction have a DBTT 150°C lower then samples orientated perpendicular to the rolling direction. Additionally, in [4] the effect of plate thickness, existence of notch and annealing on the impact bending properties were investigated. A comparison between notched and unnotched samples was made revealing that samples without a notch have a classical brittle behaviour at low temperatures and a clear transition to a ductile material behaviour at high temperatures. Delamination only occurs for notched samples and the difference in fracture behaviour was attributed to the combination of three-dimensional stress state in front of the notch and the microstructure. The results of Charpy tests performed on specimen made of recrystallized tungsten plate materials are discouraging since the sample did not dissipate energy even at 1000°C and the sample failed by an intergranular fracture. This is a clear indication that for safety – relevant parts of a fusion reactor made of W plate materials, recrystallization must be avoided by all means. Finally, the comparison of unnotched specimens made of plates with thickness of 1mm and 3mm shows a shift of DBTT of 200 K, with the thinner material performing better. This is a very important result, since it shows that a thinner plate which was exposed to a higher degree of cold work has a more beneficial microstructure having smaller grains and a higher amount of mobile edge dislocations. Both of these factors might be responsible for a lower value of DBTT. It becomes clear that a higher degree of deformation of the semi – finished tungsten product will lead to improved mechanical properties [10, 51], so going from 1mm tungsten plates to 0,1mm tungsten foils leads to impressive results (see Figure F.5).
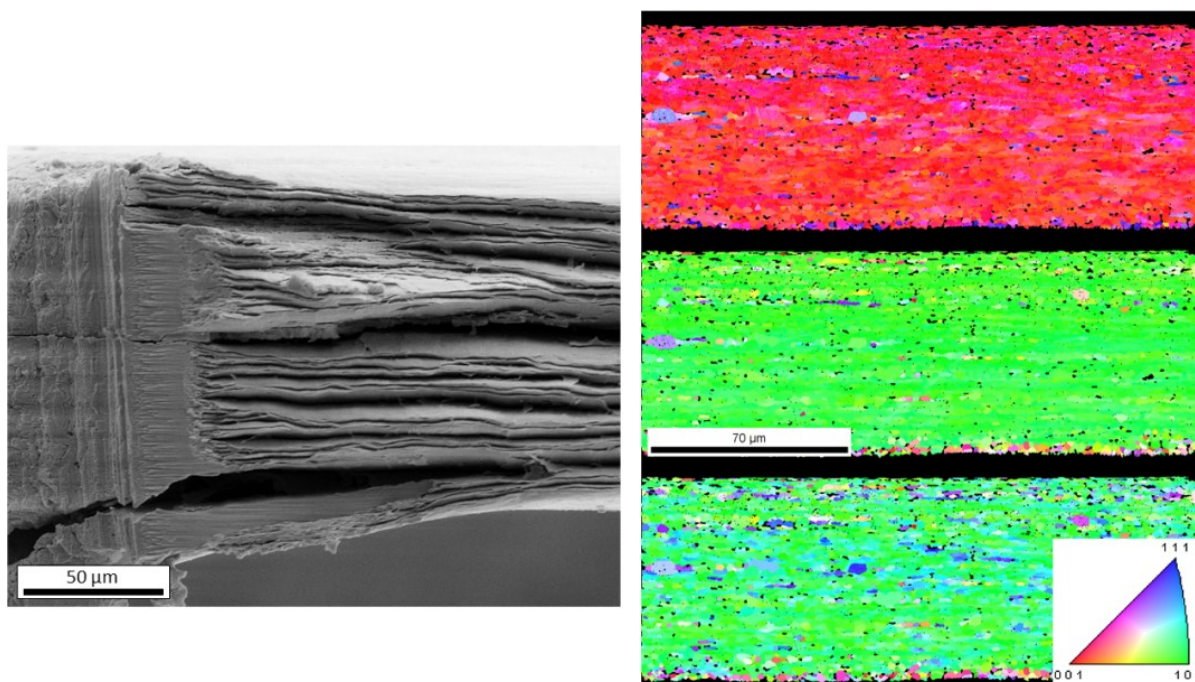
Figure F.5. a) Scanning electron micrograph of the fracture surface of a W – foil. The left part of the micrograph shows the notches introduced by razor blade sharpening and FIB – cutting. Towards the right side comes the fracture surface showing the strong delamination of individual layers of the thin tungsten foil. Fracture experiment was performed at 200°C in atmosphere, with a crosshead speed of 0,4mm/min b) Inverse pole figures maps from electron backscatter diffraction analysis for the same type of foil. The typical rotated cubic texture of thin W – sheets and W – foils is evident. The foil's normal direction (first row) mainly consists of red <100> - directions, whereas the crystals are oriented with <110> - directions parallel to rolling direction (second row) and transverse direction (third row). The micron bar applies for all inverse pole figures and the colour code for identification of crystallographic orientations is also given.

These thin tungsten foils were investigated in details in [56, 57, 58] showing superior fracture properties in comparison to plates. Even more promising are the results of fracture experiments performed on the same material, indicating that the transition temperature from brittle to ductile behaviour is around room temperature [59] which is a significant result for industrially produced tungsten. This is currently one of the leading and most promising toughening and ductilization strategies of W, where the idea is to extend favourable ductile properties of the foil to the bulk material by synthesizing a tungsten laminate [56].

F.5. Summary

At actual state of research, alloying of tungsten does not seem to be a viable option to ductilize and toughen the material. Rhenium, improving the mechanical properties markedly, is the only element that is currently in industrial use, and there are no other less abundant, i.e. cheaper elements in sight. In the last years, research was also focused on elements on the left side of tungsten in the periodic system of

elements, and it seems to come down to the fact that only d-band filling elements, being right-hand of tungsten, are beneficial.

In summary, it can be said that the alignment of the microstructure is crucial for material's good properties. A plate – like microstructure of the tungsten materials is favourable for good toughness in two out of three directions, which is better in comparison to tungsten rod materials. A higher degree of deformation leads to significantly improved mechanical properties, making tungsten foils a very interesting material for fusion application. Important to obtain a good ductility is to generate a thermally stable pancake grain structures with a thickness of the grains in the submicron or nanometre regime. Research and development towards an advantageous, purpose-designed and stabilized microstructure has to pursued.

Disclaimer

F.6. References

[1]   I. Smid, M. Akiba, G. Vieider, and L. Plöchl, "Development of tungsten armor and bonding to copper for plasma-interactive components," *J. Nucl. Mater.*, vol. 258–263, no. Part 1 A, pp. 160–172, 1998.

[2]   D. Rupp and S. M. Weygand, "Loading rate dependence of the fracture toughness of polycrystalline tungsten," *J. Nucl. Mater.*, vol. 417, no. 1–3, pp. 477–480, 2011.

[3]   A. Giannattasio and S. G. Roberts, "Strain-rate dependence of the brittle-to-ductile transition temperature in tungsten," *Philos. Mag.*, vol. 87, no. 17, pp. 2589–2598, 2007.

[4]   J. Reiser, M. Rieth, B. Dafferner, and A. Hoffmann, "Charpy impact properties of pure tungsten plate material in as-received and recrystallized condition (1 h at 2000 °C (2273 K))," *J. Nucl. Mater.*, vol. 442, no. 1–3, pp. S204–S207, 2013.

[5]   M. Fukuda, A. Hasegawa, T. Tanno, S. Nogami, and H. Kurishita, "Property change of advanced tungsten alloys due to neutron irradiation," *J. Nucl. Mater.*, vol. 442, no. 1–3, pp. S273–S276, 2013.

[6]   A. Hasegawa, T. Tanno, S. Nogami, and M. Satou, "Property change mechanism in tungsten under neutron irradiation in various reactors," *J. Nucl. Mater.*, vol. 417, no. 1–3, pp. 491–494, 2011.

[7]   J. M. Steichen, "Tensile properties of neutron irradiated TZM and tungsten," *J. Nucl. Mater.*, vol.

60, no. 1, pp. 13–19, 1976.

[8]   M. Rieth *et al.*, "Recent progress in research on tungsten materials for nuclear fusion applications in Europe," *J. Nucl. Mater.*, vol. 432, no. 1–3, pp. 482–500, 2013.

[9]   S. Wurster *et al.*, "Recent progress in R&D on tungsten alloys for divertor structural and plasma facing materials," *J. Nucl. Mater.*, vol. 442, no. 1–3, pp. 181–189, 2013.

[10]   E. Lassner and W.-D. Schubert, *Tungsten - Properties, Chemistry, Technology of the Element, Alloys and Chemical Compounds*. New York: Kluwer Academic/Plenum Publishers, 1999.

[11]   A. K. Suri, N. Krishnamurthy, and I. S. Batra, "Materials issues in fusion reactors," *J. Phys. Conf. Ser.*, vol. 208, no. 12001, p. 16, 2010.

[12]   S. J. Zinkle, "Advanced materials for fusion technology," *Fusion Eng. Des.*, vol. 74, no. 1–4, pp. 31–40, 2005.

[13]   E. E. Bloom, "The challenge of developing structural materials for fusion power systems," vol. 263, no. 1998, pp. 7–17, 2008.

[14]   W. D. Klopp, "A Review of Chromium, Molybdenum and Tungsten Alloys," *J. Less-Common Met.*, vol. 42, pp. 261–278, 1975.

[15]   S. V. ; Nagender Naigu and P. Rama Rao, *Phase Diagrams of Binary Tungsten Alloys*. Asm Intl, 1991.

[16]   R. I. Jaffee, C. T. Sims, and J. . Harwood, "The effect of rhenium on the fabricability and ductility of molybdenum and tungsten," in *Proceedings of the 3rd Plansee Seminar, Reutte*, 1958, pp. 380–411.

[17]   P. L. Raffo, "Yielding and Fracture in tungsten and tungsten rhenium alloys," *J. Less-Common Met.*, vol. 17, pp. 133 – 149, 1969.

[18]   S. Wurster, "Fracture behavior of tungsten based materials," 2011.

[19]   G. A. Geach and J. E. Hughes, "The alloys of rhenium with molybdenum or with tungsten and having good high temperature properties," in *Proceedings of the 2nd Plansee Seminar, Reutte*, 1955, pp. 245–253.

[20]   Y. Mutoh, K. Ichikawa, and M. Takeuchi, "Effect of rhenium addition on fracture toughness of tungsten at elevated temperatures," *J. Mater. Sci.*, vol. 30, pp. 770–775, 1995.

[21]   B. Gludovatz, S. Wurster, A. Hoffmann, and R. Pippan, "Fracture toughness of polycrystalline tungsten alloys," *Int. J. Refract. Met. Hard Mater.*, vol. 28, no. 6, pp. 674–678, 2010.

[22]   S. Wurster, B. Gludovatz, and R. Pippan, "High temperature fracture experiments on tungsten-rhenium alloys," *Int. J. Refract. Met. Hard Mater.*, vol. 28, no. 6, pp. 692–697, 2010.

[23]   J. G. Booth, R. I. Jaffee, and E. I. Salkovitz, "The mechanisms of the rhenium alloying effect in group VI-A Metals," in *Proceedings of the 5th Plansee Seminar, Reutte*, 1964, pp. 547 – 570.

[24]   A. Gilbert, "A fractographic study of tungsten and dilute tungsten-rhenium alloys," *J. Less-Common Met.*, vol. 10, pp. 328–343, 1966.

[25]   B. Gludovatz, S. Wurster, T. Weingärtner, a. Hoffmann, and R. Pippan, "Influence of impurities on the fracture behaviour of tungsten," *Philos. Mag.*, vol. 91, no. 22, pp. 3006–3020, 2011.

[26]   A. Gilbert, G. T. Hahn, and C. N. Reid, "Tensile properties of chromium and chromium-rhenium

alloys," in *Annual meeting on high temperature refractory metals*, 1964, p. 21.

[27]   E. Pink and R. J. Arsenault, "Low-temperature softening in body-centered cubic alloys," *Prog. Mater. Sci.*, vol. 24, pp. 1–50, 1979.

[28]   J. R. Stephens and W. R. Witzke, "Alloy Softening in Group VIa Metals alloyed with Rhenium," *J. Less-Common Met.*, vol. 23, pp. 325–342, 1971.

[29]   E. Pink, "Lergierungsentfestigung und Spröd Duktil Übergang von kubisch raumzentrierten Metallen," *Zeitschrift für Met.*, vol. 67, pp. 564–567, 1976.

[30]   R. Gröger, A. G. Bailey, and V. Vitek, "Multiscale modeling of plastic deformation of molybdenum and tungsten: I. Atomistic studies of the core structure and glide of 1/2<1 1 1> screw dislocations at 0 K," *Acta Mater.*, vol. 56, no. 19, pp. 5401–5411, 2008.

[31]   L. Romaner, C. Ambrosch-Draxl, and R. Pippan, "Effect of rhenium on the dislocation core structure in tungsten," *Phys. Rev. Lett.*, vol. 104, no. 19, pp. 1–5, 2010.

[32]   J. R. Stephens, "Dislocation structures in single crystal tungsten and tungsten alloys," *Metall. Trans.*, vol. 1, no. May, pp. 1293–1301, 1970.

[33]   J. E. Cordwell and D. Hull, "Observation of 110 Cleavage in 110 Axis Tungsten Single Crystal," *Philos. Mag.*, pp. 215–224, 1972.

[34]   J. M. Liu and B. W. Shen, "Crack nucleation in tungsten on crystallographic planes and on grain boundaries of twist misorientation," *Scr. Metall.*, vol. 17, pp. 635–638, 1983.

[35]   H. Li, S. Wurster, C. Motz, L. Romaner, C. Ambrosch-Draxl, and R. Pippan, "Dislocation-core symmetry and slip planes in tungsten alloys: Ab initio calculations and microcantilever bending experiments," *Acta Mater.*, vol. 60, no. 2, pp. 748–758, 2012.

[36]   A. Luo, D. L. Jacobson, and K. S. Shin, "Solution softening mechanism of iridium and rhenium in tungsten at room temperature," *Int. J. Refract. Met. Hard Mater.*, vol. 10, no. 2, pp. 107–114, 1991.

[37]   A. Luo, K. S. Shin, and D. L. Jacobson, "Ultrahigh temperature tensile properties of arc-melted tungsten and tungsten-iridium alloys," *Scr. Metall. Mater.*, vol. 25, pp. 2411–2414, 1991.

[38]   S. Wurster, B. Gludovatz, A. Hoffmann, and R. Pippan, "Fracture behaviour of tungsten-vanadium and tungsten-tantalum alloys and composites," *J. Nucl. Mater.*, vol. 413, no. 3, pp. 166–176, 2011.

[39]   L. Romaner, "personal communication." .

[40]   J. Hohe and P. Gumbsch, "On the potential of tungsten-vanadium composites for high temperature application with wide-range thermal operation window," *J. Nucl. Mater.*, vol. 400, no. 3, pp. 218–231, 2010.

[41]   M. Faleschini, H. Kreuzer, D. Kiener, and R. Pippan, "Fracture toughness investigations of tungsten alloys and SPD tungsten alloys," *J. Nucl. Mater.*, vol. 367–370 A, pp. 800–805, 2007.

[42]   D. Brunner, "Stress-relaxation tests in the work-hardening regime of tungsten single crystals below 300 K," *Mater. Sci. Eng. A*, vol. 483–484, pp. 525–528, Jun. 2008.

[43]   M. Rieth and B. Dafferner, "Limitations of W and W-1%La2O3for use as structural materials," *J. Nucl. Mater.*, vol. 342, no. 1–3, pp. 20–25, 2005.

[44] M. Rieth and A. Hoffmann, "Influence of microstructure and notch fabrication on impact bending properties of tungsten materials," *Int. J. Refract. Met. Hard Mater.*, vol. 28, no. 6, pp. 679–686, 2010.

[45] M. Mabuchi *et al.*, "Tensile properties at elevated temperature of W-1%La2O3," *Mater. Sci. Eng. A*, vol. 214, no. 1–2, pp. 174–176, 1996.

[46] Q. Yan, X. Zhang, T. Wang, C. Yang, and C. Ge, "Effect of hot working process on the mechanical properties of tungsten materials," *J. Nucl. Mater.*, vol. 442, no. 1–3, pp. S233–S236, 2013.

[47] E. Pink and L. Bartha, *The metallurgy of doped/non-sag tungsten*. Elsevier Science Publishers, 1989.

[48] O. Horacsek and L. Bartha, "Development of the bubble structure from selectively deforming potassium-pores in doped tungsten wires," *Int. J. Refract. Met. Hard Mater.*, vol. 22, no. 1, pp. 9–15, 2004.

[49] P. Schade, "Bubble evolution and effects during tungsten processing," *Int. J. Refract. Met. Hard Mater.*, vol. 20, no. 4, pp. 301–309, 2002.

[50] "ASTM E399-90, Standard test method for plane-strain fracture toughness of metallic materials.," in *Annual Book of ASTM Standards*, Philadelphia (PA):American Society of Testing and Materials, 1997.

[51] A. Hoffman, "personal communication." .

[52] J. Reiser, M. Rieth, B. Dafferner, S. Baumgärtner, R. Ziegler, and A. Hoffmann, "Deep drawing of tungsten plates for structural divertor applications in future fusion devices," *Fusion Eng. Des.*, vol. 86, no. 12, pp. 2949–2953, 2011.

[53] D. Rupp and S. M. Weygand, "Experimental investigation of the fracture toughness of polycrystalline tungsten in the brittle and semi-brittle regime," *J. Nucl. Mater.*, vol. 386–388, pp. 591–593, 2009.

[54] D. Rupp, R. Mönig, P. Gruber, and S. M. Weygand, "Fracture toughness and microstructural characterization of polycrystalline rolled tungsten," *Int. J. Refract. Met. Hard Mater.*, vol. 28, no. 6, pp. 669–673, 2010.

[55] S. Wurster, L. Krämer, T. Leitner, and R. Pippan, "Anisotropic Fracture Behavior of Tungsten Based Materials – Rolled Lanthanum Oxide Dispersion Strengthened Tungsten," *18th Plansee Semin.*, pp. 1–11, 2013.

[56] J. Reiser, M. Rieth, B. Dafferner, and A. Hoffmann, "Tungsten foil laminate for structural divertor applications – Basics and outlook," *J. Nucl. Mater.*, vol. 423, no. 1–3, pp. 1–8, 2012.

[57] J. Reiser, M. Rieth, B. Dafferner, A. Hoffmann, X. Yi, and D. E. J. A. C, "Tungsten foil laminate for structural divertor applications – Analyses and characterisation of tungsten foil," *J. Nucl. Mater.*, vol. 424, pp. 197–203, 2012.

[58] J. Reiser *et al.*, "Tungsten foil laminate for structural divertor applications – Tensile test properties of tungsten foil," *J. Nucl. Mater.*, vol. 434, pp. 357–366, 2013.

[59] V. Nikolic, S. Wurster, D. Firneis, and R. Pippan, "Improved fracture behavior and microstructural characterization of thin tungsten foils," *Nucl. Mater. Energy*, vol. 9, pp. 181–188, 2016.